AD/A-004 805

SOUND PROPAGATION IN SHALLOW WATER. VOLUME II. UNCLASSIFIED PAPERS

Ole F. Hastrup, et al

SACLANT ASW Research Centre
La Spezia, Italy

15 November 1974

DISTRIBUTED BY:

NTIS
National Technical Information Service
U. S. DEPARTMENT OF COMMERCE

SACLANTCEN

Conference Proceedings No. 14

SACLANT ASW
RESEARCH CENTRE

SOUND PROPAGATION IN SHALLOW WATER
VOL. II: UNCLASSIFIED PAPERS

Proceedings of a Conference held at SACLANTCEN
on 23-27 September 1974

Organized by

OLE F. HASTRUP and OLE V. OLESEN

15 NOVEMBER 1974

NORTH
ATLANTIC
ORGANIZ…

VIALE SAN BARTOLOMEO 400
I - 19026 - LA SPEZIA, ITALY

This document is released to a NATO Government at the direction of the SACLANTCEN subject to the following conditions:

1. The recipient NATO Government agrees to use its best endeavours to ensure that the information herein disclosed, whether or not it bears a security classification, is not dealt with in any manner (a) contrary to the intent of the provisions of the Charter of the Centre, or (b) prejudicial to the rights of the owner thereof to obtain patent, copyright, or other like statutory protection therefor.

2. If the technical information was originally released to the Centre by a NATO Government subject to restrictions clearly marked on this document the recipient NATO Government agrees to use its best endeavours to abide by the terms of the restrictions so imposed by the releasing Government.

ACCESSION for		
NTIS	White Section	☐
DDC	Buff Section	☐
UNANNOUNCED		☐
JUSTIFICATION		
BY		
DISTRIBUTION/AVAILABILITY CODES		
Dist.	AVAIL. and/or SPECIAL	
A		

Per form 50

Compiled and Published by

STI

SACLANTCEN
CONFERENCE PROCEEDINGS NO. 14

NORTH ATLANTIC TREATY ORGANIZATION
SACLANT ASW Research Centre
Viale San Bartolomeo 400
I 19026 - La Spezia, Italy

SOUND PROPAGATION IN SHALLOW WATER
VOL. II: UNCLASSIFIED PAPERS

Proceedings of a Conference held at SACLANTCEN
on 23-27 September 1974

Organized by

Ole F. Hastrup and Ole V. Olesen

15 November 1974

This document has been prepared from text and illustrations provided by each author. The opinions expressed are those of the authors and are not necessarily those of the SACLANT ASW Research Centre.

LIST OF PARTICIPANTS AT THE CONFERENCE

Name	Organization	Paper CP Vol/page
AKAL T.	SACLANTCEN	14/22
ARENS H.J.	Erprobungsstelle 71 der BW 233 Eckernfoerde, Berliner Strasse 115 GERMANY	14/206
AUBELL A.	Norwegian Defence Establishment Horten P.O. Box 115, N-3191 Horten NORWAY	14/112
BENNETT C.M.	Naval Coastal Systems Laboratory Panama City, Florida U.S.A.	13II/130
BLACKER D.C. (CDR)	CINCHAN, Northwood, Middlesex U.K.	
BRADLEY D.L.	Naval Ordnance Laboratory White Oak, Silver Spring, Maryland 20910 U.S.A.	13I/53
BUCKER H.P.	U.S. Naval Undersea Center San Diego, Ca., 92132 U.S.A.	14/31
CHING P.A.	The Admiralty Research Laboratory Teddington, Middlesex U.K.	13I/79
COLE B.F.	New London Laboratory NUSC, New London, Conn., 06320 U.S.A.	13I/7
COMPIANI P. (C.F.)	MARIPERMAN, La Spezia ITALY	
DIACHOK O.I.	U.S. Naval Oceanographic Office Washington D.C. 20390 U.S.A.	14/141
DIAMANTI E. (C.C.)	MARIPERMAN, La Spezia ITALY	
DINESEN J. (LT.CDR)	Royal Danish Navy Copenhagen DENMARK	

Name	Organization	Paper Vol/page
DE GUILLEBON (L.V.)	Commission d'Etudes Pratiques d'Océanographie Toulon FRANCE	
DE WITTE V. (L.V.)	Ministry of Defence Brussels BELGIUM	
HARRISON C.H.	The Admiralty Research Laboratory Teddington, Middlesex U.K.	
HASTRUP O.F.	SACLANTCEN	
INGENITO F.	Naval Research Laboratory Washington D.C. U.S.A.	14/69
JENSEN F.B.	SACLANTCEN	14/79
KANABIS W.G.	New London Laboratory NUSC, New London, Conn., 06320 U.S.A.	13I/43
KING L.A.	New London Laboratory NUSC, New London, Conn., 06320 U.S.A.	14/224
KRACHT G.	KRUPP-Atlas-Elektronik, 28 Bremen 44 Postfach 448545 GERMANY	13I/67
KUPERMAN W.A.	Naval Research Laboratory Washington D.C. U.S.A.	14/93
LAVAL R.	SACLANTCEN	14/235
LEFADEUX F.	Laboratoire de Détection Sous-Marine Le Brusc France	
MUIR T.G.	Applied Research Laboratories The University of Texas at Austin Austin, TEXAS 078712 U.S.A.	14/185
MURPHY E.L.	SACLANTCEN	14/2
OLESEN O.V.	SACLANTCEN	
O'QUINN L.D.	SACLANT Norfolk, Virginia 23511 U.S.A.	

Name	Organization	Paper Vol/page
PHELPS, G. (CDR)	SACLANTCEN (Naval Advisor)	
PIPER H.S.	The Pennsylvania State University P.O. Box 30, State College, Penn., U.S.A.	14/215
RETALLACK G.J.	SACLANTCEN (Director)	
REYNOLDS T.N.	The Admiralty Underwater Weapons Establishment Portland, Dorset U.K.	
ROSS J.M. (MAJ)	Defence Research Establishment Atlantic Dartmouth CANADA	
ROY J.	Laboratoire de Détection Sous-Marine Le Brusc FRANCE	14/252
SCHNEIDER H.G.	Forschungsanstalt d. BW für Wasserschall und Geophysik 23 Kiel, Karolinenweg 22 GERMANY	14/129
SCHOTHORST J.G.	Physics Laboratory TNO Via MOD Netherlands (Navy) THE NETHERLANDS	13I/2
SCHUNK E.	Forschungsanstalt d. BW für Wasserschall und Geophysik 23 Kiel, Karolinenweg 22 GERMANY	14/14
SKELLY M.M.	Ministry of Defence (Navy) U.K.	13I/108
SLUYTERMAN van LANGEWEYDE W.	Forschungsanstalt d. BW für Wasserschall und Geophysik 23 Kiel, Karolinenweg 22 GERMANY	14/40
STRARUP T.	Danish Defence Research Establishment Østerbrogades Kaserne DK-2100, Copenhagen DENMARK	
TACCONI G.	University of Genova, Genova ITALY	
THIELE R.	Forschungsanstalt d. BW für Wasserschall und Geophysik 23 Kiel, Karolinenweg 22 GERMANY	14/173

Name	Organization	Paper Vol/page
VETTORI G.C.	SACLANTCEN	
WASILJEFF A.	SACLANTCEN	14/156
WESTON D.E.	The Admiralty Research Laboratory Teddington, Middlesex U.K.	13I/34 13I/79
WILLE P.	Forschungsanstalt d. BW für Wasserschall und Geophysik 23 Kiel, Karolinenweg 22 GERMANY	14/52
ZIEGENBEIN J.	Institut für Hochfrequenzphysik 5307 Werthhoven, Königstrasse 1 GERMANY	

At the end of each paper will be found a brief recording of some of the discussion that followed its presentation.

CHAIRMEN AND ASSISTING SECRETARIES FOR SESSIONS

Chairman of Conference	O.F. Hastrup
Secretary of Conference	O.V. Olesen

		Chairman of Session	Assisting Secretary
Monday	Session 1	O.F. Hastrup	F.B. Jensen
	Session 2	H.P. Bucker	A. Wasiljeff
Tuesday	Session 3	B.F. Cole	E.L. Murphy
	Session 4	A. Aubell	T. Akal
Wednesday	Session 5	A. Wasiljeff	F.B. Jensen
	Session 6	D.E. Weston	A. Wasiljeff
Thursday	Session 7	D.L. Bradley	E.L. Murphy
	Session 8	C.M. Bennet	T. Akal
Friday	Session 9	O.F. Hastrup	A. Wasiljeff

GENERAL ORGANIZATION

To facilitate access to papers of different levels of security classification, the proceedings of the SACLANTCEN Conference on Sound Propagation in Shallow Water are published in the following manner:

SACLANTCEN Conference Proceedings CP-13

Title: Sound propagation in shallow water, Vol. I: Classified papers.

Part 1: Nato Confidential Papers

Part 2: Nato Secret Paper

SACLANTCEN Conference Proceedings CP-14

Title: Sound propagation in shallow water, Vol. II: Unclassified papers.

cccccccc

The following lists only the unclassified papers published in the present document; a full listing of all the papers presented at the conference is given in SACLANTCEN CP-13.

TABLE OF CONTENTS

INTRODUCTION

During the last decade most NATO nations have shown a growing interest in problems concerning antisubmarine warfare in shallow water. Previously, during and just after World War II it was felt that shallow water would never be an area for naval operations and that all research effort should therefore be concentrated in the deep-water field. Only sporadic interest was shown in shallow-water ASW, with the result that it was the shallow-water projects that generally suffered the most from cuts in defence-research expenditure. This attitude is now changing drastically and most nations have a dedicated effort in shallow-water research that will hopefully lead, if not to a complete solution of this difficult problem, at least to a much greater understanding of the basic principles and thereby to improved ASW capability in shallow water.

Shallow water is usually defined as water of less than 200 m depth or, from a geographical viewpoint, as being the continental shelves. It covers only about 8% of the total ocean but, due to the very high concentration of shipping in these areas and numerous strategic submarine routes to operating area, it has a much higher importance than the simple percentage indicates.

Because of the relative proximity of the surface and the sea floor in shallow water, those two boundaries have a stronger influence on acoustics than is experienced in deep water. This is especially so with reverberation, where the effects of the two boundaries amplify each other and create seriously-high reverberation levels.

The water column itself is less homogeneous than in deep water due to the mixing of water masses of different character, particular near river estuaries. This means that fairly complicated models are needed to describe the propagation realistically, so that prediction is therefore difficult and time consuming.

A further complication for ASW in shallow water comes from the often high ambient-noise level due to dense shipping, oil-drilling platforms or other industries. The number of false targets also seems to be higher in shallow than in deep water. Bottom features such as rocky outcrops and wrecks create echoes, and turbulence due to currents can give significant doppler-type false echoes.

The conference reported here was planned by SACLANTCEN to improve the understanding of these shallow-water problems within NATO and the NATO nations by discussing the following subjects:

(a) Propagation.

(b) Reverberation and ambient noise.

(c) Acoustic modelling.

(d) Sonar performances.

(e) Operational and systems aspects.

IMPROVEMENTS OF THE RAY-MODE ANALOGY FOR ESTIMATING THE FREQUENCY OF MINIMUM ATTENUATION FOR MODES IN SHALLOW WATER

by

E. Murphy
SACLANT ASW Research Centre
La Spezia, Italy

ABSTRACT

There is some evidence from shallow water sound propagation data that indicates that attenuation due to boundary losses can be minimal at intermediate frequencies. Also, somewhat complicated theoretical considerations show that the lowest order modes may not always be the modes with least attenuation. A simple ray-mode analogy is often discussed in the literature [see, for example, Kornhauser and Raney, J.A.S.A. 27, 1955: 689; Weston, Jnl Sound Vib. 9 (1), 1969: 80-89] that offers a simple physical basis for these features of shallow water propagation. However the ray-mode analogy lacks rigor and, more important, fails to give quantitative results for the most pertinent values of the parameters. Improvements are described that do not complicate the attractive simplicity of the ray-mode analogy too drastically, but make it possible to obtain quantitative results for more interesting parameter values, and at the same time puts the analogy on a more rigorous foundation.

INTRODUCTION

Experimental results for shallow water sound propagation [see, for example, Refs. 1, 2, 3, 4] have shown that attenuation can be minimal at intermediate frequencies. This is also found in theoretical calculations for specific problems, and in fact, it has been shown that the lowest order mode does not necessarily have minimum attenuation [see Ref. 5]. In addition, the detailed analysis in Ref. 5 for special examples has shown that a number of modes may have approximately the same low value of attenuation. As a consequence, in such circumstances, at all ranges the transmission loss is the result of a complicated interaction between these modes.

It is useful to have some simple model to give at least a qualitative picture to help anticipate the properties of attenuation for different environmental conditions. The ray-mode analogy [see, for example, Refs. 6, 7, 8, 5] is intended as such a tool, but there are serious problems with the simpler versions considered so far, and as a result the analogy fails for the most pertinent parameter values.

In this paper, it is shown, perhaps for the first time, that the concept of beam or ray displacement [see Refs.9 to 15] arises quite naturally in a proper development of the ray-mode analogy, and it is shown that the displacement representation is essential both for putting the analogy on a firmer foundation, and more important for removing the problems that prevent application of the analogy for the most pertinent parameter values. For example, one of the most important rays is the one that just grazes the boundary, and the usual ray-mode analogy fails for such ray parameters.

As the ray-mode analogy is made more complicated, then it is hardly a substitute for actual numerical calculation by complete modal analysis. However, the ray-mode analogy extended to include the phenomenon of beam or ray displacement, combined with recent results describing the nature of beam displacements for bounded underwater sound propagation problems [Refs. 11 to 13], can be a very useful aid for anticipating the behaviour of sound attenuation in shallow water for various kinds of environmental conditions.

1. REVIEW OF THE CONVENTIONAL RAY-MODE ANALOGY

We first derive the simpler ray-mode analogy using the dispersion relationship in the form developed by Brekhovskikh in Ref. 16. For sound propagation in a layer with index of refraction $n(z)$ a function of depth z in the layer [see Fig. 1] and reflection coefficients V_1 and V_2 at the two boundaries of the layer, the dispersion relationship for determining "characteristic" values of a parameter θ_0, can be written in the form

$$V_1 V_2 \, e^{ik_0 \int_{\text{cycle}} \sqrt{n^2(z) - \sin^2\theta_0}\, dz} = 1 \qquad \text{[Eq. 1]}$$

where the integral is the well-known WKB phase integral taken over one ray cycle.

The reflection coefficient V_1 is defined as follows. With the boundary 2 replaced by a semi-infinite homogeneous medium, then

$$V_1 \, e^{ik_0 \int_{\text{cycle}} \sqrt{n^2(z) - \sin^2\theta_0}\, dz}$$

is defined as the reflection coefficient for an upgoing plane wave reflected from the medium and boundary lying above boundary 2.

The reflection coefficient V_2 is defined as the reflection coefficient for a downgoing plane wave incident on boundary 2 when the region above boundary 2 is replaced by a semi-infinite homogeneous medium with sound speed equal to $c(z)$ evaluated at boundary 2.

For the moment we consider θ_0 as real and representing the angle measured with respect to the vertical, for a plane wave, or corresponding ray, at some reference level $z = z_0$. The wave number $k_0 = \omega/c_0$, where ω is the angular frequency and c_0 is the sound speed at the reference level $z = z_0$. The relationship can be interpreted as giving the discreet θ_0-values for which the corresponding up and down-going plane waves would be in constructive interference at depth $z = z_0$, after one cycle.

For real θ_0, we introduce an amplitude $A(\theta_0)$ and phase $\varphi(\theta_0)$ for the reflection coefficients, and write Eq. 1 in the following form

$$A_1 A_2 \, e^{i k_0 \int_{\text{cycle}} \sqrt{n^2 - \sin^2\theta_0}\,dz + \varphi_1(\theta_0) + \varphi_2(\theta_0)} = 1 \, . \qquad \text{[Eq. 2]}$$

This relationship requires that the phase satisfy the equation,

$$k_0 \int_{\text{cycle}} \sqrt{n^2 - \sin^2\theta_0}\,dz + \varphi_1(\theta_0) + \varphi_2(\theta_0) = 2\pi N \qquad \text{[Eq. 3]}$$

where N is an integer, and the amplitudes satisfy,

$$A_1 A_2 = 1 \, . \qquad \text{[Eq. 4]}$$

While Eq. 3 can be recognized as the well-known WKB or Bohr-Sommerfeld eigenvalue condition, we see that Eq. 4 can be satisfied for real θ_0 only when reflection is total at both boundaries.

Weston in Ref. 8 has used Eq. 3 in the following scheme in an attempt to give a simple recipe to determine a frequency of minimum attenuation for a mode [see Fig. 1]

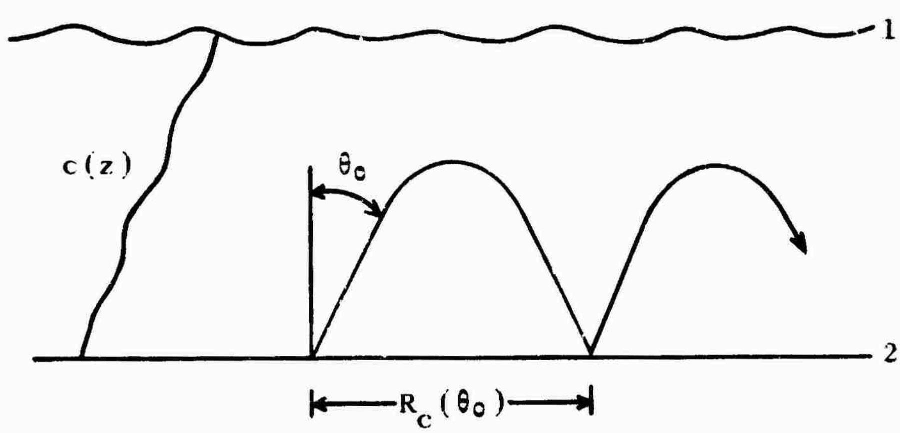

FIG. 1

1) Find $\theta_0(\lambda)$ from Eq. 3, using $\varphi_1 = -\pi$ if the ray hits the pressure release surface, and $-\pi/2$ if the ray angle θ_0 is larger and the ray is totally reflected by refraction before reaching the boundary (see Fig. 2) where $\theta_0 = \theta_c$ represents the ray parameter corresponding to the surface grazing ray.

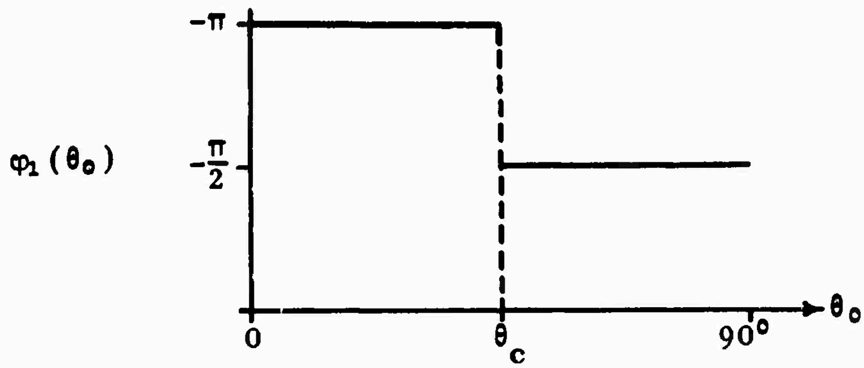

FIG. 2

2) Find the cycle range $R_c(\theta_0)$ from ordinary ray theory,

$$R_c(\theta_0) = \int_{\text{cycle}} \frac{\sin\theta_0 \, dz}{\sqrt{n^2 - \sin^2\theta_0}} . \qquad \text{[Eq. 5]}$$

3) Combine $R_c(\theta_0)$ and $\theta_0(\lambda)$ to obtain $R_c(\lambda)$.

4) With the assumption that the loss per bounce is not too sensitive to θ_0 in the range of θ_0 of interest, then the frequency of minimum attenuation is the value of λ for which R_c is a maximum.

There are two serious problems that arise in this scheme. With φ_1 discontinuous as shown in Fig. 2, then $R_c(\lambda)$ is discontinuous in the most pertinent range of λ (see the sketch in Fig. 3). This problem arises from the discontinuous φ_1 as sketched in Fig. 2. As Weston has suggested, this problem can be eliminated by obtaining from wave analysis the correct and continuous phase φ_1 as a function of θ_0.

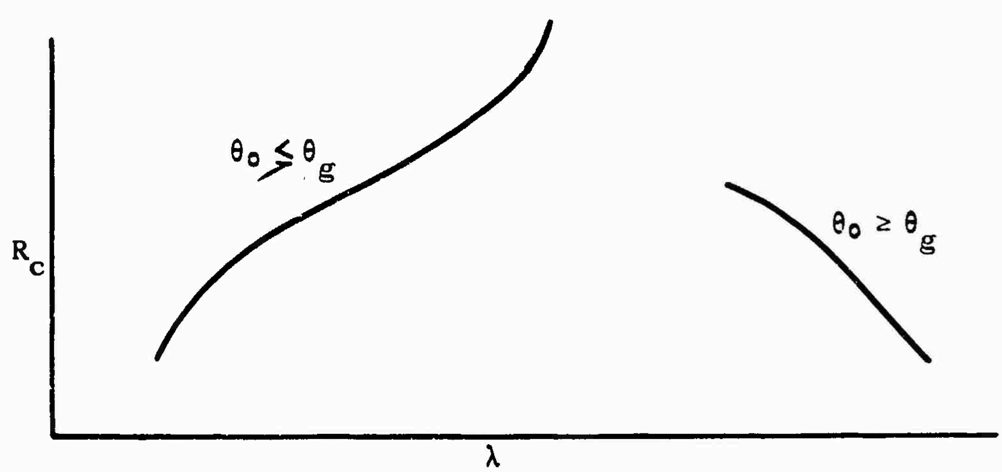

FIG. 3

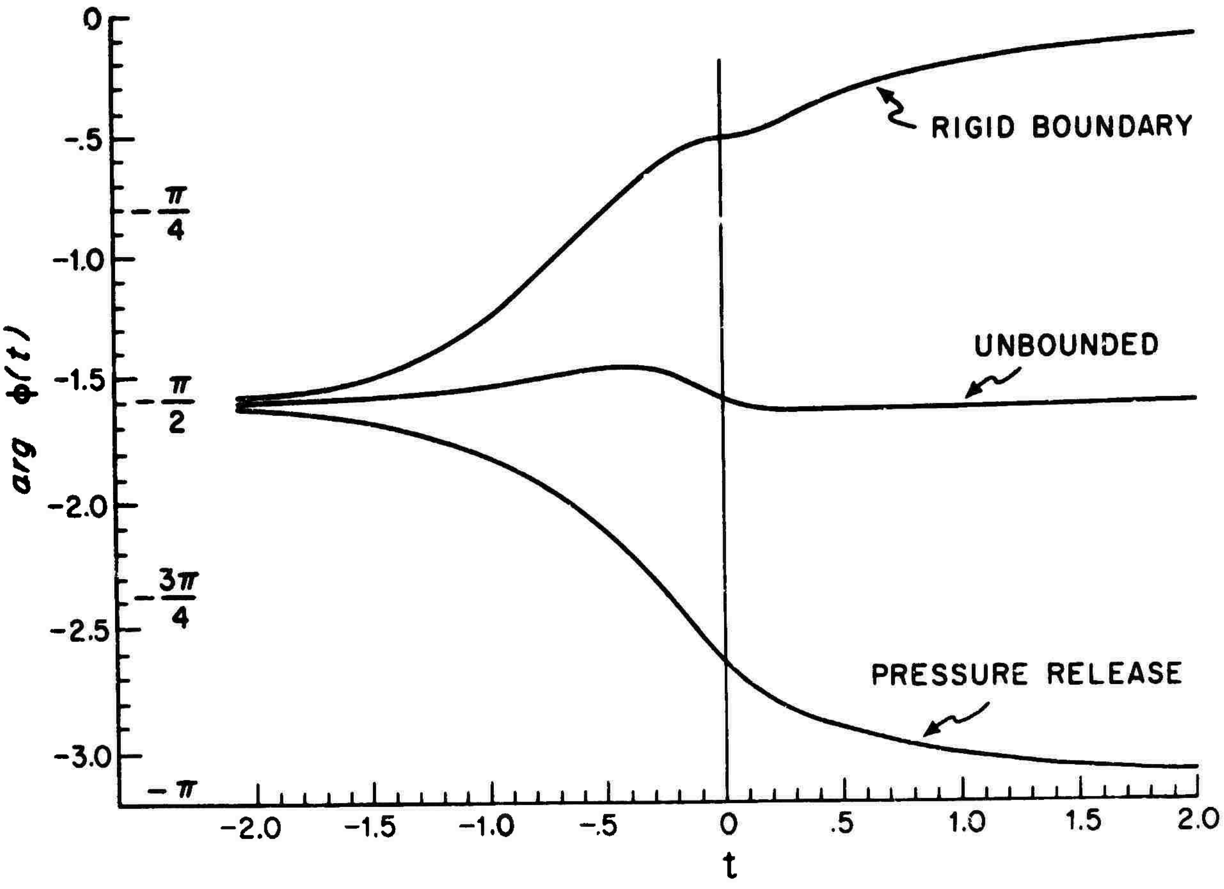
0
-.5
$-\frac{\pi}{4}$
-1.0
-1.5
$-\frac{\pi}{2}$
-2.0
$-\frac{3\pi}{4}$
-2.5
-3.0
$-\pi$
arg $\phi(t)$
RIGID BOUNDARY
UNBOUNDED
PRESSURE RELEASE
-2.0
-1.5
-1.0
-.5
0
.5
1.0
1.5
2.0
t

FIG. 4

An example of the results of such a calculation is reproduced in Fig. 4, taken from Ref. 11. In this figure the phase of the reflection coefficient is given for an $n(z)$ profile that increases monotonially in the direction away from a pressure release or a rigid boundary, or from an extremum of $n(z)$, the latter for example corresponding to the lower boundary of a surface channel. The results, as described in Ref. 11, can be written in terms of a parameter t, without specifying $n(z)$ or θ_0. When $n(z)$ and θ_0 are specified then t-values are directly related to θ_0. For nearly vertical rays, t is large and positive and the phase approaches the value for such boundaries bounding a homogeneous medium. For large negative t-values the rays have a vertex far below the boundary, and the phase approaches $-\pi/2$, the value appropriate for total reflection in an unbounded medium. With these continuous phases the problem of a discontinuous $R_c(\lambda)$ would disappear. However, this one step automatically requires a second step not considered in the past. It is well known [see, for example, Ref. 17] that when a reflection coefficient has a phase that is a continuous function of angle of incidence, then there will be displacements for the reflected ray or beam, and the amount of the displacement is related to the derivative of the phase with respect to angle of incidence. Therefore, to clear up the problem of discontinuous phases in the phase integral condition, also requires modification of the ray cycle range R_c. However, rather than being an additional difficulty, the introduction of displacements, or better, the recognition of the need to consider them, actual clears up other problems with the simpler ray mode analogy. For example, under some conditions there are problems in the determination of R_c from ordinary ray theory. An example is sketched in Fig. 5, where $c(z)$ has a surface layer. A ray turning just below the layer has a finite cycle

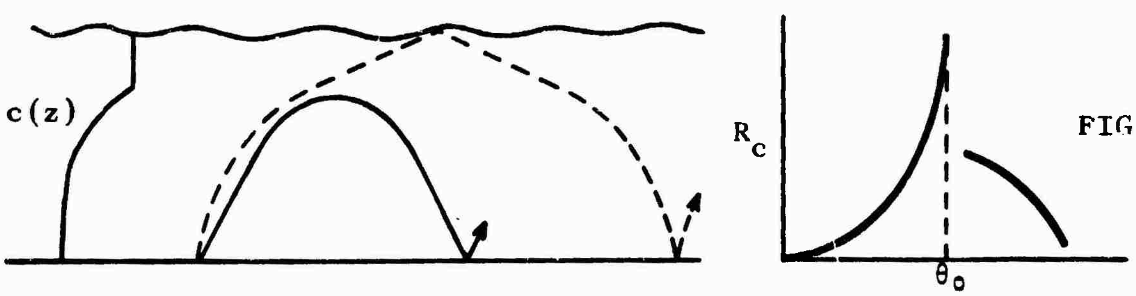

FIG. 5

range, but a ray slightly steeper enters the layer and has a large, in fact, infinite cycle distance. It turns out that while the continuous phase $\varphi(\theta_0)$ removes problems with the phase integral equation, the derivative of the phase introduces displacements that actually remove problems arising for the ordinary ray theory cycle range. At this point, we return to the original dispersion equation and develop these new points in a more systematic way.

2. RAY-MODE ANALOGY WITH DISPLACEMENTS

In Eq. 2, the dispersion equation was written in terms of an amplitude A and phase φ for the reflection coefficients when θ_0 is real. However, it was pointed out that Eq. 4 could not be satisfied for real θ_0. Now we consider θ_0 complex,

$$\theta_0 = \theta_r + i\,\theta_i$$

where θ_r is the real part and θ_i is the imaginary part, and we assume,

$$\theta_i \lll \theta_r \ .$$

Although we continue to use the functions $A(\theta_0)$ and $\varphi(\theta_0)$, they no longer represent amplitude and phase of the reflection coefficient when θ_0 is complex. We now make a Taylor series expansion for the various functions in Eq. 2, as follows

$$A(\theta_0) = A(\theta_r) + i\theta_i \left.\frac{dA}{d\theta_0}\right|_{\theta_r} \cdots\cdots \qquad \text{[Eq. 6]}$$

$$\varphi(\theta_0) = \varphi(\theta_r) + i\theta_i \cos\theta_r \left.\frac{d\varphi}{d\sin\theta_0}\right|_{\theta_r} \cdots\cdots \qquad \text{[Eq. 7]}$$

$$\int_{\text{cycle}} \sqrt{n^2 - \sin^2\theta_0}\, dz \approx \int_{\text{cycle}} \sqrt{n^2 - \sin^2\theta_r}\, dz - i\theta_i \cos\theta_r \int_{\text{cycle}} \frac{\sin\theta_r\, dz}{\sqrt{n^2 - \sin^2\theta_r}} \qquad \text{[Eq. 8]}$$

where the reason for writing the derivative in Eq. 7 with respect to $\sin\theta_0$, rather than θ_0, will become clear below. The second integral in Eq. 8 is readily identified as the ray theory cycle range integral. This is a special example where the derivative of phase, the first integral, gives a range displacement or cycle distance, the second integral.

(NOTE: Higher order derivatives of the integral in Eq. 8, where one limit is a zero of the radical and a function of θ_0, are not well-behaved. However, it is shown in some of the references cited on displacement phenomena, that with a correct phase change φ, then the sum

$$\varphi + \int_{\text{cycle}} \sqrt{n^2 - \sin^2\theta_0}\ dz$$

is well-behaved and, therefore, a Taylor series expansion can be made for the sum of these two phases. However, the terms correct to first order are as given in Eqs. 7 and 8, and for heuristic reasons φ and the phase integral have been treated separately in Eqs. 7 and 8.)

With relations, Eqs. 6 to 8 applied to Eq. 2 for complex θ_0, we obtain, to first order, the following equations, that replace Eqs. 3 and 4

$$k_0 \int_{\text{cycle}} \sqrt{n^2 - \sin^2\theta_r}\ dz + \varphi_1(\theta_r) + \varphi_2(\theta_r) = 2\pi N \qquad \text{[Eq. 9]}$$

$$A_1(\theta_r)A_2(\theta_r)e^{+\theta_i k_0 \cos\theta_r \left\{ \int_{\text{cycle}} \frac{\sin\theta_r \, dz}{\sqrt{n^2 - \sin^2\theta_r}} - \frac{1}{k_0}\frac{d\varphi_1}{d\sin\theta_0}\Big|_{\theta_r} - \frac{1}{k_0}\frac{d\varphi_2}{d\sin\theta_0}\Big|_{\theta_r}\right\}} = 1 \quad \text{[Eq. 10]}$$

where Eq. 9 involves only θ_r, and so determines θ_r to first order, while Eq. 10 then determines θ_i, also to first order. Equation 9, in this approximation, is again just the usual eigenvalue equation. However, it is the second equation, Eq. 10, that establishes the ray-mode analogy when the phenomenon of displacement is identified. In Refs. 9 to 15, it is shown that the range displacement, call it D, arising from a phase change for reflection that is a function of the angle of incidence, is given by the relation,

$$D = -\frac{1}{k_0}\frac{d\varphi}{d\sin\theta} \, . \quad \text{[Eq. 11]}$$

With this notation, Eq. 10 can be written in the form,

$$A_1(\theta_r)A_2(\theta_r) = e^{-\theta_i k_0 \cos\theta_r R_D} \quad \text{[Eq. 12]}$$

where R_D is the cycle distance with displacements,

$$R_D = R_C + D_1 + D_2 \quad \text{[Eq. 13]}$$

and D_1 and D_2 are displacements arising from the boundary, or ray vertex phenomena. Equation 12 has a very simple interpretation that is the ray-mode analogy. The range dependence for a given mode in shallow water can be written, approximately, [see Ref. 17, p.354] as follows,

$$e^{ik_0 r \sin\theta_r}$$

where r is the range. For $\theta_i \ll \theta_r$, we have,

$$e^{ik_0 r \sin\theta_r} \, e^{-\theta_i k_0 r \cos\theta_r} \, .$$

Comparison in this form, with Eq.12, then shows that θ_i is such that in one displaced cycle distance $r = R_D$, the decrease in amplitude is given by $A_1(\theta_r)A_2(\theta_r)$, that is to say, it is just the loss due to the single surface and bottom bounce in one cycle.

Therefore, the basis for the ray-mode analogy has been developed from the modal dispersion equation, and an essential ingredient has been the recognition of the displacement contribution. More important, as established in Refs. 9 to 15, the displacements are such as to make $R_D(\theta_r)$ a smooth continuous function. This is illustrated in Fig. 6, taken from Ref. 11, where the ray theory cycle range and the displaced cycle range, are plotted as a function of grazing angle $\delta = \frac{\pi}{2} - \theta_r$, for various kinds of boundaries bounding a medium with linear n^2 increasing with depth, with gradient $dn^2/dz^2 = 25 \times 10^{-8}$ ft^{-1}, and source-receiver depth of 1250 ft, for $\lambda = 100$ ft.

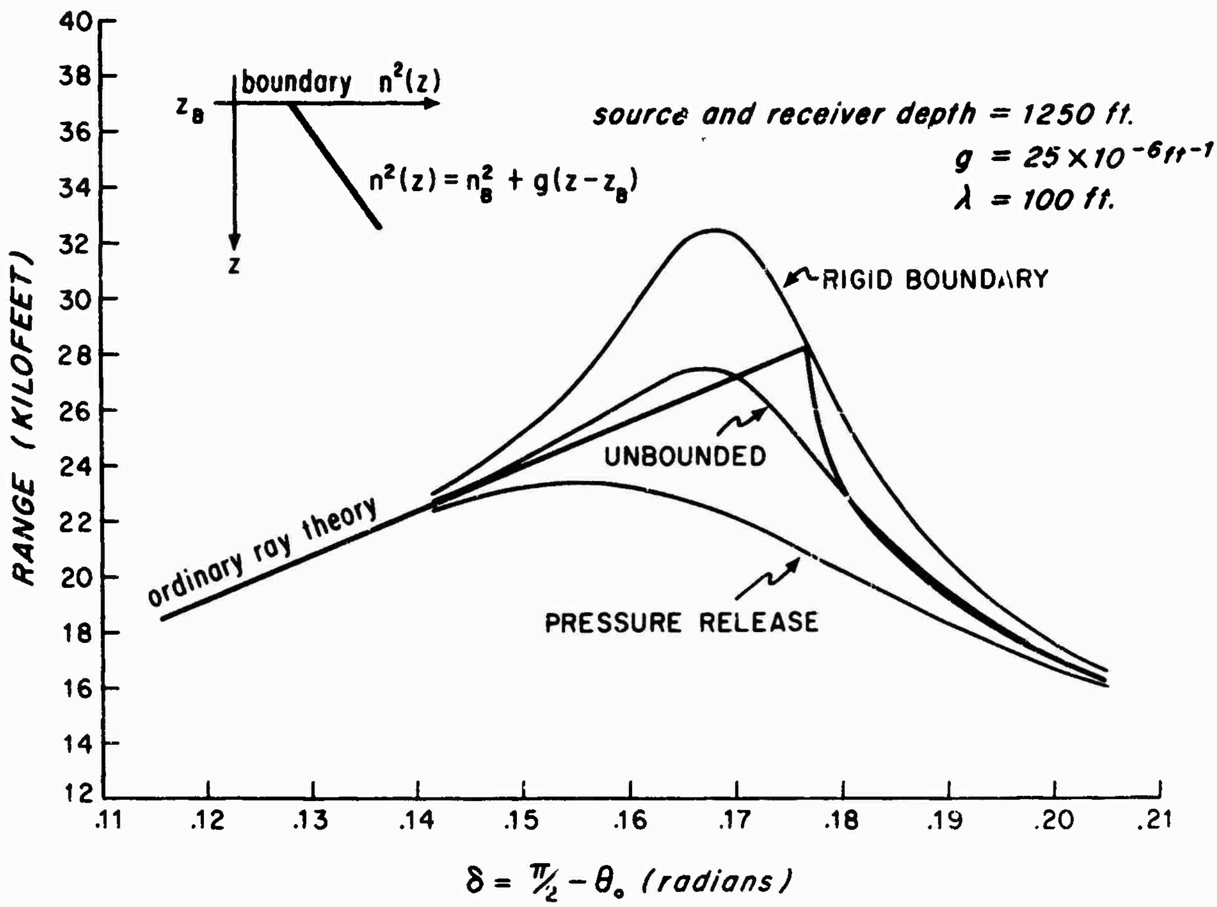
RANGE (KILOFEET)
40
38
36
34
32
30
28
26
24
22
20
18
16
14
12
.11
.12
.13
.14
.15
.16
.17
.18
.19
.20
.21
$\delta = \pi/2 - \theta_0$ (radians)
boundary $n^2(z)$
z_B
z
$n^2(z) = n_B^2 + g(z - z_B)$
source and receiver depth = 1250 ft.
$g = 25 \times 10^{-6} ft^{-1}$
$\lambda = 100$ ft.
RIGID BOUNDARY
UNBOUNDED
PRESSURE RELEASE
ordinary ray theory

FIG. 6

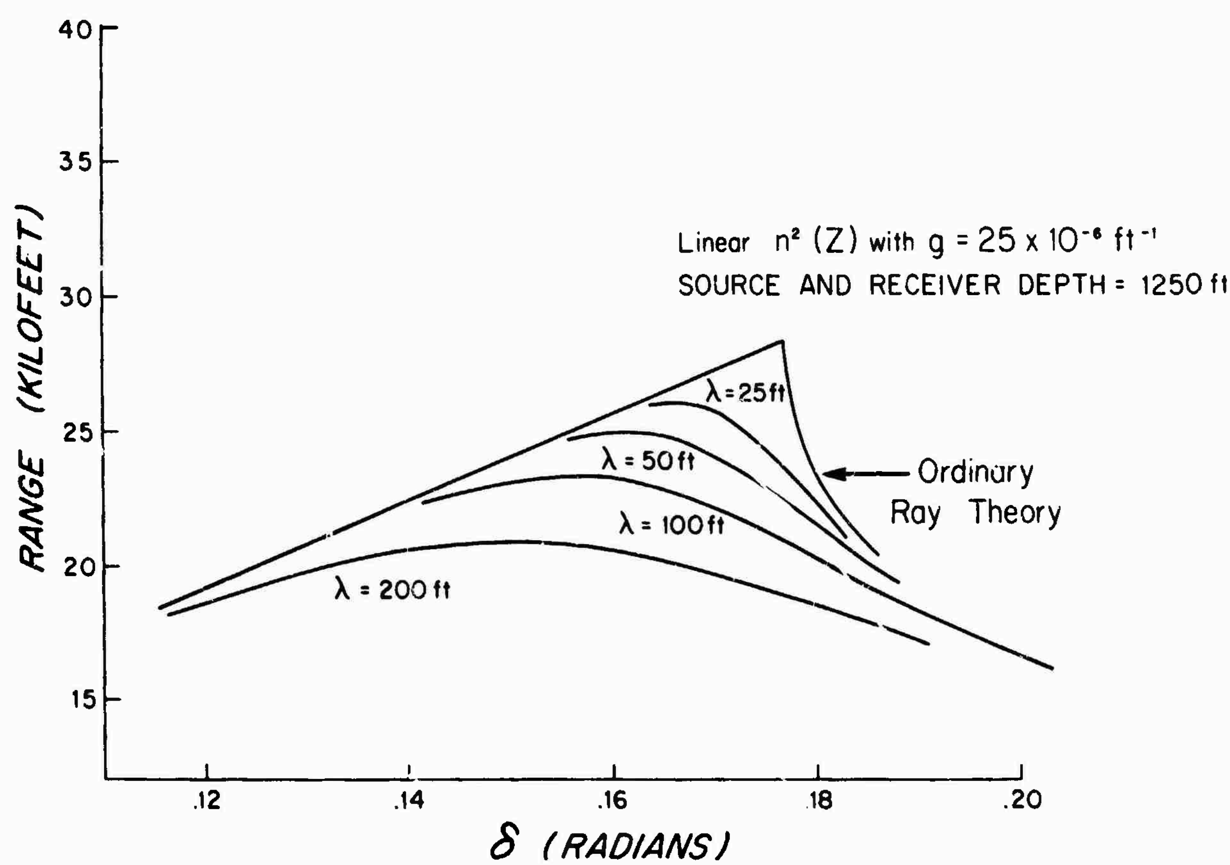
RANGE (KILOFEET)
40
35
30
25
20
15
.12
.14
.16
.18
.20
δ (RADIANS)
Linear n^2 (Z) with $g = 25 \times 10^{-6}$ ft $^{-1}$
SOURCE AND RECEIVER DEPTH = 1250 ft
λ = 25 ft
λ = 50 ft
λ = 100 ft
λ = 200 ft
Ordinary
Ray Theory

FIG. 7

It can be seen that, depending on the kind of boundary, and the angle, the displacements can be positive or negative. The displaced cycle distance is now wavelength dependent since the displacements are wavelength dependent. An example of the wavelength dependence is given, from Ref. 11, in Fig. 7.

In Ref 5, the simplest version of the ray-mode analogy is developed from the eigenvalue problem, but with such drastic approximations that no term like the displacement term arises in the final result, only R_c.

The approximations fail for the most pertinent, near grazing rays. With the displacement term, we can apply the analogy over the full range of the parameters including boundary grazing rays. Along these lines, we note that in Ref. 5, it is shown that a number of modes have approximately equal attenuations in a problem with downward refraction for which rays turn near a pressure release surface. On the basis of the effect of displacements for the pressure release problem as illustrated in Fig. 7, we might anticipate that a number of modes may have similar attenuation since cycle range curves are flattened by the displacements in the region of the maximum range. On the other hand, for a rigid boundary, as illustrated in Fig. 6, displacements are toward longer range, the peak is narrow and sharp.

In summary, the recognition of the significance of displacement phenomena in the proper development of the ray-mode analogy, and recent work on the nature of the displacements [Refs. 9 to 15], have put the analogy on a firmer foundation and have removed some of the pathological aspects of the simpler model.

ACKNOWLEDGEMENTS

The author expresses his appreciation to A. Wasiljeff, O.V. Olesen, and O. Hastrup for many helpful discussions.

REFERENCES

1 WESTON, D.E. Propagation of sound in shallow water. Jnl Brit. I.R.E. 26, 1963: 329-337.

2 KIBBLEWHITE, A.C., and DENHAM, R.N. Experiment on sound propagation in shallow water with velocity structure. Jnl Acoustical Society America, 44, 1968: 104-112.

3. WILLE, P., THIELE, R., and SCHUNK, E. Shallow-water sound attenuation in a standard area. Jnl Acoustical Society America, 54, 1973: 1708-1720.

4. MURPHY, E. and OLESEN, O.V. Broadband sound propagation trials in shallow water near the Island of Elba, SACLANTCEN SM-39. La Spezia, Italy, SACLANT ASW Research Centre, 1974

5. KRUPIN, V.D. A special effect in a waveguide having a negative sound velocity gradient. Soviet Physics-Acoustics 18, 1973: 460-469.

6. KORNHAUSER, E.T. and RANEY, W.P. Attenuation in shallow-water propagation due to an absorbing bottom. Jnl Acoustical Society America, 27, 1955: 689-692.

7. BUCKER, H.P. Normal-mode sound propagation in shallow water. Jnl Acoustical Society America, 36, 1964: 251-258.

8. WESTON, D.E. Rays, modes, interference and the effect of shear flow in underwater acoustics. Jnl Sound Vib., 9 (1), 1969: 80-89.

9. MURPHY, E.L. Modified ray theory for the two-turning-point problem. Jnl Acoustical Society America, 47, 1970: 899-908.

10. MURPHY, E.L. Ray representation of diffraction effects in the split-beam sound field. Jnl Acoustical Society America, 43, 1968: 610-618.

11. MURPHY, E.L. and DAVIS, J.A. Modified ray theory for bounded media. Jnl Acoustical Society America (Scheduled for publication, December 1974).

12. DAVIS, J.A. and MURPHY, E.L. Modified ray theory in the presence of a boundary. Woods Hole Oceanographic Institution, Report No. 71-48, July 1971.

13. MURPHY, E.L., DAVIS, J.A. and DOUTT, J.A. Application of modified ray theory to underwater sound propagation. Woods Hole Oceanographic Institution. Report No. 71-49, July 1971.

14. DAVIS, J.A. Propagation loss as predicted by modified ray theory. Woods Hole Oceanographic Institution. Report No. 72-88, December 1972.

15. DAVIS, J.A. Behaviour of modified ray theory. Woods Hole Oceanographic Instituion. Report No. 72-89, December 1972.

16. BREKHOVSKIKH, L.M. The dispersion equation for normal waves in laminar media. Paper delivered at Conference of the Commission of Acoustic of the Acad. Sci. USSR, February 1955.

17. BREKHOVSKIKH, L.M. Waves in Layered Media. Academic Press Inc., New York, 1960.

DISCUSSION

Dr Wille asked if this theory held for time dispersion relations too. Dr Murphy agreed that it could and said that in this paper he had considered only cw and spatial displacements arising from phase changes on reflection that are continuous functions of angle of incidence. It is well-known that when the phase change is also a function of frequency, as it was in the work he presented, there can be time displacements for transient signals, with time delays related to the derivative of the phase with respect to frequency. However, there is a problem with combined space and time displacement representations. In the cw analysis, the field of a point source is represented as an integral or angular "spectrum" in the variable θ. The displacement representation arises from application of the stationary phase method to approximate the integral. For a transient one makes a second spectral analysis, but now as an integral over frequency. Again, application of the stationary phase method, but now on the frequency variable, leads to arrival time displacements. The problem with combined space and time displacements is that if you apply the stationary phase method first to the θ-integration, the remaining frequency integral may no longer be in a form of which the stationary phase procedure can also be applied to the frequency integration, and vice versa. What representation is appropriate will depend on the nature of the transient, for example, on its spectrum.

ON THE DIRECT MEASUREMENT OF THE ACOUSTIC IMPEDANCE OF THE SEA BOTTOM

by

E. Schunk
Forschungsanstalt d. BW für Wasserschall
und Geophysik, Kiel, Germany

ABSTRACT

The acoustic behaviour of the sea-bottom is characterized by its impedance which normally has to be computed from the physical properties of the particular sediment. The disadvantage of this method is that each single parameter such as the sound velocities and the elastic constants of the medium must be obtained from laboratory measurements on bottom samples or in situ measurement, respectively. Furthermore. several of the necessary parameters, e.g. the shear-wave velocity and the attenuation, are rather difficult to determine and finally all the information concerning bottom properties is limited to the upper few metres, depending on the sampling or measuring devices used. These difficulties can be avoided by measuring the acoustic bottom impedance direct. A simple method for realization is discussed and a preliminary experimental set-up is described. Results of the first test runs are presented and will be compared with impedance values computed from core-sample data in the usual way.

INTRODUCTION

The acoustic behaviour of the sea-bottom is characterized by its impedance or its reflection coefficient, respectively, which has to be either determined experimentally in expensive sea trials or computed from the physical properties of the particular sediment. The first method of measuring the reflection coefficient is applicable only to greater water depth where it is possible to separate the direct and bottom-reflected signal — a technique which has been widely used, e.g. by SACLANTCEN, during the last ten years — whereas the method of computing the reflection from the sediment properties has the disadvantage that each single parameter such as the sound velocities and the elastic constants of the medium must be obtained from laboratory measurements on bottom samples or in situ measurements, e.g. the shear-wave velocity and the attenuation, are rather difficult to determine and finally all the information concerning bottom properties is limited to the upper few metres, depending on the sampling or measuring devices used.

Additional difficulties may be introduced by the type of bottom, e.g. as in our standard test area in the Central North Sea where the upper layer mostly consists of sand requiring special equipment like vibrocorers in order to get bottom samples at all. According to measurements carried out by Schirmer [Ref. 1], the values of the compressional wave velocity determined from such probes may differ considerably from in situ values. Figure 1 illustrates two profiles of compressional wave velocity in sand sediments. The upper curve shows measurements on quasi-undisturbed sediment taken by a box-grab sampler with a cross-section of 20 x 2 cm but a length of only 20 cm whereas the solid curve represents measurements on a sample taken by means of a vibrocorer of 10 x 10 cm cross-section. The reduction in sound velocity is probably caused by a considerable loss of the water content and by changes of the internal structure of the sediment due to the strong vibrations of the corer. Although the values of the box-grab sample seem to be more reliable, especially as a better fit with model computations of propagation loss can be achieved, they are insufficient for describing the complete behaviour of the bottom because of the limited sample length.

In order to avoid these difficulties in the determination of the sound velocity in sand sediments the exact knowledge of which would be the most important condition for the computation of the reflection coefficient, we tried to apply a technique of the direct measurement of the acoustic impedance proposed by Mechel [Ref. 2], at the 6th International Congress on Acoustics in 1968 for airborne sound to underwater conditions.

1. BASIC THEORY

Starting from the definition of the acoustic admittance and introducing the force-equation Mechel found a simple general method for measuring acoustic impedances. A sound field of any arbitrary geometry and the time-dependence $e^{j\omega t}$ may be described by

$$p(\bar{r}, t) = P(r)\, e^{j\varphi(\bar{r})} \cdot e^{j\omega t}$$

with the real amplitude $P(\bar{r})$ and the phase-factor $e^{j\varphi(r)}$ both depending on the vectorial space coordinate $\bar{r}$. The linearized force-equation

$$\rho \cdot \frac{\partial \bar{v}}{\partial t} = -\text{grad } p$$

yields for the normal component v_n of the particle velocity

$$v_n = \frac{j}{k \cdot z} \cdot \frac{\partial p}{\partial n}$$

with the wave number $k = w/c$ and the characteristic impedance $Z = \rho c$. The complex acoustic admittance G at a point on the interface S

follows from

$$G \equiv \left.\frac{v_n}{p}\right|_S = \frac{j}{kZ}\,\frac{\partial p/\partial n}{p}$$

$$= \frac{j}{kZ}\,\frac{\partial}{\partial n}\,\ln\left[P(\bar{r})e^{j\varphi(\bar{r})}\right]\Big|_S$$

$$= \frac{1}{kZ}\left[-\frac{\partial}{\partial n}\,\varphi(\bar{r}) + j\,\frac{\partial}{\partial n}\,\ln P(\bar{r})\right]\Big|_S .$$

This result means that the real part of the acoustic admittance can be determined from the slope of the phase of the sound pressure vs distance curve, the imaginary part is given by the change of the logarithm of the amplitude.

2. CAPABILITY OF THE METHOD

This technique permits the determination of the bottom impedance for oblique incidence of the sound wave as well as of impedance distributions for inhomogeneous interfaces as it yields local impedances. The accuracy of this method is characterized by the fact that it is a differential technique, that means that the accuracy will become optimal where phase and amplitude show the strongest changes in front of an interface, or, with respect to underwater application, where the bottom impedance values are low and the impedances of water and sediment are matched to each other, respectively.

3. DESCRIPTION OF EQUIPMENT

For the first field tests an experimental set-up was chosen as illustrated in Fig. 2. An electro-dynamic underwater transducer (J 11) was used as sound source. The grazing angle of the incident sound could be varied between 14° and 22°. The component of the sound pressure normal to the sea-bottom has been received by a movable, motor-driven hydrophone (LC 10), preamplified and recorded aboard the ship on magnetic tape. Figure 3 shows the hydrophone, its drive-shaft and the watertight case for the preamplifier and the motor, the operation-status of which was controlled by magnetic relays. The total measuring interval was 44.5 cm.

4. ANALYSIS AND RESULTS

The tape-recorded signals were played back, measuring the phase by means of a phase-meter relative to the generator signal recorded as well and registering it vs bottom distance. Similarly, the pressure amplitude was registered on a logarithmic level recorder. Figures 4a to 4c illustrate the measured amplitude and corresponding phase distribution in front of the water/bottom interface as a function of distance from the bottom for the frequencies of 2 kHz, 5 kHz and 10 kHz for a grazing angle of 22°. Figures 5a to 5c show measurements at the same frequencies for a grazing angle of 14° for the incident sound. Here the original registrations have been depicted. For both cases (Figs. 4 and 5) the angles of incidence have been evaluated from the SWR in front of the bottom and found to agree well with the values chosen. The gradients of these phase- and amplitude curves taken at the bottom yield the real and imaginary part, respectively, of the admittance according to theory. In all cases the complex reflection coefficient has been computed from the admittance and compared to values determined from the sound velocity and the density obtained from a bottom sample taken in the same area (c_1 = 1990 m/s; ρ_1 = 2.15 10^3 kg/m^3; - boulder clay) [see Ref. 3]. Attenuation factors of 1 dB/λ and 2 dB/λ have been used. The results have been summarized in Table 1, giving the absolute value (module) and the phase angle of all complex reflection coefficients.

TABLE 1

		Reflection Coefficient				
Grazing Angle		from impedance			from sample	
		2 kHz	5 kHz	10 kHz	1 dB/λ	2 dB/λ
22°	Absolute Value	0.81	0.95	0.57	0.97	0.94
	Phase Angle	-84°	-25°	141°	-69°	-69°
14°	Absolute Value	0.60	0.24	0.47	0.97	0.95
	Phase Angle	-69°	-88°	-32°	-100°	-100°

DISCUSSION AND CONCLUSIONS

The reflection coefficients computed from the measured impedances differ in most cases from those evaluated from the core-sample data. Especially for the grazing angle of 14°, the absolute values of the former are much too small. For the time being we have to renounce any interpretation of that effect as several reasons can easily be found to be responsible for that difference. A few of them may be mentioned here.

If you take into account that the impedance values have been gained from three different launchings of the equipment and that the bottom properties of the test area varied rather fast within short distances, reaching from sand to clay and mud or boulder clay, the probability of the bottom impedance being different for successive stations and for the position where the core-sample was taken is rather high. Furthermore, bottom roughness on which there was no information available may introduce additional errors, e.g. by pretending lower reflection coefficients for convex curvatures and higher ones for concave curvatures.

In spite of the somewhat disappointing results for the reflection coefficients, the text-book-like looking measured curves of phase and amplitude as shown in Figs. 4 and 5 are rather encouraging. Nevertheless, before a final decision with respect to the applicability of this new method can be taken, controlled measurements at a bottom of well-known properties (e.g. tank experiment) will have to be carried out. In addition, it is intended to investigate how far the information contained in those parts of the phase- and amplitude curves farther away from the bottom can be included in the determination of the bottom impedance.

REFERENCES

1. F. Schirmer in "Shallow-water Sound Attenuation in a Standard Area" by P. Wille, R. Thiele and E. Schunk, Jnl Acoustical Society America, 54, 1973: 1708-1726.

2. F. Mechel, "New Method of Impedance Measurement", 6th International Congress on Acoustics (1968), H-5-16.

3. F. Schirmer, Institut für Geophysik, Universitat Hamburg, private communication.

DISCUSSION

In response to several questions, Dr Schunk explained that this approach for obtaining the reflection coefficient through the impedance of the bottom was especially developed for shallow waters and should be accepted as a competing method to the various methods of direct measurement. He also pointed out that in measuring local impedance the curvature of the bottom could influence the result; how big this effect is could only be shown by tank experiments.

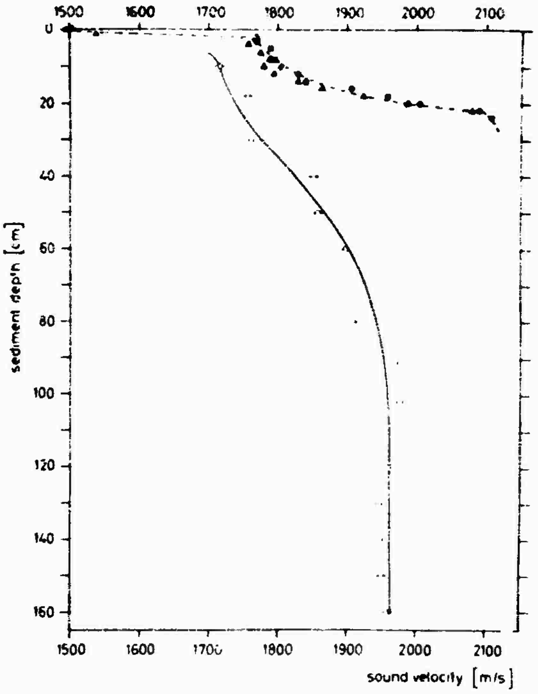

FIG. 1

PROFILES OF COMPRESSIONAL WAVE VELOCITY IN SAND SEDIMENT

(.......... box-grab samples, 0-------0 vibrocorer sample)

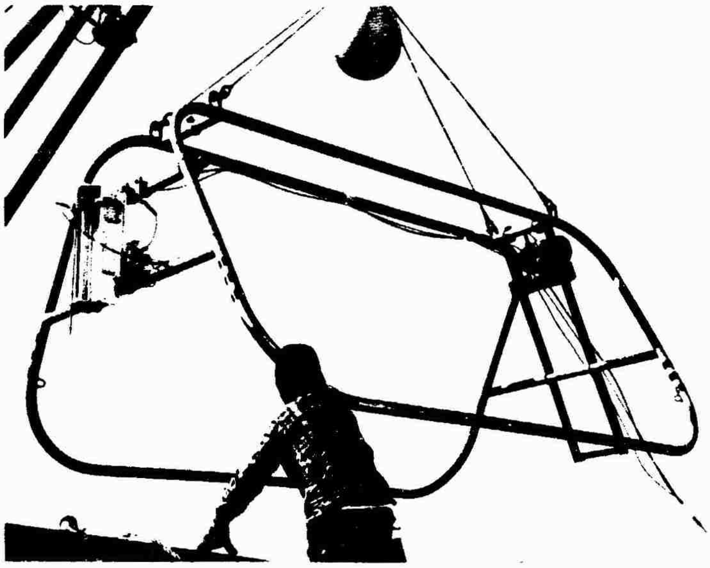

FIG. 2

TOTAL VIEW OF EQUIPMENT

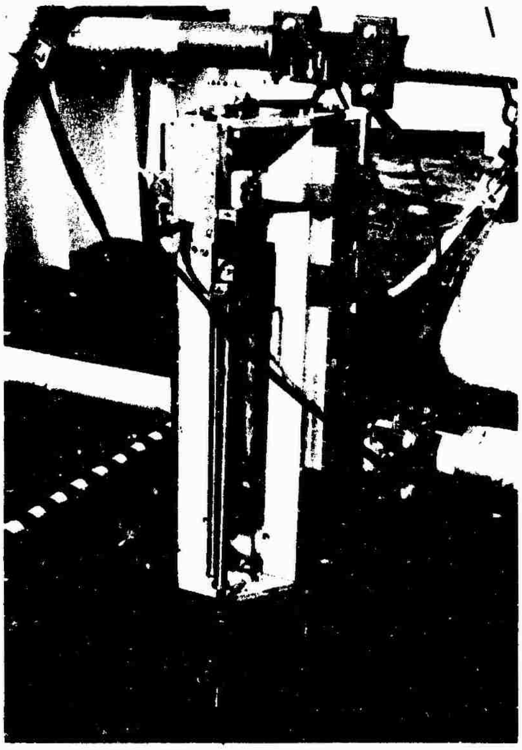

FIG. 3

RECEIVING PART OF THE EQUIPMENT

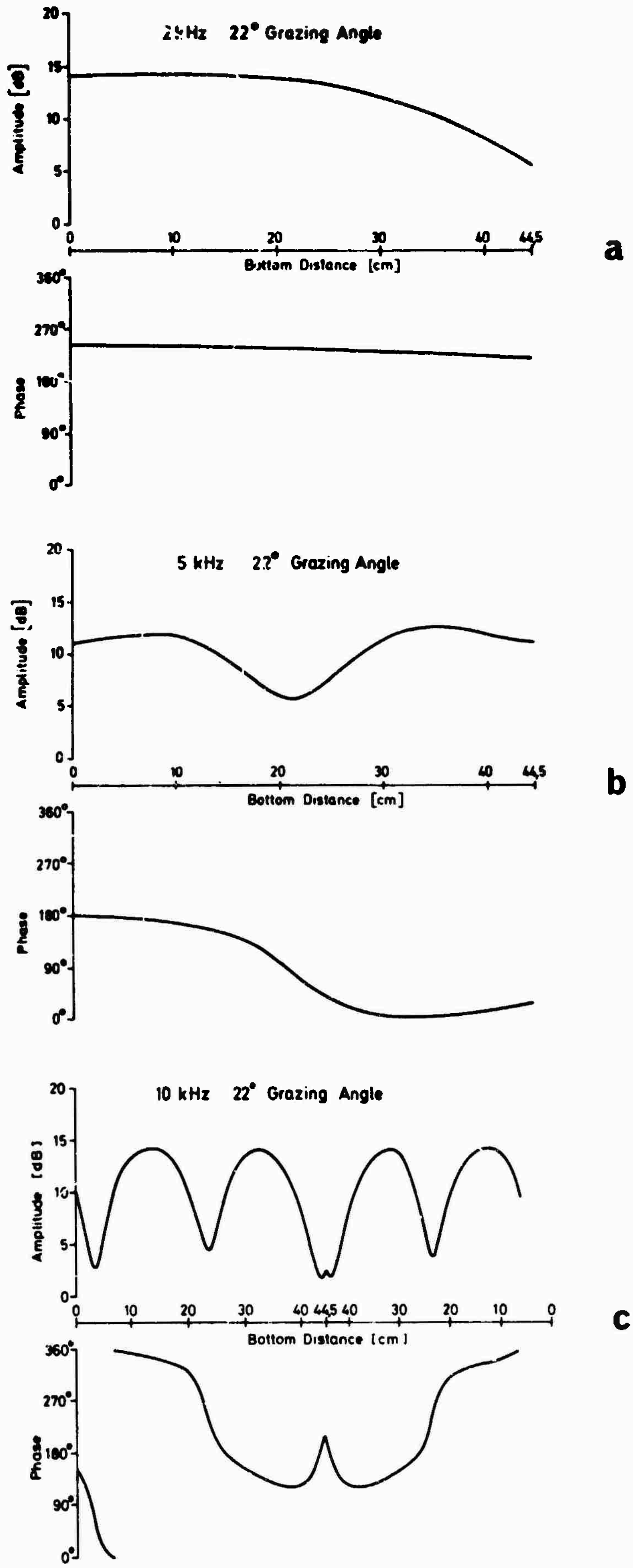

FIG. 4 AMPLITUDE AND PHASE OF RECEIVED SIGNALS vs BOTTOM DISTANCE FOR A GRAZING ANGLE OF 22°

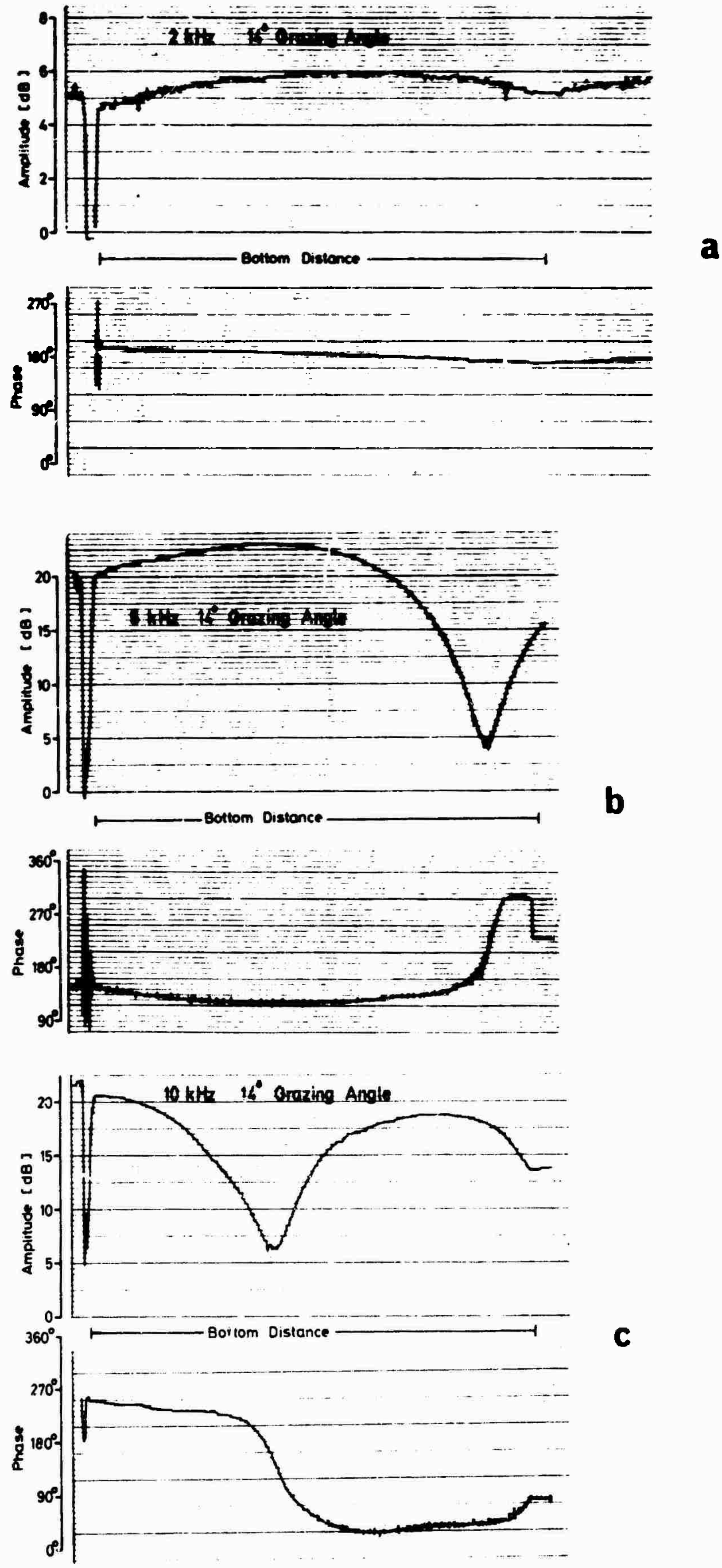

FIG. 5 AMPLITUDE AND PHASE OF RECEIVED SIGNALS vs BOTTOM DISTANCE FOR A GRAZING ANGLE OF 14°

THE PHYSICAL CHARACTERISTICS OF THE SEA FLOOR THAT AFFECT SHALLOW WATER PROPAGATION

by

T. Akal
SACLANT ASW Research Centre
La Spezia, Italy

ABSTRACT

In shallow water, due to the multiple reflected propagation paths, acoustic propagation generally depends upon the characteristics of the boundaries. Physical properties of the sediments and roughness of the sea floor surface are the two main parameters which control the reflectivity and reverberation characteristics of the bottom. In the areas where acoustic experiments were conducted, these physical characteristics of the sea floor have been studied with the data acquisition and analysis techniques developed at the Centre. Here, these techniques are briefly discussed and some of the acoustic parameters are compared with the sea floor parameters.

INTRODUCTION

The propagation of sound in shallow water depends upon many environmental variables of the sea surface, water medium and bottom in shallow water areas. Due to the multiple reflected propagation paths, acoustic propagation characteristics are very sensitive to the boundary conditions.

The velocity structure of the water column controls the influence of the sea surface or the bottom on propagation. In summer, under the downward-refracting conditions the propagation is mainly influenced by the sea-floor characteristics; whereas, in winter, the influence of the sea-floor is reduced due to the upward-refracting conditions.

In contrast to the deep sea-floor, the continental shelves mostly consist of different types of sediments with considerable spatial variation, and wide spectrum of bottom roughness. Figure 1 shows an example of a bathymetric profile, where, within a short distance, different types of sediment and bottom roughness exist.

Bottom composition and bottom roughness are the two main parameters, which control the reflectivity and scattering characteristics of the sea-floor. As the capability of computer facilities has increased, the importance of including these parameters in the new generation of prediction models is being increasingly recognized. Figure 2 shows the basic input parameters to acoustic models.

1. BOTTOM COMPOSITION

The amount of sound energy reflected from the bottom depends upon the physical properties of the sediments. It is well known that the reflectivity of the bottom can be expressed as a function of the compressional and shear wave velocities, the attenuation of these waves and the density.

Most of our knowledge of the physical properties of the sediments has been acquired through core sampling. The previous studies have shown that porosity of the marine sediments (which can be measured very easily) stands out as the most important parameter, causing variations in compressional sound velocity and density. The statistical relationship between these properties is shown in Fig. 3 [Ref. 1]. High porosity material is a poor reflector and reflectivity increases with decreasing porosity.

Since the attenuation of compressional and shear wave velocities are very difficult parameters to measure, these quantities can be deduced from either the results obtained by Hamilton [Ref. 2] or the values obtained from laboratory and field measurements of natural and artificial sediments. Figure 4 summarizes the measured attenuation values reported by several investigators [Ref. 3]. It indicates the order of magnitude of attenuation to be expected for saturated sediments. At all frequencies the attenuation is higher in sand and muddy sand, compared to silts and clays. It also shows that the attenuation is approximately linearly dependent on the frequency, thus sediment acoustic attenuation can be expressed as dB/λ.

Displays of relative sound speed and relative density vs porosity also give a general idea of the acoustical characteristics of an area. Figure 5 summarized the bottom composition of the two acoustic trial zones, that are situated north and southeast of the Island of Elba [Ref. 4]. The northern area consists of much more low porosity material (highly reflective sea-floor, higher attenuation within the sediment) compared to the southeastern area. Figure 6 compares the spatial variation of bottom material in these areas, where as the northern area mainly consists of high velocity and high density sediments, with very thin low velocity material in the upper part. (This would only effect very high frequencies). The southeastern area consists of low velocity and low density material with a thin high velocity later at a depth of approximately 3 m.

Figure 7 compares the results of transmission loss measurements over the areas mentioned above in winter and summer conditions, for 50 m source and receiver, and in 1/3 octave filter bands for 0.2, 0.8 and 3.2 kHz centre frequencies. In winter under upward-refracting conditions, the transmission loss, does not show any pronounced dependence for these different bottom conditions. Whereas in summer, under downward refracting conditions, the transmission loss shows a very significant dependence on the differences in the sea floor [Ref. 5]

2. BOTTOM ROUGHNESS

The acoustic properties of sediments have been under study by the scientific community for several years and this has been the subject of a large number of papers. The study of bottom roughness has been neglected mainly due to the difficulties of making quantitative measurements of bottom roughness.

The sea floor contains a wide spectrum of roughness, from features of the order of tens to hundreds of kilometres to those of the order of centimetres. It is well known that scattering depends on the dimension of bottom irregularities, and our main interest is in the scale of roughness that is comparable to the acoustic wave lengths. It requires different techniques to resolve this wide range of roughness.

The spectrum range of the sea floor roughness and resolution capabilities of the measurement techniques are shown in Fig. 8. Figure 9 illustrates the characteristics of the equipment used to study the roughness of the sea-floor. The system consists of a standard 12 kHz echo sounder (66° beamwidth), a 3.5 kHz transducer with 23° beamwidth, a 50 kHz narrow-beam (6°) echo sounder, towed close to the bottom (10 to 15 m) and underwater stereo cameras. The upper part of Fig. 10 shows an example of a recording obtained from an area, which illustrates the characteristic "hyperbola" structures found over rough bottom. The same figure also compares the bottom profiles obtained with three different pieces of equipment over the same track. The spectrum of the 50 kHz system profile is also displayed in the same figure.

Whereas the echo sounder provides information along individual tracks, the stereo cameras can provide a mosaic over small areas, and photogrammetric techniques can be subsequently employed to provide very fine-scale contour charts of the sea floor. We have developed a very simple method of digitizing these contours to obtain, through the computer, two-dimensional power spectra and autocorrelation function of the surfaces. Examples of this are shown in Fig. 11. The technique has the advantage of revealing the directionality of the roughness. This technique can be applied to any kind of contoured data to obtain two-dimensional statistical properties of a surface.

CONCLUSIONS

1. Physical properties of the sediments is the main parameter that affect the shallow water propagation in summer condition.
2. There is a need to be able to deduce the compressional and shear wave attenuation and shear wave velocity.
3. Methods developed to obtain one and two dimensional sea floor roughness spectra provide the quantitative description of the bottom roughness and use of these data in acoustic models.
4. Studies on sea floor roughness may give the possibility of predicting the interested dimension of bottom irregularities from simply measurable parameters, i.e. normal echo soundings, sediment type, etc.

REFERENCES

1. AKAL, T. The relationship between the physical properties of underwater sediments that affect bottom reflection. Marine Geology, 1972.

2. HAMILTON, E.L. Compressional-wave attenuation in marine sediments. Geophysics, 37 (4), 1972.

3. ANDERSON, A.L. A caustics of gas-bearing sediments ARL. The University of Texas at Austin, May 1974.

4. AKAL, T. Acoustic characteristics of the sea floor: experimental techniques and some examples from the Mediterranean Sea. Physics of Sound in Marine Sediments, edited by L. Hampton, Plenum Publishing Corporation.

5. MURPHY, E. and OLESEN, O.V. Broadband sound propagation trials in shallow water near the Island of Elba, SACLANTCEN SM-39. La Spezia, Italy, SACLANT ASW Research Centre, 1974.

DISCUSSION

In answer to a question by Dr Wille on how the stereophotographs were evaluated, Mr Akal explained that this work had been done by the Italian Istituto Geografico Militare in Florence, applying aerial surveys techniques to obtain a quantitative evaluation of the shape of the sea floor. Dr Wille asked what density of photographs is required to give a statistical description of the sea floor in an area. Mr Akal explained that, of the many photographs taken, only fifteen had been analysed so far. It was therefore too early to say, although obviously this would differ between areas in which the bottom features changed within tens of metres and those in which they remained constant for many kilometres.

Major Ross asked why most of the statistical relationships between physical properties of sediment used porosity as an index parameter and what was the relation between porosity and grain size. Mr Akal explained that the porosity of marine sediments stands out as the most important parameter causing variations in acoustic characteristics of the sediments. The amount of pore space in sediments results from such interrelated factors as the size, shape and minerology of the solid grains, which usually result in a general decrease in porosity with increasing grain size. Mr Hastrup pointed out that it is also because it is easier to measure porosity than grain size.

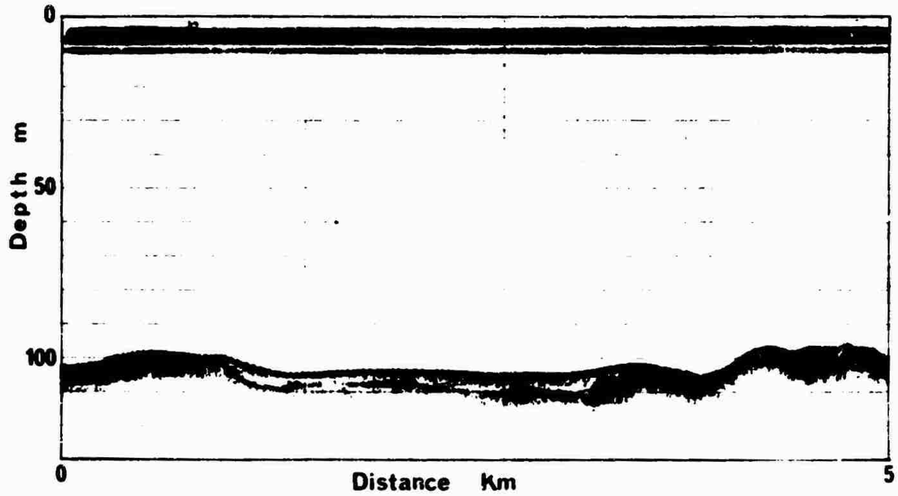

FIG. 1

BOTTOM COMPOSITION

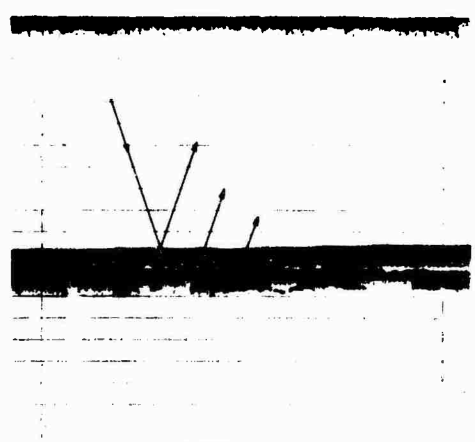

Input parameter to acoustic models

PHYSICAL PROPERTIES OF SEDIMENTS

Compressional and shear wave velocity

Density

Attenuation of compressional and shear waves

FIG. 2

BOTTOM ROUGHNESS

STATISTICAL PROPERTIES OF SEA FLOOR SURFACE

One dimensional and/or two dimensional spectra of bottom roughness, Autocorrelation fonction

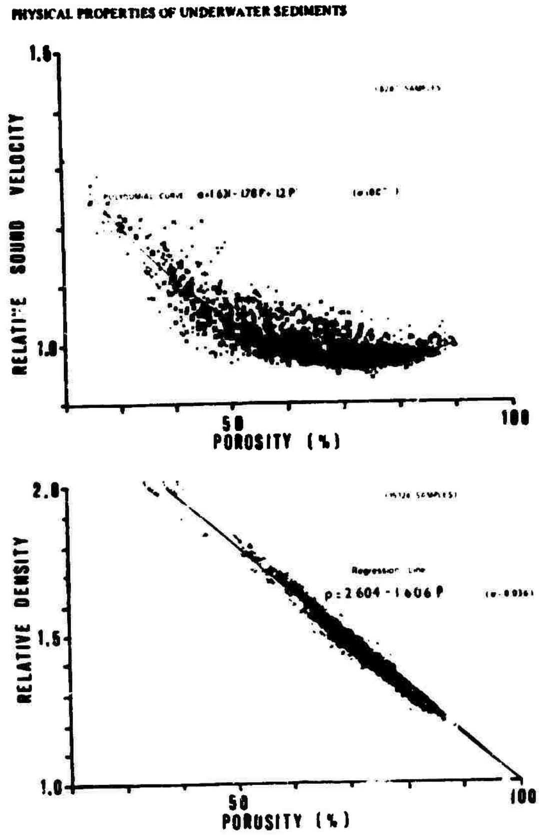

FIG 3

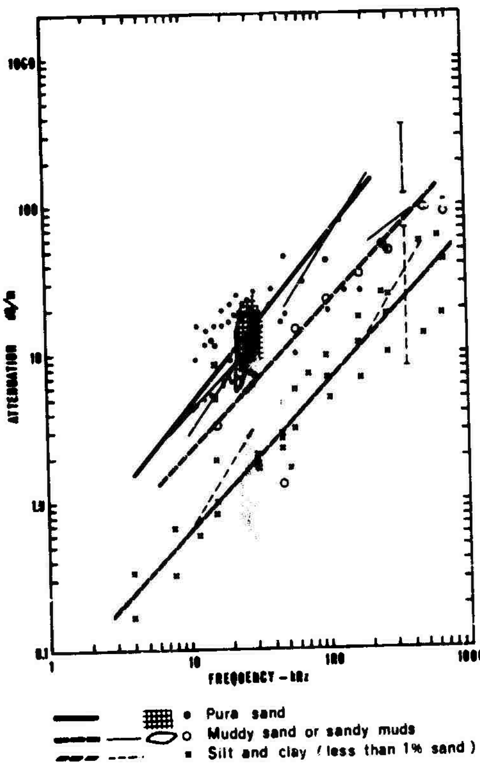

FIG. 4

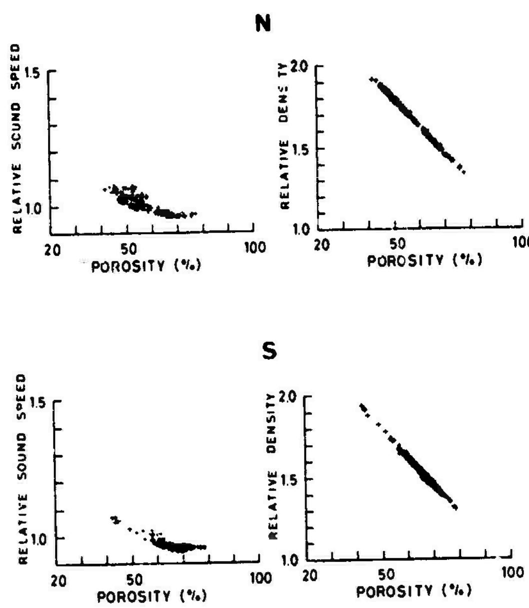

FIG. 5

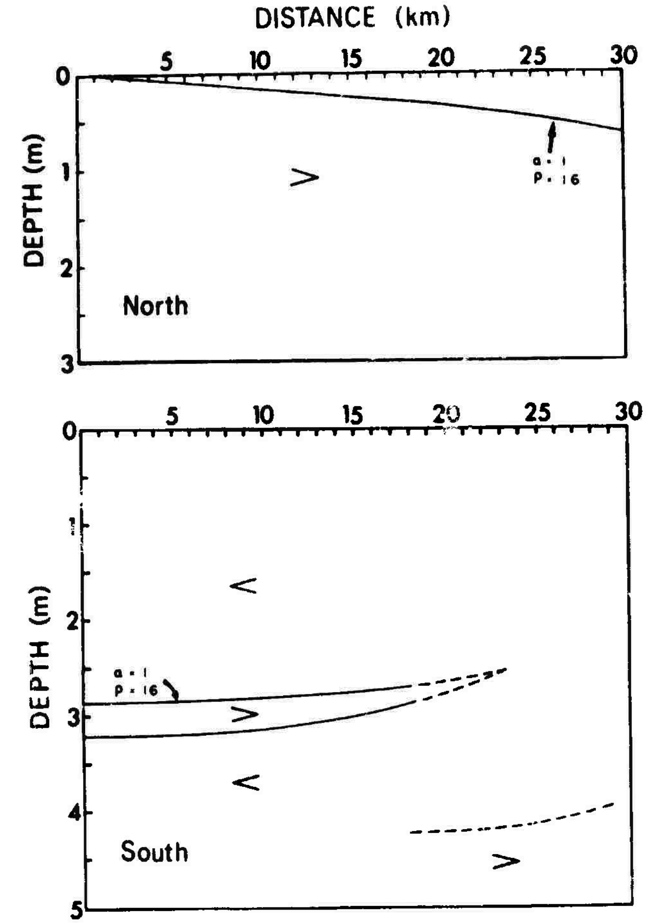
DISTANCE (km)
5 10 15 20 25 30
DEPTH (m)
0 1 2 3
North
0 1 2 3 4 5
South

FIG. 6

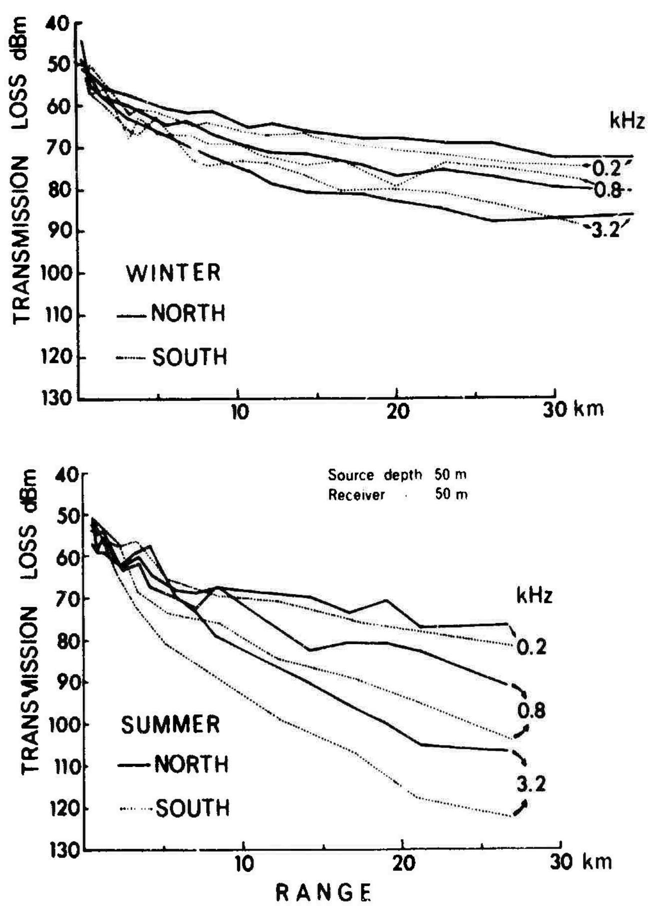
TRANSMISSION LOSS dBm
40 50 60 70 80 90 100 110 120 130
kHz
0.2
0.8
3.2
WINTER
NORTH
SOUTH
10 20 30 km
Source depth 50 m
Receiver 50 m
SUMMER
NORTH
SOUTH
RANGE

FIG. 7

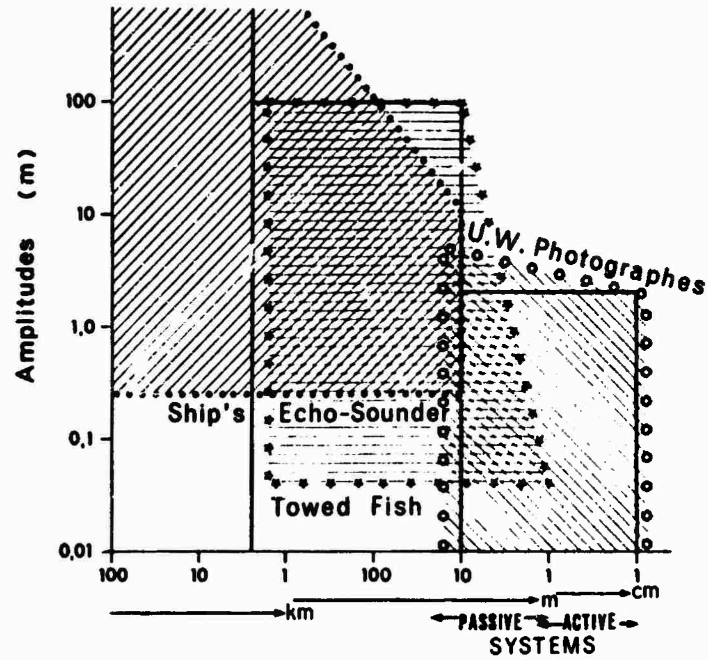

FIG. 8

GROSS FEATURES	INTERMEDIATE FEATURES	SMALL FEATURES
RIDGES	BANKS	RIPPLES
ABYSSAL PLAINS	VALLEYS	BOULDERS
TRENCHES	HILLS	MOUNDS
ETC.	ETC.	ROCK OUTCROPS
		ETC.

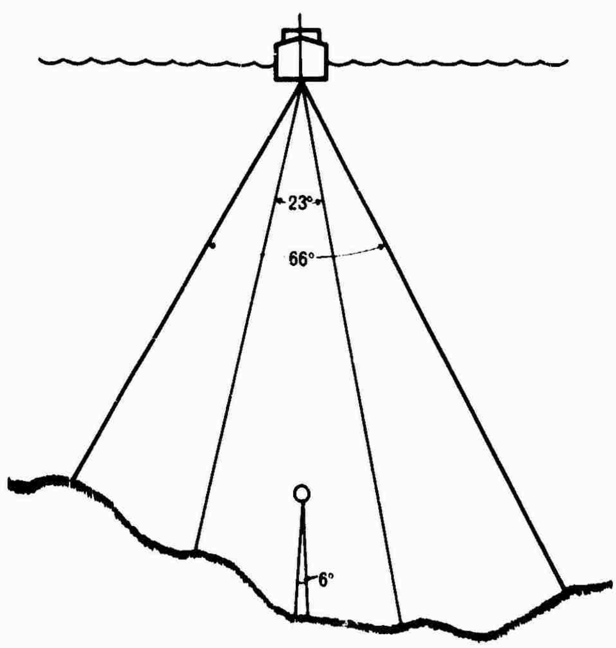

66° Beamwidth 12 kHz
23° » 3.5 »
6° » 50 »

FIG. 9

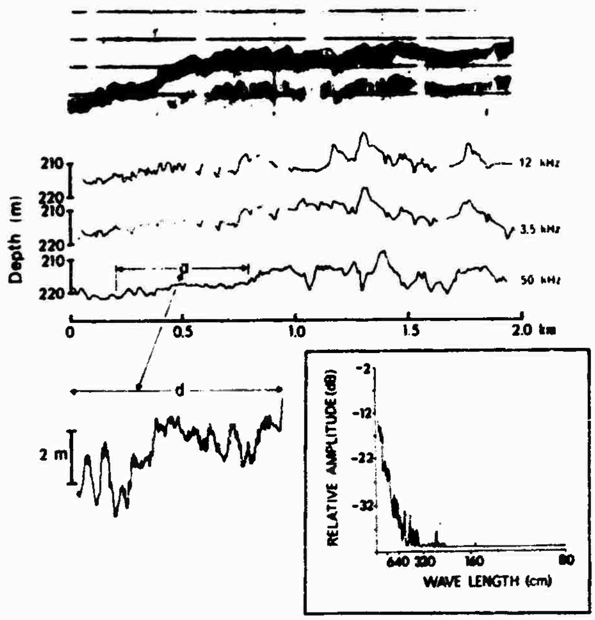

FIG. 10

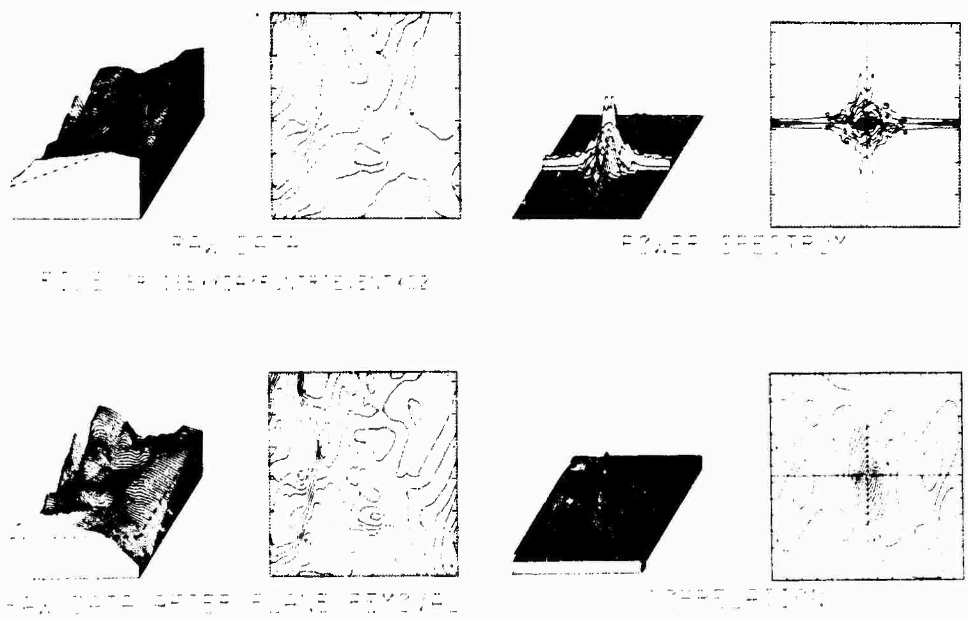

FIG. 11a

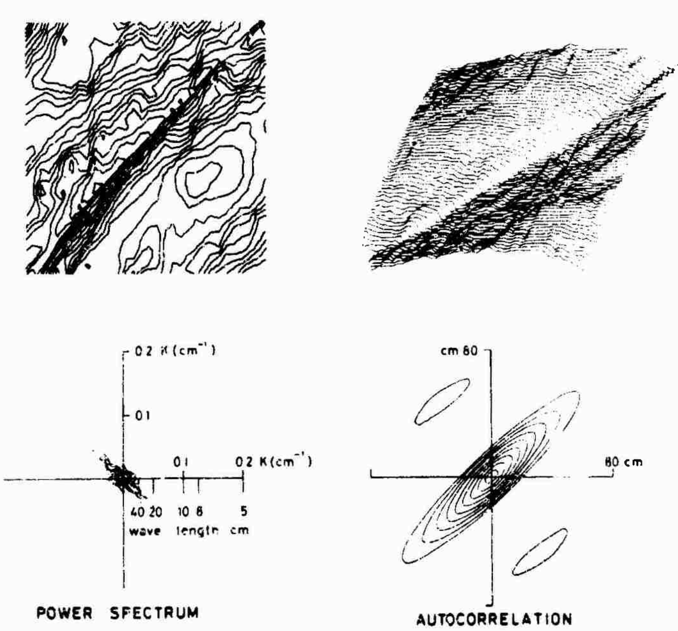

FIG. 11b

THREE REPRESENTATIONS OF SHALLOW-WATER SOUND PROPAGATION

by

H.P. Bucker
US Naval Undersea Center, San Diego, Ca., USA

INTRODUCTION

In th' , report we will consider three methods of solving sound propagation problems in shallow water: wave theory, ray theory, and by use of numerical marching solutions. For each method five different topics will be discussed. These are: the representation of the sound field; the effects of the sound speed profile; the effects of boundary losses; the effects of scattering; and the effects of horizontal changes in the sound speed or boundaries of the channel.

1. REPRESENTATIONS OF THE SOUND FIELD

The wave equation is shown in Fig. 1. As shown, the sound pressure p can be written as a product of the square root of the density times a scalar potential function. The square of the effective wave number, K^2, is equal to $(\omega/c)^2$, ω is the angular frequency and c is the sound speed, plus other factors envolving spatial derivities of the density. At frequencies above ~ 100 Hz these density terms can be omitted. There are several methods of solving the wave equation such as the natural mode expansion [Ref. 1], the fast field method [Ref. 2], the ray mode method [Ref. 3], and the method of virtual modes [Ref. 4]. In this presentation we will restrict ourselves to the natural mode expansion which is shown on the bottom line. We have used the method of separation of variables and Cauchy's Theorem to write the potential function as a sum of residues plus a branch line contour. In the expression,

r	is the horizontal range,
$\varphi_n(z_0)$	is the solution of the z separated wave equation that satisfies the boundary conditions evaluated at the source depth z_0,
$\varphi_n(z)$	is the same function evaluated at the receiver depth z,
k_n	is the horizontal wave number for the nth mode,
N_n	is a type of normalization factor.

Now let us consider the ray representation of the sound field as shown in Fig. 2. The ray theory representation is a solution of the eikonal equation shown at the top of the figure. In the limit $\omega \to \infty$ the eikonal equation $\to$ the wave equation. One might say that ray solutions are asymptotic solutions of the wave equation. In general, it is difficult to determine the frequency above which the ray solution will give accurate predictions of the sound field for a specified shallow-water channel. The ray solution is written as a sum of eigen rays which are those rays that travel from the source to the receiver. The amplitude of the ray A_n, depends upon the accumulated boundary loss, R, the angle of the ray at the source, γ_s, the horizontal distance and a measure of the spreading $\delta h/\delta\gamma_s$ (δh is the vertical separation of neighboring rays at range r that have angular spread $\delta\gamma_s$ at the source). In the neighborhood of a caustic line (a line along which $\delta h \to 0$) corrections to this simple formulation must be made. The phase θ_n is a sum of the integral of $(\omega/c)ds$, where ds is a segment along the ray path, plus the accumulated phase shift due to boundary reflections, equal to $-\ell\pi/2$, where ℓ is the number of times that the ray has touched a caustic line.

The third representation of the sound field is shown in Fig. 3. Here we assume a solution of ψ that is a product of U times a Hankel function of the first kind. By suitable choice of k_o we hope to concentrate the rapid r variations in $H^{(1)}_{(k_o r)}$, so that U will only vary slowly with range. Following Leontovich and Foch [Ref. 5] we delete the second partial of U with respect to r which results in a parabolic equation amenable to a marching solution. Shown at the bottom of Fig. 3 is the split-step numerical developed by Tappert and Hardin [Ref. 6]. To go from range r to range $r+\Delta r$ requires a discrete Fourier transform, some simple modification of the coefficients, and the inverse transform. The starting values of U can be obtained from either of the two representations mentioned earlier, that is from ray theory or wave theory.

2. EFFECT OF THE SOUND-SPEED PROFILE

There are many ways for accounting for the variation of sound speed with depth; however, two models seem to be most popular for the natural mode solutions. In the first, as shown in Fig. 4, the inverse square of the sound speed is written as a linear form of z. The solution for the z-dependent part of the potential function can then be written as either a sum of exponential functions or as a sum of Airy functions [Ref. 1]. In the second model a numerical solution for U(z) is used [Refs. 7, 8].

For the ray theory many models have been developed. On this subject we will only make three observations. First, if there are many receiver locations some form of the ray sweep-out technique [Ref. 9] should be used. That is, instead of concentrating on a single receiver and finding what pairs of rays bracket this receiver it is much faster to look at the rays a pair at a time and ask what receivers are bracketed by the rays. Second, to remove false caustics you must either use a profile representation that has a continuous value of dc/dz [Ref. 10], or you must smooth the range or depth vs γ_s curves

before calculating the sound intensity. Finally, caustic corrections must be made. The general methods of caustic correction [Ref. 11] are known except for a few pathological cases. However, they are not particularly easy to apply.

The parabolic method has no problems with arbitrary sound-speed variations. The sound speed effects the solution only through the term K^2.

3. EFFECT OF BOUNDARY LOSSES

For the natural mode wave solution we can introduce the boundary losses by means of reflection coefficients. We will illustrate this for the case of surface reflection but the same technique can be used at the bottom. Consider Fig. 5 and imagine that there is an isovelocity layer near the surface of depth z_p. Then the potential functions are as shown in the top part of the figure. There is an up-going plane wave incident on the surface which is reflected as a down-going wave with the specular reflection coefficient S. In general the modulus of S is less than one, which indicates energy loss due to scattering or energy transfer through the surface. The usual interface conditions requiring continuity of pressure and the vertical component of particle velocity are imposed so that we can solve for the coefficients A and B. Then we shrink the thickness of the layer to zero which removes the isovelocity layer but leaves the reflection coefficient S in the solution as shown in the figure.

For the ray theory we simply modify the reflected ray by the amplitude loss and phase shift contained in the reflection coefficient. Although this is easy to do, there can be complications because the reflection coefficients are for plane waves and because the ray theory cannot account for energy splitting where part of the ray is reflected at the interface and the rest travels into the sediment to emerge with reduced amplitude at a further range. There may also be energy travelling along a bottom interface, which is sometimes called the lateral wave. This appears in the natural mode solution as the contribution of a branch-line contribution [Ref. 12] but does not appear in the usual ray formulations.

Current practice for introducing boundary effects in the Parabolic model is illustrated in Fig. 6. The surface reflection is effected by reflecting the profile and minus the potential function about the surface. This corresponds to a reflection coefficient, S, equal to -1. At the bottom the sediments must be modelled by the proper value of K^2 which contains the sound speed and the density. This can be done if sediment parameters are known but could be a problem if only experimental values of bottom loss are available. It should also be noted that the bottom must be extended deep enough and with values of K^2 having a sufficiently large imaginary component that the potential function goes smoothly to zero at maximum depth. If this is not accomplished then high frequency noise (similar to the Gibbs phenomena) will be generated near the bottom, which will travel up as the solution progresses in range and will eventually contaminate the potential function at all depths.

4. EFFECT OF BOUNDARY SCATTERING

We shall next consider the effects of scattering of sound energy at the surface. Equations will be derived for surface scattering but the principle is the same for bottom scattering. Also the method will work equally well for the three sound-level representations, so we will only discuss the case for the wave theory representation.

The first step is to determine the upgoing sound energy incident on the surface. The imaginary isovelocity layer at the surface discussed earlier provides the separation of up- and down-going waves. We scatter from the up-going wave of mode n, at the surface by means of a surface-scattering coefficient σ to the receiver. Ray theory is used to determine the propagation loss from the surface to the receiver. In Fig. 7 the first term in the square bracket [ ] represents energy scattered from the mode to the receiver while the second term represents energy scattered from the source into the mode. Similar corrections can be made for the ray theory and for the parabolic method.

5. EFFECT OF HORIZONTAL CHANGES

Horizontal changes in the sound-speed profile or in the bottom topology or type of sediment pose a serious problem for the analyst using wave solutions. There are sophisticated methods that can be used, e.g. see Milder [Ref. 13] and Weinberg [Ref. 14]. However, these assume orthogonal wave functions which is not the case when there is significant bottom loss. At NUC we have been using the earlier formulations of Weston [Ref. 15] and Pierce [Ref. 16]. The basic concept is that the dispersion equation is invariant for slow horizontal variations so that the sound energy remains in a given mode. The sound field is calculated as shown in Fig. 8. The source term $\varphi(z_0)$ is calculated using the profile and bottom losses at the source location, the receiver term $\varphi(z)$ is calculated using the profile and bottom losses at the receiver location, and the history of the mode accumulates in the term $\exp(i\int_0^r k_n\,dr)$. For example, if the mode goes through a region of high loss then $\int_0^r k_n\,dr$ will accumulate a large imaginary component which will attenuate the mode.

The ray theory has no serious problems with horizontal changes. A fast and effective method is to divide the ocean into triangular segments as shown in Fig. 9. This technique was described at the Ray Tracing Conference held here [Ref. 17] in September 1971. The sound speed c is fitted as a linear function to three points, the corners of the triangle, where the sound speed is known. Next a rotation is made to tilted coordinate system in which c is a linear function of only one of the coordinate directions, in this case z'. The ray paths are therefore arcs of circles. After solving for the radius of curvature, ρ, the ray can be quickly traced through the triangle.

A linearly-segmented bottom is easily treated by replacing the under side of the lowest triangle with a bottom segment over the appropriate range interval. Smooth bottom topology can be programmed at the expense of complicated algorithms.

The parabolic method also works very well in cases where there are profile or bottom topology changes. The sound speed only effects the value of K^2 and the bottom effects the solution by means of changes in the sound speed and density.

SUMMARY

We have looked at three representations (natural mode, ray theory, and parabolic solution) of the sound field that have proven useful in underwater sound problems. We have also looked at the effects of sound-speed profiles, boundary losses, boundary scattering, and horizontal changes on the representations. As we have seen, a representation may be best for treating some of the factors but not so good in other cases. It is desirable to have all three types of models so that solutions can be cross-checked and so that the most accurate method is available when the need arises.

REFERENCES

1. H.P. Bucker, "Sound Propagation in a Channel with Lossy Boundaries," J. Acoust. Soc. Amer. 48, 1187-1194 (1970).

2. S.G. Chamberlain, "Final Report for Sound Propagation Study," Raytheon Submarine Signal Div. Report on Contract N00014-67-C-0241 (March 1970).

3. G.A. Leibiger, "Application of Normal Mode Theory to Propagation of 3.5 kHz Pulses in Shallow Water," Vitro Labs. Report VL-2476-9-0 (June 1968).

4. F.M. Labianka, "Normal Modes, Virtual Modes and Alternative Representations in the Theory of Surface Duct Sound Propagation," J. Acoust. Soc. Amer. 53, 1137-1147 (1973).

5. M.A. Leontovich and V.A. Fock, "Solution of the Problem of Propagation of Electromagnetic Waves Along the Earth's Surface," J. Phys. U.S.S.R. 10, 13-... (1946).

6. C.W. Spofford, "A Synopsis of the AESD Workshop on Acoustic Propagation Modelling by Non Ray-Tracing Techniques, 22-25 May 1973, Washington, D.C.," AESD TN-73-05 (Nov. 1973).

7. D.R. Hartree, Numerical Analysis, pp. 134-165, Oxford University Press, London (1958).

8. J. Cybulski, F. Ingenito, and A.V. Newman, "Normal Mode Solutions for Arbitrary Sound Speed Profiles," J. Acoust. Soc. Amer. 48, 91(A) (1970).

9. H.P. Bucker, "The Ray Sweep-Out Method," J. Acoust. Soc. Amer. 52, 283-286 (1971).

10. M.A. Pedersen, "Acoustic Intensity Anomalies Introduced by Constant Velocity Gradients," J. Acoust. Soc. Amer. 33, 465-474 (1961).

11. R.L. Hollford, "Modifications to Ray Theory Near Cusped Caustics," in B.T.L. Report, Continuation of LRAPP (Final Report) (Feb. 1972).

12. L.M. Brekhovskikh, Waves in Layered Media, pp. 270-280, Academic Press, New York (1960).

13. D.M. Milder, "Ray and Wave Invariants for Sofar Channel Propagation," J. Acoust. Soc. Amer. 46, 1256-1263 (1969).

14. H. Weinberg and R. Burridge, "Horizontal Ray Theory for Ocean Acoustics," J. Acoust. Soc. Amer. 55, 63-79 (1974).

15. D.E. Weston, "Guided Waves in a Slowly Varying Medium," Proc. Phys. Soc. (London), 73, 365-384 (1959).

16. A.D. Pierce, "Extension of the Method of Normal Modes to Sound Propagation in an Almost-Stratified Medium," J. Acoust. Soc. Amer. 37, 19-27 (1965).

17. H.P. Bucker, "Some Comments on Ray Theory with Examples from Current NUC Ray Trace Models," pp. 32-36 in SACLANTCEN Proceedings No. 5 (Geometrical Acoustics) (15 Dec. 1971).

DISCUSSION

Mr Akal asked about the (bottom) parameters used for calculating the bottom reflection and scattering coefficients in the models. Dr Bucker explained that about ten years ago the interest was mainly on frequencies from 3 to 4 kHz for which models of elastic solids plus absorption worked well if the first 10 to 20 ft of the sediment was accurately described. Later, when interest turned to much lower frequencies, these models did not work so well and the important thing was to obtain the gradient accurately. New models were developed in which the sound speed and the layers had a gradient so that at sufficiently low frequencies the sound will be refracted out. In the last five years seismologists have used deltametric techniques for calculating dispersion curves for earthquakes. It is thought that these can be used through hundreds of layers without losing accuracy and take both the shear effects and the gradients effects into account. It is found that if the sound goes deep the attenuation is less than Hamilton predicts due clearly to the attractive concept that as a sediment compacts the attenuation undoubtedly becomes less. One can have fairly high loss in the first layers but if the frequency is low enough to break though this high-loss region, there is generally very good bottom reflection.

$$p = \sqrt{\rho}\,\psi$$

$$\nabla^2\psi + K^2(x,y,z)\psi = 0$$

$$\text{where, } K^2 = (\omega/c)^2 + \frac{1}{2\rho}\nabla^2\rho - \tfrac{3}{4}\left(\frac{1}{\rho}\,\text{grad}\,\rho\right)^2$$

NATURAL MODE SOLUTION:

$$\psi = (2\pi/r)^{1/2} \sum_n \phi_n(z_0)\,\phi_n(z)\,\exp(ik_n r)/N_n$$

$$+ \text{ BRANCH LINE INTEGRAL(S)}$$

FIG. 1 WAVE THEORY REPRESENTATION OF THE SOUND FIELD

$$\left(\frac{\partial\psi}{\partial x}\right)^2 + \left(\frac{\partial\psi}{\partial y}\right)^2 + \left(\frac{\partial\psi}{\partial z}\right)^2 + K^2 = 0$$

[EIKONAL EQUATION]

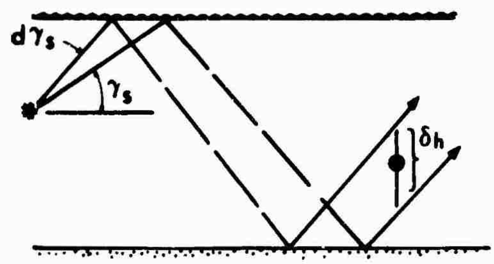

$$\Psi = \sum A_n \exp(i\theta_n)$$

$$A_n = R \cdot [\cos\gamma_s\,\delta\gamma_s\,/\,r\delta h]^{1/2}$$

$$\theta_n = \int_0^r K\,ds + \epsilon - \ell\pi/2$$

FIG. 2 RAY THEORY REPRESENTATION OF THE SOUND FIELD

$$\nabla^2\psi + K^2\psi = 0 \qquad \text{(WAVE EQUATION)}$$

$$\psi(r,z) = U(r,z)\,H_0^{(1)}(k_o r) \qquad \text{(SEPARATION OF VARIABLES)}$$

$$\underbrace{\cancel{\frac{\partial^2 U}{\partial r^2}}}_{\text{Can be neglected in many cases}} - i2k_o\frac{\partial U}{\partial r} + \frac{\partial^2 U}{\partial z^2} + (K^2 - k_o^2)U = 0 \qquad \text{(PARABOLIC EQ. Leontovich and Foch)}$$

$$U(r+\Delta r, z) = e^{\frac{-i\Delta r}{2}(K^2-k_o^2)}\underbrace{\left(e^{\frac{i\Delta r}{2K_o}\frac{\partial}{\partial z^2}}\right)_{op} U(r,z)}_{F^{-1}\left| e^{-\frac{i\Delta r}{\partial k_o}s^2}\,F\,U(r,z)\right|}$$

SPLIT STEP ALGORITHM, Tappert and Hardin

FIG. 3 NUMERICAL REPRESENTATION OF THE SOUND FIELD

I. WAVE THEORY: A. $1/C^2 = 1/C_o^2 + bz$; $\psi \begin{cases} \exp(\pm i\ell z)\,;\ b = 0 \\ A_i[\xi(z)]\,;\ A_i[\xi e^{i2\pi/z}] \end{cases}$

B. Numerical solution for ψ.

II. RAY THEORY: A large number of solutions for specific forms of $C(z)$ are known.

III. PARABOLIC METHOD: Numerical solution accounts for arbitrary variation.

FIG. 4 EFFECT OF THE SOUND SPEED PROFILE

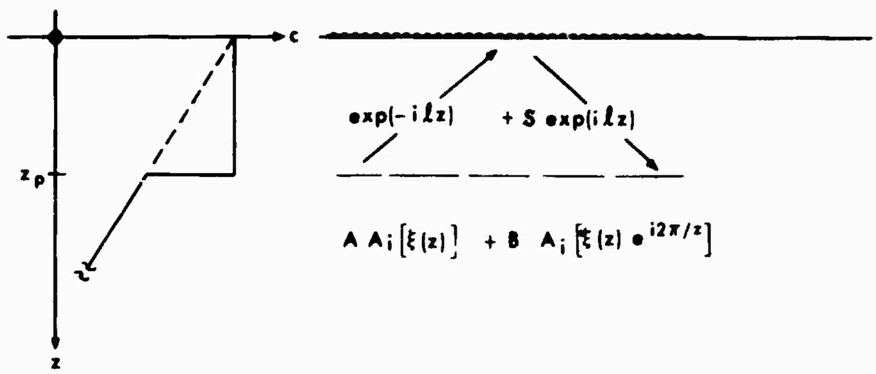

Take the limit $z_p \to 0$

$$A = [b'(S+1) - i\ell b\,(S-1)]/[ab' - a'b]$$

$$B = [a'(S+1) - i\ell a\,(S-1)]/[a'b - b'a]$$

Where, $a = A_i[\xi(0)]$ $\qquad b = A_i[\xi\,0)\,e^{i\,2\pi/z}]$

$a' = dA_i(\xi)/dz\,\big|_{z=0}$ $\qquad b' = d\,A_i(\xi e^{i2\pi/z})/dz\,\big|_{z=0}$

FIG. 5 INTRODUCTION OF S INTO THE NATURAL MODE SOLUTION

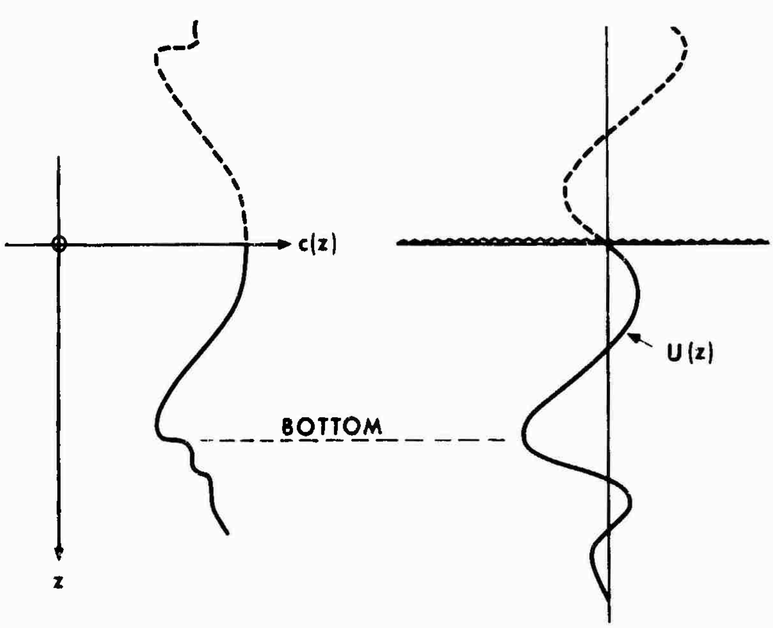

FIG. 6 BOUNDARY EFFECTS FOR PARABOLIC SOLUTION

$$I_s(r)/I_0 = \frac{2\pi}{r}\, e^{-\alpha_n r}\left[\left|\frac{\Phi_n(z_0)}{N_n}\right|^2 G(z) + \left|\frac{\Phi_n(z)}{N_n}\right|^2 G(z_0)\right]$$

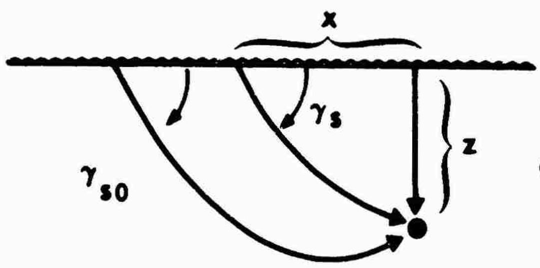

$$G(z) = \int_{\gamma_{s0}}^{\pi/2} \frac{\sigma\, e^{\alpha_n x}}{\sin \gamma_r}\, d\gamma_s$$

$$\left[\alpha_n = 2\,\mathrm{Im}(k_n)\right]$$

FIG. 7 SURFACE SCATTERING (wave theory)

$$\psi = (2\pi/r)^{1/2} \sum_n \phi_n(z_0)\, \phi_n(z)\, \exp(ik_n r)\,/N_n$$

$\phi_n(z_0)$ --- Calculate for Source Profile and Bottom Loss

$\phi_n(z)$ ---- Calculate for Receiver Profile and Bottom Loss

$$\exp(ik_n r) \rightarrow \exp\left(i \int_0^r k_n\, dr\right)$$

FIG. 8 NATURAL MODE SOLUTION FOR HORIZONTAL VARIATIONS

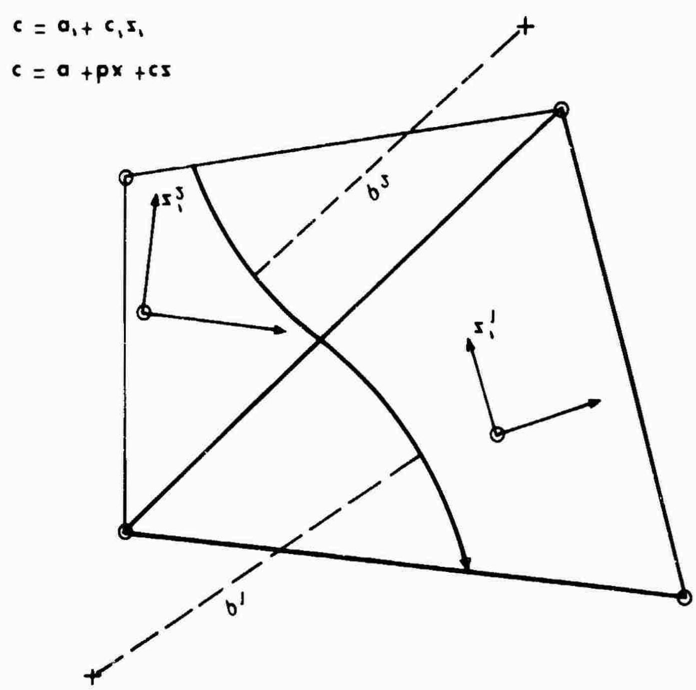

FIG. 9 RAY PATHS IN TRIANGULAR SEGMENTS

ON CLASSIFICATION OF SHALLOW WATER SOUND SPEED PROFILES BY ACOUSTICAL CRITERIA

by

W. Sluyterman van Langeweyde
Forschungsanstalt d. BW für Wasserschall
und Geophysik, Kiel, Germany

ABSTRACT

The underwater sound propagation is mainly controlled by the sound velocity profile — shortly named profile —. Therefore, investigations concerning the problem of sonar range predictions should be approached from this side. For practical use a partition into profile classes becomes necessary. By means of an idealized ray tracing model the influences of the profiles on the acoustical intensity fields are studied. In this way the features leading to the classes will be found and weighted not by comparing the profiles themselves but the resulting intensity fields. A method of profile simplification being controlled in its consequence on the intensity field provides a pre-classification independent of the source depth. Comparisons of intensity fields computed under systematical variations of the profiles lead to the definition of the "profile type" which does not yet consider the source depth. The additional specification of the source depth determines the "coarse classes" of the profile — source depth — combinations. Profile or source depth changes within such a coarse-class will not show any discontinuities in the intensity fields. The systematical computations additionally provide guideline for the realization of the subpartition of the coarse classes.

The sound speed profile — hereafter referred to simply as profile — influences sound propagation mainly in two ways:

1. It operates directly on the spatial distribution of the sound intensity, and
2. Indirectly affects the intensity field by directing the sound energy towards the boundaries where it is reflected, scattered and absorbed.

The considerable variability of the oceanographic states of the medium causes drastic changes in acoustical ranges. This variability cannot be altered, but must be accepted as a fact of nature. The only manageable solution for the sonar user in shallow water is to predict, as precisely as possible, what environmental conditions he must take into account. For military purposes it is especially important to obtain an accurate sonar range prediction at the time and position of

the assigned task. Because of the relationship between the primarily interesting sonar ranges and the profiles, investigations concerning the problem of sonar range predictions should be approached from the oceanographic side.

To reach a usable method of range prediction it is necessary to reduce the infinite number of possible profiles into a finite number of profile classes. It is not sufficient to treat the profiles only in regard to their shape or oceanographic properties. The final partition is an acoustical rather than an oceanographic task. The criteria for a partition of sound speed profiles as an aid for an acoustical range prediction can only be found by examining the properties of the acoustical field. Through existing relationships these properties can be transferred to those profile features which primarily affect the acoustical field.

Before a partition of sound speed profiles according to their acoustical effects can be made, the relationship between the profiles and sound fields must be known. In this paper this relationship will be simulated by a numerical ray tracing model. This model is a many-rays program which computes in the range-depth plane a matrix of values for the sound intensity field. It also accounts for scattering surfaces and absorbing bottoms.

The partitioning problem was investigated in three parts:

1. First a method of profile simplification, controlled by its effects on the intensity fields, provides a preclassification independent of source depth.
2. Then comparisons of intensity fields, computed under systematical variations of the profiles, lead to definitions of coarse classes of profile source-depth combinations.
3. Independent of source depth, profile types are defined from which the potential coarse classes can be deduced.

Figure 1 shows two profiles and the corresponding intensity fields.

1. Upper: summer profile of the North Sea, water depth 55 m.
2. Lower: winter profile of the Baltic, water depth 85 m.

The different types of profiles give rise to different structure in the sound fields, computed for a source depth of 21 m (star). For these fields and for all those to follow these standards have been used:

1. The entire water column is shown.
2. The range extends from 1 n.mi to 30 n.mi.
3. The source depth is 21 m.
4. Two adjacent curves mean a difference of 2 dB, and each 10 dB curve is represented by a bold line.
5. The cylindrical spreading and medium loss have not been added to these calculations.

A range of 30 n.mi and a source depth of 21 m were chosen so that comparisons could be made with field experiments conducted with explosive signals.

In the ray model, profiles are approximated by straight line segments so that they can be uniquely defined by a finite number of points. As a first step in the partition the number of profile points is reduced under control of the acoustical consequences. This is done by means of a progressive adjustment procedure which retains or only insignificantly displaces the salient profile points.

This point reduction scheme can best be explained with the simple 7-point profile shown in Fig. 2. The procedure starts by finding the straight line between points 1 and 2. The third point is checked with this segment and if within a given tolerance of 2ε another straight line using all three points is calculated by the least squares method. If the next point lies within the tolerance of the new line segment it is incorporated with the previous points and a new best fit line is calculated using all 4 points. This procedure is iterated until a succeeding point is found which lies outside the tolerance of the last computed line segment. This line constitutes the first profile segment and the uppermost point 1' is determinated by its intersection with the surface. With the last point used in calculation of the preceding best fit line and the next point, which was outside the 2ε-tolerance, the entire procedure is repeated so that the next profile segment and point 2' can be found. The execution of the procedure over the entire water-column creates depending on the value of 2ε a new profile having the same or fewer points than the original profile.

At this point one question is naturally raised, "Is the use of this profile simplification allowed from the acoustical point of view and if it is, up to what range of tolerance may it be used?"

Figure 3 shows a sequence of profiles with the depth written in metres and the numbers above the scale indicating sound speed in m/s. Adequately displaced it is also valid for subsequent profiles. Profile 1 was measured in 55 m of water. One reading is obtained every metre with a resolution of 0.1 m/s. The succeeding profiles were calculated from the original data using the progressive adjustment procedure with increasing tolerance ranges. In this example, the proecdure was started with a value of ε set at 0.05 m/s and subsequently increased in 0.05 m/s steps.

Now the question is, "How do the corresponding intensity fields behave?" To answer this question the intensity fields shown in Fig. 4 were calculated using a source depth of 21 m.

a) The <u>first four fields</u> uniformally show a zone of high intensity between about 20 to 30 m.

b) By <u>field 6</u> the intensity decreases steplike.

c) In <u>field 10</u> the intensity again raises rapidly

d) The <u>fields 11 to 14</u> are nearly constant, and

e) At <u>field 15</u> the structure is totally changed.

The following points a) to e) correspond to the respective points above. With these profile features the intensity field properties are explained.

The source at a depth of 21 m and the two profile maxima at 20 and 28 m, which have a sound speed greater than the profile has at the source depth, constitutes a duct (Fig. 3).

a) This duct is not altered in the first four profiles.

b) In profile 6 the sound speed of the source depth exceeds that of the lower maximum for the first time.

c) In profile 10 the source is located in the region of the slightly positive gradient of the uppermost layer.

d) From profile 11 to profile 14 the layer above the thermocline remains invariable.

e) Profiles 15 and 16 are totally different from the original profile.

At first glance one would decide that a smoothing of the original profile in excess of step 5 would not be allowed from an acoustical standpoint.

Now field computations were carried out, which start from the assumption that those small profile maxima were horizontally unsteady. The first three profiles of Fig. 5 show some possible variations. Profiles 4 and 5 are not discussed in this paper.

Profile 1 is smooth.

In profile 2 two maxima of the same magnitude and at the same depth as in the last example are applied.

In profile 3 the same variation but in the opposite direction was applied.

Again the source is at a depth of 21 m for the calculated fields of Fig. 6.

Fields 1 and 2 were calculated respectively using profiles 1 and 2 and show the expected structure.

Field 3 was calculated using profile 3. Although it is similar to field 1 it demonstrates that the deviation to the left hardly affects the acoustical field. It does not create any new turning points of the rays, but only causes a slight displacement of the rays.

Now let a horizontal variability be permitted, for instance by alternating profiles. In this case the influence of the focusing group disappears.

Field 2-1, computed from profile 2 alternating with profile 1, is very similar to field 1.

Likewise field 2-3, computed from profiles 2 and 3 is very similar to field 3, which again, as already mentioned, is nearly the same as field 1.

As the duct gradually decomposes more and more rays are lost and will not be recaptured even when the duct is regenerated later.

Hence horizontal unsteadinesss of these small maxima has a similar acoustical consequence as their removal by the progressive smoothing. That means that the simplification of a profile can be allowed in spite of rapid changes in the acoustical field. The upper limit of the allowable range of tolerance certainly depends on the magnitude of the estimated horizontal variability.

The profile simplification by the progressive adjustment with a depth independent tolerance range according to the oceanographic behaviour of the medium is a preclassification independent of the source depth.

A further acoustically justified partition is not possible without considering the source depth. Because of the important roll of the source depth it will be called <u>reference depth</u> from now on. The sound speed at the reference depth will be called <u>reference sound speed</u>.

In conformity of Snell's Law, rays only have their turning points at those depths where the sound speed is greater than the reference sound speed. At such a depth a turning point will only occur, if from there to the reference depth there is no sound speed greater than the reference sound speed. But just the fact, there are turning points or not is responsible for rapid changes of the intensity field.

Intensity field calculations by systematical profile variations as in Fig. 7 illustrate this fact. In profile 11 the lower maximum exceeds the slight maximum at the upper edge of the thermocline. With the source at 21 m this causes the differences seen in the fields numbered from 1 to 10 and in the last two fields of Fig. 8.

Profile variations of this kind have been observed in the Baltic. The profiles of Fig. 9 where measured at the same position of the Baltic. The time between profiles 1 and 2 was [illegible] minutes and between profiles 3 and 4 was 15 minutes. In the five hours between the measurement of these two pairs of profiles, the lower maximum had developed to such an extent that it exceeded the upper maximum at the edge of the thermocline.

Further special investigations of acoustical effects by profile properties were conducted to find the most important and class defining profile features.

The profile maxima are equally important above as well as below the reference depth. For the partitioning purpose it is of special significance when a profile part has a sound speed greater or less than the reference sound speed. If a relative maximum exists which has a higher sound speed the significant roll of the reference sound speed is transferred to this relative maximum. It is valid for the piece of profile between this maximum and the next boundary. If this maximum is exceeded by another maximum towards the boundary this maximum again takes over the definitive roll up to the next boundary. For the parts above and below the source, the membership of the <u>coarse class</u> is determined by those maxima, which

- have higher sound speed than the reference sound speed, and which
- occur with increasing sound speed in the order from the source to the respective boundary.

If the first number is agreed upon for the upper and the second for the lower part, a pair of numbers uniquely determine the coarse class of a profile source-depth combination.

The artificial profile of Fig. 10 serves to illustrate its potential coarse classes and source depth dependence. The pairs of numbers to the left of the profile identify coarse classes for those cases when the source is placed at the depth where the numbers are written.

Without being forced to fix the source depth prior to classifying sound speed profiles one can describe the profile qualitatively with its coarse class possibilities by a sequence of numbers. If the maxima are enumerated according to increasing sound speed, as in example of Fig. 10 from 1 to 6, the order of the numbered maxima with increasing depth would be

5, 6, 2, 1, 3, 4, 4, 0 .

(A boundary maximum is included and a boundary without a maximum is numbered with 0.) This sequence results in a <u>profile type</u> which is independent of a source depth, but from which all potential coarse classes of the profile can be deduced.

Thus a partitiion of sound speed profiles can be obtained in three steps:

1. Preclassification by progressive adjustment.
2. Partition into profile types.
3. Finding the coarse classes, when the source depth has been fixed.

The coarse partition is not fine enough for practical sonar range prediction, but it is a necessary step before a further subpartition by acoustical criteria can be accomplished. Continuous profile variations, which do not cause a change in the coarse class, do not result in discontinuities in the acoustical field. These investigations have shown that it is not correct to represent a sound speed profile by another one obtained by averaging a set of profiles without regard to the source depth and their coarse classes. The intensity field calculated from a mean profile in general does not represent the mean intensity field obtained by averaging intensity fields resulting from the individual profiles.

This investigation also points out some criteria that can be used as a basis for subpartitioning coarse classes. But it is not reasonable to construct fine classes with the universality that was done with the coarse classes. It should be carried out with concrete profile information. This reduces the number of profile types and simplifies the specification of criteria.

REFERENCES

1. CAPERON, J., SCHIPMOLDER, B. and HARWOOD, W. Three-Line analysis of bathythermographs, SACLANTCEN TR 107. La Spezia, Italy, SACLANT ASW Research Centre, 1968.

2. SLUYTERMAN, van Langeweyde, W. Considerations of numerical and experimental propagation models for two-dimensional variation of medium properties. In: CONOLLY, B.W. and CLARKE, R.H. (eds) Geometrical acoustics (Ray tracing) (NU), SACLANTCEN Conference Proceedings CP-5. La Spezia, Italy, SACLANT ASW Research Centre, 1971: 302-306.

3. SCHNEIDER, H.G. Berücksichtigung der Grenzflächenrauhigkeit bei Schallstrahlenrechnung, FWG-Bericht 72-3.

4. REEVES, J.L. and SOLOMON, L.P. Sensitivity of ray theory to input data. In: CONOLLY, B.W. and CLARKE, R.H. (eds) Geometrical acoustics (Ray tracing), SACLANTCEN Conference Proceedings CP-5. La Spezia, Italy, SACLANT ASW Research Centre, 1971: 114-129.

5. SOLOMON, L.P. A technique investigating the sensitivity of ray theory to small changes in environmental data. Acoust. Soc. Am. Proceedings of 86th Meeting, Los Angeles Hilton, 30 Oct - 2 Nov 1973.

6. WILLE, P., THIELE, R. and SCHUNK, E. Shallow-water sound attenuation in a standard area. Jnl Acoustical Society America, 54, 1973: 1708.

7. SCHIRMER, F. Eine Untersuchung akustischer Eigenschaften von Sedimenten der Nord- und Ostsee", Dissertation Universität Hamburg, Fachbereich Geowissenschaften (1971).

8. SCHELLSTEDE, G. and KROLL, W. Standardauswertung zur Ausbreitungsdämpfung von Knallsignalen im Flachwasser. FWG-Bericht 1973-7.

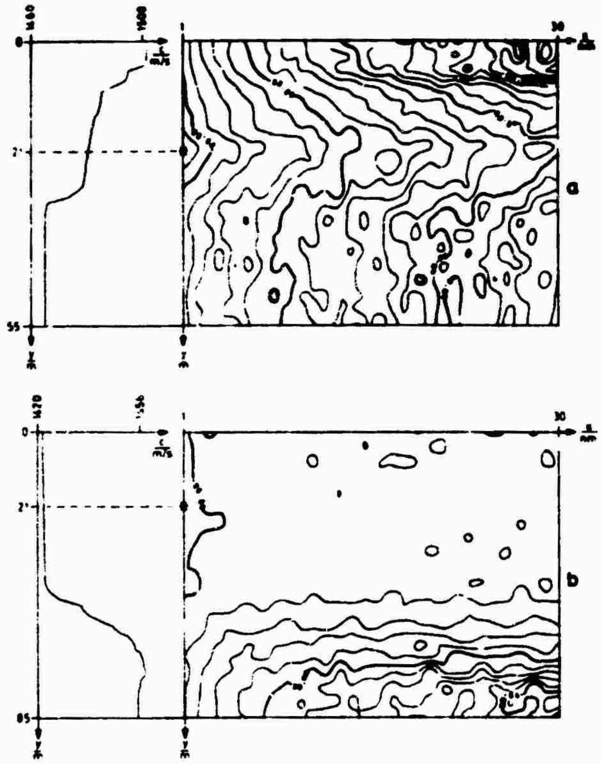

FIG. 1 SOUND SPEED PROFILES AND CORRESPONDING SOUND INTENSITY FIELDS WITH A SOURCE DEPTH OF 21 m
a) NORTH SEA SUMMER, b) BALTIC WINTER

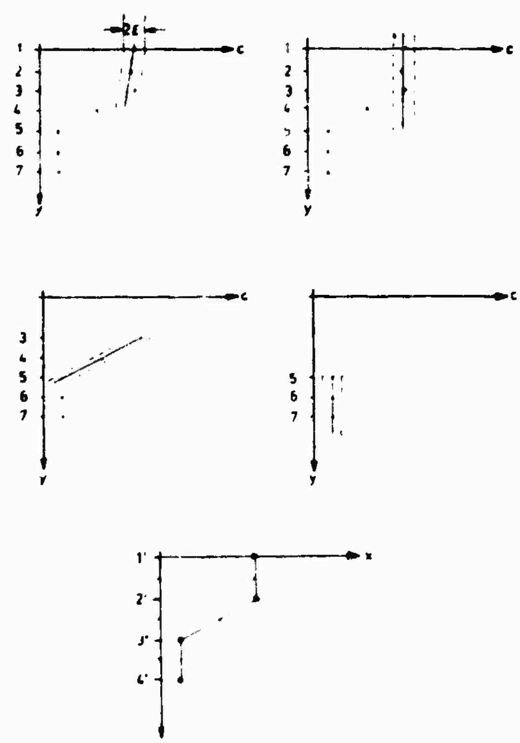

FIG. 2 PROFILE SMOOTHING PROCEDURE USING A SIMPLE PROFILE

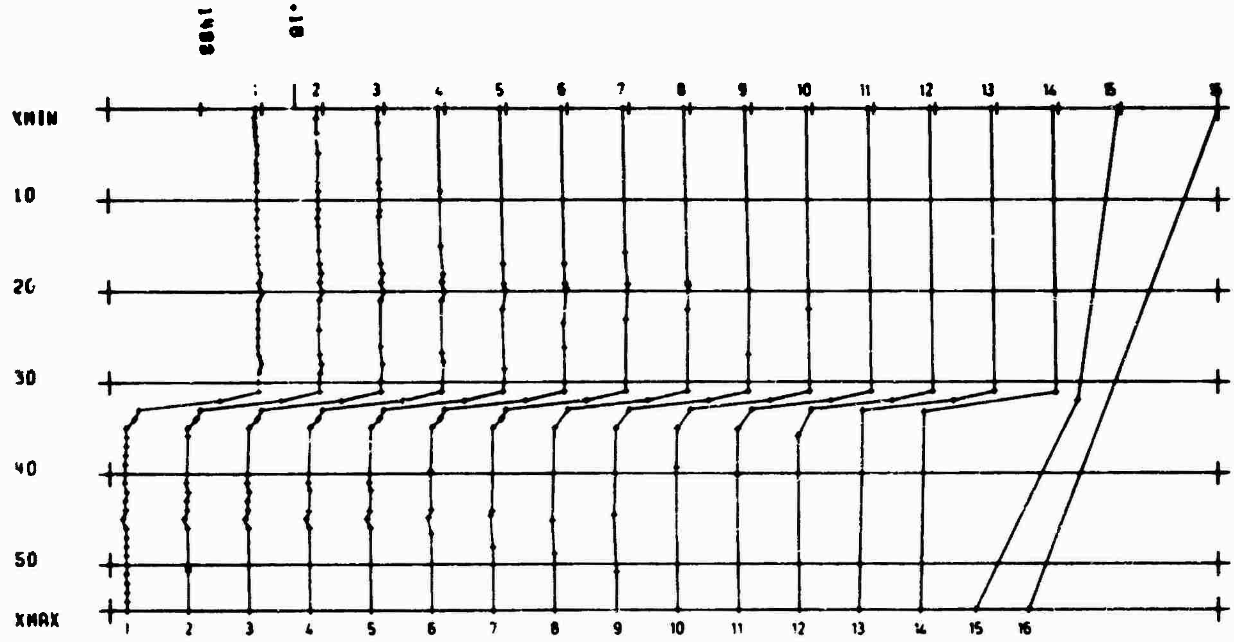

FIG. 3 SERIES OF SYSTEMATICALLY SMOOTHED PROFILES

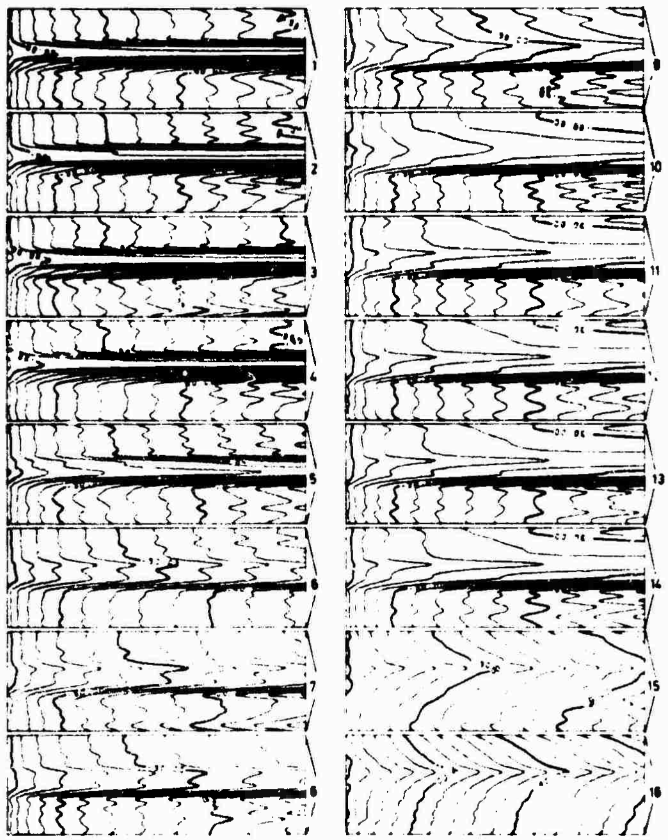

FIG. 4 SERIES OF INTENSITY FIELDS CALCULATED WITH THE PROFILES OF FIG. 3 AND A SOURCE DEPTH OF 21 m

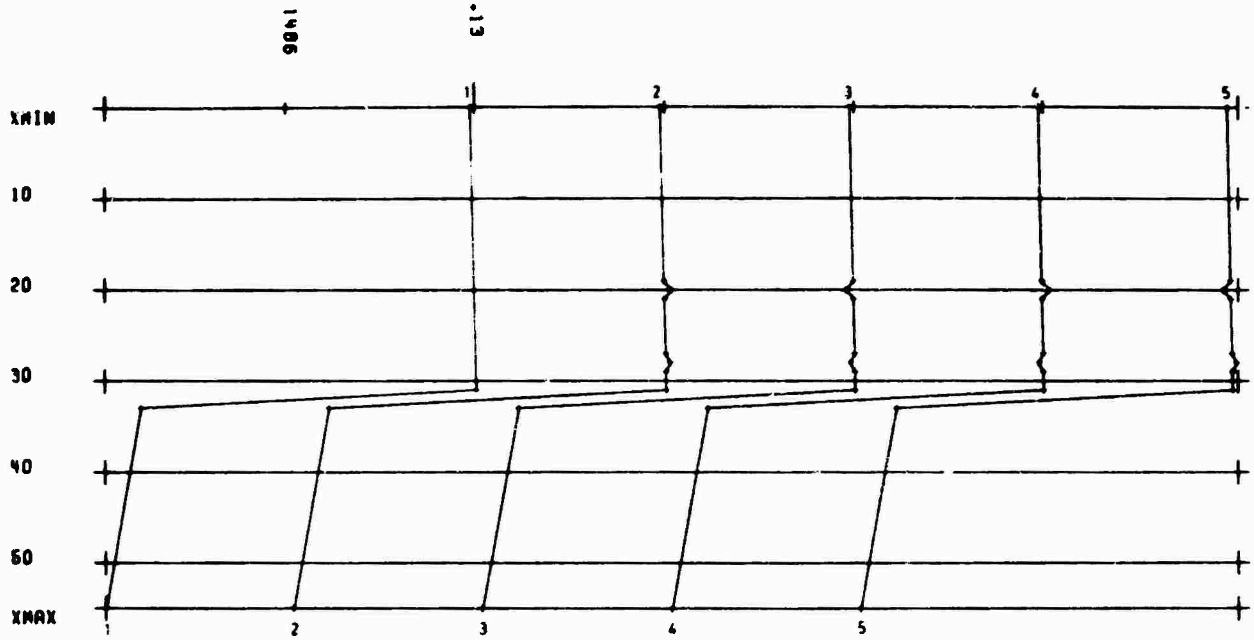

FIG. 5 SERIES OF SYSTEMATICALLY VARIATED PROFILES

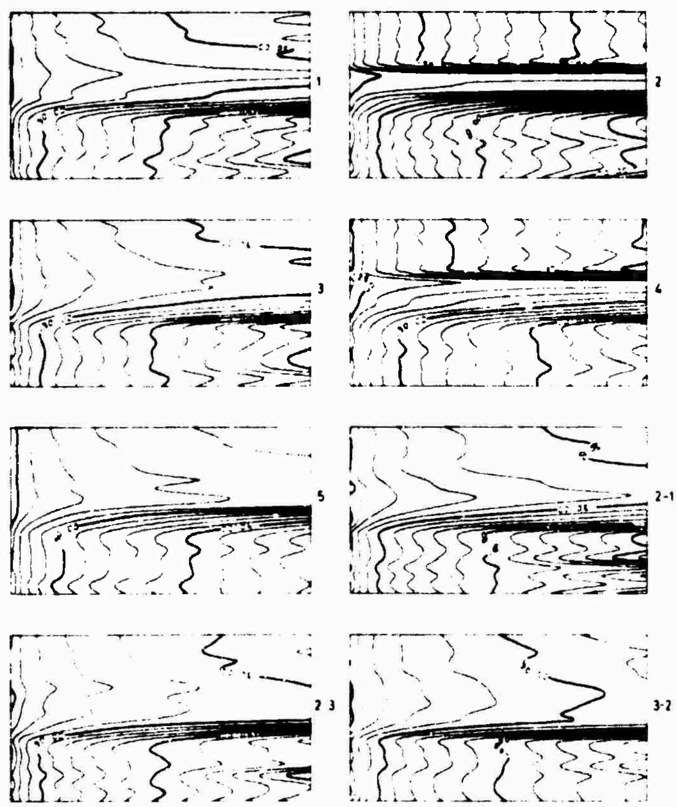

FIG. 6 SERIES OF INTENSITY FIELDS CALCULATED WITH ONE OR MORE PROFILES FROM FIG. 5 AND A SOURCE DEPTH OF 21 m

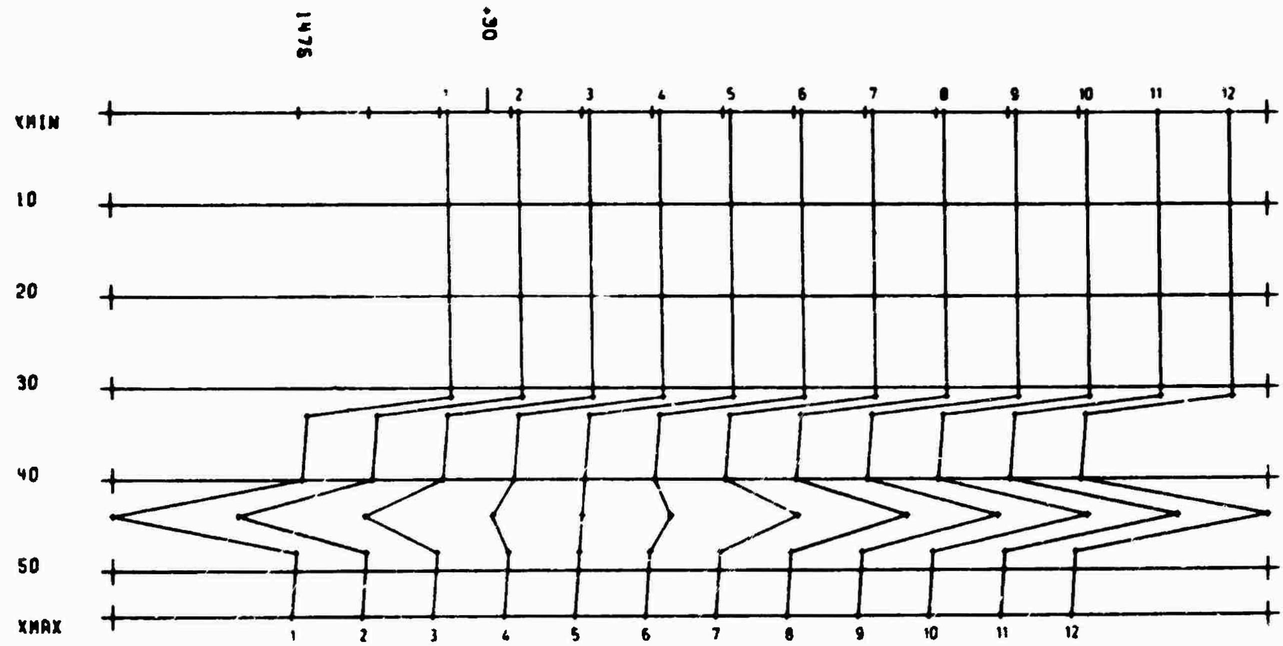

FIG. 7 SERIES OF SYSTEMATICALLY VARIATED PROFILES

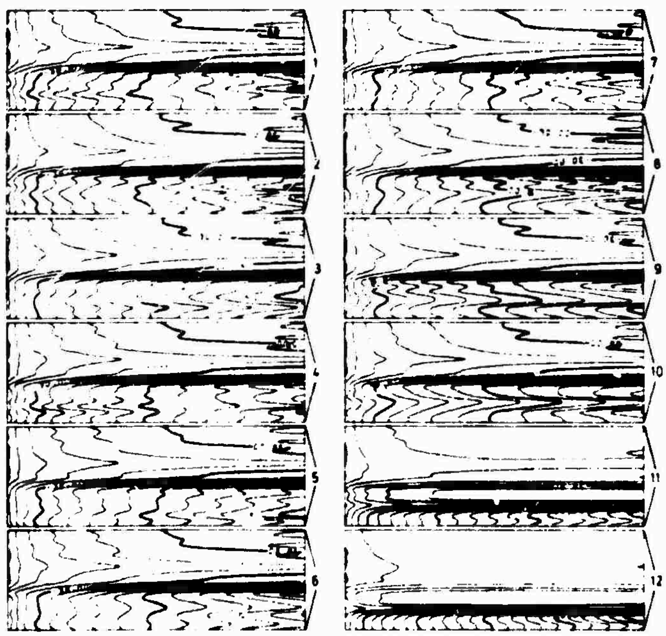

FIG. 8 SERIES OF INTENSITY FIELDS CALCULATED WITH THE PROFILES OF FIG. 7 AND A SOURCE DEPTH OF 21 m

FIG. 9 SERIES OF PROFILES MEASURED AT THE SAME POSITION BUT DIFFERENT TIME IN THE BALTIC

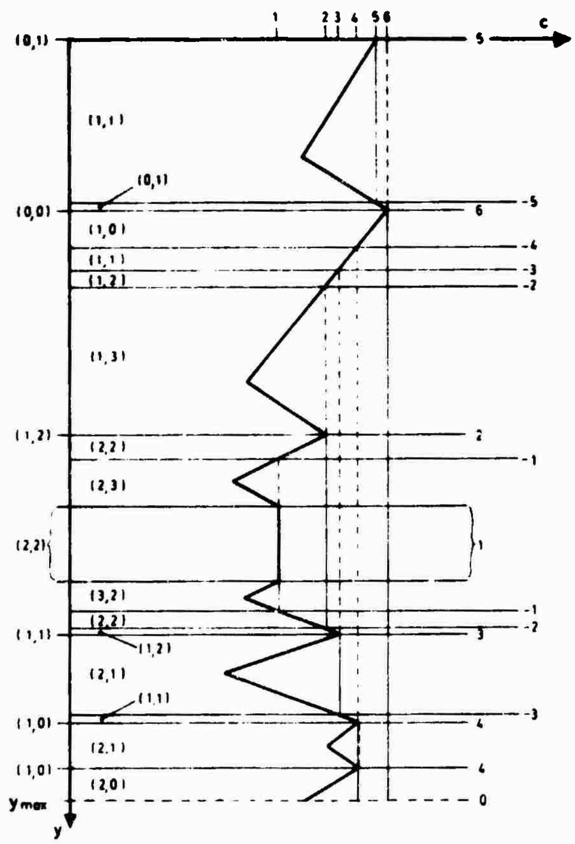

FIG. 10 ARTIFICIAL PROFILE ILLUSTRATING THE SOURCE DEPTH DEPENDENCE OF THE COARSE CLASS AND THE PROFILE TYPE

MEASUREMENTS OF SOUND ATTENUATION IN STANDARD AREAS OF NORTH SEA AND BALTIC

by

G. Schellstede and P. Wille
Forschungsanstalt d. BW für Wasserschall
und Geophysik, Kiel, Germany

ABSTRACT

The measurements are presented for a selection of different environmental conditions referring to sound intensity decay laws, vertical intensity distribution and frequency dependence of attenuation. The temperature-salinity stratification of the Baltic area offers the possibility of a SOFAR-type sound propagation in shallow water whereas the North Sea area is mainly suitable to study the influence of the bottom under downward refraction conditions. To achieve quasi synoptic control of the sound fields and environmental fields only by combined ship-aircraft measurements, the sea areas were chosen for weak spatial and slow temporal variations of the environmental parameters. The fulfillment of these prerequisites and the measurement and evaluation techniques are discussed with regard to the aptitude of the standard area measurements for testing and fitting prediction models.

INTRODUCTION

Sound propagation models, which are simple enough for practical application, must confine themselves on the strongest environmental influences and neglect all the minor ones. Since the acoustic hierarchy of the environmental parameters may differ with respect to sea area and time, there will be no universal propagation model for shallow water. So it seems unavoidable, to investigate the sea areas of interest individually with regard to important and less important environmental properties and to tailor the model to the sea area in question. Then one may hope to learn, which criteria make different sea areas acoustically similar.

To estimate the hierarchy of the environmental influences, a sufficient separation of the different processes involved is needed. This seems to be possible perhaps in very simple standard areas, which are selected for their extremely weak horizontal variation of all environmental parameters.

The measurements we present here, stem from standard areas of North Sea and Baltic as shown in Fig. 1. Up to now, one succeeds at the most to model the sound propagation behaviour of the North Sea [Ref. paper of H.G. Schneider: "Modelling the Propagation Loss in Shallow Water"]. On the contrary, the acoustical behaviour of the Baltic is in part not even qualitatively understood. Therefore we confine ourselves to the comparison of the observations.

1. MEASURING METHOD

We have standardized the propagation measurements as follows: [Ref.: P. Wille, R. Thiele, E. Schunk: "Shallow Water Sound Attenuation in a Standard Area", Journal of the Acoustical Society America, 54 (1973) p.1708].

As illustrated in Fig. 2, each individual propagation measurement consists of a series of 30 TNT-bombettas which are air-dropped within 10 min along a range of 30 n.mi. The measuring time is short enough with respect to stationary sea state and allowes for tests of reproduceability. The detonation depth is always 26 m. The receiving array — horizontal or vertical — has 10 separate hydrophones.

The data acquisition of the sea state, oceanographic stratification and sea bottom will not be discussed here.

2. ENVIRONMENTAL CONDITIONS

The temperature profiles of North Sea summer show a main thermocline with gradients of 1 to 3°C/m; often there is a second, weaker thermocline near the sea surface, depending strongly on weather conditions. Figure 3 shows some examples. During winter, the North Sea is completely isothermal. There is no salinity stratification. The upper sediment of the bottom consists of sand which is from a few decimetres up to 2 m thick.

The variation of temperature stratification in the horizontal direction is often relatively weak which is demonstrated by this towed Delphin measurement conducted by Deutsches Hydrographisches Institute (see Fig. 4). However, when there are storms, the variations may be significantly stronger. Model computations by H.G. Schneider show that these weak horizontal variations may be neglected with respect to sound propagation.

In the central Baltic, there is a sound channel formation during summer, the sound speed increasing towards the bottom from salinity and towards the surface from temperature. The upper thermocline corresponds to the North Sea behaviour. October profiles are shown in Fig. 5; note that the thermocline was deeper than the fuse depth of the explosive sources for all our acoustic measurements.

The sound speed at the upper part of the increase of salinity is often but not in all cases higher than within the mixed layer. The horizontal variation of the thermohaline structure is stronger than for the North Sea and probably varies faster. Obviously our provisional stratification measurement is not sufficient as input for propagation model computation for the Baltic. During the winter there is no thermocline; the salinity increase however does not vanish. The sea bottom of the Baltic area consists of mud up to a few metres thickness for almost all the Baltic measurements.

3. ATTENUATION LOSS; SOUND LEVEL SLOPE VS DISTANCE

Each of the 10 hydrophone signals was filtered digitally to obtain third octave extracts from 40 Hz to 10 kHz. The signal energy was integrated for the complete signal duration and corrected for background noise. The cylindrical spreading loss of 10 lg R has been removed.

The resultant slopes are shown in Fig. 6, and can be described in most cases as an exponential decrease consisting of both boundary and medium losses. The slope of the regression line in dB/km is computed for least squares. It is possible to describe the propagation law as a superposition of an assumed spreading function of $R^{-\beta}$ together with the exponential dissipation loss $e^{-\alpha R}$. The fitting of the propagation law by a suitable spreading coeffcient β will be discussed later. For the following figures, $\beta = 1$, that means cylindrical spreading is always used. For the range interval of 1 to 30 n.mi this has been proved to be a sufficient description. Then the standard deviation of the sound level data is typically 1 to 2 dB.

For a few Baltic measurements illustrated by Fig. 7, however, one finds stronger deviations from a pure exponential slope; the sound channel mentioned above may produce caustics.

4. ATTENUATION LOSS; FREQUENCY DEPENDENCE

The dissipation α usually increases monotonically with frequency above a few 100 Hz and can be determined with low error from the propagation measurements. Figure 8 demonstrates that all ten separate hydrophone channels give values of α that lie within a narrow band of scatter. The prerequisite of such small scatter is a horizontal receiving array.

All attenuation loss measurements made in both standard areas result in the area of variation presented in Fig. 9. For each series the mean curve for the ten hydrophones is used.

Obviously the North Sea measurements taken together form an area that is of approximately constant width within the frequency range investigated; the difference in the attenuation coefficient corresponds to a factor of 5 to 10. In the Baltic however this factor approaches 30 between 100 and 300 Hz but is only a factor of 3 between 1 kHz and 2 kHz. Even this simple superposition of all measurements shows the mean attenuation in the Baltic to be significantly higher at low frequencies and lower at high frequencies than in the North Sea. The salinity increase of the Baltic seems to effectively screen the highly absorbing mud bottom at high frequencies but not at the lower frequencies.

The North Sea behaves in a simpler manner than the Baltic with regard to the frequency dependence of attenuation. The steepest and the levelest slope of all the North Sea series differ less than factor 2 as shown in Fig. 10. There was no simple connection observable between the frequency slope of attenuation and environmental parameters, for example sea state and medium stratification. However, the slope tends to be steeper if the temperature profile reduces the energy density near the rough sea surface by downward refraction. If one tries to simplify the slope of the attenuation curve by a single function, one gets $\alpha \sim f^{0.38}$ for winter and $\alpha \sim f^{0.55}$ for summer conditions as a mean for ten series under both conditions.

Figure 11 shows that for the Baltic, the summer attenuation can be nearly frequency independent, if the sea state is low. The often observed minimum of α near 100 Hz has almost vanished if the mean of all ten hydrophones is taken.

However the steep slope of α for winter conditions is very similar to that found in the North Sea (Fig. 12). At higher frequencies neither the amount nor the slope of the attenuation function differs significantly for both areas. Only the minimum near 100 Hz is more pronounced for the Baltic winter.

5. INFLUENCE OF WAVE HEIGHT ON THE ATTENUATION LOSS

The North Sea attenuation continues to behave simpler than the Baltic with respect to the influence of sea state. In Fig. 13 there are only examples of winter conditions where the additional contribution of medium stratification is absent. The average attenuation loss does increase with wave height, but with no significant frequency dependence of propagation loss on wave height. For North Sea summer the influence of sea state is even less. If there is any connection of propagation loss to the sea state spectrum, it is at most very weak.

The comparison with the Baltic summer results illustrated in Fig. 14 shows that there is not only a strong increase in attenuation by sea state (variations of factor 8 occur) but especially a significant frequency dependence above 1 kHz. However the measurements give no more than a connection to the wave height. Differences in the sea state spectrum seem to be of minor influence on the attenuation for the Baltic too. However, for most examples the wind driven sea was rather stationary.

The maximum attenuation is remarkably similar for both North Sea and Baltic, but a reduction of wave height in the North Sea produces only a slight decrease in attenuation. Lowering the wave height in the Baltic however has a strong effect on the attenuation. Presumably, the focusing effect of the summer sound channel which can only be found in the Baltic deteriorates as the sea state becomes stronger, causing an increase in boundary loss. So, one cannot exclude the possibility that the sea state has primarily indirect influence on the attenuation in the Baltic by disturbing the eveness of the stratification.

6. INFLUENCE OF SEA STATE DIRECTION ON ATTENUATION

The following examples differ only with respect to sea state direction. The sound propagation direction is either parallel or perpendicular to the wind. Since the directional spectrum of the sea state is increasingly isotropic towards shorter wave lengths, one would expect mainly the longer sound waves to be influenced by the sea state direction. Indeed, there is no significant difference above 500 Hz. If there would occur Bragg scattering of longer sound waves at the perpendicular wave crests, then the attenuation is expected to be higher for parallel wind condition. This seems to be confirmed by Fig. 15. The difference is indeed significant, as the reproduceability of the measurements shows when repeated for the same direction within one hour. In most cases this reproduceability was even better (standard deviation ≈ 10% of the scale used).

For higher sea states this difference was even more remarkable for both directions as shown by Fig. 16. However, this time the higher attenuation is found in the perpendicular direction, negating the interpretation that the attenuation should increase or at least change for the parallel sea state condition.

This comparison serves to demonstrate that influence of sea direction on attenuation cannot hastly be concluded after only a few observations. It may be that influence of sea direction on attenuation can be measured under certain conditions however, during all our measurements it was surely masked by other and stronger processes. To obtain deviations of the observed amount it is only necessary that the aircraft course changes slightly. Computations show that even small variations in the sediment subsoil structure may have a strong effect on the attenuation at lower frequencies. At higher frequencies the acoustic penetration will not reach deeper than the sand layer of a few decimetres, therefore, the sea bottom behaves like a horizontally invariant parameter. So, at higher frequencies there is neither a significant influence on sea state direction nor of variation of the sand sediment subsoil on the attenuation in the North Sea.

7. DEPENDENCE OF ATTENUATION ON RECEIVER DEPTH (NORTH SEA)

The attenuation measurements mentioned up to now were presented as mean values for all ten separate hydrophones even if measured by the vertical array.

If the attenuation is plotted separately for the different hydrophone depths (Fig. 17), one will find a remarkable depth dependence below 1 kHz, especially for winter conditions. In fact, the highest attenuation is found near the sea surface and the lowest near the bottom. Above 1 kHz the depth dependence is inverted and much weaker: the near surface hydrophone gives the lowest attenuation.

This behaviour corresponds to the measured two-dimensional sound intensity fields. Figure 18 shows that the isobars run approximately parallel to the surface at low frequencies; at high frequencies one finds isobars in horizontal orientation near the bottom.

Less obvious but significant is the depth dependence of the attenuation for summer condition. Again, the attenuation near the surface is highest at low frequencies and lowest at high frequencies as shown in Fig. 19.

8. CONTRIBUTION OF THE MEDIUM TO ATTENUATION LOSS

Surely the frequency dependence of the attenuation is not the consequence of a single process. The measurements in the Baltic have shown the influence of the sea surface to be at least a competitive mechanism.

Subtracting the deep sea medium loss from the measured North Sea attenuation, a substantial loss increase by frequency is left over (Fig. 20). This is valid for a correction with mean maximum and minimum deep sea values. The remaining loss can be modelled rather satisfactorily using a stratified dissipative bottom and a frequency dependent surface scattering, both contributions being of the same order. The extent to which bottom scattering is involved must be left open, however.

For the Baltic attenuation, the reduction by an assumed deep sea loss gives only a slight decrease (Fig. 21), if mean values for all hydrophone channels are taken. Now the characteristic sound speed profile of the Baltic summer provides a unique opportunity to determine the medium loss for shallow water in a manner similar to that employed in the deep water SOFAR-channel. Unfortunately the fuse depth of the air dropped bombettas could not be adjusted to the channel axis; therefore all shots were fired in the mixed layer.

Surprisingly one finds for several Baltic propagation series deep minima of the attenuation coefficient at the depth of the sound channel and within a relatively small frequency interval (Fig. 22). It seems likely that part of the sound energy comes into the sound channel by local inhomogeneities or scattering and remains trapped.

This assumption is supported by the observation of extremely long reverberation duration for the same fuse depth. Since part of the guided sound energy will escape by scattering again, one would hardly expect to obtain quantitative results for the shallow water medium loss from these propagation measurements. However, far away from the source, the sound channel will surely loose more energy than gain, because off channel axis, the energy density is already much lower. Therefore the true medium loss value should not be higher than estimated from this data and compared to Thorp's deep sea loss. (We hope to prove this by suitable bombettas in the next future).

So we may conclude that the North Sea medium loss is not higher than in the deep ocean too, because pollution as a possible reason for higher loss is even less than for the Baltic. Up to now there is no explanation for the frequency selection of low losses, however.

Figure 23 shows that there are propagation series without any sound speed profile peculiarities which show a second loss minimum at low frequencies near the channel axis. This is not understood either. There are examples with both minima, or one or even none. In any case, the fuse depth was inside the mixed layer.

Figure 24 illustrates a sound intensity field with focusing profile and focusing effect.

Figure 25 is an example of a focusing profile but no guided energy within the channel. Perhaps the channel has been defocusing along the sound path in this case.

9. REMARKS ON PROPAGATION LAWS

Let us finish with a remark on propagation laws. It seems more a question of suitable fitting than of the physics involved to describe the sound level slope for a limited range interval by

$$R^{-3/2} \quad \text{or} \quad R^{-1} \cdot e^{-\alpha R} \quad \text{or} \quad R^{-\beta} \cdot e^{-\alpha R} \quad \text{respectively.}$$

If β is determined by a regression function for the different frequency bands and hydrophone channels independently, one may look for interconnections between the distribution of β and parameters like hydrophone depth, frequency, sea state or stratification. From the measurements, there is no significant correlation — perhaps with one curious exception which has to do with direction of sea state and may be due to the limited set of data.

Figure 26 shows the distribution of β to exhibit a maximum near 1 if wind and sound propagation are perpendicular. If they are parallel, the maximum is shifted between 1.4 and 1.5. If the contrary would be the case, one could perhaps assume the perpendicular wave crests make

the angular distribution of sound incidence at the boundaries more stationary. Following these examples however any interpretation would be rather speculative. So some of the Baltic shallow water results contribute more to new questions than to decide between competing assumptions.

DISCUSSION

Miss Ching asked for comments on her belief that surface bubbles might be causing the considerable increase in propagation loss associated with higher wind strength, which it was impossible to explain in terms of increased surface roughness. Dr Wille said that he had the same suspicions but the difficulty in measuring bubble concentrations had so far prevented a quantitative investigation; however the idea must not be excluded.

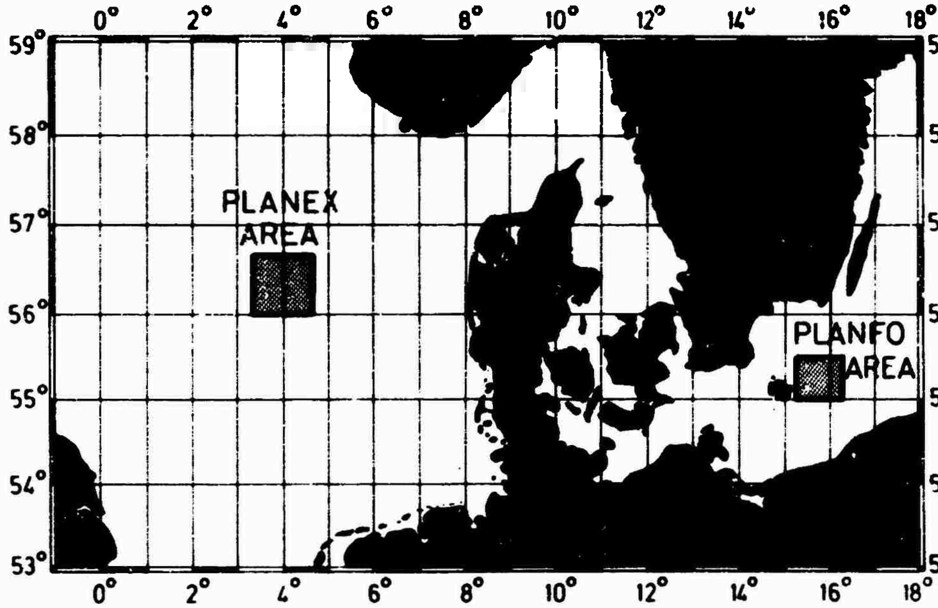

FIG. 1 STANDARD AREAS IN NORTH SEA AND BALTIC SEA

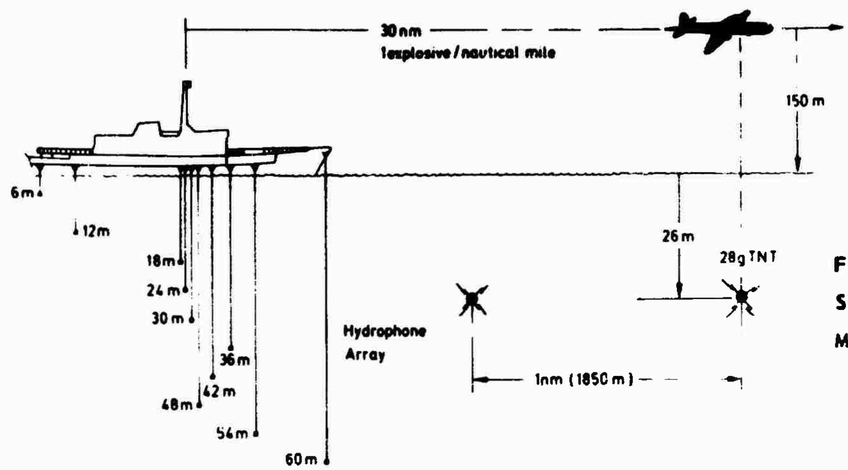

FIG. 2

STANDARDIZED SOUND PROPAGATION MEASUREMENT (SHIP – AIRCRAFT)

FIG. 3

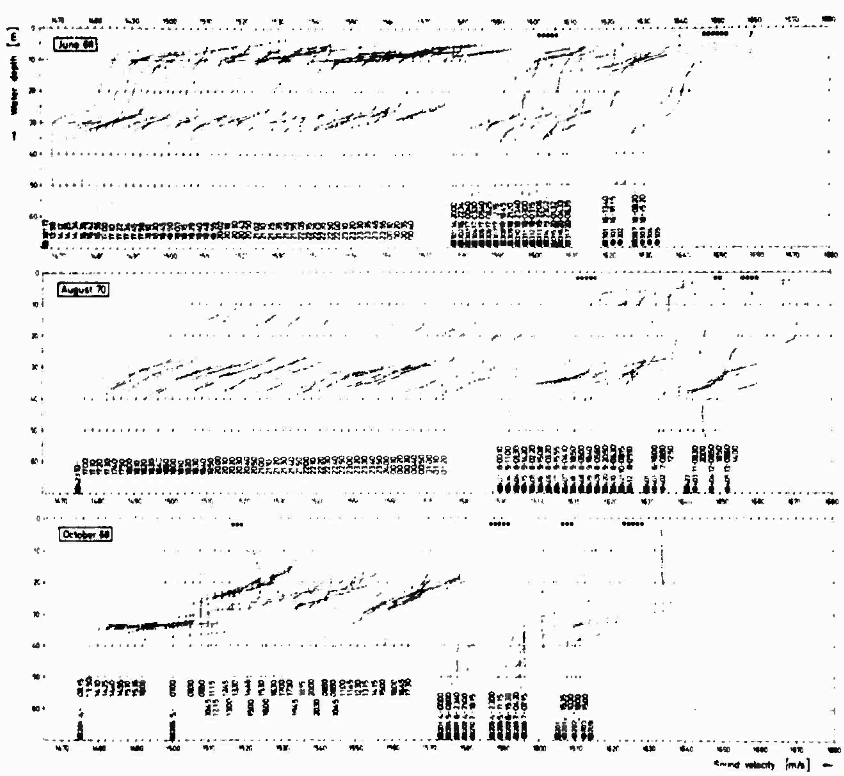

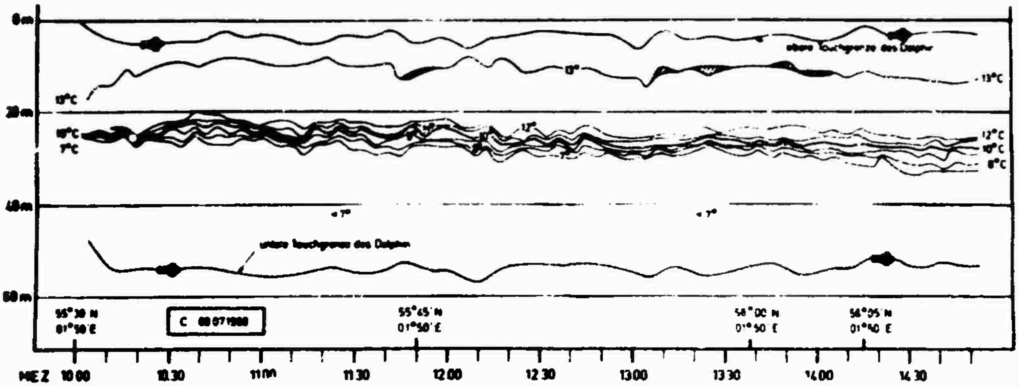

FIG. 4

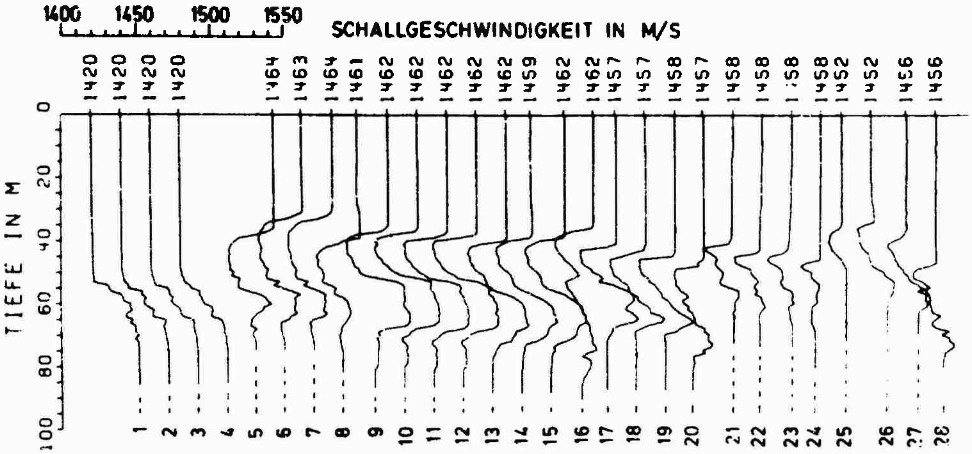

FIG. 5 SOUND VELOCITY PROFILES - BORNHOLM REGION

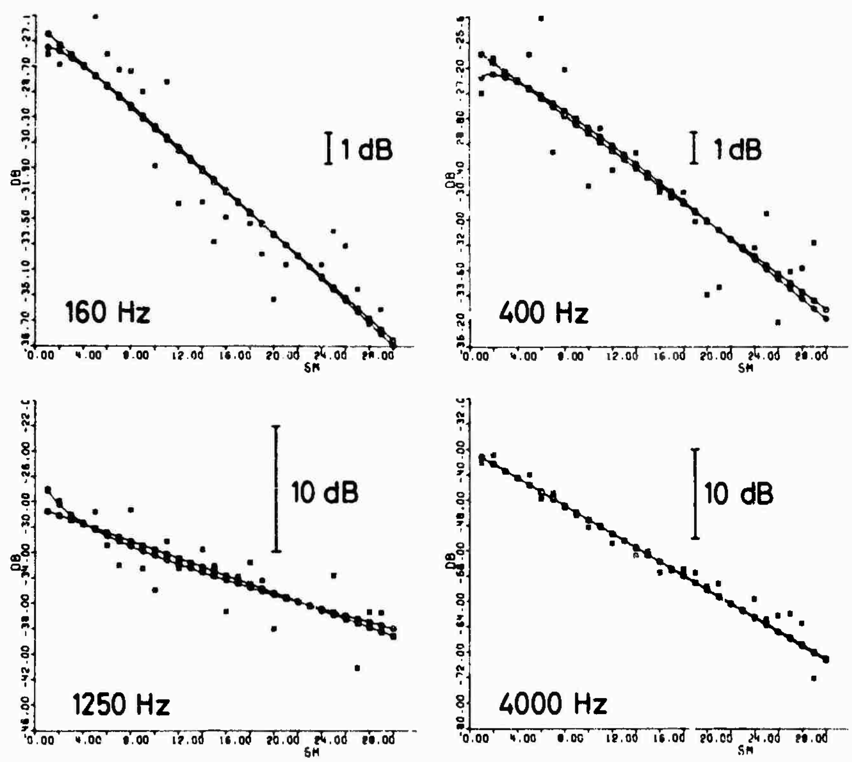

FIG. 6 SOUND LEVEL vs DISTANCE - NORTH SEA, WINTER

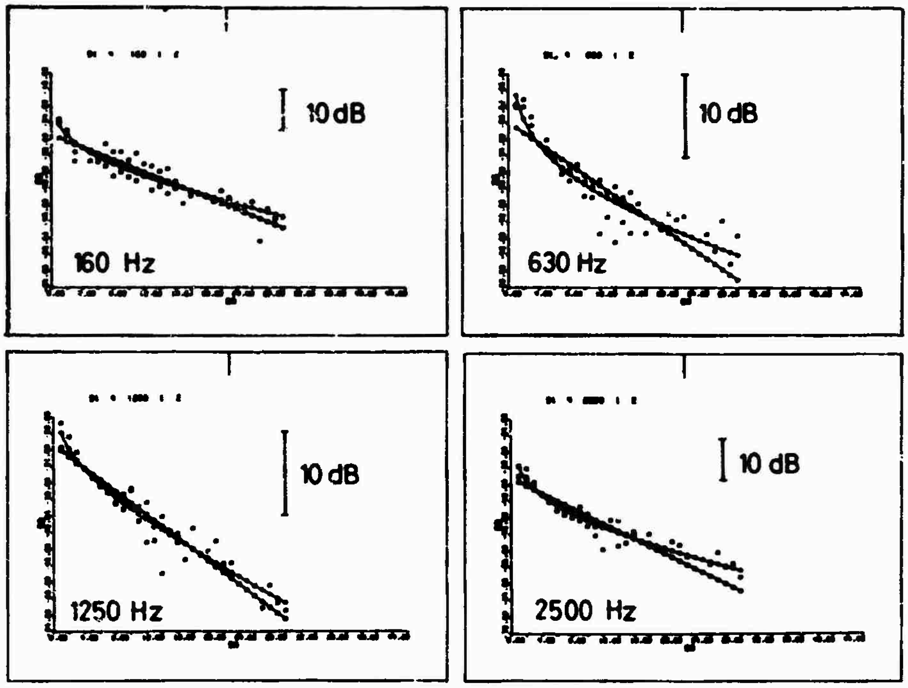

FIG. 7 SOUND LEVEL vs DISTANCE – BALTIC SEA, LATE SUMMER

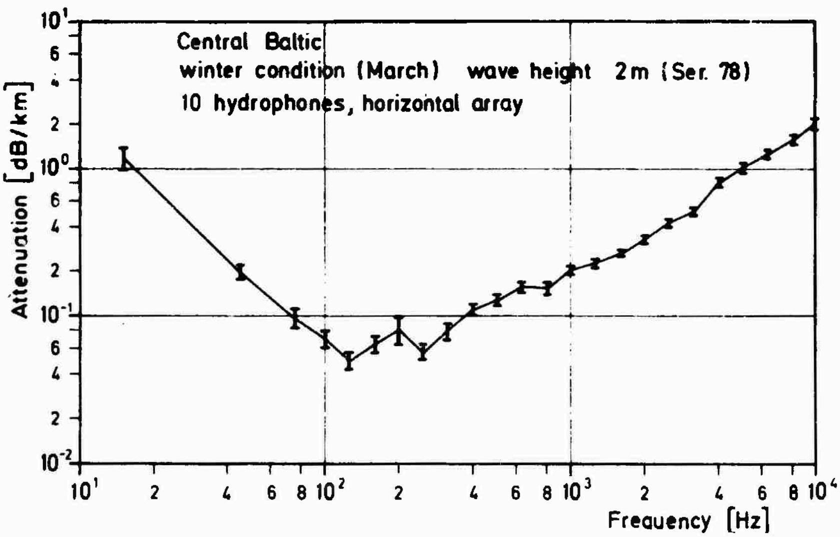

FIG. 8 COMPARISON OF ATTENUATION LOSS SPREADING – 10 SIMULTANEOUS MEASUREMENTS

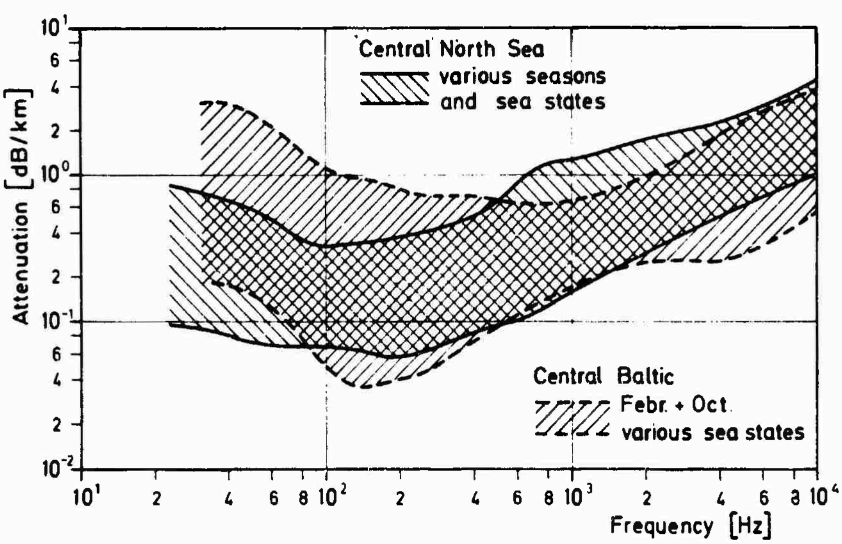

FIG. 9 COMPARISON OF ATTENUATION LOSS RANGE – BALTIC SEA, NORTH SEA

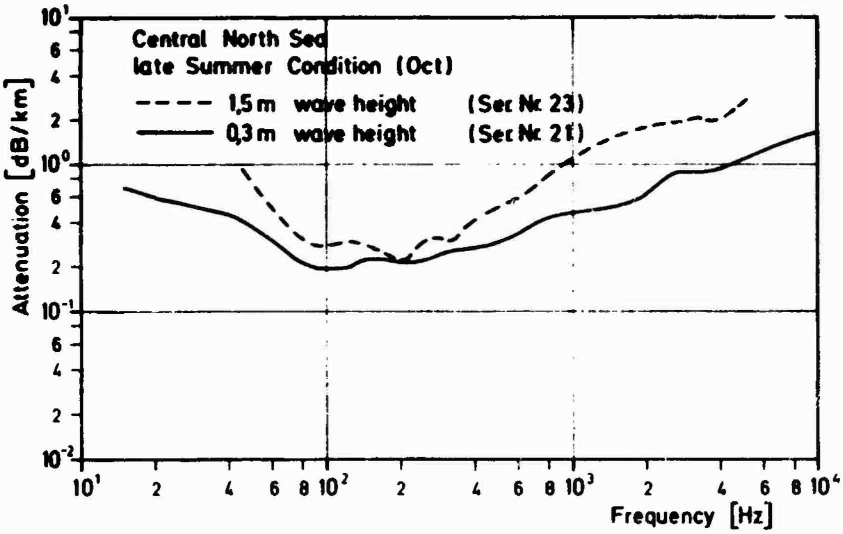

FIG. 10 MAXIMUM AND MINIMUM SLOPE OF ATTENUATION LOSS CURVE – NORTH SEA

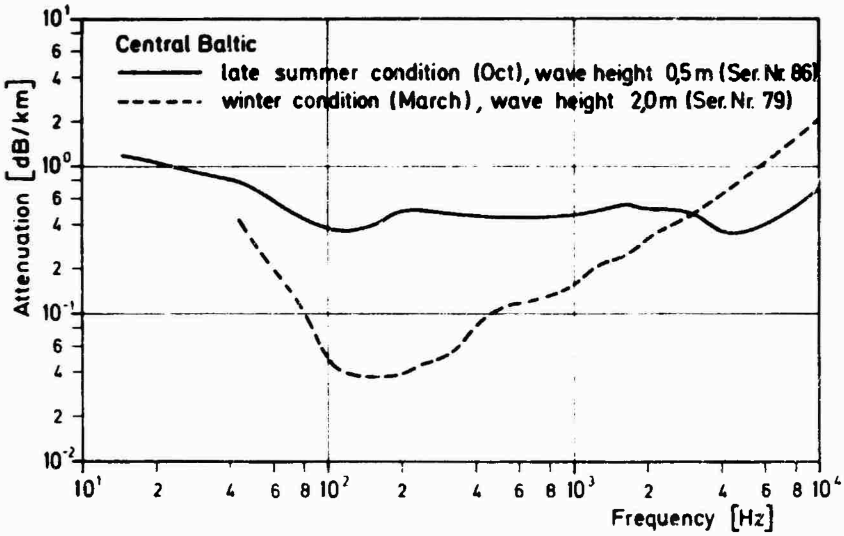

FIG. 11 MAXIMUM AND MINIMUM SLOPE OF ATTENUATION LOSS CURVE – BALTIC SEA

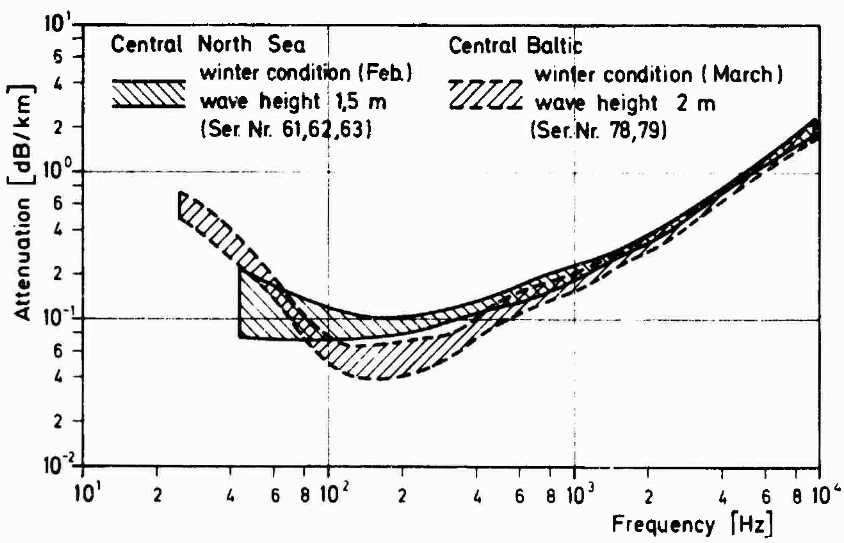

FIG. 12 COMPARISON OF ATTENUATION LOSS – BALTIC SEA, NORTH SEA

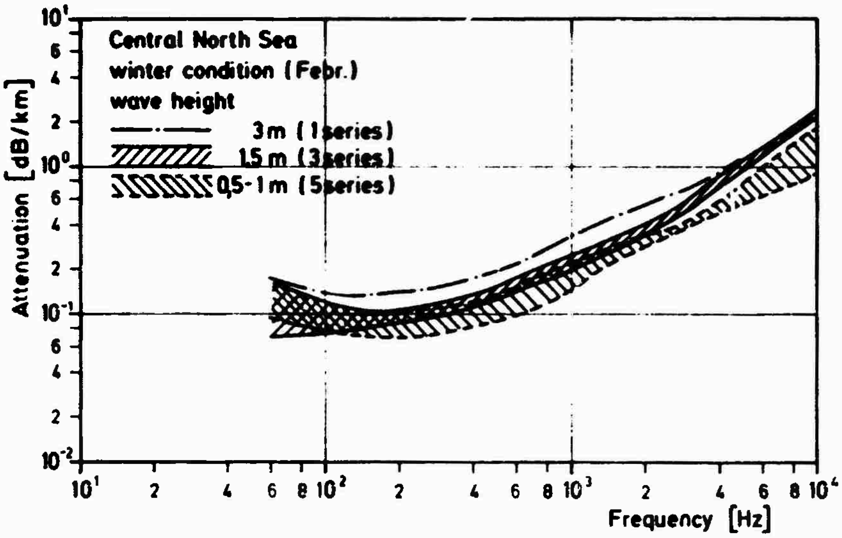

FIG. 13 INFLUENCE OF WAVE HEIGHT ON ATTENUATION - NORTH SEA

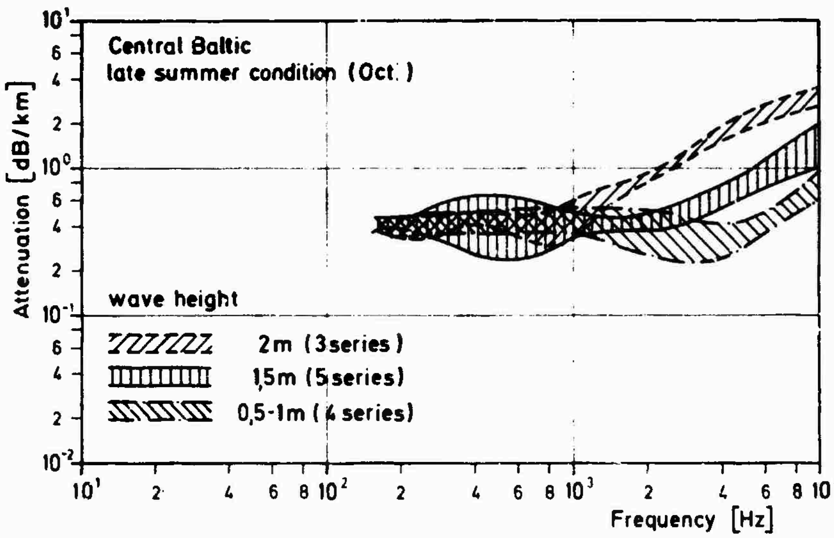

FIG. 14 INFLUENCE OF WAVE HEIGHT ON ATTENUATION - BALTIC SEA

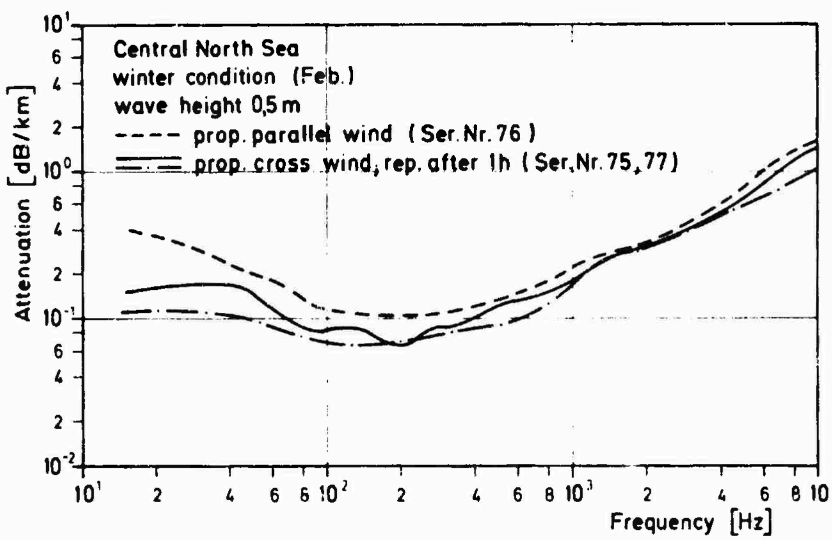

FIG. 15 POSSIBLE INFLUENCE OF SEA WAVE DIRECTION ON ATTENUATION

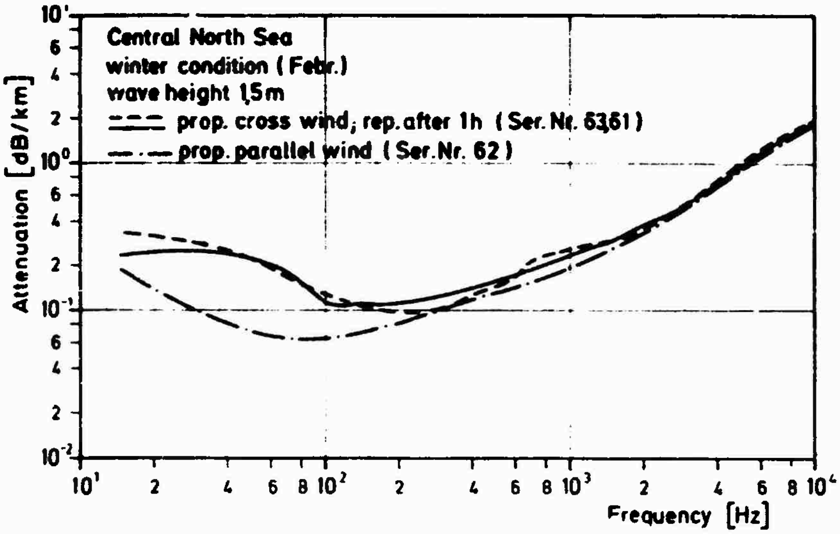

FIG. 16 POSSIBLE INFLUENCE OF SEA WAVE DIRECTION ON ATTENUATION

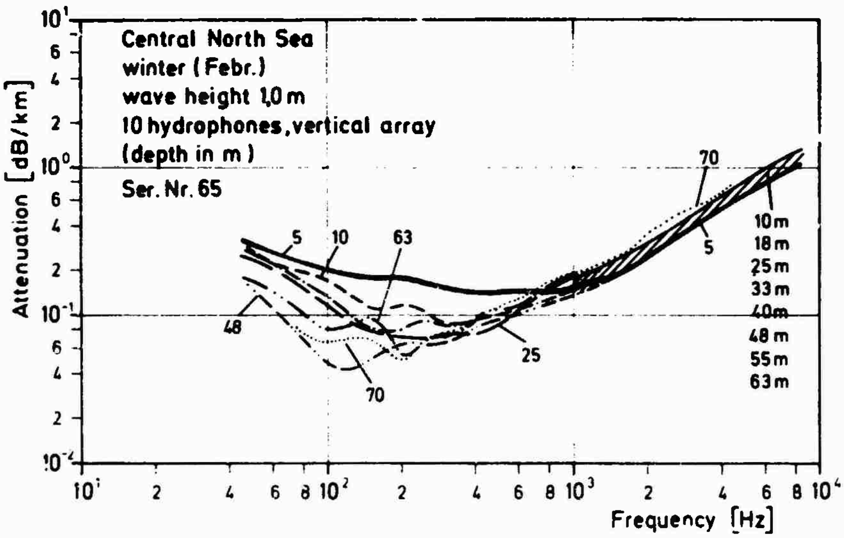

FIG. 17 ATTENUATION FOR DIFFERENT RECEIVER DEPTHS, WINTER CONDITION

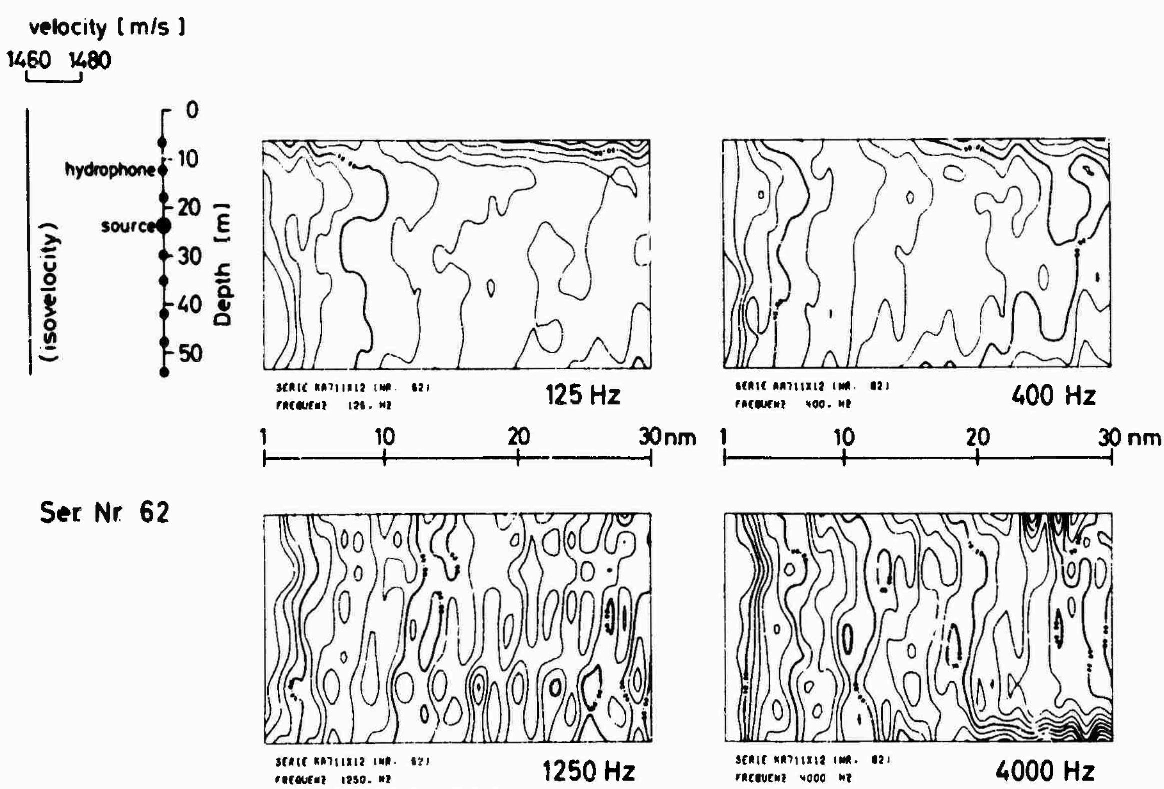

FIG. 18 MEASURED FIELD OF SOUND INTENSITY – NORTH SEA, WINTER CONDITION

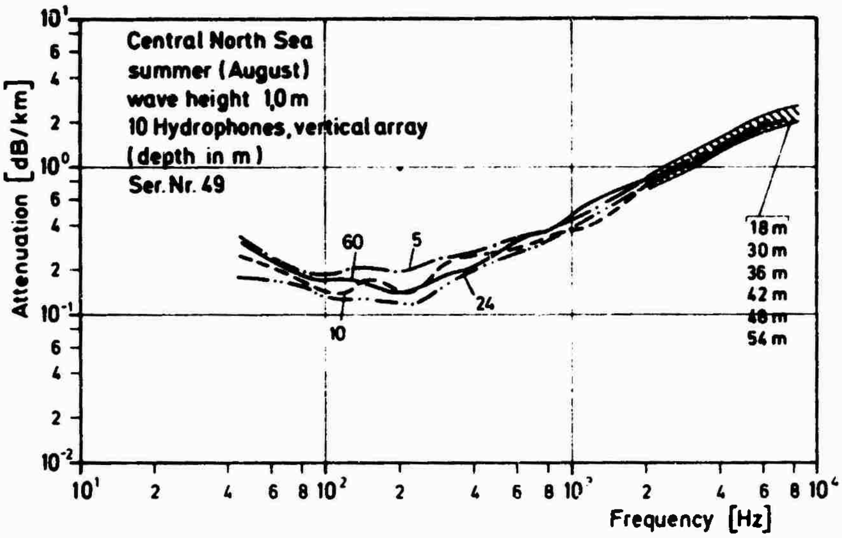

FIG. 19 ATTENUATION FOR DIFFERENT RECEIVER DEPTHS, SUMMER CONDITION

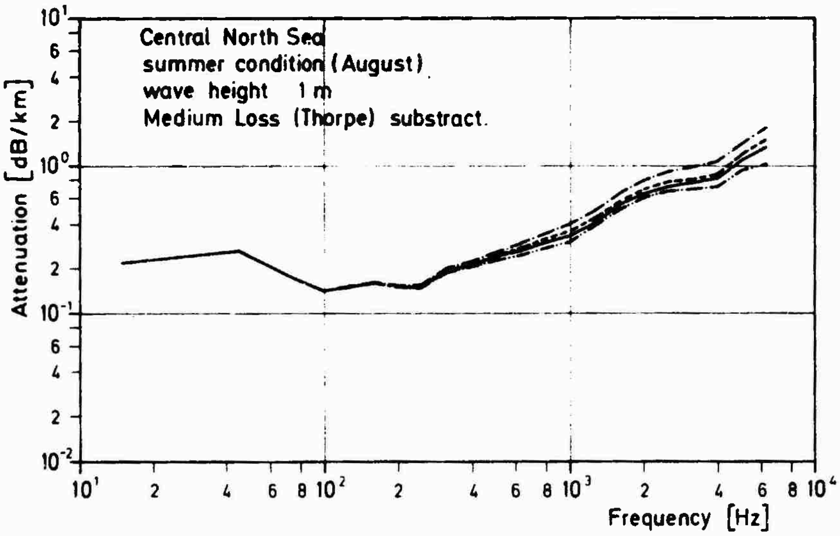

FIG. 20 POSSIBLE CONTRIBUTION OF MEDIUM ATTENUATION – NORTH SEA

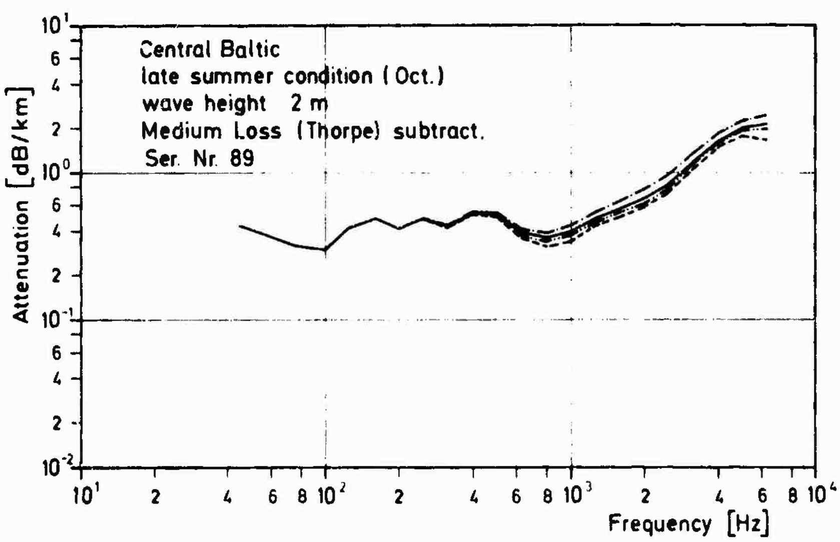

FIG. 21 POSSIBLE CONTRIBUTION OF MEDIUM ATTENUATION – BALTIC SEA

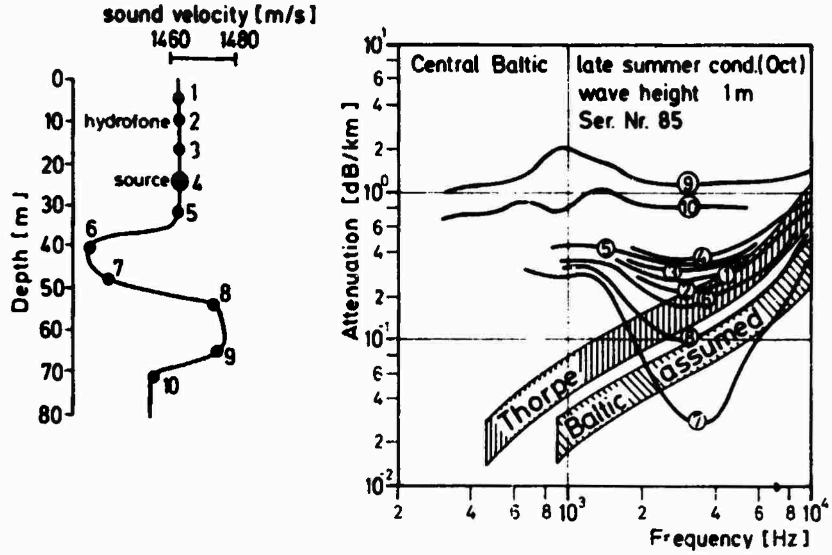

FIG. 22 ATTENUATION NEAR AXIS OF TEMPERATURE SALINITY CHANNEL - BALTIC SEA

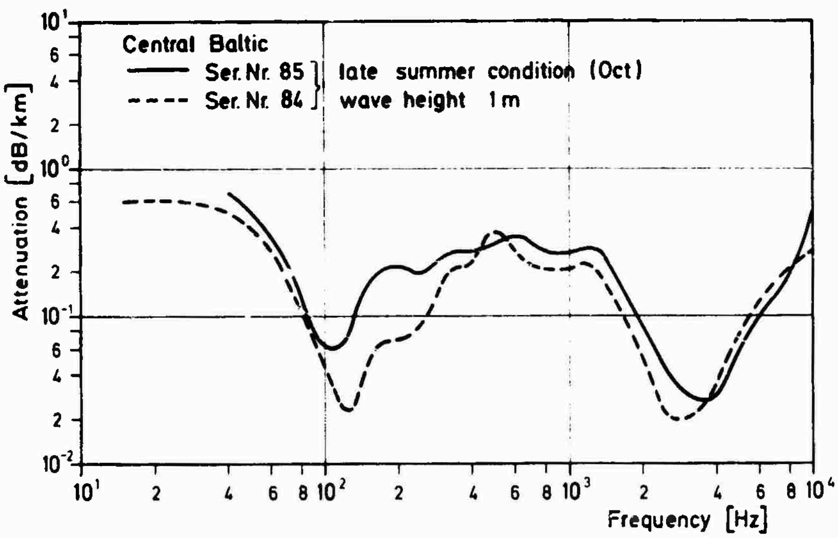

FIG. 23 ATTENUATION NEAR CHANNEL AXIS - BALTIC SEA (EXAMPLES OF TWO MINIMA)

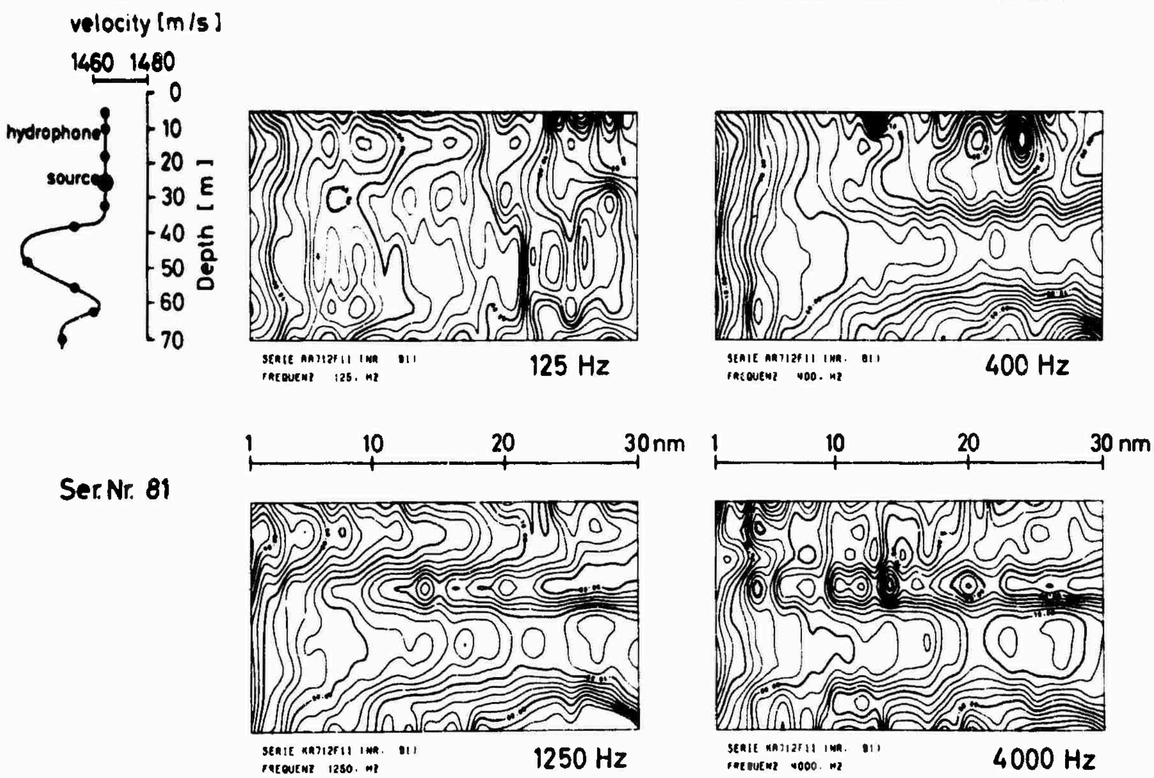

FIG. 24 MEASURED FIELD OF SOUND INTENSITY - BALTIC SEA, LATE SUMMER CONDITION

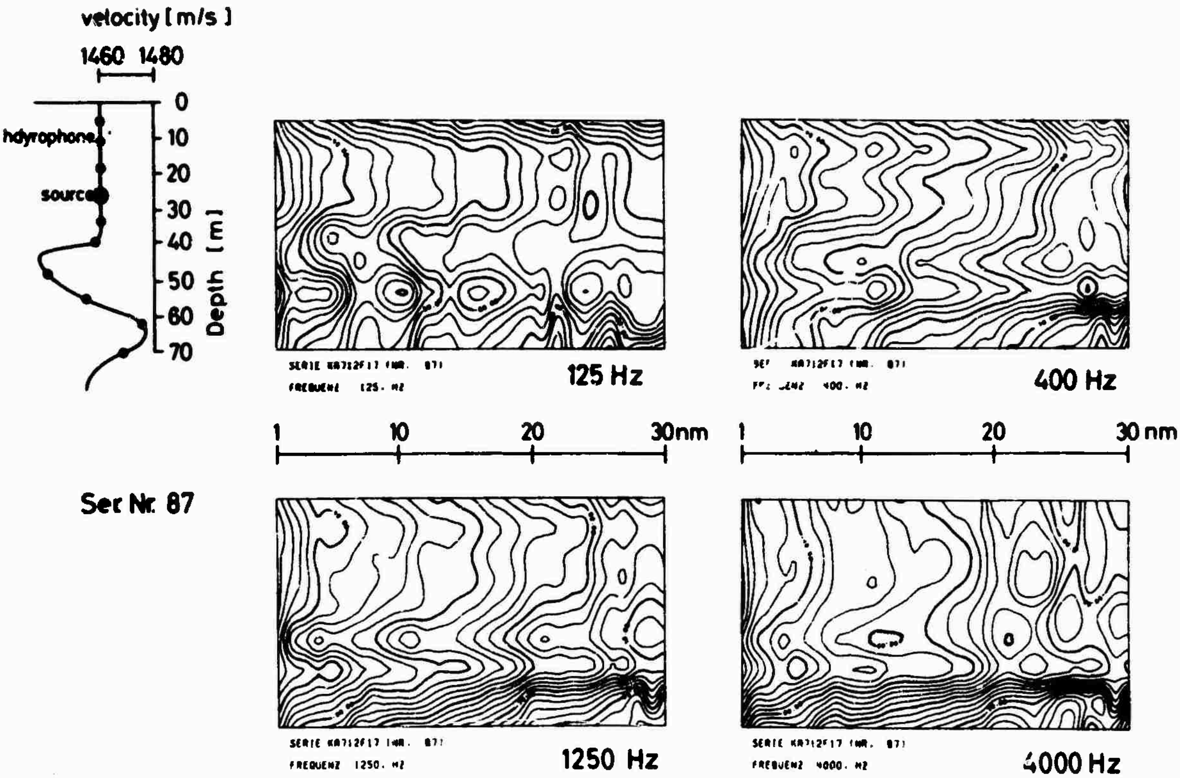

FIG. 25 MEASURED FIELD OF SOUND INTENSITY – BALTIC SEA, LATE SUMMER CONDITION

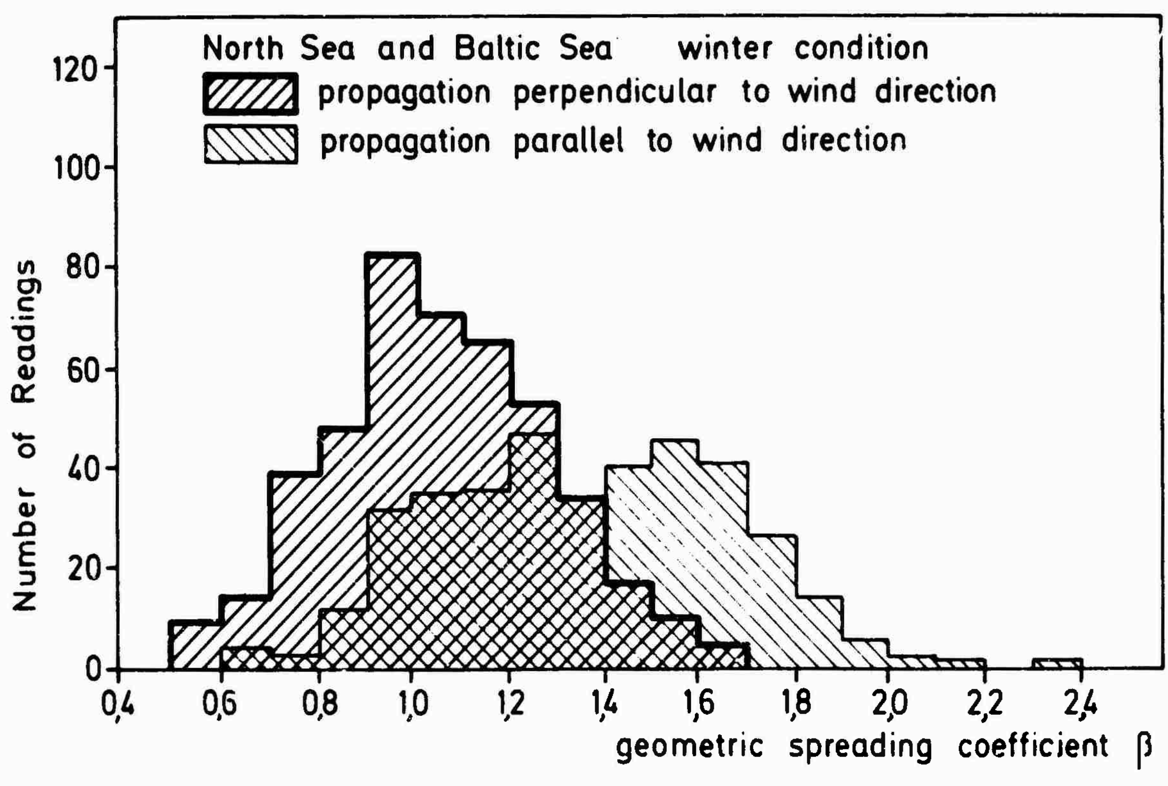

FIG. 26 DISTRIBUTION OF GEOMETRIC SPREADING COEFFICIENT β

EXCITATION, PROPAGATION, AND ATTENUATION OF ACOUSTIC NORMAL MODES IN SHALLOW WATER

by

F. Ingenito
US Naval Research Laboratory, Washington, DC, USA

ABSTRACT

The problem of acoustic propagation in shallow water was approached by studying, both experimentally and theoretically, the discrete normal modes of the duct. Mode separation was achieved experimentally by two methods, a temporal method depending on the differing group velocities of the modes and a spatial filtering method depending on their vertical pressure distributions. Varying the depth of the source and using a vertical array of hydrophones spanning most of the water column, modal excitations and modal pressure distributions were measured. Mode attenuations were obtained by making measurements on a mode at a series of ranges. Data were taken at frequencies of 400, 750, and 1500 Hz for a variety of sound-velocity profiles in several different areas. As many as three modes were identified and measured. Results were compared with normal mode calculations applied to idealized models of the areas. Relative arrival times, modal excitations and vertical pressure distributions agreed well with the calculations. Comparisons of measured mode attenuations with calculations were made, but the results were less conclusive because of the lack of independent knowledge of the bottom properties. Of particular interest are the data taken over a consolidated bottom, where shear-wave excitation is probably important and over a sloping bottom where mode conversion may be taking place.

INTRODUCTION

It is generally conceded that the full apparatus of wave theory is required to treat the problem of sound propagation in shallow water. However, simplifying assumptions must be made about the ocean environment in order for the problem to be tractable mathematically. If it is assumed that the surface and bottom boundaries are smooth and parallel and that the environmental properties are dependent only upon depth, the wave equation, expressed in cylindrical coordinates, separates into two ordinary differential equations. The range equation can then be solved in closed form and the depth equation, together with the boundary conditions, define an eigenvalue problem which can be solved numerically. The solution indicates that propagation occurs in the normal modes of the system, each modal field characterized by a distinctive field distribution and propagation velocity.

This is an attractive and fairly simple picture, but the assumptions of normal mode theory do not hold exactly in the real ocean, so the question arises as to whether the normal mode method is useful in a realistic situation. This paper will present the results of experiments designed to validate normal mode theory and some modifications of the basic model.

1. THEORY

The geometry is shown in Fig. 1. A layer of water is bounded above by air (this is considered to be a pressure release boundary) and below by several bottom layers (only two are shown in the figure). The final semi-infinite bottom layer has a constant sound velocity and density while the sound velocities in the other layers, including the water, can vary with depth. All the densities are constants. Normal mode theory predicts that at long ranges from a harmonic point source of unit source strength the pressure $p(r, z, t)$ (including only the N discrete modes) is

$$p(r,z,t) = \omega\rho^2 \left(\frac{1}{8\pi r}\right)^{1/2} \sum_{n=1}^{N} \frac{u_n(z_0)u_n(z)}{k_n^{1/2}} e^{i[k_n r - \omega t] - \delta_n r}, \qquad \text{[Eq. 1]}$$

where r is the range,

z_0 is the source depth,

z is the receiver depth,

ω is the radial frequency and

ρ is the water density.

The modal wave numbers k_n and the normalized functions $u_n(z)$ are determined by the solution of the eigenvalue problem defined by the depth dependent part of the separated wave equation. A modal attenuation term $e^{-\delta_n r}$ has been added to account for losses in the system.

Equation 1 predicts that with the source at a constant depth z_0 the vertical pressure distribution of the nth mode is proportional to $u_n(z)$. Similarly if the receiver is held at a fixed depth z the source excitation of a mode is proportional to $u_n(z_0)$. We have performed a series of experiments under a variety of environmental conditions to test these predictions and also to measure the mode attenuation coefficients δ_n [Refs. 1, 2 and 3].

2. EXPERIMENTAL MODE RESOLUTION AND IDENTIFICATION

To make measurements on individual modes it is necessary to isolate and identify them. Two methods were used to resolve the modes. The first method makes use of the fact that the normal modes usually

have different group velocities. Thus, if the source emits very short pulses and the receiver is at sufficiently long range the modes can be separated in time. Using a vertical array of receivers covering most of the water depth their vertical pressure distributions can be measured. Figure 2 shows an example of the received signal from a 750 Hz omnidirectional source. This is an oscillographic recording of the outputs of twelve hydrophones spaced two metres apart in approximately 30 m of water. Time progresses from left to right. The hydrophones are arranged vertically so that observation of the phase changes in a distinct arrival can be used to identify a mode. The first arrival has a single 180° phase change, between the 11 m and 13 m hydrophones, indicating a null in that region. The second arrival has no phase changes and therefore no nulls. We conclude that the earliest arrival is the second mode and the next is the first mode. Theoretical calculations of the relative time of arrival agree with this conclusion. The vertical pressure distributions can then be measured directly from the oscillographic recording. A known calibration signal is also recorded so that absolute measurements can be made.

The second method of mode resolution is based on the orthogonality of the normal modes. Again a vertical array of receivers spaced over the depth of the water is used. The gain and polarity of each identical hydrophone is set to be proportional to the calculated amplitude of the desired mode at the hydrophone depth and the outputs of all the hydrophones are summed. Because of the orthogonality of the modes the array acts as a "mode filter" suppressing the other modes relative to the selected mode. Naturally it is necessary to calculate the mode functions in advance to properly shade the array.

In our experiments the first method was usually employed when enough temporal separation was available; the "mode filter" was sometimes used to measure mode excitation and mode attenuation. In any case, since all the hydrophone outputs were recorded on magnetic tape, either method could be employed in the analysis of the data.

3. RESULTS FOR RANGE-INDEPENDENT ENVIRONMENTS

Figures 3, 4, and 5 show comparisons between measured pressure amplitude distributions and the mode amplitude functions $u_n(z)$ for three types of sound velocity profiles: isovelocity, upward refracting, and downward refracting. The measured velocity profile for each case is shown in the right of the figure. Each of the measured values represents the average peak pressure amplitude for ten transmissions occurring within approximately seven minutes for each set. The calculated mode amplitude functions have been so scaled that the maximum value within each mode matches the pressure amplitude at that depth. It can be seen that the measurements and calculations agree reasonably well in all three cases.

Measurements of the source excitation can be made by varying the source depth while fixing attention on a single receiver, or by the "mode filter" method described above. The results can be compared with the mode amplitude function $u_n(z_0)$. Figure 6 shows an example of such measurements for the first three modes at 750 Hz. This type of measurement is subject to a problem not encountered in measurements of the vertical pressure distribution. Because of the time required to raise and lower the source, it took two hours to obtain the data shown in the figures, leading to some ambiguity between spatial and temporal effects. In addition, phase changes in the source excitation are not observable; this is indicated in the figure by plotting all points with the same phase.

The mode attenuation coefficients δ_n were obtained by measuring the pressure amplitude as a function of range with source and receiver depths held constant. Alternatively, the mode filter could be used with the source depth held constant. The source ship took stations at various ranges from the receivers and at each station the source was lowered to several depths previously chosen to maximize the strength of the desired modes. At each source depth a five minute run of approximately 50 three-cycle pulses was made. In one day it was possible to do five range stations, enough to obtain the attenuation coefficients from the slopes of the pressure amplitude vs range curves. Usually the sound velocity profile, which was measured at each range station, changed only slightly during the day. More drastic changes could be corrected for in the analysis. An example of the results is shown in Fig. 7. The data were taken over a very smooth semi-consolidated bottom. The measured attenuation coefficients as functions of frequency and mode number give clues as to the causes of the loss. The analysis of the data shown in the figure, plus data not shown, is not complete, but it is believed that the major cause of the loss was the excitation of shear waves in the bottom. The shear velocity of the bottom in this area is high but less than the sound velocity in the water, so that shear waves excited in the bottom carry energy away from the water layer. Other mode attenuation measurements over unconsolidated bottoms have given reasonable agreement with theory [Ref. 3].

4. RANGE-DEPENDENT ENVIRONMENTS

We have collected a substantial body of data, from which the examples given in this paper have been selected, which tends to show the basic correctness of the normal mode picture in range-independent situations. If the water is not of constant depth, or the sound velocity profile changes with range, or both, the wave equation does not separate and normal mode theory breaks down. In areas where the changes in depth and sound velocity with range are gradual, as is frequently true on the continental shelf, a simple extension of the normal mode method is often used [Ref. 4]. It is assumed that the normal mode gradually adapts to local conditions and that any energy initially in a mode remains in that mode. Mathematically $u_n(z_0)$ in Eq. 1 is replaced by the mode amplitude function calculated using the depth and sound velocity profile at the source and $u_n(z)$ is replaced by the function calculated using the depth and velocity profile at the receiver. The wave number k_n is replaced by an

averaged wave number given by the expression $\frac{1}{r}\int_{0}^{r} k_n(r')dr'$. This means that the vertical pressure distribution and source excitation are determined solely by local conditions.

We have recently performed experiments in an area of changing water depth to test this theory [Ref. 5]. In these experiments the receiving array was kept fixed while the source ship took stations at increasing ranges from the receivers. The measurements and analysis were performed as described above.

Figures 8 and 9 show some of the results as the source ship moved into shallower water. The vertical pressure amplitude distribution did not vary significantly with range. At zero range in the figures a typical pressure distribution is shown compared with the mode amplitude function calculated at that point. Source excitation measurements taken at about 9 km and 17 km from the source are also shown in the figures. The latter are compared with mode amplitude functions calculated using the depth and velocity profiles at those ranges. For this region of very gradual slope very good agreement is obtained, verifying the correctness of the assumptions.

When the bottom slope is much greater however, the results are quite different. Figures 10 to 12 show data taken as the source ship moved into deeper water and the depth changed more rapidly. We notice that while the pressure distribution is still predicted quite accurately, the predictions of source excitations become worse as depth and bottom slope increase.

For example, in Fig. 10 at the 12 km range a significant source excitation is measured for the first mode at the shallowest depth, contrary to the calculated mode excitation function. At this source depth higher order modes are excited, and it appears that energy from these modes is being converted into the first mode. The other figures also show a failure of the modified normal mode method in this case.

A further complicating factor, not shown in the figures, was a significant change in the sound velocity profile as the water depth increased. Whereas at the receivers the profile was very nearly isovelocity, a negative gradient developed near the bottom and became more pronounced at the longer ranges. The combination of increasing bottom slope and changing velocity profile apparently exceeded the limits of the validity of the model. A more detailed model accommodating these effects is needed.

Mode attenuation experiments were also performed in the same area, but the data has not been reduced and analysed.

CONCLUSIONS

We conclude that the normal mode model works well in the real ocean in range-independent situations, and it can be easily modified to accommodate situations in which the environment varies slowly with range. For more rapid changes, the method fails and a model including mode coupling effects is needed.

Finally, Eq. 1 can be used to compute propagation loss. We have recently taken propagation loss data using both CW and explosive sources in conjunction with our normal mode measurements. This data, when reduced and analysed can be used to validate a propagation loss model based on normal mode principles.

ACKNOWLEDGEMENTS

This work was supported by NAVSEA Code 06H1-4 and the US Office of Naval Research.

REFERENCES

1. R.H. Ferris, F. Ingenito, and A.L. Faber, "Experimental Separation and Identification of Acoustic Normal Modes in Shallow Water," NRL Report 7174 (1970).

2. R.H. Ferris, J. Acoust. Soc. Am. 52, 981 (1972).

3. F. Ingenito, J. Acoust. Soc. Am. 53, 858 (1973).

4. e.g., R.N. Denham, J. Acoust. Soc. Am. 39, 1170 (1966).

5. S.N. Wolf, to be published.

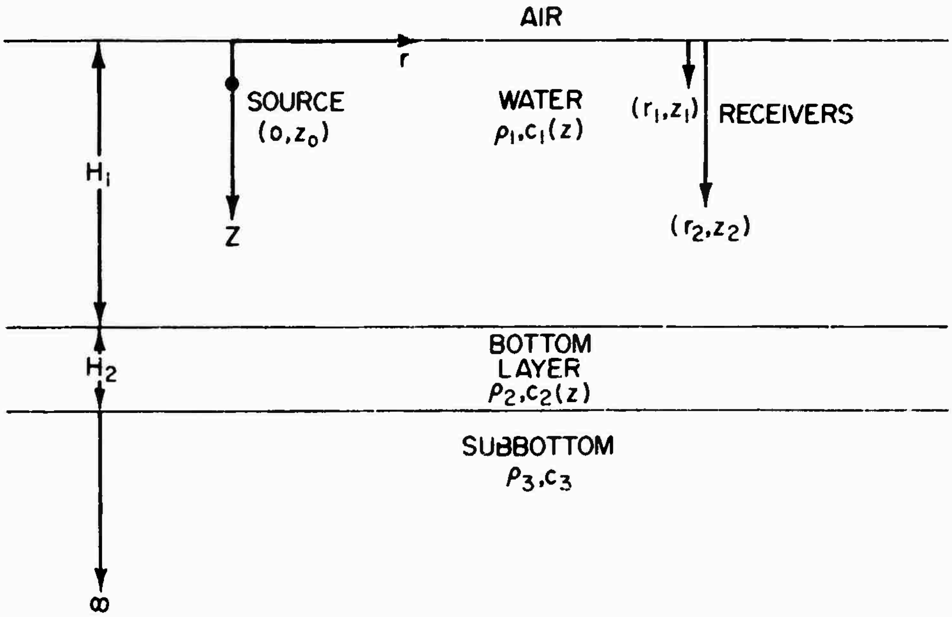
AIR
r
SOURCE
(o,z_0)
WATER
$\rho_1,c_1(z)$
(r_1,z_1)
RECEIVERS
H_1
Z
(r_2,z_2)
BOTTOM
LAYER
$\rho_2,c_2(z)$
H_2
SUBBOTTOM
ρ_3,c_3
∞

FIG. 1

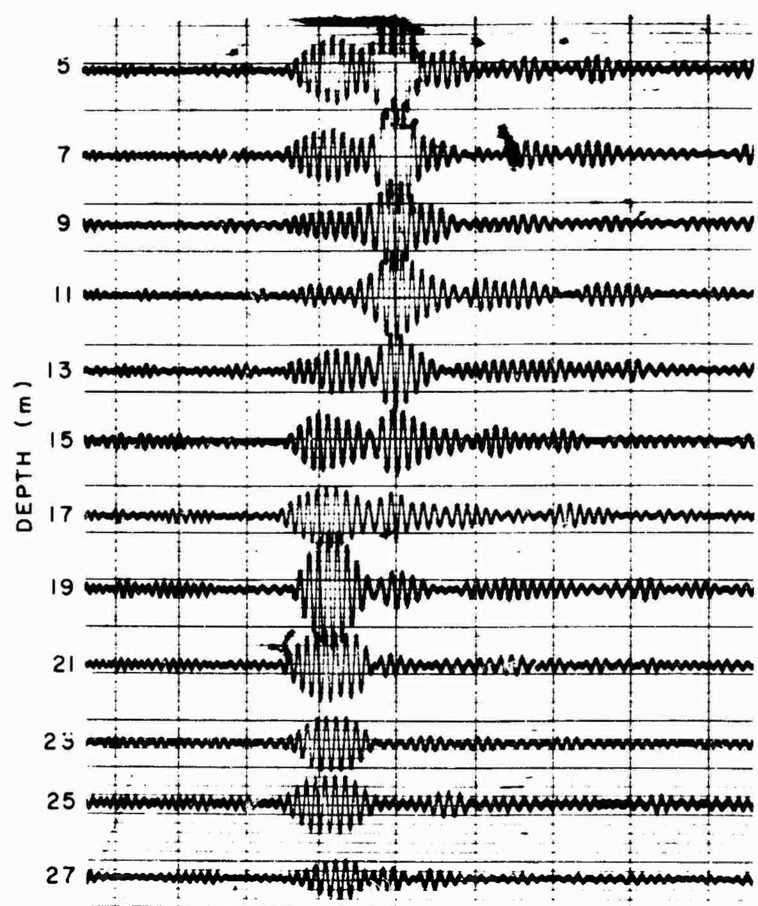
DEPTH (m)
5
7
9
11
13
15
17
19
21
23
25
27

FIG. 2

FIG 3

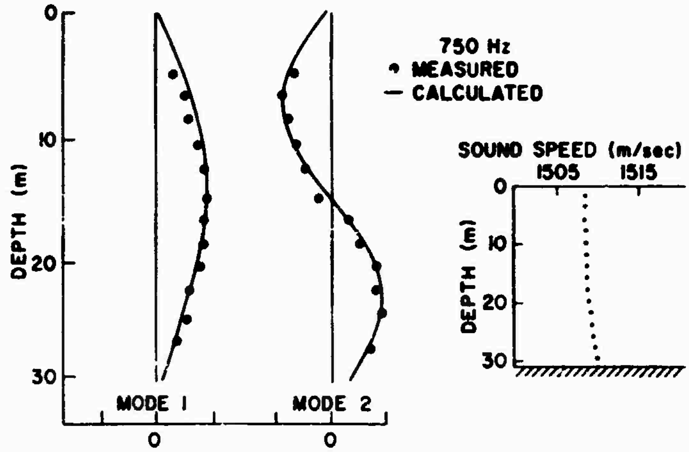

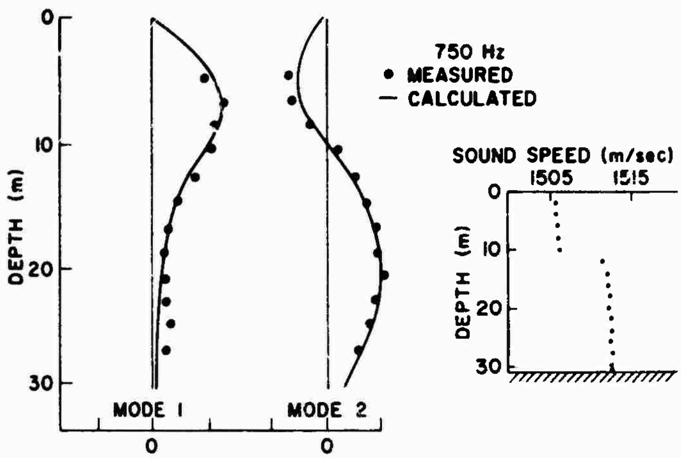

FIG. 4

FIG. 5

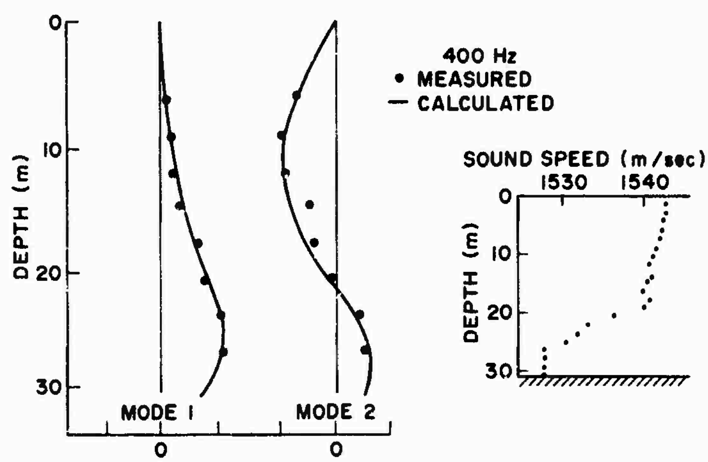

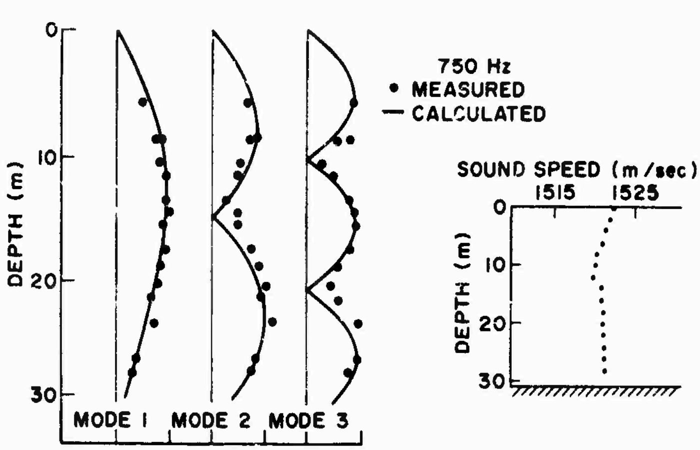

FIG. 6

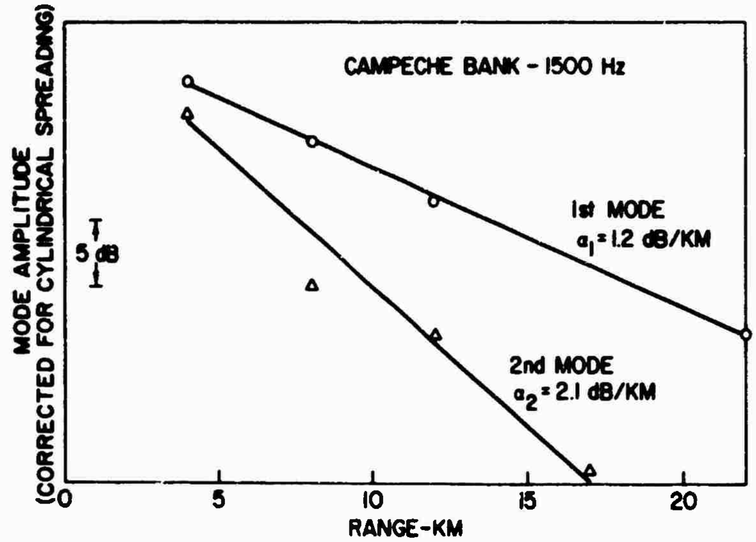

FIG. 7

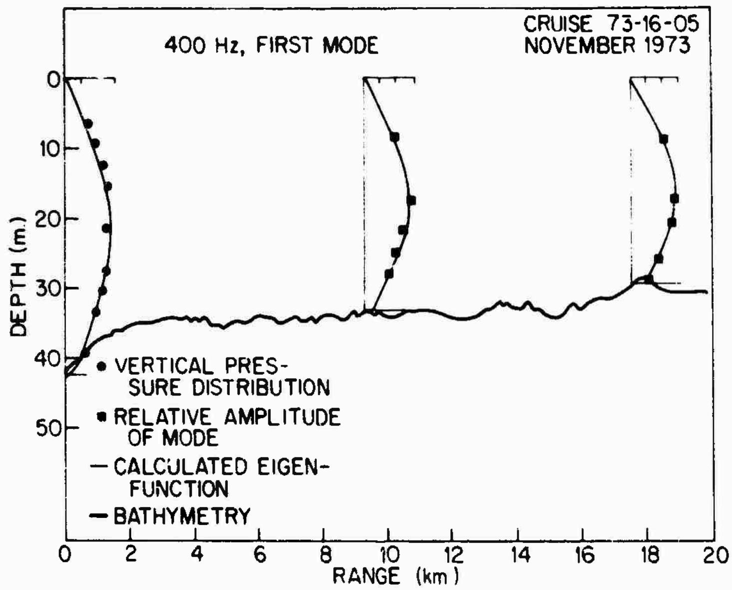

FIG. 8

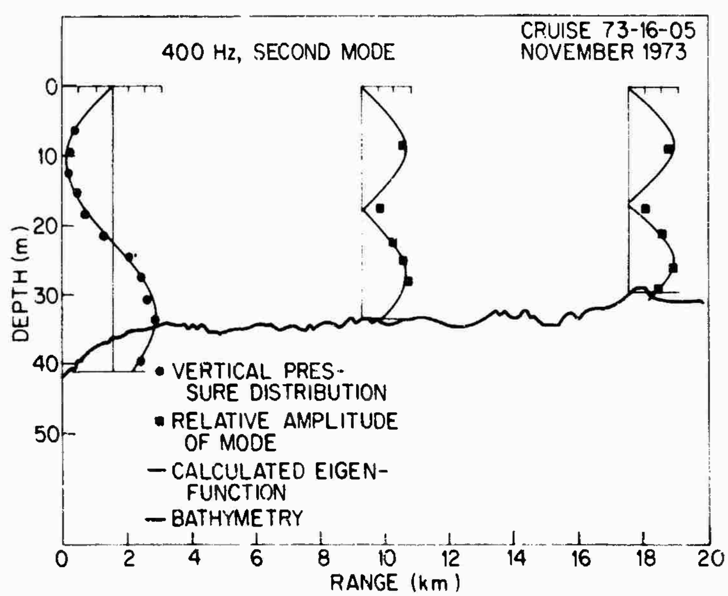

FIG. 9

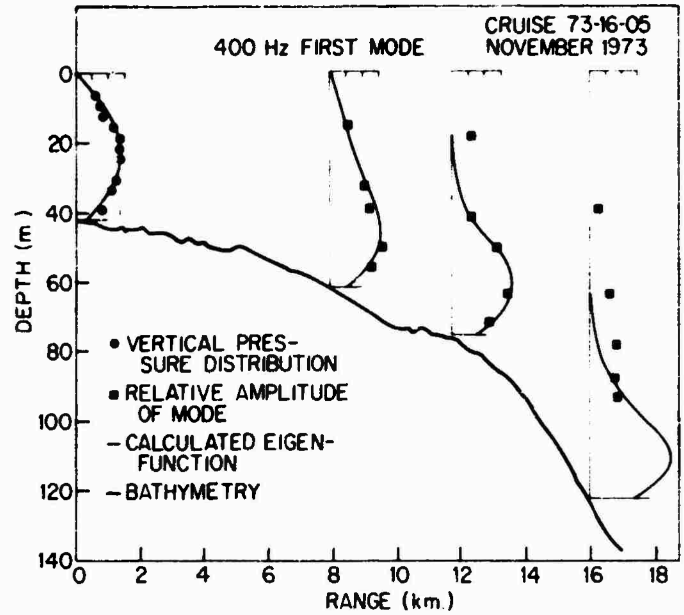

FIG. 10

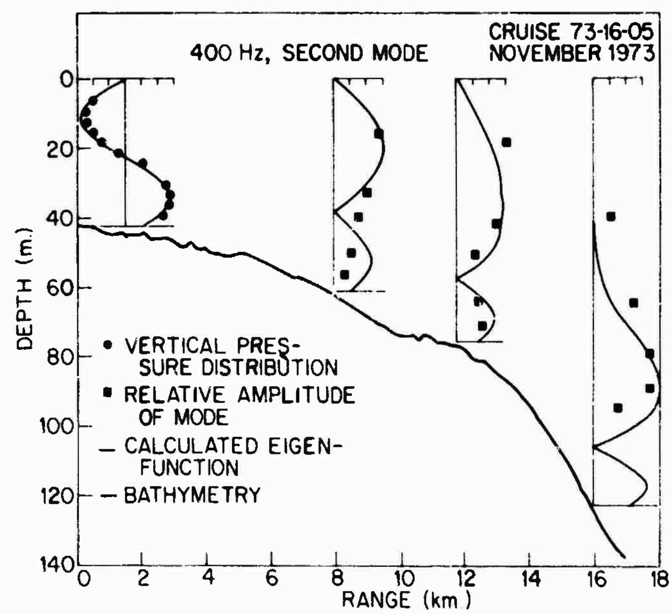

FIG. 11

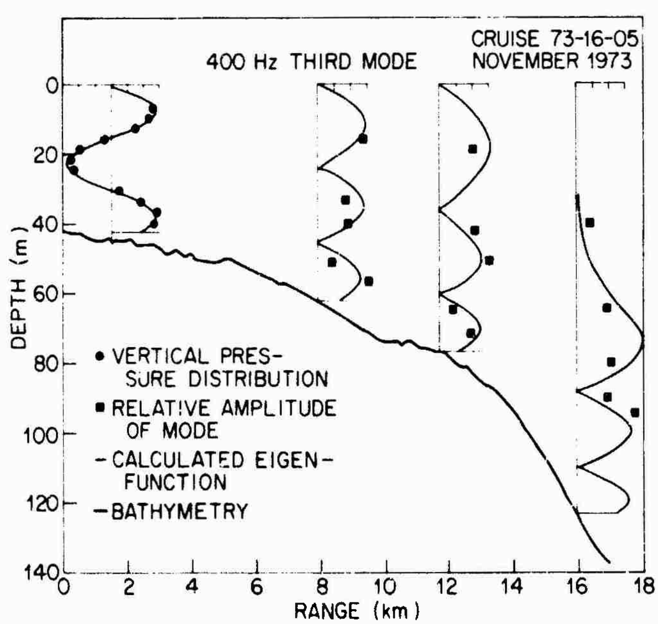

FIG. 12

COMPARISON OF TRANSMISSION LOSS DATA FOR DIFFERENT SHALLOW-WATER AREAS WITH THEORETICAL RESULTS PROVIDED BY A THREE-FLUID NORMAL-MODE PROPAGATION MODEL

by

F.B. Jensen
SACLANT ASW Research Centre
La Spezia, Italy

ABSTRACT

The sound propagation experiments were carried out in two different shallow-water areas under both summer and winter conditions. The acoustic runs were performed along tracks 35 km long in water of nearly constant depth (~110 m). The signals received from explosive sources by an array of hydrophones distributed over the water column were processed digitally to obtain transmission loss in 20 one-third octave filter bands with centre frequencies from 0.1 to 8 kHz. The experimental data have been compared with theoretical results provided by a range-independent normal-mode computer program based on a three-fluid propagation model, and the agreement found between theory and experiment is generally excellent for the entire frequency range.

INTRODUCTION

A scanning of the literature on sound propagation in the ocean shows that a detailed comparison of broadband transmission loss data for shallow water with predictions given by a normal-mode propagation model does not exist. There could be several reasons for that, since the following three conditions have to be fulfilled to be able to carry out such a comparison successfully. First, you must be in possession of a sufficiently good sound propagation model. SACLANTCEN has had a good model at its disposal since April this year, when it received a new computer program from US Naval Research Laboratory, Washington, D.C., based on a three-fluid normal-mode propagation model. Second, you must have the necessary computer facility for handling big programs and be able to spend several hours of CPU time per week, since the mode calculation at high frequencies is very time consuming. At SACLANTCEN the computer facility has been excellent since the beginning of 1974, when a new UNIVAC 1106 computer was installed. The third condition is that you must have some high-quality experimental data from a shallow-water area that can be appropriately described by your computer model. Since 1969 SACLANTCEN has carried out an extensive program of broadband sound propagation measurements in various shallow-water areas under different environmental conditions. A substantial part of these

data have now been processed and a report was issued in April this year [Ref. 1]. Thus, for the past six months we have at SACLANTCEN been able to carry out a detailed comparison of experimental and theoretical results for sound propagation in shallow water in the frequency range 0.1 to 8 kHz. The results of this study will be presented in the following.

1. THE COMPUTER PROGRAM

The program used for calculating sound propagation losses in the ocean consists of two parts of which part one, containing the mode calculation, is a slightly improved version of a program named FLUIDT (600 statements) developed at US Naval Research Laboratory, Washington, D.C., while part two, containing the transmission loss calculation, is a program named MODEADD (1000 statements) developed at SACLANTCEN.

The mode calculation program FLUIDT treats the ocean as an idealized three-fluid model, see Fig. 1. The first fluid layer (the water) is characterized by having constant depth H, constant density ρ_0, flat surface, flat bottom, and a sound speed c_0 that varies only with depth. The water is bounded above by air and below by a two-layer fluid bottom. The upper part of the bottom is characterized by having constant thickness H_1, constant density ρ_1, and a compressional wave velocity c_1 that varies only with depth. This bottom layer is bounded below by a semi-infinite sub-bottom with constant density ρ_2 and constant compressional wave velocity c_2.

The FLUIDT program solves the depth-dependent part of the Helmholtz equation for this three-fluid model by means of a finite difference technique. For a given source frequency the number of trapped modes are found, and the mode amplitude functions are calculated. Further, the effect on each normal-mode amplitude in the water due to an assumed small wave attenuation in both bottom layers is calculated and expressed as a mode attenuation coefficient.

For further details on the mode solution technique, see Ref. 2, which actually treats a two-fluid model, but so far no official documentation exists for the three-fluid model.

The second part of the computer program called MODEADD calculates the transmission loss by adding up the modes. According to Ref. 3, the pressure field from a point source of unit source strength is at long ranges given by

$$P(r,z,t) = \frac{\omega\rho_0^2}{H} \sqrt{\frac{1}{8\pi r}} \sum_{n=1}^{NM} \frac{u_n(z_0)u_n(z)}{\sqrt{k_n}} \cdot e^{-\alpha_n r} \cdot e^{i(k_n r - \omega t - \frac{\pi}{4})} \quad \text{[Eq. 1]}$$

where

H = water depth

k_n = wave number

NM = number of modes

P = pressure

r = range

t = time

u_n = mode amplitude

z = depth

z_0 = source depth

α_n = modal attenuation coefficient

ρ_0 = water density

ω = source frequency .

Since we are only interested in the amplitude of the pressure field, the time-dependent factor $e^{-i\omega t}$ will be dropped from Eq. 1 in the following.

By introducing the abbreviations

$$A_n = \frac{u_n(z_0)u_n(z)}{\sqrt{k_n}} \cdot e^{-\alpha_n r} \qquad \text{[Eq. 2a]}$$

$$\theta_n = k_n r - \frac{\pi}{4}, \qquad \text{[Eq. 2b]}$$

equation 1 takes the form

$$P(r,z) = \frac{\omega\rho_0^2}{H} \sqrt{\frac{1}{8\pi r}} \sum_{n=1}^{NM} A_n \cdot e^{i\theta_n} \qquad \text{[Eq. 3]}$$

or

$$P(r,z) = \frac{\omega\rho_0^2}{H} \sqrt{\frac{1}{8\pi r}} \sqrt{\left(\sum_{n=1}^{NM} A_n \cos\theta_n\right)^2 + \left(\sum_{n=1}^{NM} A_n \sin\theta_n\right)^2} . \qquad \text{[Eq. 4]}$$

In this expression for the pressure field the modes have been phase coherently added.

Since the pressure amplitude at a distance of 1 m from a point source of unit source strength is given by

$$P_1 = \frac{\omega\rho_0^2}{4\pi} \qquad \text{[Eq. 5]}$$

the transmission loss in dB re 1 m may be determined from the equation

$$TL = -20 \lg \frac{P}{P_1} \qquad \text{[Eq. 6]}$$

leading to

$$TL = -20 \lg \left[\frac{\rho_0}{H} \sqrt{\frac{2\pi}{r}} \sqrt{\left(\sum_{n=1}^{NM} A_n \cos \theta_n \right)^2 + \left(\sum_{n=1}^{NM} A_n \sin \theta_n \right)^2} \right]. \qquad \text{[Eq. 7]}$$

This expression for the transmission loss does not include loss due to volume attenuation in the water. The term to be added to the right hand side of Eq. 7 to include the volume attenuation may be found in Ref. 4:

$$TLVOL = (0.007 \cdot f^2 + 0.155 \cdot \frac{1.7\, f^2}{1.7^2 + f^2})\, R \qquad [\text{dB re } 1\,\text{m}] \qquad \text{[Eq. 8]}$$

where f is the source frequency in kHz and R the range in km.

The modal attenuation coefficient α_n appearing in Eq. 2a is composed of two contributions, one from each of the two bottom layers. Thus, α_n may be written

$$\alpha_n = \gamma_n' \beta_1 + \gamma_n'' \beta_2 \qquad [m^{-1}] \qquad \text{[Eq. 9]}$$

where γ' and γ'' are the dimensionless attenuation coefficients for the various modes due to an absorption of compressional waves in the two bottom layers. The γ-values are calculated by the mode program. β_1 and β_2 are the attenuation coefficients for compressional waves in the top bottom layer and the sub-bottom layer, respectively.

From an extensive collection of experimental data on compressional-wave attenuation in marine sediments, Hamilton [Ref. 5] concludes that the attenuation in dB/m is approximately dependent on the first power of frequency. Thus, it is convenient to express the attenuation coefficients β_1 and β_2 in dB/wavelength, since a fixed number for each β can then be used throughout the whole frequency range. If β_1 and B_2 are given in dB/WL, Eq. 9 becomes

$$\alpha_n = \gamma_n' \beta_1 \frac{\omega}{2\pi \bar{c}_1 (20 \lg e)} + \gamma_n'' \beta_2 \frac{\omega}{2\pi c_2 (20 \lg e)} \qquad [m^{-1}] \qquad \text{[Eq. 10]}$$

where c_1 is the mean sound speed in the top bottom layer and c_2 is the sound speed in the sub-bottom.

The MODEADD program calculates the transmission loss from Eqs. 7 and 8. Several options exist in the program, e.g. calculation of transmission loss vs range for a given source and receiver depth,

calculation of depth-averaged transmission loss vs range or frequency for a given source depth, or calculation of energy distribution over depth at a given range for different source depths. Examples will be shown later.

2. THE EXPERIMENTS

Shallow-water sound propagation measurements have been carried out in areas north and southeast of the Island of Elba along tracks 35 km long in water of nearly constant depth, approximately 110 m. In these areas there are no significant tidal effects, biological activity is negligible, the bottom is smooth, and there is very little reverberation. Therefore, repeated propagation trials can be performed in which only one environmental parameter is changed, such as: the bottom (in which the two areas differ), the sound speed structure (different seasons), or the sea state.

The propagation data presented in this paper were collected during cruises in August 1969 and February 1970. The measured sound-speed profiles are shown in Fig. 2, and it is seen that while the winter profiles taken north and southeast of Elba are almost identical, the summer profiles differ quite a bit with the steepest gradient recorded southeast of Elba. During the four acoustic runs, the signals from explosive sources were recorded by an array of hydrophones distributed over the water column, and the signals were processed digitally to obtain transmission loss in 20 one-third octave filter bands with centre frequencies from 0.1 to 8 kHz. For further details on the experimental procedure, see Ref. 1.

The experimental data were collected under essentially range-independent conditions: almost constant water depth for the entire acoustic track, and only slight variations in the sound-speed profile with range. Further, the bottom in the two areas was almost flat, and the experiments were carried out in relatively calm sea. This means that the possibility of getting acceptable predictions from the range-independent propagation model described earlier is good. The only difficulty seems to be the establishment of an appropriate model for the bottom, which on the other hand is an extremely important thing, especially when modelling acoustic propagation under downward refracting summer conditions, where the transmission losses exceed those measured under winter conditions by 20 to 30 dB.

3. PARAMETERS CHOSEN FOR THE "AVERAGE" BOTTOM

The bottoms north and southeast of Elba differ in the sense that a low-velocity sediment layer of thickness 5 to 6 m exists southeast of Elba but not north of Elba [Ref. 6]. The result of sound speed measurements in the bottom southeast of Elba is shown in Fig. 3. Three bottom cores were taken, one close to the receiving ship, one at range 10 km, and one at range 20 km. We see that the measured

compressional wave velocity in the upper 2 to 3 m is lower than the sound speed in the water just above the bottom (1470 m/s compared to 1508 m/s). It is also seen that a high-velocity sand layer is mixed into the low-velocity layer at depth 2.5 to 3.5 m.

Figure 3 shows that the measured sound-speed profile in the bottom varies with range. However, the sound propagation model requires as input an "average" bottom, and such a one can in fact be determined only by comparing predicted transmission losses with actually measured data. Thus, some physical parameters for the bottom will be considered as free parameters, and their values will be adjusted to give the best agreement between theory and experiment.

The parameter values chosen to represent an average bottom southeast of Elba are given in Fig. 3. Both the water depth $H = 106$ m and the thickness $H_1 = 6$ m of the top bottom layer were determined from echo soundings. The average density $\rho_1 = 1.5\ \rho_0$ for the top bottom layer was determined from density measurements in the core samples. The density $\rho_2 = 1.8\ \rho_0$ for the sub-bottom was determined from experimental data reported in the literature. Since compressional-wave attenuation was not measured in the core samples, an initial estimate for the two β-values were found in Ref. 5, but the final β-values were determined as to give the best agreement between theoretical and experimental transmission loss data. The dashed line shown in the figure is the average sound-speed profile chosen for the bottom. The introduction of a high-velocity sand layer in the model was necessary to get agreement between experimental and theoretical results at high frequencies.

The bottom north of Elba has no low-velocity sediment layer as seen from Fig. 4. Here the bottom is hard with a high-velocity layer close to the upper boundary. The attenuation coefficient β_1 for the top bottom layer is found to be larger for the hard bottom north of Elba (0.13 dB/WL) than for the soft bottom southeast of Elba (0.06 dB/WL), which was also to be expected from porosity measurements in the core samples.

4. COMPARISON OF THEORETICAL AND EXPERIMENTAL RESULTS

As previously mentioned, the influence of the bottom on the sound propagation in shallow water is largest under summer conditions, and therefore the adjustment of bottom parameters for a given model should be done by comparing predictions with data collected during summer trials. Figure 5 shows the depth-averaged transmission loss vs frequency at four different ranges for the summer experiment southeast of Elba. This way of presenting the experimental data is ideal for making comparison with theory and for adjusting bottom parameters, since by taking depth-averaged transmission loss, the receiver-depth parameter is eliminated from the problem. While experimental data exist for 20 frequencies in the range 0.1 to 8 kHz, the theoretical transmission losses have been determined for only 7 different frequencies, and this to limit the computation time, which is around $2\frac{1}{2}$ h for producing the dashed curves in Fig. 5. It is seen that a good agreement between theory and experiment has been obtained for the whole frequency range.

Now, by changing the sound-speed profile from a downward refracting summer profile to a slightly upward refracting winter profile, one more or less expects the same good agreement to exist between theory and experiment. However, as seen in Fig. 6 some disagreement exists particularly at two frequencies: 100 Hz and 400 Hz.

The adjustment of bottom parameters for the area north of Elba was carried out by comparing predictions with the summer data shown in Fig. 7. An excellent agreement between theory and experiment has been obtained. However, when comparing the calculated transmission losses with winter data (Fig. 8), it is seen that too low a loss is predicted at high frequencies.

As an illustration of the good agreement that generally exists between theoretical and experimental transmission loss data, a few examples for the southeastern area will be shown. In Figs. 9 and 10 the depth-averaged transmission loss vs range is given for two selected frequencies for summer and winter conditions, respectively.

In Figs. 11 and 12, transmission loss data for a single hydrophone are compared with predictions at two different frequencies. While the results shown are for a source depth of 30 m and a receiver depth of 50 m, the agreement between theory and experiment is just as good for a shallow receiver at 15 m depth and for a deep receiver at 100 m depth. Also for winter data the agreement between predicted and measured transmission losses are good, see Figs. 13 and 14. Here the source depth is 51 m and the receiver depth 50 m, but the agreement is just as good for the shallow and deep receiver.

Finally, it should be mentioned that having spent 50 to 100 h of computer time in finding an appropriate "average" bottom for the two areas, the production run on the computer took 12 h, and then transmission loss curves were produced for 7 different frequencies, for 3 different receiver depths, for transmission loss vs range, for depth-averaged transmission loss vs range and frequency, and all these calculations for 4 different trials: north and southeast of Elba for summer and winter. The maximum number of modes calculated was 325 for a source frequency of 6.4 kHz.

SUMMARY AND CONCLUSIONS

The good agreement found between experimental and theoretical transmission loss data clearly demonstrates that the three-fluid normal-mode program could become a powerful tool in shallow-water sound-propagation studies. However, the model applies only to nearly range-independent propagation cases, and besides, the computation time involved in modelling a broadband shallow-water experiment is presently so high, that it causes a natural limitation in the applicability of the program. Furthermore, the complexity of the three-fluid model requires a lot of information about the bottom, and that information is usually not available.

It is evident that one way of increasing the applicability of the computer program would be by putting more effort into the collection of bottom information, e.g. by measuring the compressional-wave attenuation in the upper bottom layers, since this would lead to a reduction of the number of free bottom parameters, and thus make the task of finding an appropriate "average" bottom much faster than at present. Further, the computer program could definitely be speeded up by changing some of the most time-consuming calculation loops.

Since the three-fluid model described in this paper is a range-independent model, and since propagation conditions in the ocean are essentially range dependent, it seems more important to try to develop a range-dependent normal-mode program than to refine the existing range-independent programs. It is clear that a range-dependent program would be much more complex than the existing models and require more information about various physical parameters for water and bottom, but such a program could very well be faster in use than the range-independent program, since the problem of parameter adjustment for the bottom would be avoided and thus 25 to 50 h of computer time saved per trial zone.

In short, the conclusions of this study may be summarized as follows:

1. When the propagation conditions are nearly range independent, it is possible with the three-fluid sound propagation model described here to obtain good agreement between theoretical and experimental transmission loss data for a broad frequency range.

2. The computer program based on the three-fluid model is at present too slow and ought to be speeded up considerably.

3. More information about the bottom is required.

4. The future modelling effort should be put into the development of a range-dependent normal-mode program rather than into the refinement of existing range-independent programs.

REFERENCES

1. MURPHY, E. and OLESEN, O.V. Broadband sound propagation trials in shallow water near the Island of Elba, SACLANTCEN SM-39. La Spezia, Italy, SACLANT ASW Research Centre, 1974.

2. NEWMAN, A.V. and INGENITO, F. A normal mode computer program for calculating sound propagation in shallow water with an arbitrary velocity profile. NRL Memorandum Report 2381, January 1972.

3. INGENITO, F. Measurements of mode attenuation coefficients in shallow water. Jnl Acoustical Society America, 53 (3), 1973: 858-863.

4. SKRETTING, A. and LEROY, C. Sound attenuation between 200 Hz and 10 kHz, SACLANTCEN TR 156. La Spezia, Italy, SACLANT ASW Research Centre, 1969.

5. HAMILTON, E.L. Compressional-wave attenuation in marine sediments. Geophysics, 37 (4), 1972: 620-646.

6. AKAL, T. et al Measured and computed physical properties of sediment cores - Island of Elba zone, SACLANTCEN M-82. La Spezia, Italy, SACLANT ASW Research Centre, 1972.

DISCUSSION

In answer to a question by Mr Cole about the ratio of the thickness of the bottom layer of the model to the wavelength of 400 Hz sound, Mr Jensen explained that these two lengths were comparable and it was therefore not surprising that some disagreement between theory and experiment could occur at that particular frequency [see Fig. 6].

Major Ross asked if there had been any need to invoke bottom or surface roughness to account for the agreement between theory and experiment over the wide frequency range. Mr Jensen answered that neither bottom nor surface roughness is included in the model, but that the slight disagreement found between theory and experiment at high frequencies for the winter data north of Elba [see Fig. 8] could possibly be accounted for by including surface scattering.

Prof Tacconi asked for an elaboration on the need for more information about the bottom. Mr Jensen said that what was primarily needed was information about bottom roughness and information about the attenuation of compressional waves and shear waves in the different bottom layers down to a depth of not less than one wavelength of the lowest frequency sound considered.

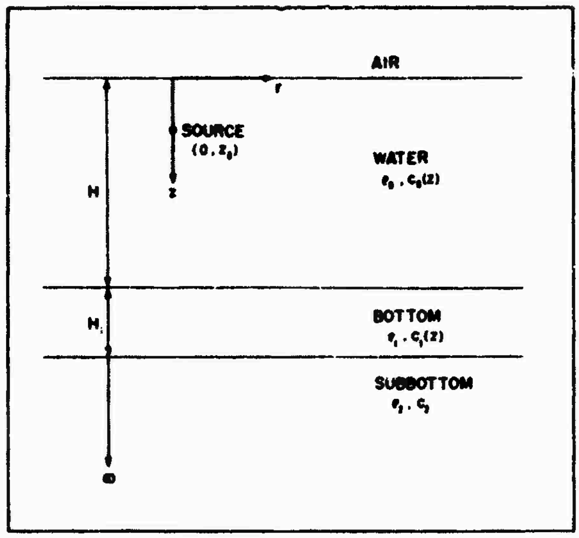

FIG. 1
CONFIGURATION OF THREE-FLUID SOUND PROPAGATION MODEL

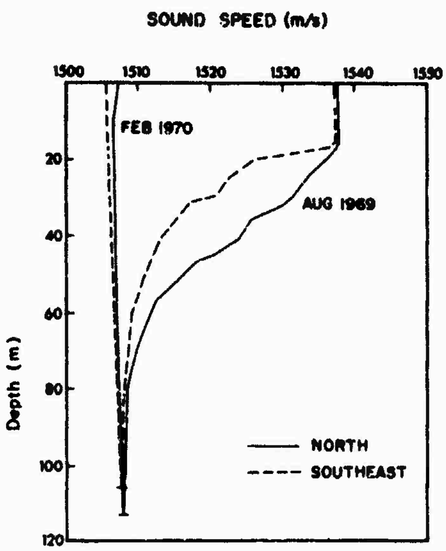

FIG. 2
SOUND SPEED PROFILES MEASURED NORTH AND SOUTHEAST OF ELBA IN 1969 AND 1970

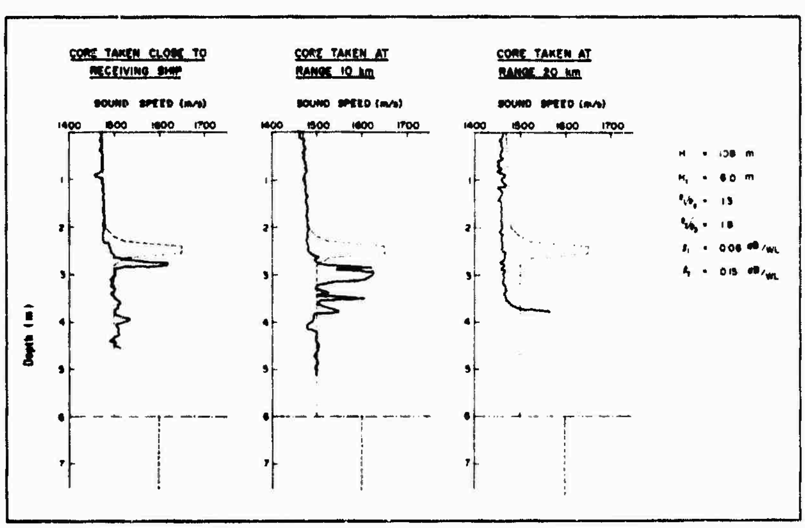

FIG. 3 MEASURED COMPRESSIONAL WAVE VELOCITY IN THE UPPER PART OF THE BOTTOM SOUTHEAST OF ELBA

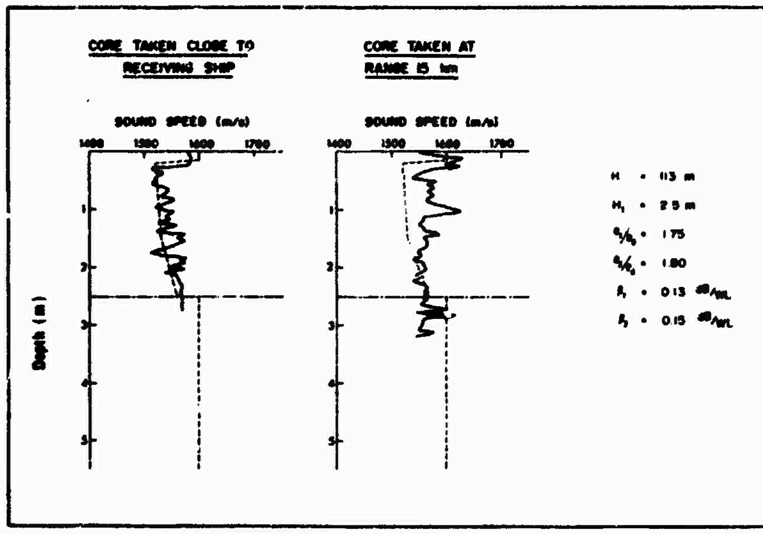

FIG. 4 MEASURED COMPRESSIONAL WAVE VELOCITY IN THE UPPER PART OF THE BOTTOM NORTH OF ELBA

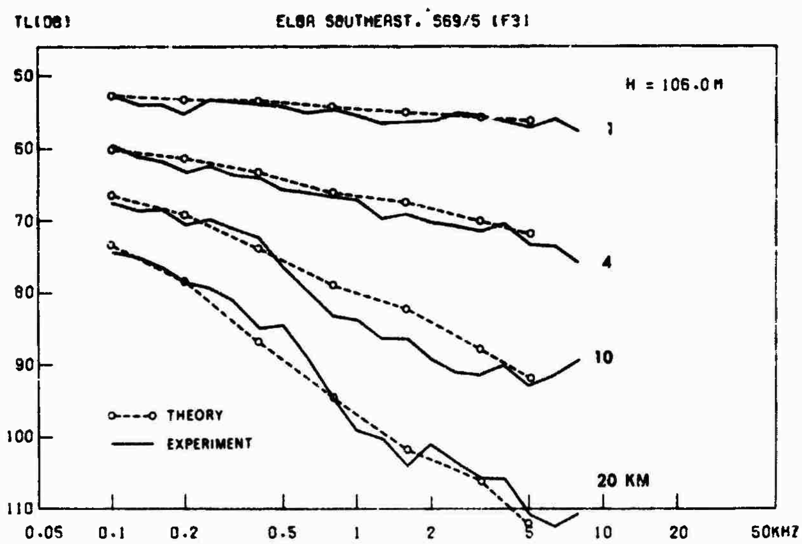

FIG. 5 DEPTH AVERAGED TRANSMISSION LOSS vs FREQUENCY AT RANGES 1, 4, 10, AND 20 km FOR SUMMER TRIAL SOUTHEAST OF ELBA

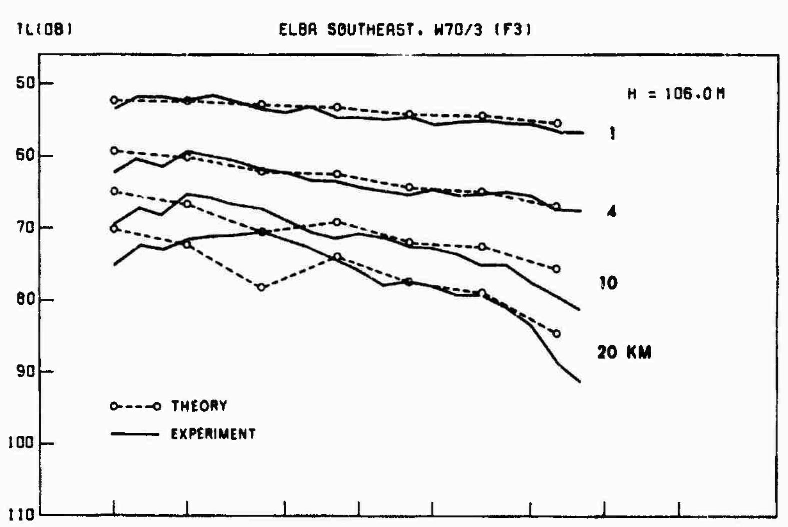

FIG. 6 DEPTH AVERAGED TRANSMISSION LOSS vs FREQUENCY AT RANGES 1, 4, 10, AND 20 km FOR WINTER TRIAL SOUTHEAST OF ELBA

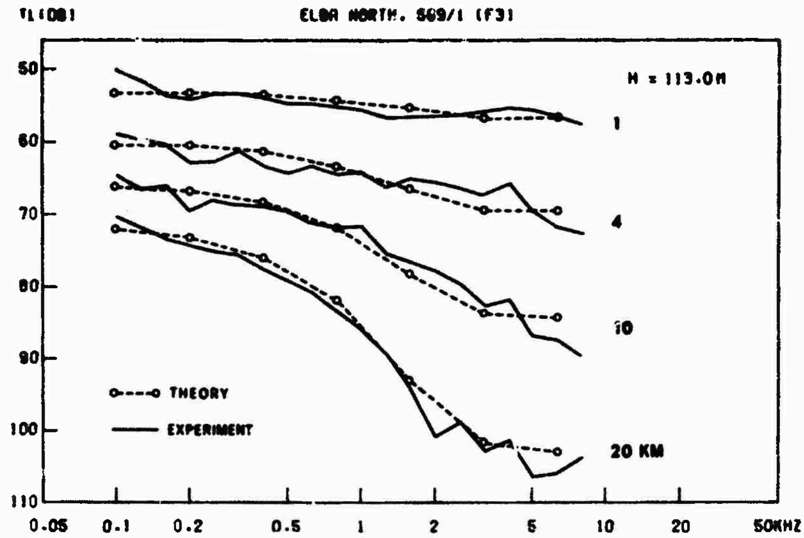

FIG. 7 DEPTH AVERAGED TRANSMISSION LOSS vs FREQUENCY AT RANGES 1, 4, 10, AND 20 km FOR SUMMER TRIAL NORTH OF ELBA

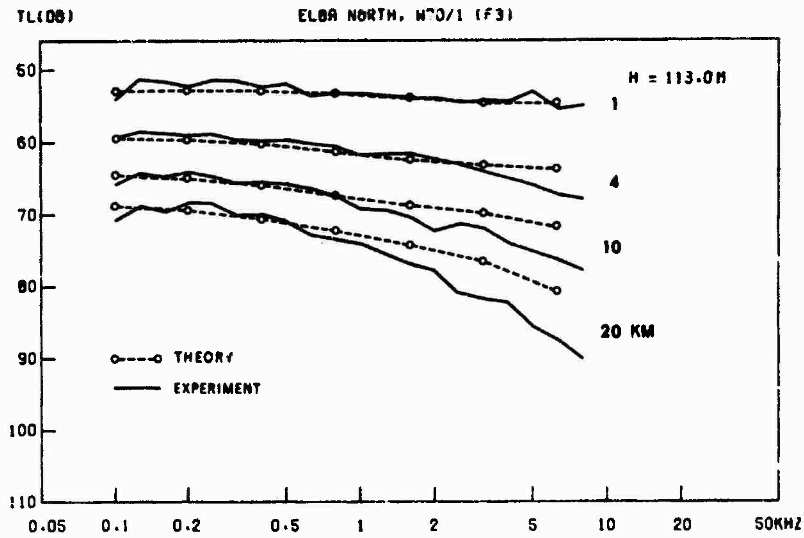

FIG. 8 DEPTH AVERAGED TRANSMISSION LOSS vs FREQUENCY AT RANGES 1, 4, 10, AND 20 km FOR WINTER TRIAL NORTH OF ELBA

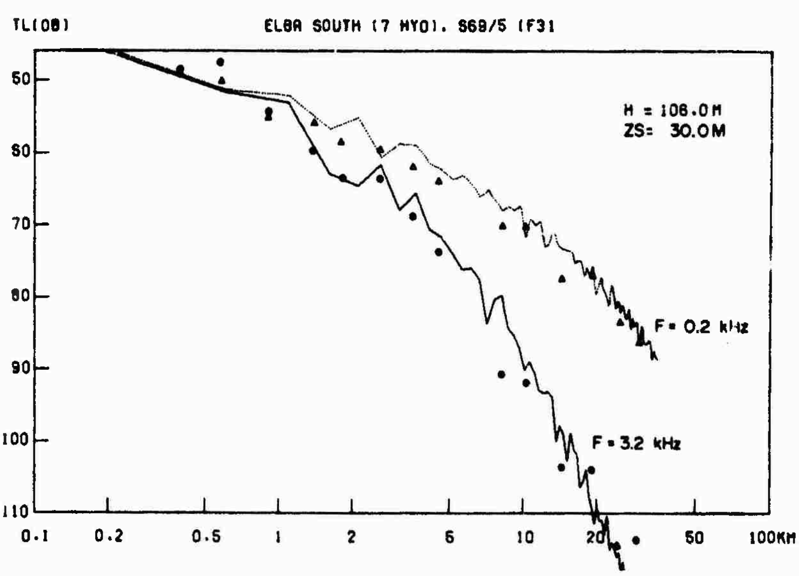

FIG. 9 DEPTH-AVERAGED TRANSMISSION LOSS vs RANGE FOR SUMMER TRIAL SOUTHEAST OF ELBA

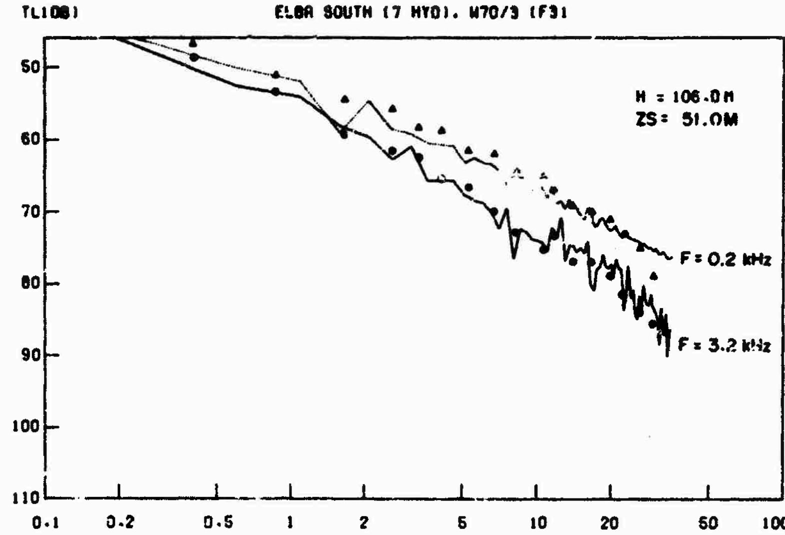

FIG. 10 DEPTH AVERAGED TRANSMISSION LOSS vs RANGE FOR WINTER TRIAL SOUTHEAST OF ELBA

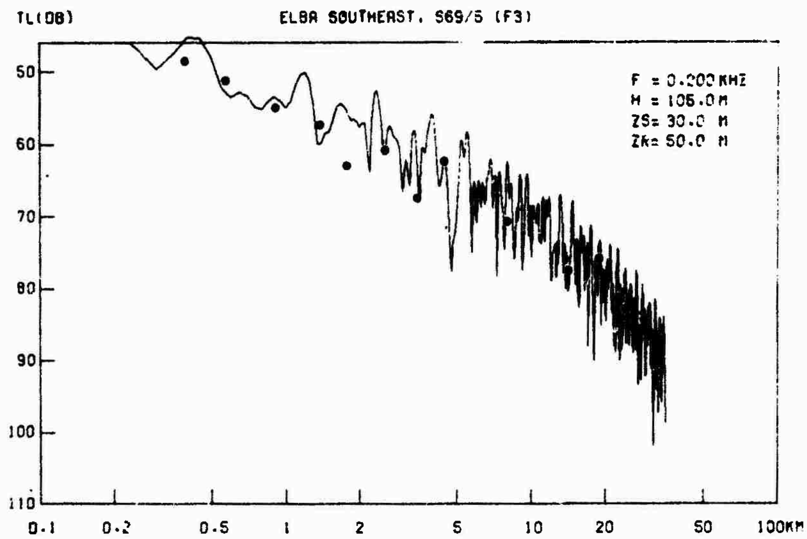

FIG. 11 TRANSMISSION LOSS vs RANGE FOR SUMMER TRIAL SOUTHEAST OF ELBA
F = 0.2 kHz

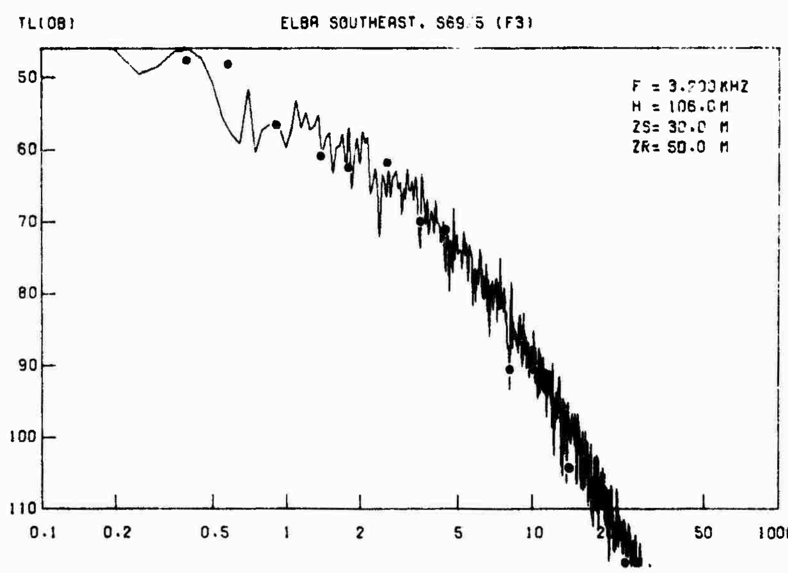

FIG. 12 TRANSMISSION LOSS vs RANGE FOR SUMMER TRIAL SOUTHEAST OF ELBA
F = 3.2 kHz

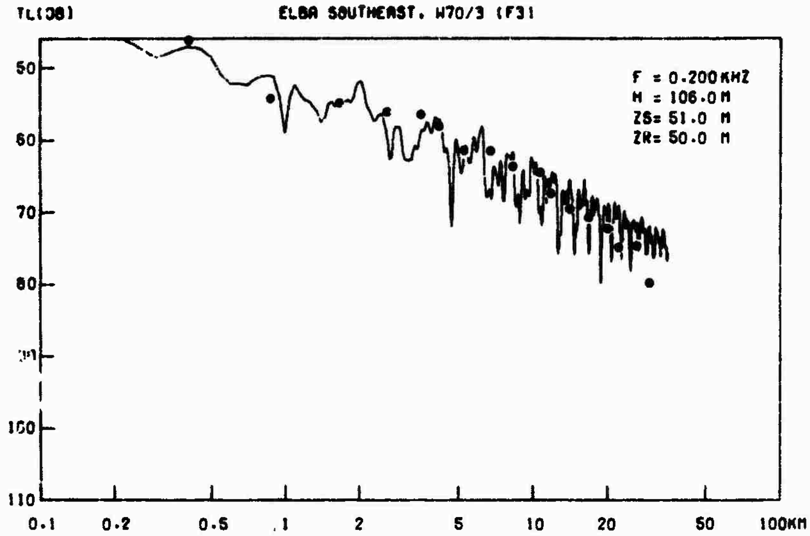

FIG. 13 TRANSMISSION LOSS vs RANGE FOR WINTER TRIAL SOUTHEAST OF ELBA F = 0.2 kHz

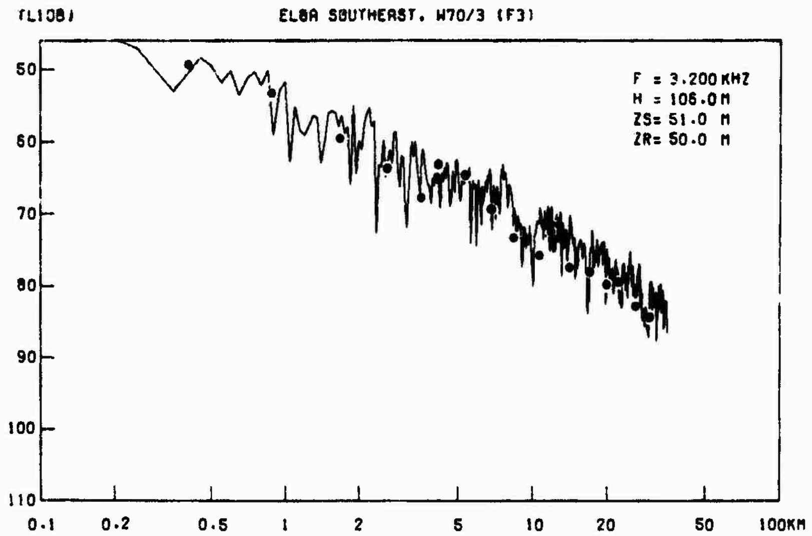

FIG. 14 TRANSMISSION LOSS vs RANGE FOR WINTER TRIAL SOUTHEAST OF ELBA F = 3.2 kHz

ATTENUATION FROM BOUNDARY SCATTERING IN SHALLOW WATER

by

W.A. Kuperman
US Naval Research Laboratory, Washington, DC, USA

ABSTRACT

The major contributions to propagation loss in shallow water are cylindrical spreading, bottom attenuation, and scattering at the sea surface and bottom. The first two of these contributions are well determined in wave-theory models. On the other hand, a generally-accepted method for including boundary-scattering effects in shallow-water wave theories has not been established. In this study, losses due to scattering at the surface and bottom of a duct are derived using a boundary-perturbation wave theory. The boundary roughness is assumed to be random, the rms height being small compared to the acoustic wavelength. However, no restriction is placed on the correlation distances of the boundaries and therefore this formalism is not limited to the Kirchoff regime. The method used is to derive new boundary conditions which the average acoustic field satisfies and then to solve the wave equation with these new boundary conditions. In the limit of infinite correlation distance of the boundary roughness, the results agree with those obtained earlier by other investigators using the Kirchoff approximation. This model permits the calculation of the loss of the average acoustic field using specific models of the sea surface, for example, the Pierson-Moskowitz spectra for a fully-developed sea. In addition, by characterizing the bottom as a randomly-rough two-fluid interface, loss due to bottom roughness is included in this model. Scattering contributions to the normal mode attenuation coefficients are calculated and the significance of these contributions are determined by comparison with experimental data obtained in selected shallow-water areas.

INTRODUCTION

This paper considers those effects on acoustic propagation in shallow water due to the random roughness of the boundaries. Essentially, rough boundaries will cause a decay in the average field as a function of range. The effects of boundary roughness can be included in wave-propagation models by using appropriate boundary conditions on the mean field. These boundary conditions characterize the roughness and will depend on the rms height of the roughness and the correlation function describing the horizontal variation of the surface statistics. One can then solve the wave equation for the mean field with these new boundary conditions.

In what follows, we shall outline the derivation of a general form of rough-boundary conditions. That is, we will consider the boundary conditions associated with a randomly-rough two-fluid interface. In the limit of the density of the second fluid going to zero, such a class of boundary conditions also includes the pressure-release condition. The combination of pressure release and fluid/fluid boundary conditions describes the waveguide problem that is considered to be the most fundamental description of shallow-water propagation.

In order to be reasonably assured that the derived boundary conditions will give plausible results in a waveguide, we first use these conditions to derive reflection and transmission coefficients at a randomly-rough two-fluid interface. It will then be shown that in the Kirchoff approximation, these results will reduce to those obtained earlier by Eckart [Ref. 1], Clay [Ref. 2], Medwin and Hagy [Ref. 3]. Calculated results from the reflection of sound from an ocean surface described by the Pierson-Moskowitz model of a fully-developed sea will be presented. It will be shown that in this example, the reflection coefficient is a function of wind speed and wind direction. This is not the case in the Kirchoff approximation.

These boundary conditions are then applied to the waveguide problem. The result is that the wave numbers associated with each normal mode become complex. The imaginary part of each wave number can be interpreted as the attenuation coefficient associated with a particular normal mode. At no point in the derivation is any ray approximation made; the formalism is strictly wave theoretic. Calculated results are presented for various ocean conditions where velocity profile, wind speed, and wind direction are varied.

1. BOUNDARY CONDITIONS

Figure 1 displays the two-fluid rough-surface geometry. The fields are described by velocity potentials v_1 and v_2 in the regions with sound speeds and densities c_1, ρ_1 and c_2, ρ_2 respectively. The rough surface is described by the random function $\alpha(\vec{r}_\perp)$ where $\vec{r}_\perp = (x,y)$. The rms values of α and its transverse gradient are taken to be small as compared to the acoustic wavelength. We require that the pressure and velocity be continuous across the interface. Therefore, we must have

$$\rho_1 v_1(\vec{r}_\perp, z)\Big|_{z=\alpha(\vec{r}_\perp)} = \rho_2 v_2(\vec{r}_\perp, z)\Big|_{z=\alpha(\vec{r}_\perp)} \qquad \text{[Eq. 1]}$$

$$\frac{\partial v_1}{\partial n}\Bigg|_{z=\alpha(\vec{r}_\perp)} = \frac{\partial v_2}{\partial n}\Bigg|_{z=\alpha(\vec{r}_\perp)} \qquad \text{[Eq. 2]}$$

where $\frac{\partial}{\partial n}$ is the local partial derivative normal to the interface. With α taken small, we can expand Eqs. 1 and 2 in a Taylor series about the plane $z=0$. We retain terms to order α^2. Next, following

the perturbation method of Bass [Ref. 4] (originally developed for a pressure-release surface) we decompose the velocity potentials into average ($\langle v_i \rangle$) and stochastic (w_i) parts:

$$v_i = \langle v_i \rangle + w_i, \qquad i = 1, 2 . \qquad \text{[Eq. 3]}$$

We then insert Eq. 3 into the Taylor expansions of the above boundary conditions and average over the ensemble of surfaces. After some algebra, we obtain two sets of boundary conditions at the plane $z = 0$.

$$\rho_1 \langle v_1 \rangle - \rho_2 \langle v_2 \rangle = f_1 (w_i, \langle v_i \rangle) \qquad \text{[Eq. 4]}$$

$$\frac{\partial \langle v_1 \rangle}{\partial z} - \frac{\partial \langle v_2 \rangle}{\partial z} = f_2 (w_i, \langle v_i \rangle) ; \quad i = 1, 2 \qquad \text{[Eq. 5]}$$

and

$$\rho_1 w_1 - \rho_2 w_2 = g_1 (\langle v_1 \rangle, \langle v_2 \rangle) \qquad \text{[Eq. 6]}$$

$$\frac{\partial w_1}{\partial z} - \frac{\partial w_2}{\partial z} = g_2 (\langle v_1 \rangle, \langle v_2 \rangle) . \qquad \text{[Eq. 7]}$$

The functions f_1 and f_2 have leading terms of order $\langle \alpha^2 \rangle$ (we later show that $w_i \sim \alpha$) and are given by

$$f_1 = \rho_2 \langle \alpha \frac{\partial w_2}{\partial z} \rangle - \rho_1 \langle \alpha \frac{\partial w_1}{\partial z} \rangle + \frac{\langle \alpha^2 \rangle}{2} \left[\rho_2 \frac{\partial^2 \langle v_2 \rangle}{\partial z^2} - \rho_1 \frac{\partial^2 \langle v_1 \rangle}{\partial z^2} \right] \qquad \text{[Eq. 8]}$$

and

$$f_2 = \langle \alpha \frac{\partial^2 w_2}{\partial z^2} \rangle - \langle \alpha \frac{\partial^2 w_1}{\partial z^2} \rangle + \frac{\langle \alpha^2 \rangle}{2} \left[\frac{\partial^3 \langle v_2 \rangle}{\partial z^3} - \frac{\partial^3 \langle v_1 \rangle}{\partial z^3} \right] - \langle (\vec{\nabla}_\perp \alpha) \cdot \vec{\nabla}_\perp (w_2 - w_1) \rangle \qquad \text{[Eq. 9]}$$

where $\vec{\nabla}_\perp$ is the transverse gradient. As $\alpha \to 0$, f_1 and f_2 vanish as $\langle \alpha^2 \rangle$. This indicates that the average perturbed field will be of the form $\langle v_i \rangle \approx u_i + O(\alpha^2) + \ldots$ where u_i are the solutions of the unperturbed problem. On the other hand, the leading terms for g_1 and g_2 are of the order α. Therefore, the leading term in an expansion for w_1 and w_2 will be proportional to α,

$$g_1 = \rho_2 \alpha \frac{\partial \langle v_2 \rangle}{\partial z} - \rho_1 \alpha \frac{\partial \langle v_1 \rangle}{\partial z} \qquad \text{[Eq. 10]}$$

$$g_2 = \alpha \left[\frac{\partial^2 \langle v_1 \rangle}{\partial z^2} - \frac{\partial^2 \langle v_1 \rangle}{\partial z^2} \right] - (\vec{\nabla}_\perp \alpha) \cdot \vec{\nabla}_\perp \langle v_2 - v_1 \rangle) . \qquad \text{[Eq. 11]}$$

To lowest order (α), g_1 and g_2 are known functions, since the leading terms in the perturbation series for the v_i's are the unperturbed solutions, the u_i's. Using a Fourier transform method [Ref. 5] we can solve for w_i and then $\langle \alpha \frac{\partial w_i}{\partial z} \rangle$ and $\langle \alpha \frac{\partial^2 w_i}{\partial z} \rangle$; the latter two appear in f_1 and f_2. With these quantities known, the rhs* of Eqs. 4 and 5 are the new boundary conditions for the average fields in the presence of a randomly-rough interface.

2. REFLECTION AND TRANSMISSION COEFFICIENTS

Boundary conditions 4 and 5 are rather complicated because of the form of f_1 and f_2. Nevertheless, these boundary conditions are tractable. The boundary conditions simplify if the Kirchoff approximation is made. Below, we outline the derivation of relfection and transmission coefficients under the Kirchoff assumption and compare results with those relevant results appearing in the literature. Following this, we work out the reflection coefficient without assuming the Kirchoff approximation in the case when $\rho_2 \to 0$. This latter case reduces the algebra by an order of magnitude and hence simplifies the presentation of this perturbation method.

2.1 Kirchoff Approximation

The Kirchoff approximation assumes that "the field near every region of the surface is essentially what it would have been if the surface had been flat with a slope equal to that of the irregular surface at the point in question [Ref. 6]." In the present theory we can apply the Kirchoff approximation by taking the autocorrelation function of the surface to be unity. In this limit, there is a considerable simplification of f_2 since it can be shown that the term involving the transverse gradients vanish. Physically, this is consistent with the Kirchoff approximation which assumes the surface to be locally flat and therefore one does not expect any effects arising from horizontal gradients.

Now, let us assume that we have a plane wave impinging on the interface from region I. The velocity potentials in regions I and II satisfy the wave equation (assuming a time dependence of $e^{-i\omega t}$)

$$\left[\vec{\nabla}^2 + \frac{\partial^2}{\partial z^2} + k_{\perp}^2 + k_{iz}^2 \right] v_i = 0; \quad i = 1,\ 2. \qquad \text{[Eq. 12]}$$

Equation 12 assumes that Snell's law is satisfied for the average (coherent) field. Though we just state this, it can actually be derived from the theory to order $\langle \alpha^2 \rangle$. From Eq. 12 we can obtain the values of the triple derivatives at the boundary that are needed to specify f_2 to lowest order in α

$$\langle \alpha_2 \rangle \left(\frac{\partial^3 \langle v_2 \rangle}{\partial z^3} - \frac{\partial^3 \langle v_1 \rangle}{\partial z^3} \right) = \langle \alpha^2 \rangle \left(k_{1z}^2 - k_{2z}^2 \right) \frac{\partial \langle v_2 \rangle}{\partial z} . \qquad \text{[Eq. 13]}$$

---

* rhs = right-hand side.

To order α^2 we can replace $\frac{\partial\langle v_i\rangle}{\partial z}$ on the rhs of Eq. 13 by $\frac{\partial u_i}{\partial z}$, u_i being the solution of the unperturbed problem. As a matter of fact, by this same reasoning, all the v_i's on the rhs of both Eqs. 4 and 5 can be replaced by their corresponding u_i's. Next, let us represent the unperturbed solutions as

$$u_1 = e^{i\vec{k}_\perp \cdot \vec{r}_\perp}\left[e^{-ik_{1z}z} + R_0\, e^{ik_{1z}z}\right] \qquad \text{[Eq. 14]}$$

$$u_2 = e^{i\vec{k}_\perp \cdot \vec{r}_\perp} T_0\, e^{-ik_{2z}z} \qquad \text{[Eq. 15]}$$

where R_0 and T_0 are the Rayleigh reflection and transmission coefficients:

$$R_0 = \frac{\rho_2 k_{1z} - \rho_1 k_{2z}}{\rho_2 k_{1z} + \rho_1 k_{2z}} \qquad \text{[Eq. 16]}$$

$$T_0 = \frac{2\rho_1 k_{1z}}{\rho_2 k_{1z} + \rho_1 k_{2z}}\,. \qquad \text{[Eq. 17]}$$

After much algebra, the boundary conditions of Eqs. 4 and 5 reduce to

$$\rho_1\langle v_1\rangle - \rho_2\langle v_2\rangle = \frac{\langle\alpha^2\rangle}{2} T_0\, e^{i\vec{k}_\perp\cdot\vec{r}_\perp}\left[\rho_2(k_{2z}^2 - k_{1z}^2) + 2k_{1z}(\rho_1 k_{2z} + \rho_2 k_{1z})\right] \qquad \text{[Eq. 18]}$$

$$\frac{\partial\langle v_1\rangle}{\partial z} - \frac{\partial\langle v_2\rangle}{\partial z} = \frac{i\langle\alpha^2\rangle}{2\rho_1} T_0 e^{i\vec{k}_\perp\cdot\vec{r}_\perp}\left[\rho_1 k_{2z}(k_{1z} + k_{2z})^2 - 2(\rho_2 k_{1z}^3 + \rho_1 k_{2z}^3)\right] \qquad \text{[Eq. 19]}$$

Finally, we assume the same form for the v_i's as given for the u_i's in Eqs. 14 and 15, replacing R_0 and T_0 by R and T respectively. These forms are substituted in Eqs. 16 and 17, and we solve for R and T. The results are

$$R = R_0(1 - 2\langle\alpha^2\rangle k_{1z}^2) \qquad \text{[Eq. 20]}$$

$$T = T_0\left[1 - \tfrac{1}{2}\langle\alpha^2\rangle(k_{2z} - k_{1z})^2\right]. \qquad \text{[Eq. 21]}$$

If we are considering a pressure-release surface, $R_0 = -1$ and therefore $R = -1 + 2\langle\alpha^2\rangle k_z^2$. This result is identical to order $\langle\alpha^2\rangle$ to that obtained by Eckart [Ref. 1] using the Kirchoff approximation. Beckmann and Spizzichino [Ref. 7] have shown that reflection results from a rough interface separating two different media can be obtained by assuming that the Rayleigh reflection coefficient is locally valid in the Kirchoff approximation. Clay [Ref. 2], using

the Rayleigh reflection coefficient together with the Eckart method obtained a coefficient identical to Eq. 20 to order $\langle \alpha^2 \rangle$.

Medwin and Hagy [Ref. 3] used a similar procedure to derive a coherent transmission coefficient for the case where the density of the second medium was much larger than that of the first medium. Their results [Eqs. 7 and 8 of their paper] and the above results for T [Eq. 21] are equivalent to order $\langle \alpha^2 \rangle$. In addition, Eq. 21 indicates that the form of the Medwin Hagy results (to order $\langle \alpha^2 \rangle$) is valid for arbitrary density ratio and not just in the limit of high density in the second medium as they originally assumed.

We have shown in this subsection that in the Kirchoff approximation we recover results from this theory that are in agreement with those obtained earlier by investigators who developed theories initially based on the Kirchoff assumption. Next, we present some results for a non-Kirchoff case. We consider a pressure-release surface so that the mathematics does not obscure the actual method. The general two-fluid case can be solved just as in this subsection but with an order of magnitude more of mathematical manipulation. Those results will be presented elsewhere.

2.2 Reflection from the Ocean Surface

Let us return to Eqs. 4 and 7 and set $\rho_2 = 0$ and $\rho_1 = 1$:

$$\langle v \rangle = - \langle \alpha \frac{\partial w}{\partial z} \rangle \; ; \quad z = 0 \; . \qquad \text{[Eq. 22]}$$

The term involving the second derivative vanishes to order $\langle \alpha_2 \rangle$. Similarly, Eqs. 5 and 10 reduce to

$$w = -\alpha \frac{\partial \langle v \rangle}{\partial z} ; \quad z = 0 , \qquad \text{[Eq. 23]}$$

where to lowest order we can replace $\langle v \rangle$ by u, the unperturbed solution. Equation 22 specifies that we must know the derivative of w on the surface. We indicated in the last section that we can solve the system of Eqs. 5 and 6 using a Fourier transform method. This is accomplished by noting that the stochastic field must originate from the boundary and hence can be expressed in the following plane wave representation

$$w = \frac{1}{2\pi} \int d\vec{\xi}_\perp \, e^{i\vec{\xi}_\perp \cdot \vec{r}_\perp} e^{i\xi_z z} a(\vec{\xi}_\perp) ; \quad \xi_z = \sqrt{k^2 - \xi_\perp^2} . \qquad \text{[Eq. 24]}$$

By Fourier transforming Eq. 23 we obtain a value for a $(\vec{\xi}_\perp)$ which we may insert in Eq. 24 and then we can determine $\frac{\partial w}{\partial z}$. Substituting this value into Eq. 22 we obtain after much algebra and after taking an ensemble average

$$\langle v \rangle = \frac{1}{(2\pi)^2} \int d\vec{\xi}_\perp \, d\vec{\xi}_1 (i\xi_z) \, e^{i(\vec{\xi}_\perp - \vec{\xi}_1)\cdot\vec{r}_\perp} P(\vec{\xi}_1) \frac{\partial}{\partial z} \langle v(\vec{\xi}_\perp - \vec{\xi}_1) \rangle , \qquad \text{[Eq. 25]}$$

where $P(\vec{\xi}_1)$ is the Fourier transform of the autocorrelation function $N(\vec{\rho})$ of the surface, $\vec{\rho}$ being the displacement vector between two points on the surface. To lowest order, the Fourier transform of the derivative of the field $\frac{\partial}{\partial z}\langle v(\vec{\xi}_\perp-\vec{\xi}_1)\rangle$ can be shown to be $-4\pi i k_{1z}\cdot\delta^2[\vec{k}-(\vec{\xi}_\perp-\vec{\xi}_1)]$, δ^2 being a two-dimensional Dirac delta function. We can then carry out the integration of ξ_1 to obtain

$$\langle v\rangle = \frac{2k_{1z}}{2\pi}\, e^{i\vec{k}_\perp\cdot\vec{r}_\perp}\int d\vec{\xi}_\perp\,(\xi_z)\,P(\vec{k}_\perp-\vec{\xi}_\perp) \qquad \text{[Eq. 26]}$$

and therefore

$$R = -1+\frac{2k_{1z}}{2\pi}\int d\vec{\xi}_\perp\,\xi_{1z}\,P(\vec{k}_\perp-\vec{\xi}_\perp). \qquad \text{[Eq. 27]}$$

The Kirchoff approximation is easily recoverable from Eq. 27. Recall, that in this approximation we take $N(\vec{\rho})=1$ so that its transform is simply $P(\vec{k}_\perp-\vec{\xi}_\perp) = 2\pi\delta^2(\vec{k}_\perp-\vec{\xi}_\perp)$ and hence the integral just reduces to $2\pi k_z$. We are then left with precisely the leading term of the Eckart result for the specular reflection of a plane wave from a pressure-release surface.

However, Eq. 27 allows us to calculate the reflectivity as a function of the directional spatial properties of the surface. In the Kirchoff approximation, the mean value of the reflected field does not depend on the surface correlation properties [Ref. 8].

In considering the ocean surface it should be noted that it is fortuitous that the reflectivity as given by Eq. 27 is expressed in terms of the directional wave-height spectrum P and not the correlation function N. This is because for most ocean-surface models, the correlation function can only be obtained numerically from the spectrum [Refs. 9, 10].

As an indication of the directional properties of the reflection coefficient, we have calculated R from Eq. 20 inserting the Pierson-Moskowitz spectrum [Ref. 11] with the same cosine-squared assumption used by Fortuin [Ref. 12]. We have done this for three windspeeds, 5, 10, and 15 m/s with the direction of acoustic propagation taken parallel, perpendicular, and at 45° to the wind direction. The calculations were performed for three frequencies, 400, 750, and 1500 Hz. The results are presented in Figures 2 to 10 for angles of interest in shallow water. Superimposed on each graph is the Kirchoff result which usually falls in-between the directional results. The graphs indicate that there is a directional effect on the mean field that is reflected from the ocean surface. However, it must be noted that the Pierson-Moskowitz spectrum represents the wind waves of a fully-developed sea. It does not take swell into consideration and therefore has limited use in describing the real ocean. This spectrum was used because it was available. Equation 27 can just as well be evaluated using experimental results obtained from monitoring the ocean surface.

3. ATTENUATION IN SHALLOW WATER

In this Chapter we consider the propagation of sound in shallow water. Again, to keep the presentation as simple as possible, we will only consider the ocean-surface roughness. The bottom-roughness case is a straightforward though lengthy extension of what is to follow and will be presented elsewhere.

We are interested in determining the acoustic field in shallow water (a waveguide) resulting from the presence of a harmonic point source placed at an arbitrary depth z_0 in a water channel whose velocity profile may also be a function of depth. Figure 11 displays the geometry where we also include a third layer which may support shear waves. The acoustic field in the water column satisfies the equation

$$\left[\vec{\nabla}_\perp + \frac{\partial^2}{\partial z^2} + k_1^2(z) \right] \varphi = -\delta^2(\vec{r}_\perp)\,\delta(z - z_0) \, . \qquad \text{[Eq. 28]}$$

The velocity potential satisfies the standard continuity conditions at the bottom interfaces, and, if we are to include surface roughness, φ also satisfies the rough-surface boundary condition specified by Eq. 26. It turns out that it will be convenient to solve Eq. 28 using the transverse Fourier transform of φ

$$\varphi(\vec{r}_\perp, z) = \frac{1}{2\pi} \int d\vec{\eta}\; e^{i\vec{\eta}\cdot\vec{r}_\perp} v(\vec{\eta}, z) \qquad \text{[Eq. 29]}$$

where $v(\vec{\eta}, z)$ must therefore satisfy the z-dependent inhomogenous equation

$$\frac{\partial^2 v}{\partial z^2} + (k_1^2 - \eta^2)\, v = -\delta(z - z_0) \, . \qquad \text{[Eq. 30]}$$

We seek a normal mode solution of Eq. 30

$$v = \Sigma\, a_n v_n(z) \qquad \text{[Eq. 31]}$$

where v_n are the eigenfunctions satisfying the homogenous form of Eq. 30.

$$\frac{\partial^2 v_n}{\partial z^2} + (k_1^2 - k_n^2)\, v_n = 0 \, . \qquad \text{[Eq. 32]}$$

The solution of Eq. 28 can then be written as

$$\varphi(\vec{r}_\perp, z) = -\frac{\rho_1}{2\pi} \sum_n \int d\vec{\eta}\; \frac{v_n(z_0)\, v_n(z)}{k_n^2 - \eta^2}\; e^{i\vec{\eta}\cdot\vec{r}_\perp} . \qquad \text{[Eq. 33]}$$

The contour is appropriately chosen to give outgoing waves. This is actually the normal mode solution since Eq. 33 contains summations of integral representations of Hankel functions.

For the perturbed problem, the v_n's of Eq. 32 must satisfy the Fourier-transformed version of the boundary conditions given by Eq. 26 at the plane $z=0$

$$\langle v_n \rangle = i f(\vec{\eta}) \frac{\partial \langle v_n \rangle}{\partial z} \qquad \text{[Eq. 34]}$$

where $f(\eta)$ is of order $\langle \alpha^2 \rangle$ and is given by

$$f(\vec{\eta}) = \frac{1}{2\pi} \int d\vec{\xi}\ \xi_z\ F(\vec{\eta} - \vec{\xi}_\perp) \qquad \text{[Eq. 35]}$$

Using boundary condition Eq. 34 to solve for the eigenvalues of Eq. 32, we obtain the results that the new eigenvalues become complex at order $\langle \alpha^2 \rangle$, $K_n \cong k_n + i\delta_n$, with

$$\delta_n = \frac{\rho_1\, f(\eta)}{2\, k_n} \left| \frac{\partial \langle v(z=0) \rangle}{\partial z} \right|^2 , \qquad \text{[Eq. 36]}$$

k_n being the real eigenvalue of the unperturbed problem.

Returning to Eq. 33, we see that the existence of δ_n will shift the poles of the integrand off the real axis. To lowest order $\langle \alpha^2 \rangle$, the imaginary part of the location of the pole will then be

$$\delta_n = \frac{\rho_1\, f(k_n)}{2\, k_n} \left| \frac{\partial \langle v(z=0) \rangle}{\partial z} \right|^2 \qquad \text{[Eq. 37]}$$

Equation 37 represents the attenuation coefficient due to scattering at the ocean surface. In the Kirchoff approximation we have $f(k_n) = \langle \alpha^2 \rangle (k^2 - k_n^2)^{1/2}$, so that

$$\delta_n = \frac{\rho_1 \langle \alpha^2 \rangle \sqrt{k_1^2(0) - k_n^2}}{2\, k_n} \left| \frac{\partial \langle v(z=0) \rangle}{\partial z} \right|^2 . \qquad \text{[Eq. 38]}$$

There is some previous work with which we can compare the above Kirchoff result. Clay [Ref. 13] calculated the modal attenuation coefficients in isovelocity shallow water based on the principle that each time the ray associated with a normal mode bounces off the ocean surface, it is diminished in amplitude by the Eckart reflection coefficient. The number of bounces is calculated from a "skip distance" of a particular normal mode's ray representation.

The result given by Eq. 38 is very close to the Clay result, but it is slightly smaller. This discrepancy can be explained by the same argument used to explain the attenuation of the acoustic field in the water column due to a lossy bottom. As the surface causes the field to diminish in the water column, the acoustic field must still obey certain continuity conditions at the bottom boundary, so that attenuation in the water column cannot occur without some effect on the acoustic field in the ocean bottom. The result is that there

will be a small flux of energy from the bottom through the interface to compensate for the decrease of the field in the water column and also meet the continuity conditions at the fluid/fluid boundary. When one just uses a skip-distance reflection argument, such a compensation effect is not taken into account. If we take the Clay result and make both boundaries of the waveguide pressure release (or one boundary rigid) then there will be no such effect since the field must simply vanish at both boundaries (or the derivative vanish at the rigid boundary). For this case, Eq. 38 is identical with the Clay result.

The general result given by Eq. 37 depends on the direction of the acoustic propagation relative to the anisotropic ocean surface. Just as for the reflection coefficient, we can also calculate the normal mode attenuation coefficients using a Pierson-Moskowitz wave spectrum. We present some results for various velocity profiles in Figs. 12 to 22. Figures 12 and 18 display the velocity profiles. The graphs following each profile refer to the previous profile. The Kirchoff result is also presented. The bearing angles relative to the wind direction are the same as those used in reflection-coefficient calculations. The windspeed used was 10 m/s.

SUMMARY

In this paper we have presented a wave theoretic method to predict the effect of boundary roughness on propagation loss in shallow water. When possible, we connected our results with those obtained by earlier investigators to demonstrate sufficient consistency in order to make any new result plausible in the light of standard underwater acoustic theory. The presentation has been limited in order that the method, rather than specific results, could be presented in this short time.

ACKNOWLEDGEMENTS

This work was supported by NAVSEA Code 06H1-4 and the US Office of Naval Research.

REFERENCES

1. C. Eckart, J. Acoust. Soc. Am. 25, 566 (1953).

2. C.S. Clay, J. Geophys. Res. 71, 2037 (1966).

3. H. Medwin and J.D. Hagy, J. Acoust. Soc. Am. 51, 1083 (1972).

4. F.G. Bass, Izv. Vyssh. Uchebn., Zaved., Radiofiz 4, 476 (1961); (JPRS:10223).

5. Yu. K. Alekhin, Dokl. Acad. Nauk SSSR 189, 499 (1969) Sov. Phys. Dokl. 14, 1095 (1970).

6. W.C. Meecham, J. Rational Mech. Anal., 5, 323 (1956).

7. P. Beckmann and A. Spizzichino, The Scattering of Electromagnetic Waves from Rough Surfaces (Macmillan Co., New York, 1953).

8. L. Fortuin, J. Acoust. Soc. Am., 52, 302 (1972).

9. R.H. Mellen, J. Acoust. Soc. Am., 55, 1084 (1974).

10. J.G. DeBoer, "On the Correlation Functions in Time and Space of Wind-Generated Ocean Waves," SACLANTCEN Technical Report 160, (1969).

11. W.J. Pierson and L. Moskowitz, J. Geophys. Res., 69, 5181 (1964).

12. L. Fortuin, "The Sea Surface as a Random Filter for Underwater Sound Waves," Ph.D. Dissertation (Uitgeverij Waltman, Delft, 1973). SACLANTCEN SR-7.

13. C.S. Clay, J. Acoust. Soc. Am. 36, 833 (1964).

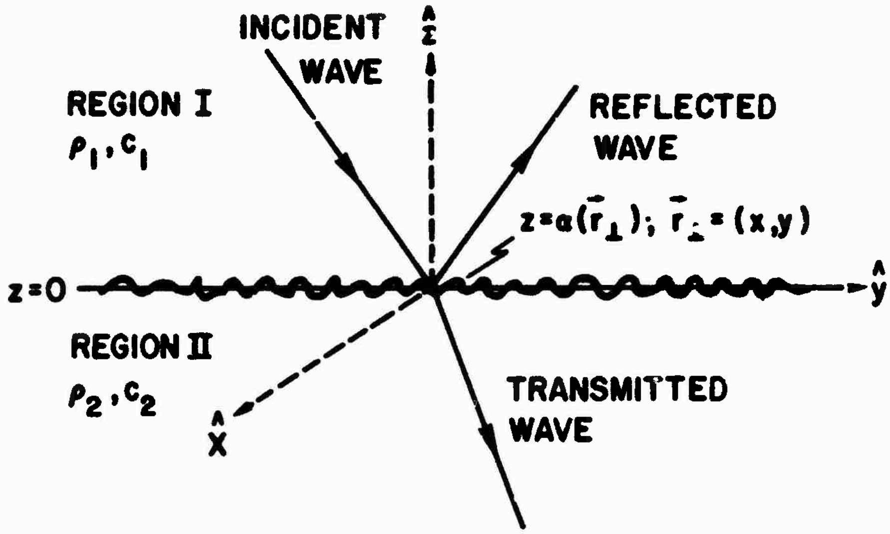

FIG. 1

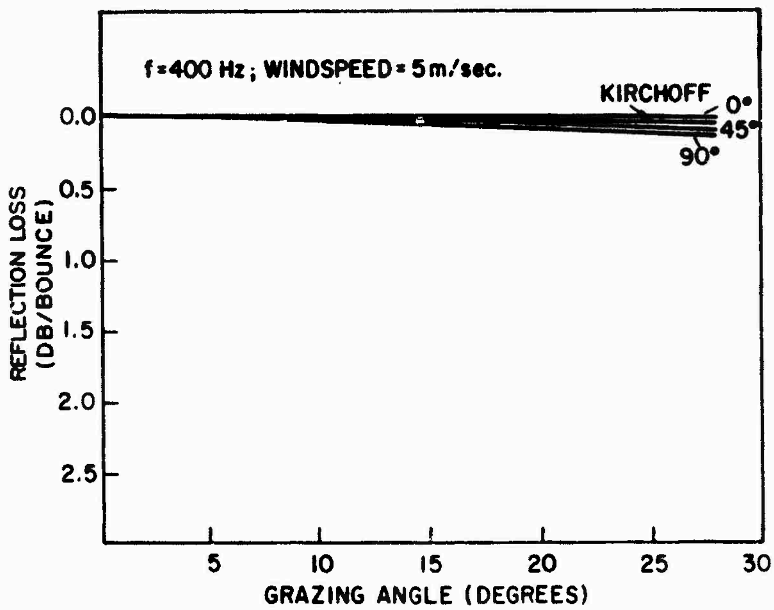

FIG. 2

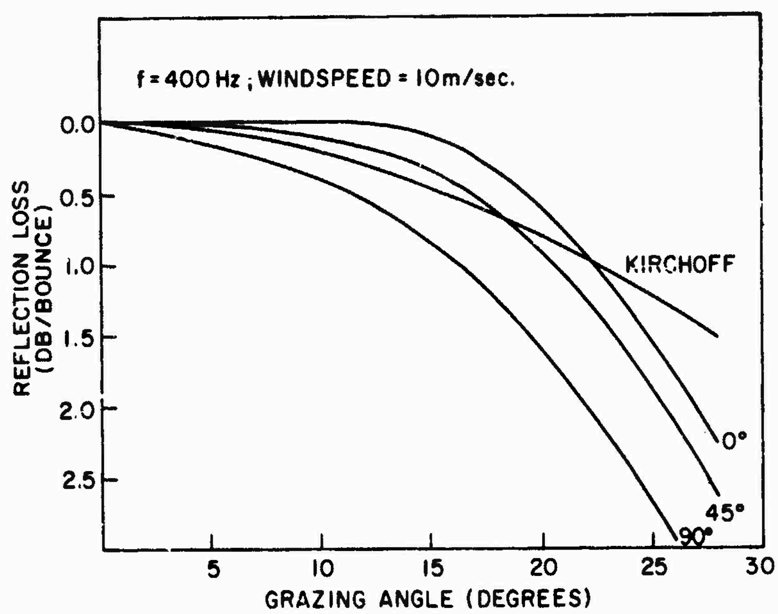

FIG 3

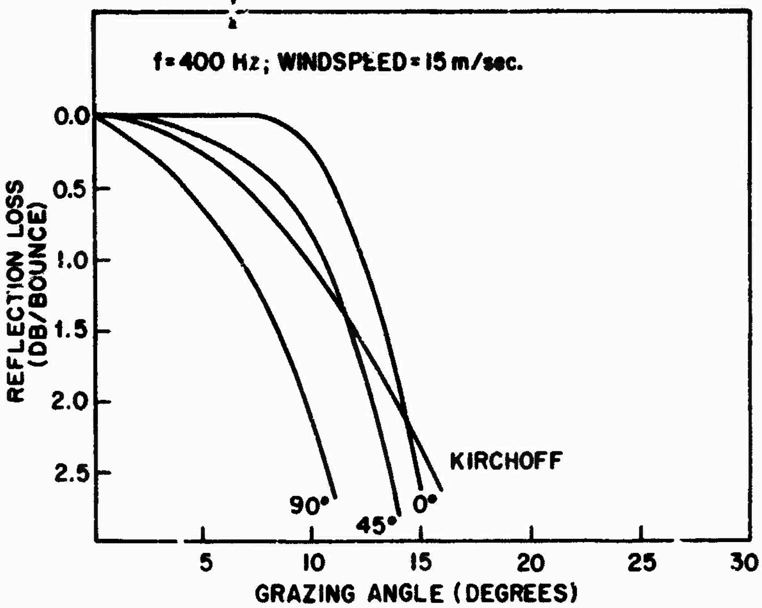

FIG. 4

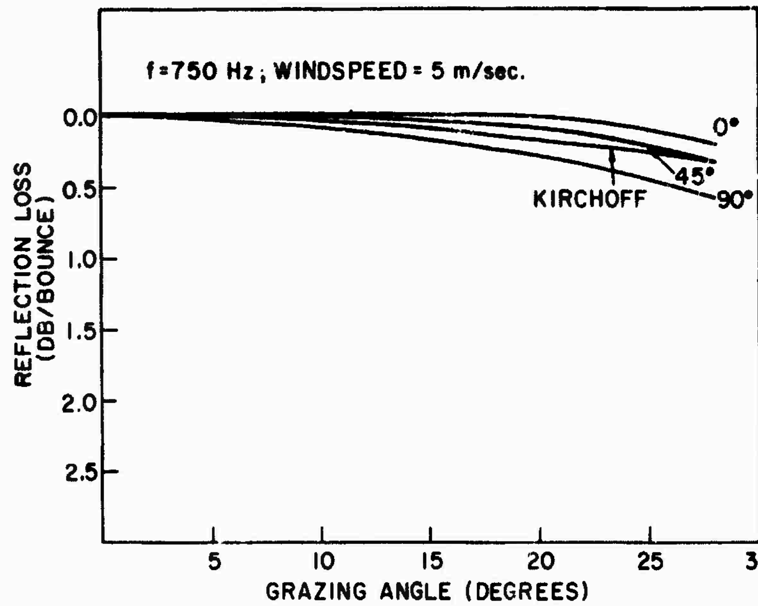

FIG. 5

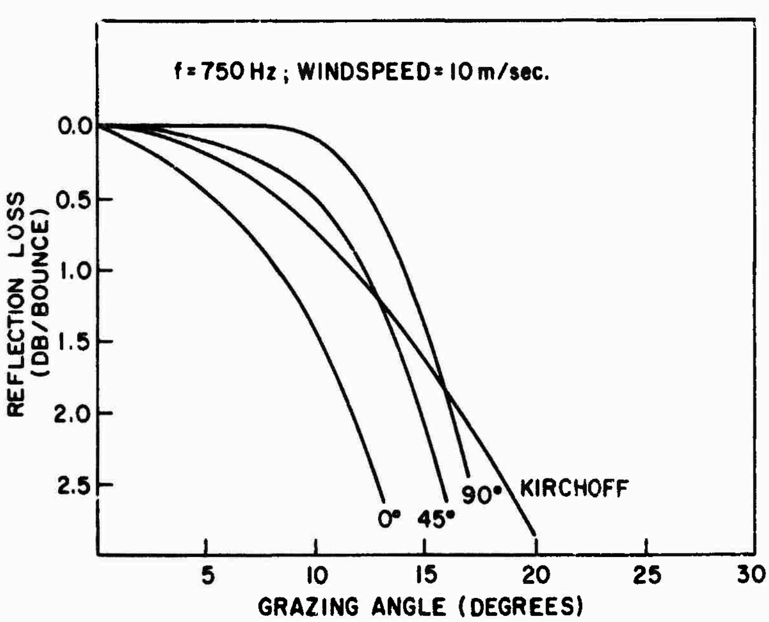

FIG. 6

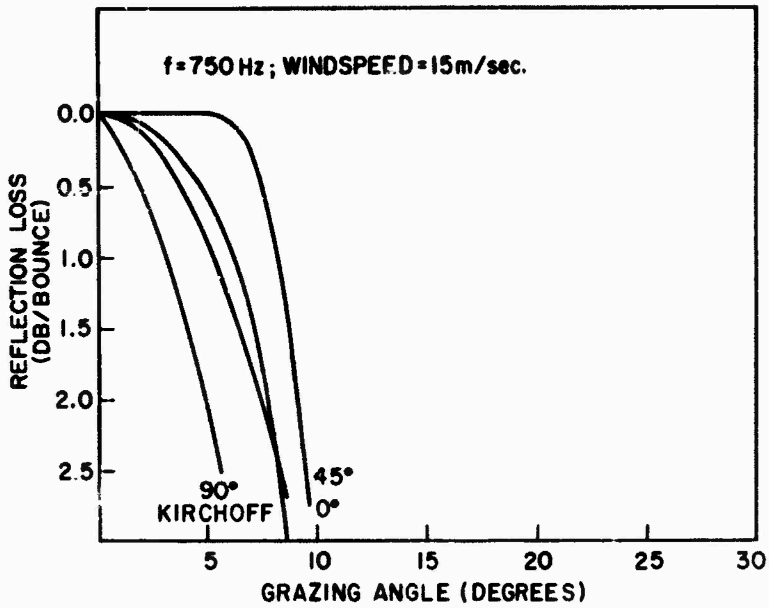

FIG. 7

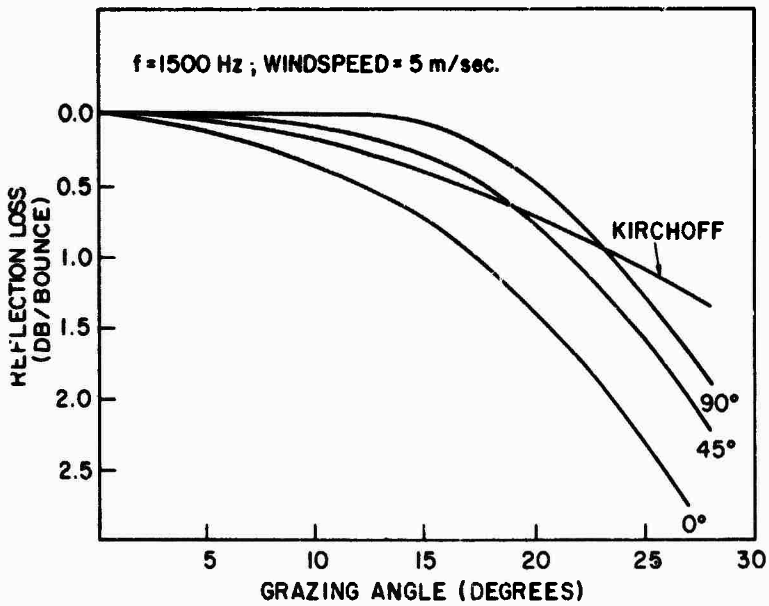

FIG. 8

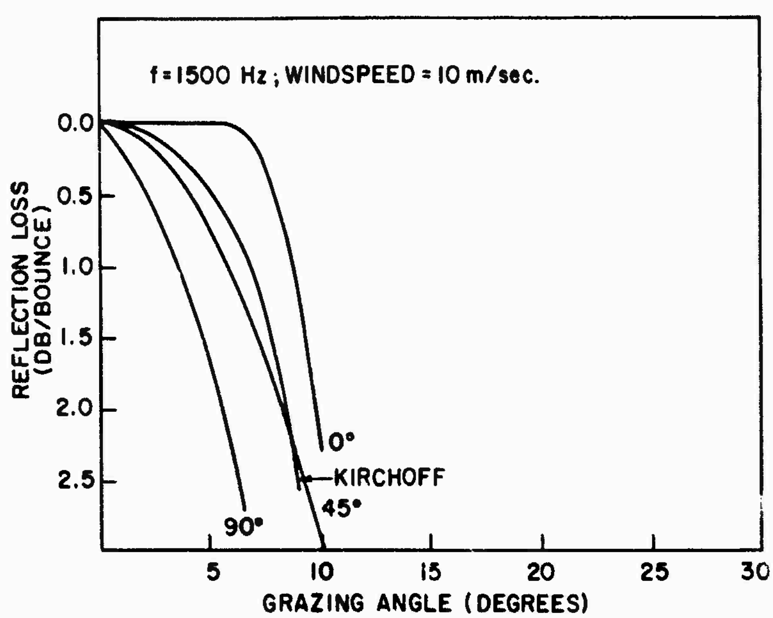

FIG. 9

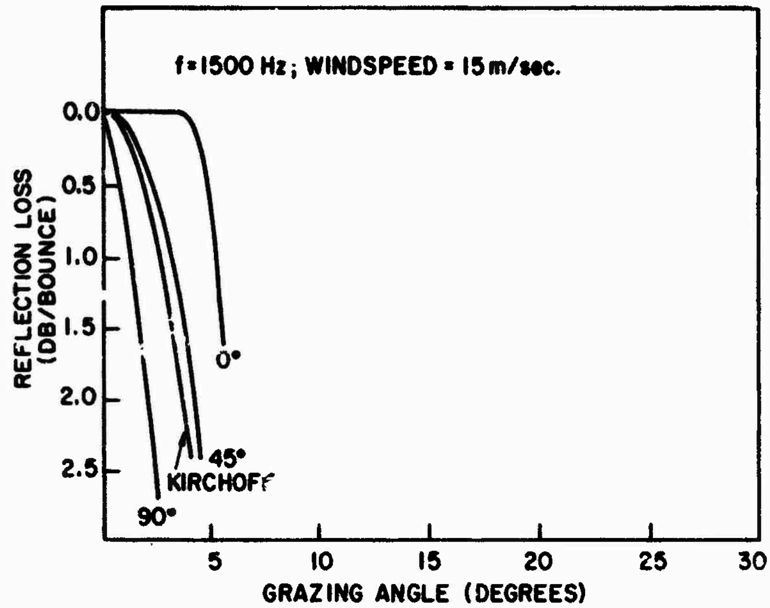

FIG. 10

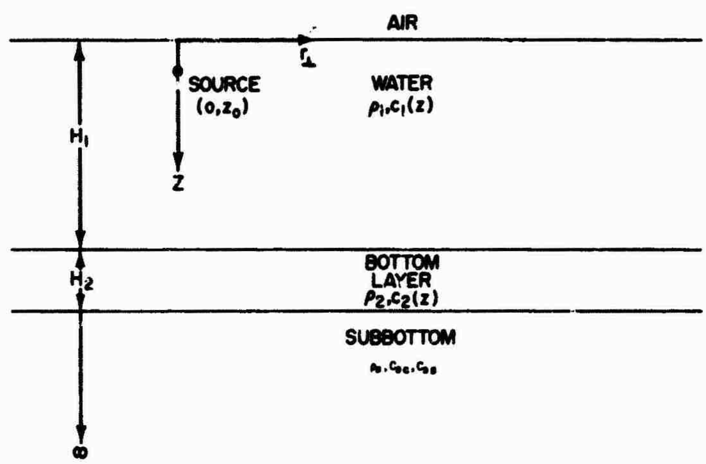

FIG. 11

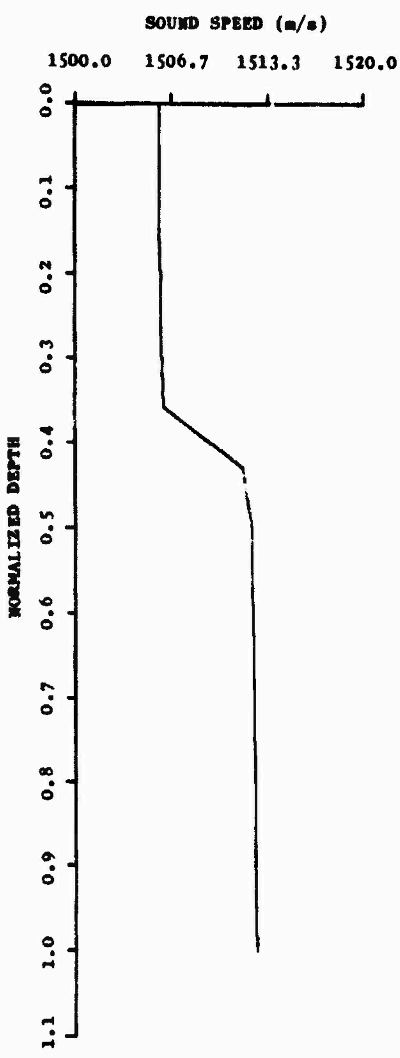

FIG. 12

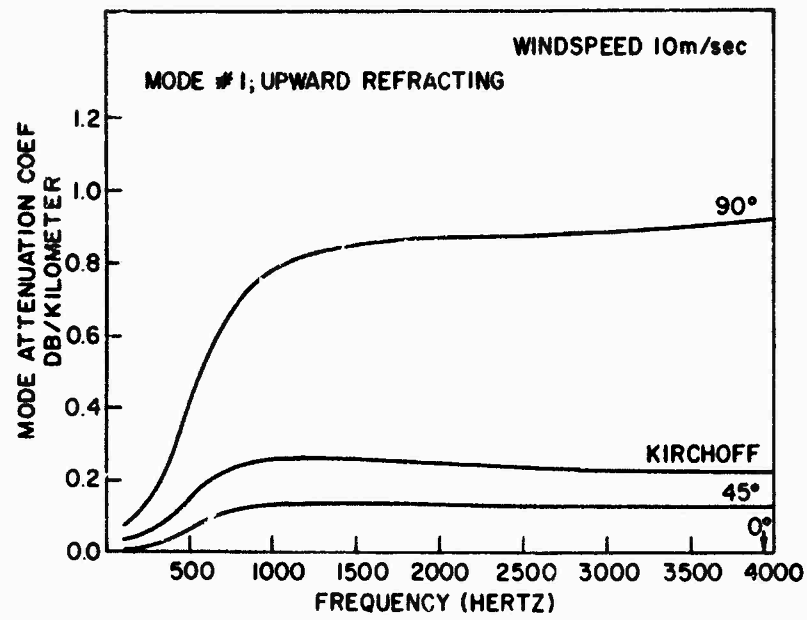
WINDSPEED 10m/sec
MODE #1; UPWARD REFRACTING
MODE ATTENUATION COEF DB/KILOMETER
1.2
1.0
0.8
0.6
0.4
0.2
0.0
90°
KIRCHOFF
45°
0°
500 1000 1500 2000 2500 3000 3500 4000
FREQUENCY (HERTZ)

FIG. 13

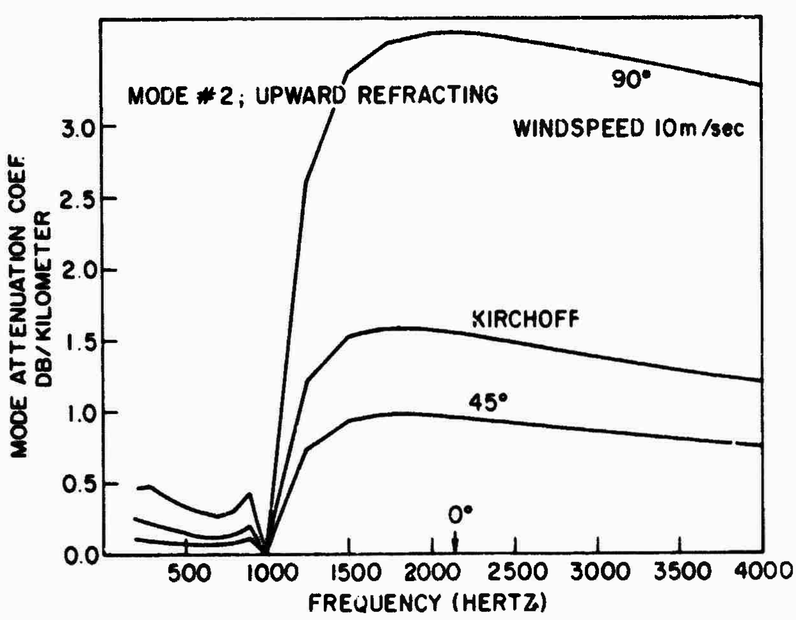
MODE #2; UPWARD REFRACTING
90°
WINDSPEED 10m/sec
MODE ATTENUATION COEF DB/KILOMETER
3.0
2.5
2.0
1.5
1.0
0.5
0.0
KIRCHOFF
45°
0°
500 1000 1500 2000 2500 3000 3500 4000
FREQUENCY (HERTZ)

FIG. 14

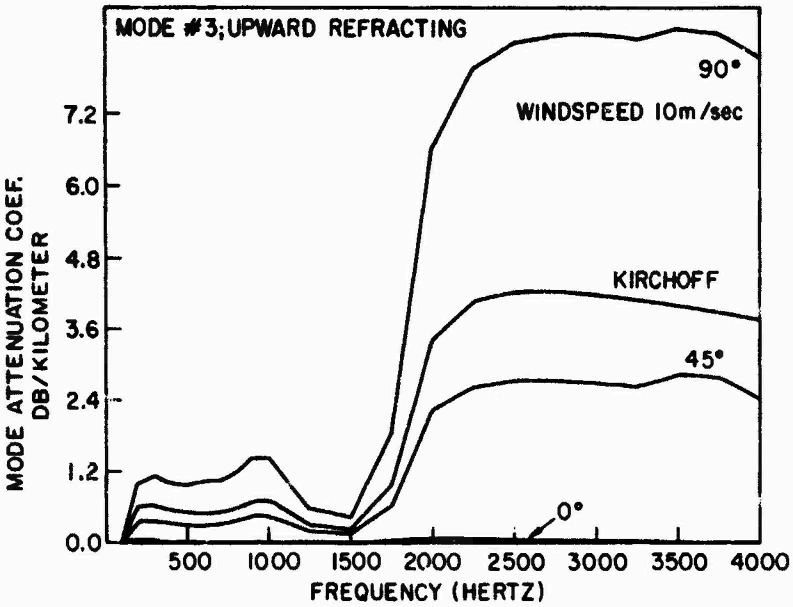

FIG. 15

FIG. 16

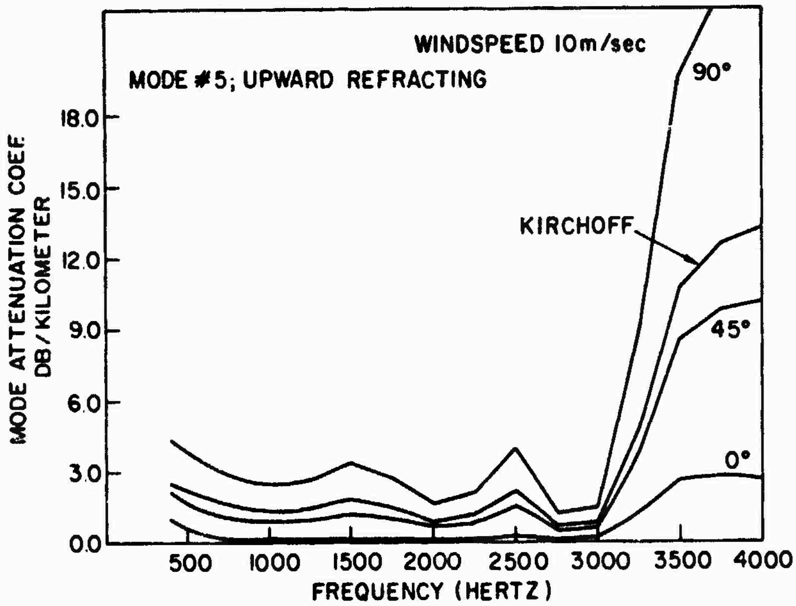

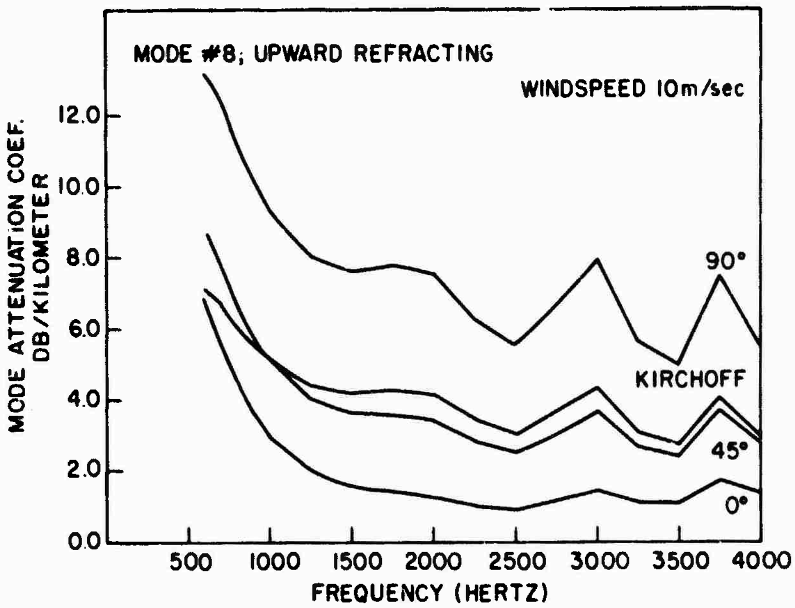

FIG. 17

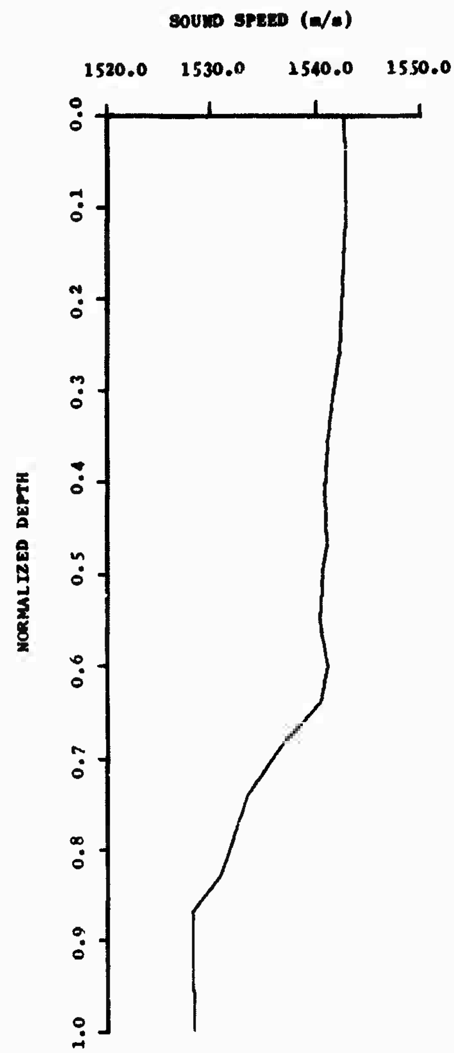
SOUND SPEED (m/s)
1520.0
1530.0
1540.0
1550.0
NORMALIZED DEPTH
0.0
0.1
0.2
0.3
0.4
0.5
0.6
0.7
0.8
0.9
1.0

FIG. 18

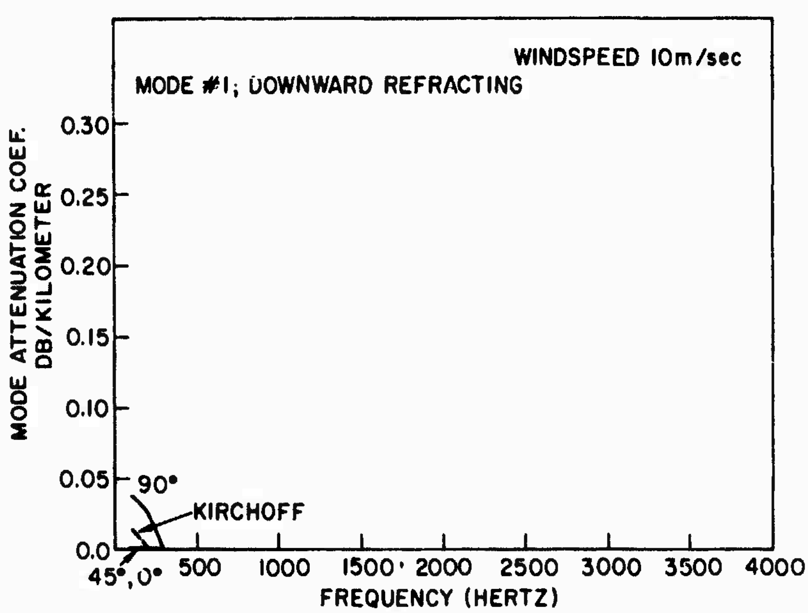
WINDSPEED 10m/sec
MODE #1; DOWNWARD REFRACTING
MODE ATTENUATION COEF.
DB/KILOMETER
0.30
0.25
0.20
0.15
0.10
0.05
0.0
90°
KIRCHOFF
45°,0°
500
1000
1500
2000
2500
3000
3500
4000
FREQUENCY (HERTZ)

FIG. 19

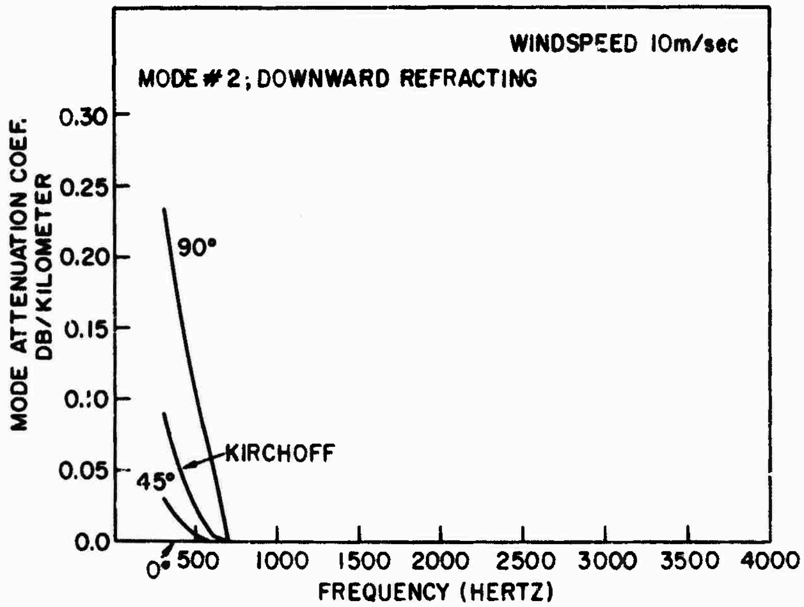

FIG. 20

FIG. 21

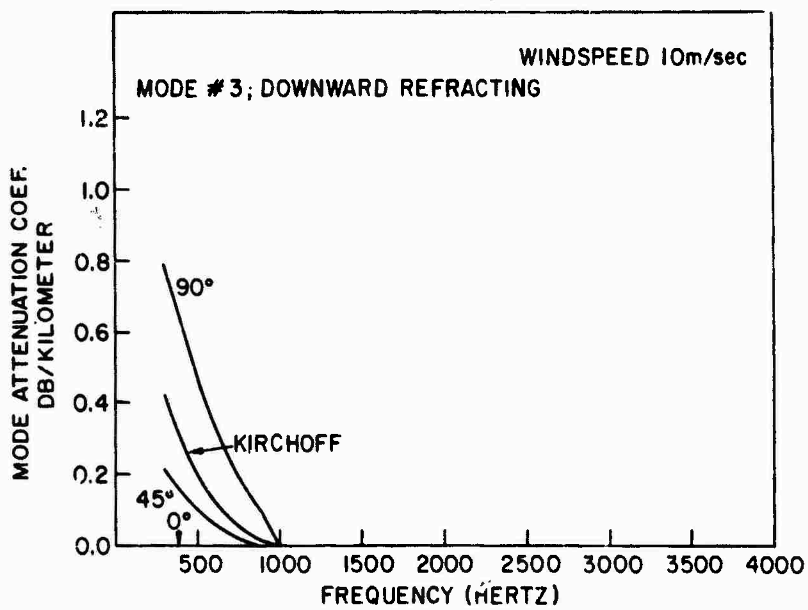

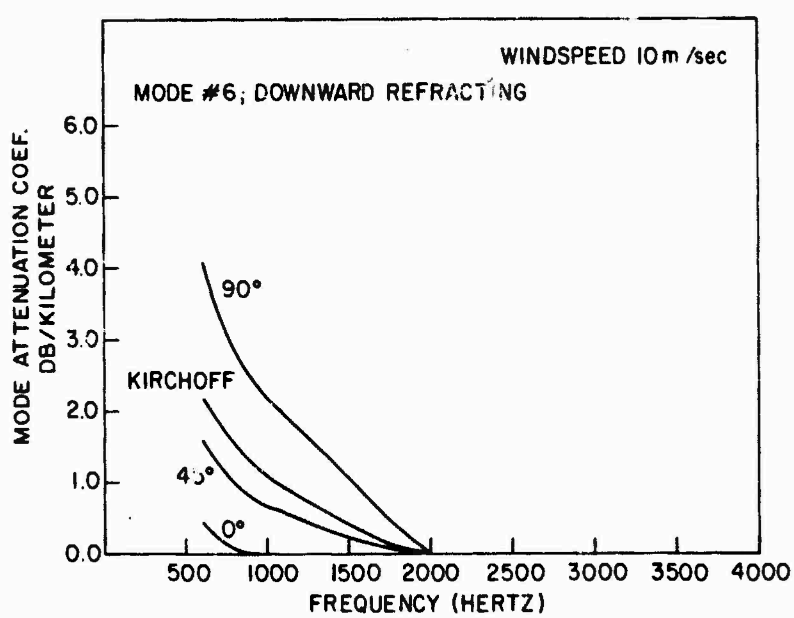

FIG. 22

SOME RESULTS OF COMPUTATIONS OF TRANSMISSION LOSS BASED ON AN ACOUSTIC PROPAGATION MODEL

by

Arne Aubell
Norwegian Defence Research Establishment, Horten, Norway

SUMMARY

An acoustic propagation model based on the ray theory has been constructed. The principle and parameters of this model are briefly described. The model has been used for computation of transmission loss. Some examples are presented showing satisfactory agreement between measured and computed results. In some cases the model has explained peculiarities of the measured transmission loss.

INTRODUCTION

Acoustic modelling of transmission loss has become popular during the last years. The type of model chosen for a specific task depends on the depth of the sea area under consideration. The term "depth" is here used in acoustic meaning, i.e. it is expressed in wavelengths. Thus, when the depth in wavelengths is greater than about 10, a model based on the ray propagation theory may be used. This ratio between water depth and wavelength is considered to be a safe limit for the validity of the ray solution. When the depth is 2 wavelengths or less, the ray theory does not apply any longer, and a model based on normal mode propagation must be used [Ref. 1]. It is required that a practical model must comprise all significant parameters for sound propagation without using excessive computer time. It should be remembered, however, that even a very complicated model represents a simplification of the ocean and that the results which may be obtained from it are only approximations to the truth.

Generally, in Norwegian waters the conditions are such that the ray theory model may be preferred, although there are exceptions. Our model has, so far, been used in connection with long-range, low-frequency transmissions.

1. BASIC PRINCIPLES OF THE ACOUSTIC MODEL

The NDRE ocean model has been dealt with in detail in Refs. 2 and 3. For the sake of completeness a brief summary will be given that presents its characteristics.

The basic principle is shown in Fig. 1. It is seen that the model is based on the following laws and parameters:

a) the law of geometric spreading formulated by the ray theory

b) vertical and horizontal sound velocity distribution

c) bottom topography

d) energy loss by bottom reflection, L_{rb}

e) energy absorption in the water volume, L_{abs}

f) energy scattering loss by reflection from the sea surface, L_{rs} .

The effects of reverberation and short-time variation of the hydrographic conditions are ignored.

The ray path coordinates and the intensity are expressed by the well-known formulae [Ref. 1], Eq. 1 and Eq. 2.

$$x_i = \int_{z_i}^{z_{i+1}} \frac{dz}{\sqrt{\frac{c_m^2}{c^2(z)} - 1}} \qquad \text{[Eq. 1]}$$

where c_m = constant = $\frac{c(z_i)}{\cos \varphi_i}$ and where x_i is the step in horizontal direction taken by the ray between the depths z_i and z_{i+1}, Fig. 2. The intensity I at the point (x_i, z_{i+1}) may be expressed by

$$\frac{I}{P} = \frac{\cos \varphi_i}{x \cdot \left|\frac{\partial x_i}{\partial \varphi_i}\right| \cdot \left|\sin \varphi_{x_i}\right|} \qquad \text{[Eq. 2]}$$

In the formula expressing the horizontal step, Eq. 1, the integrand is brought into the form

$$\frac{1}{A + 2Bz + Cz^2}, \text{ (Fig. 3)},$$

where there is a set of coefficients A_i, B_i, C_i valid in the sea layer between Z_i and Z_{i+1}. To carry out the integration in Eq. 1, $1/c^2(z)$ is expressed as

$$\frac{1}{c^2(z)} = A1_i\, z^2 + A2_i \cdot z + A3_i \qquad \text{[Eq. 3]}$$

where the coefficients $A1_i$, $A2_i$, $A3_i$ are found from the measured sound velocity profile.

[Eq. 4 is in Fig. 3]

The measured bathymetric profile is divided into segments and between the distances x_i and x_{i+1} the depth is expressed by a third degree polynomial (Fig. 4).

$$y = B1_i x^3 + B2_i x^2 + B3_i x + B4_i \qquad \text{[Eq. 5]}$$

where the coefficients are derived from the bathymetry in such a way that the slope is everywhere continuous.

It is supposed, further, that the three loss parameters, Fig. 1, are known and expressed in suitable form for the computation.

A theoretical work by Marsh, Schulkin and Kneale [Ref. 4] is used for estimating the surface reflection loss.

Numerical computation of ray path coordinates, intensities and transmission loss is carried out by means of a system of computer programmes. The first programme performs the curvilinear approximation to the measured depth-velocity profiles. The second computes the coefficients of the third degree polynomials that are used as approximation to the bottom profile. The results of these two programmes are checked before they are used as parameters in the following computations. There is a programme for determination of eigenrays based on the vertical and horizontal sound velocity distribution and the bottom topography. The main programme calculates among other things the intensity at the end of each ray. The transmission loss at a specific distance is finally obtained by addition of the pressures with random directions. This is equivalent to expressing the total loss as

$$T_{tot} = -10 \cdot \lg \left[\sum_{i=1}^{N} 10^{-\frac{1}{10} T_i} \right] \qquad \text{[Eq. 6]}$$

where

T_i = the energy transmission loss in dB for a single ray path

N = number of eigenrays.

2. COMPARISON BETWEEN MEASURED AND COMPUTED LOSS

2.1 General

The model has been used to study the transmission along several tracks some of which will be dealt with in this paper. Only frequencies below 1000 Hz have been considered. Exact determination of the reflection losses at the bottom and scattering loss at the surface is difficult. The scattering of the energy at the surface is dependent on a "wave height times frequency" parameter [Ref. 4]. The wave height is mostly estimated by eye which is an inaccurate method. However, as long as low frequencies are considered, this introduces no great error.

Information on the acoustic properties of the bottom is generally very vague and incomplete. The bottom reflection loss is dependent on the bottom material and thus may be widely variable. Adequate information concerning this type of loss would, for instance, be furnished by measurements along the track at distances separated by some 20 km. Such a lot of information does not exist for any of the tracks that are studied here. To find approximately correct data for the reflection loss another method has been adopted. The transmission loss measurement in one position of the track has been used to determine a loss function which is used in subsequent computations. This position is usually chosen at a distance of 10 to 20 km from the receiver.

Computations have been carried out along 5 tracks to find the degree of agreement between the measured and calculated transmission loss.

2.2 Track 1

The bathymetric profile along the first of these tracks, denoted track 1, is shown in Fig. 5. Transmission measurements were carried out using explosive charges of weight $\frac{1}{2}$ kg as acoustic source. Detonation depth was 40 m. The analysis was done in frequency octave bands.

The vertical sound velocity distribution was measured in 5 positions. The 5 profiles are supposed to describe the sound velocity conditions in 5 regions along the track as indicated in Fig. 5. It is seen that there is a positive gradient in the upper layer, a strong negative gradient between some 100 m and 200 m depth, and a weak positive gradient beneath 200 m. The receiver was positioned at 200 m depth. At distances exceeding 5 km energy propagates from the source at 40 m to the receiver at 200 m along bottom reflected paths. The general situation is described by the sound ray path diagrams, Figs. 6 to 8. Only a few characteristic rays are shown in each figure. Some of the bottom reflected rays are refracted in the negative gradient region. Owing to the irregular bottom the number of eigenrays at a specific propagation distance is quite great.

Information on bottom loss is insufficient. Measured values for two frequency bands are given in Fig. 9. For the band 600 to 1200 Hz an approximation was constructed and used in the following calculation. The computed transmission loss for the frequency 900 Hz is presented in Fig. 10. The agreement between the measured and computed loss is considered to be satisfactory, if the band 600 to 1200 Hz can be represented by its centre frequency, which is approximately 900 Hz.

2.3 Track 2

Track 2 will be presented next. The bottom topography is shown in Fig. 11. The receiver is situated to the right at a depth of 90 m. The source at 15 m depth moves in the indicated direction. Only the last 60 km of the track is dealt with here. The sound velocities in the area are described by the measurements plotted in Fig. 11.

As regards the bottom reflection loss on track 2 no information was available. The received energy at a distance of 10 km between source and receiver was used for determination of the bottom loss.

There is a negative sound velocity gradient everywhere. The result of this fact is that energy propagation takes place by reflected rays, some of which are shown in Fig. 12. The path taking the least reflection number is shown. The measured and computed transmission losses are presented in Fig. 13 along a distance of 60 km of the track.

2.4 Track 3

Three more tracks will be dealt with. Track 3 is shown in Fig. 14. The receiver is located at the extreme left in the figure while the source moves to the right.

The track is divided into 5 regions corresponding to measurements in 5 stations. The sound velocity in each region is supposed to be described by one of the 5 curves in Fig. 14. There is a steep negative gradient at some 50 m depth and a surface duct that becomes narrower towards deeper water. Because of the existing sound velocity distribution only bottom reflected paths carry energy. Energy propagating in the surface duct will remain there owing to the widening of the duct. A characteristic ray path is shown in Fig. 15. Measured transmission loss is shown in Fig. 16. It would be interesting to compute the transmission loss along the track because there is almost a discontinuity of the curve at about 100 km. This computation has been carried out. The result is presented in Fig. 17. The agreement between the two curves is satisfactory, and the abrupt increase of the loss at 102 km distance is confirmed. It is mainly caused by the steep slope at the bottom between 90 and 100 km distance.

2.5 Track 4

Bathymetry along track 4 is shown in Fig. 18. The bottom is relatively flat. It is supposed that the velocity profile denoted "18" in Fig. 18 describes the conditions existing along the entire length of the track. Because of the negative gradient at some 50 m depth ray paths will be as illustrated in Fig. 19. Curves showing measured and computed loss for signal frequency 116 Hz are given in Fig. 20. This case presents no features of particular interest.

2.6 Track 5

The fifth track that will be mentioned here is shown in Fig. 21. The receiver was located at 800 m depth and the source moved up-slope. The sound velocity profiles, numbered from 14 to 18, describe the velocity conditions along track 5 as shown in Fig. 21. The surface duct existing in the upper 50 m layer becomes narrower in the direction of the receiver. The measured transmission loss is shown in Fig. 22 for two frequencies of which only 116 Hz will be dealt with here.

For special reasons the 116 Hz curve is discontinuous, but there are indications that the transmission loss measured by the hydrophone at 800 m depth, decreases as the source distance exceeds some 60 n.mi. This is an interesting phenomenon.

If it is true that the transmission loss decreases with increasing distance, then this results from an increased number of eigenrays, which again is due to a combined effect of the bathymetry and the horizontal and vertical sound velocity distribution. In Figs. 23 to 25 characteristic sound rays have been plotted for 3 different distances. It is seen from Fig. 23 that at distances up to 50 km propagation takes place along ray paths that are reflected at the boundaries. At distances exceeding 50 km the surface duct widens. Some of the acoustic energy propagates in this duct, but leaks out when it reaches the area where the duct becomes more narrow. This is shown in Fig. 24 for the distance 70 km. Thus a bundle of rays propagates over great distances without having to make contact with the lossy bottom. When at a distance of 60 km from the receiver some of the rays leave the surface duct, these rays need only 2 bottom reflections to reach the receiver. This behaviour becomes even more pronounced at greater distance, see Fig. 25 for 90 km. Calculations show that the number of eigenrays increases at distances exceeding 60 km. The corresponding computed transmission loss is presented in Fig. 26, which shows that the transmission loss does decrease in accordance with the measurement. This tendency continues until at 120 km the distance becomes so great that the loss again starts increasing.

CONCLUSION

The described acoustic model has proved to be useful for prediction of transmission loss at long ranges and low frequencies provided that all parameters are known.

However, it is not capable of giving a quick answer, because preparation of the input data takes some time. In particular, the determination of eigenrays is time consuming at long ranges in the case of irregular sound velocity — and bathymetric profiles.

REFERENCES

1. Officer, C.B. Introduction to the Theory of Sound Transmission, Book, McGraw-Hill Book Company, Inc. New York, 1958.

2. Aubell, A. Theoretical Calculation of Intensities and Transmission Loss in the Ocean, Internal Report U-261, Norwegian Defence Research Establishment, Horten, Norway, 1970.

3. Aubell, A. Theoretical Calculation of Transmission Loss in the Ocean, Paper read at the Conference on Geometrical Acoustics held at SACLANTCEN, 27-30 September 1971.

4. Marsh, H.W., Schulkin, M., Kneale, S.G. Scattering of Underwater Sound by the Sea Surface, J. Acoust. Soc. Amer. 33, 3, 334-340, 1961.

DISCUSSION

Cdr Blacker found the bathymetric profiles used in this study very similar to those used by the US NAVOCEANIC acoustic surveys and Mr Aubell confirmed that he was going to apply his model to those survey data in the near future.

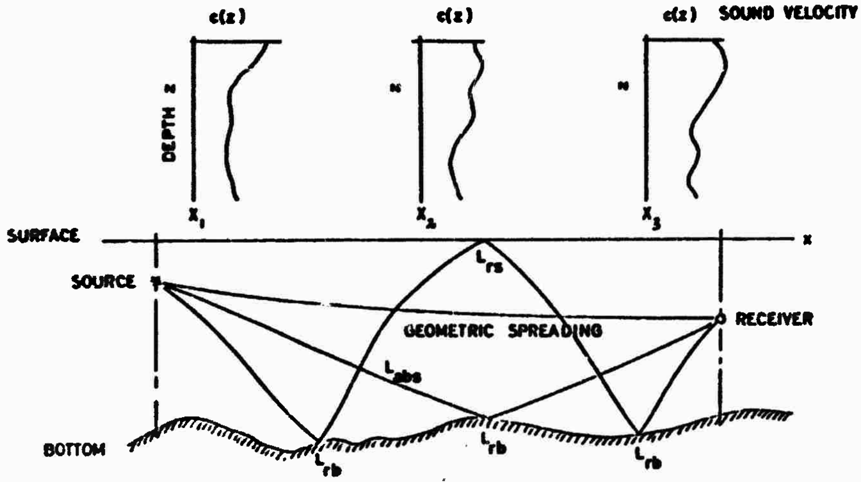

FIG. 1 OCEAN MODEL FOR THE COMPUTATION OF TRANSMISSION LOSS PARAMETERS:

a) Vertical and horizontal sound velocity distribution
b) Bottom topography
c) Energy loss by bottom reflection, L_{rb}
d) Energy absorption in the water volume, L_{abs}
e) Energy scattering loss by reflection from the sea surface, L_{rs}

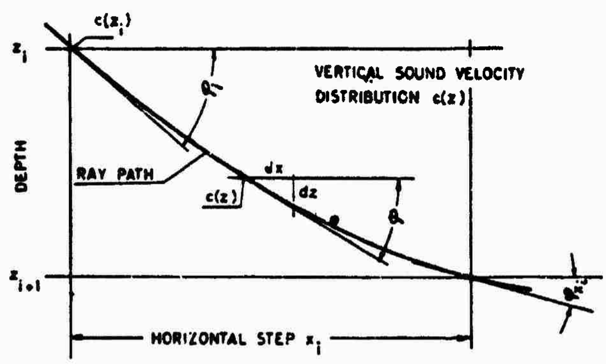

$$x_i = \int_{z_i}^{z_{i+1}} \frac{dz}{\sqrt{\frac{c_m^2}{c^2(z)} - 1}}$$, WHERE $c_m = \text{const} = \frac{c(z_i)}{\cos\varphi_i}$ Eq. (1)

SOURCE OF INTENSITY P AT $(0, z_i)$
INTENSITY AT (x_i, z_{i+1}) z]

$$\frac{I}{P} = \frac{\cos\varphi_i}{x_i \cdot \left|\frac{\partial x}{\partial \varphi_i}\right| \cdot \left|\sin\varphi_{x_i}\right|}$$ Eq. (2)

$$\frac{I}{P} = \frac{\cos^2\varphi_1}{\sum_i^{n-1} x_i \cdot \left|\sin\varphi_i\right| \cdot \left|\sum_i^{n-1}\left(x_i + \int_{z_i}^{z_{i+1}} \frac{dz}{\left(\sqrt{\frac{c_m^2}{c^2(z)} - 1}\right)^3}\right)\right| \left|\sin\varphi_2\right|}$$

FIG. 2 BASIC FORMULAE

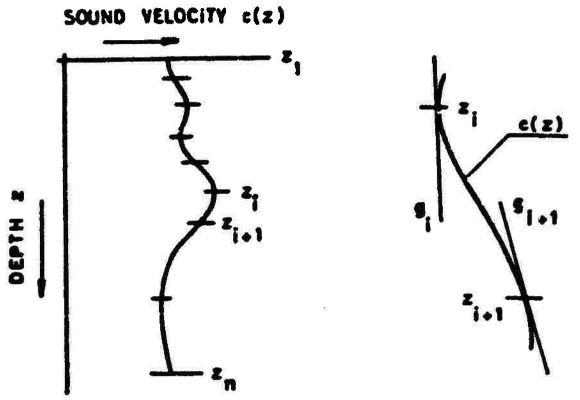

FIG. 3
DIVISION OF THE SEA DEPTH INTO LAYERS

$$x_i = \int_{z_i}^{z_{i+1}} \frac{dz}{\sqrt{\frac{c_m^2}{c^2(z)} - 1}} \qquad \text{Eq. (1)}$$

$$\frac{1}{\sqrt{\frac{c_m^2}{c^2(z)} - 1}} = \frac{1}{\sqrt{A + 2B\cdot z + C\cdot z^2}}$$

$$\frac{1}{c^2(z)} = A1_i\cdot z^2 + A2_i\cdot z + A3_i \qquad \text{Eq. (3)}$$

$$-2\cdot\frac{g_i}{c^3(z_i)} = 2A1_i\cdot z_i + A2_i \text{, WHERE } g_i = \left(\frac{dc(z)}{dz}\right)_{z=z_i} \qquad \text{Eq. (4)}$$

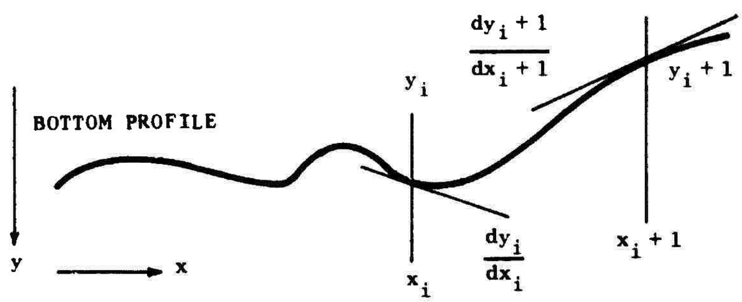

APPROXIMATION BY

$$y = B1_i \cdot x^3 + B2_i \cdot x^2 + B3_i \cdot x + B4_i \qquad \text{Eq. (5)}$$

FIG. 4 DIVISION OF BOTTOM PROFILE IN SEGMENTS

FIG. 5
BOTTOM PROFILE ALONG TRACK 1 AND SOUND VELOCITY DISTRIBUTION

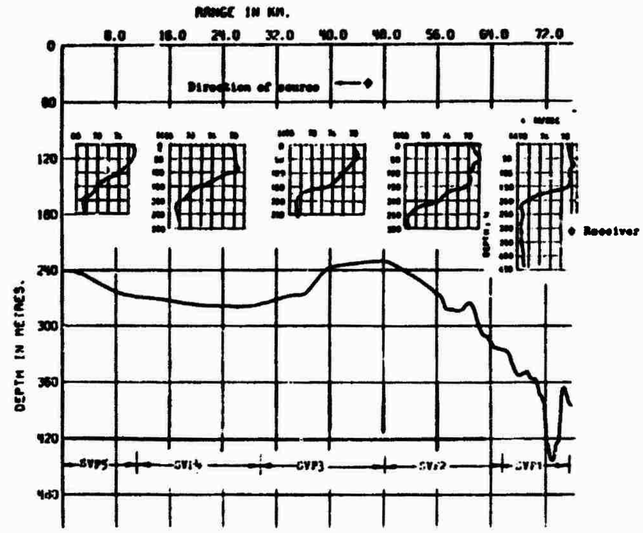

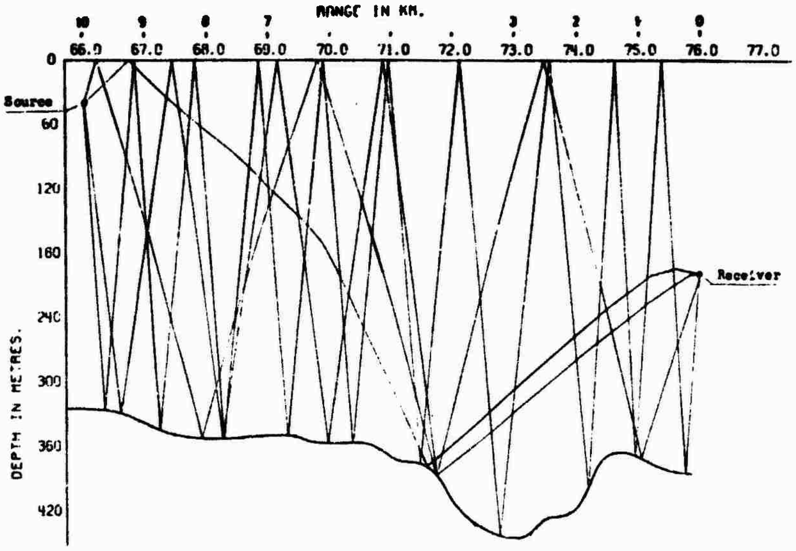

FIG. 6 TRACK 1. FOUR RAY PATHS OVER 10 km DISTANCE

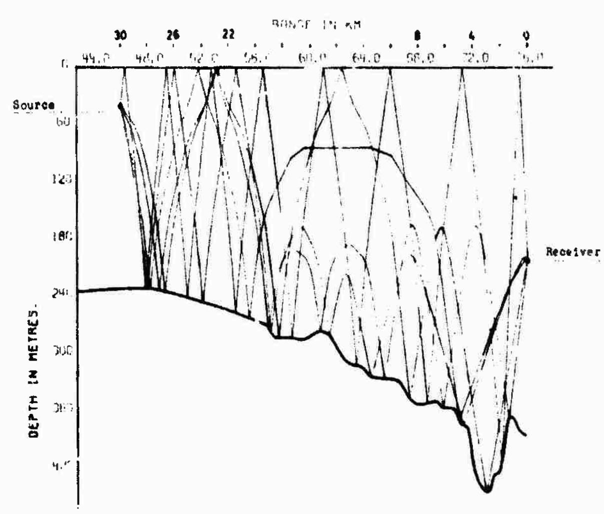

FIG. 7 TRACK 1. FIVE RAY PATHS OVER 30 km DISTANCE

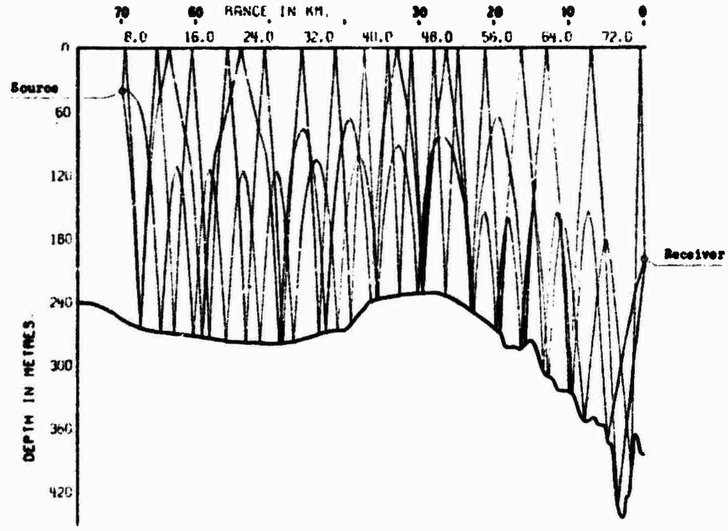

FIG. 8 TRACK 1. THREE RAY PATHS OVER 70 km DISTANCE

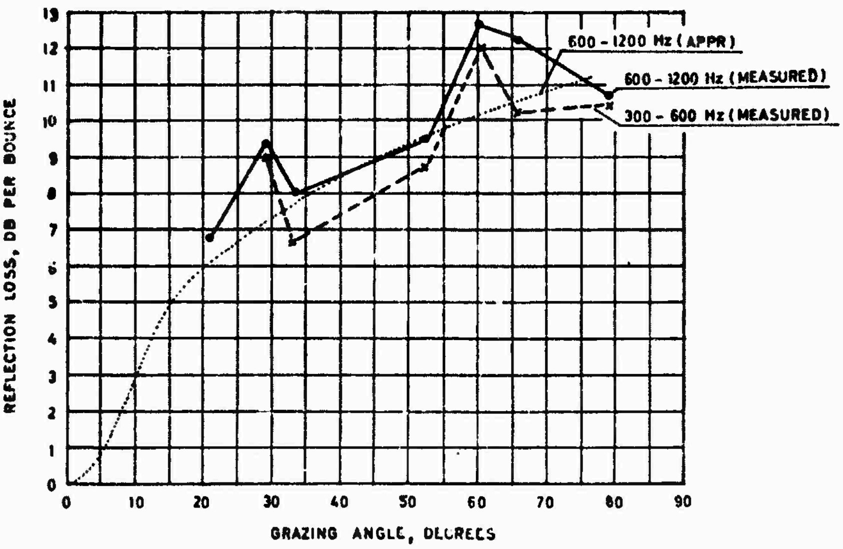

FIG. 9 TRACK 1. BOTTOM REFLECTION LOSS MEASURED IN ONE POSITION

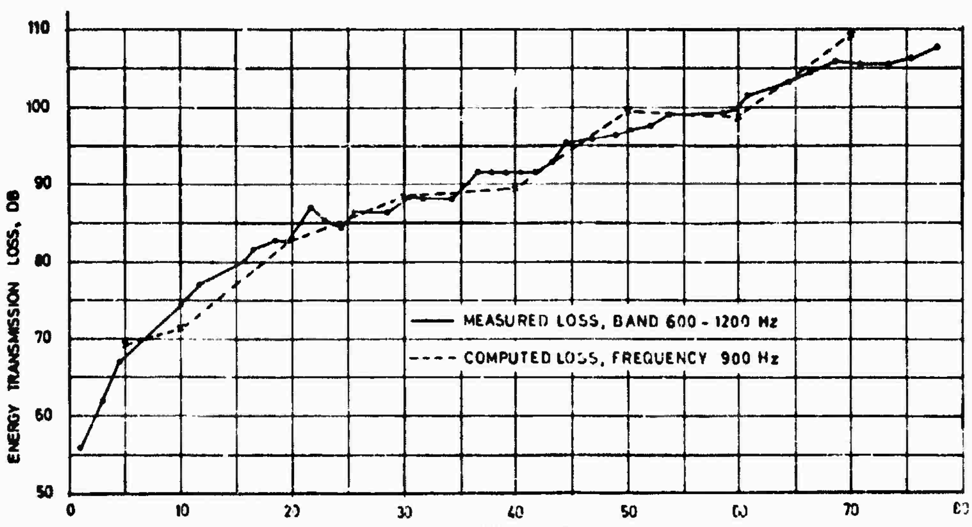

FIG. 10 TRACK 1. COMPARISON BETWEEN MEASURED AND COMPUTED TRANSMISSION LOSS

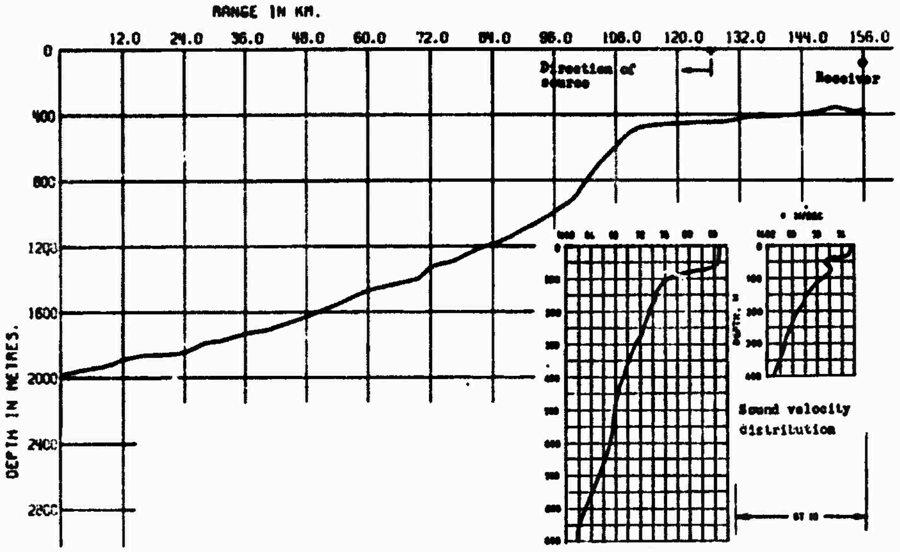

FIG. 11 BOTTOM PROFILE ALONG TRACK 2

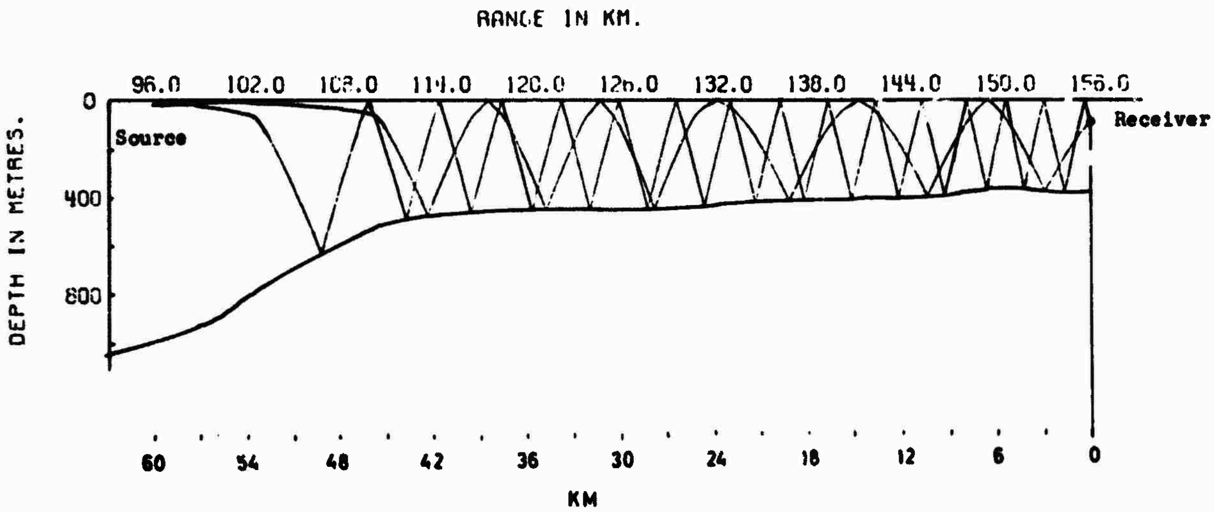

FIG. 12 TRACK 2. RAY PATHS OVER 60 km DISTANCE

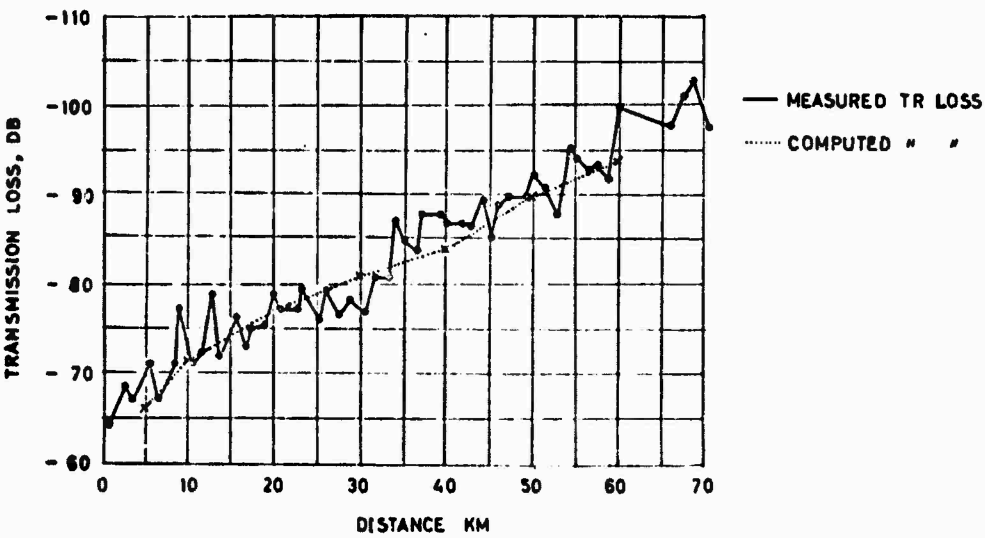

FIG. 13 TRACK 2. COMPARISON BETWEEN MEASURED AND COMPUTED TRANSMISSION LOSS, FREQUENCY 116 Hz

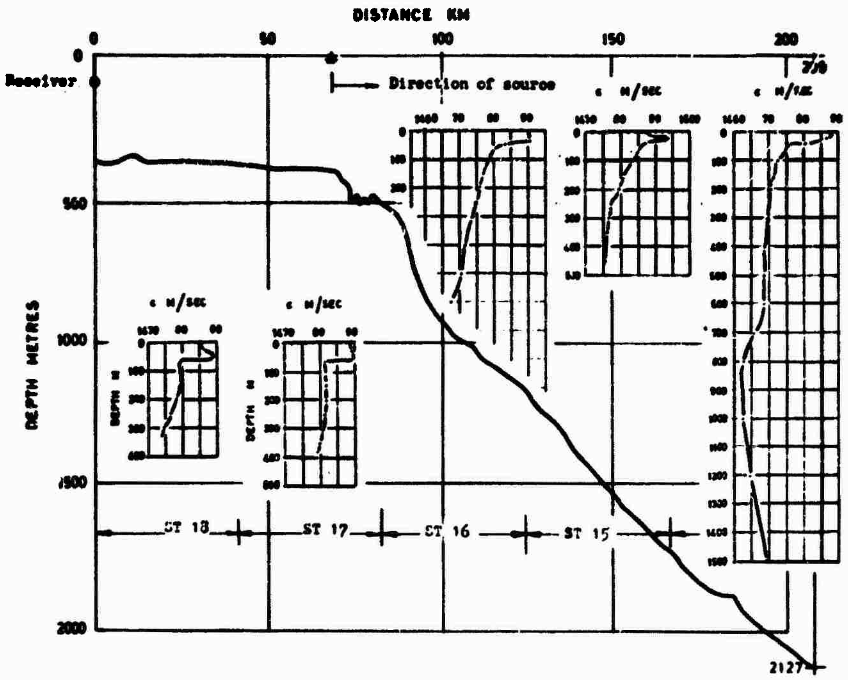

FIG. 14 TRACK 3. BATHYMETRIC PROFILE AND SOUND VELOCITY DISTRIBUTION

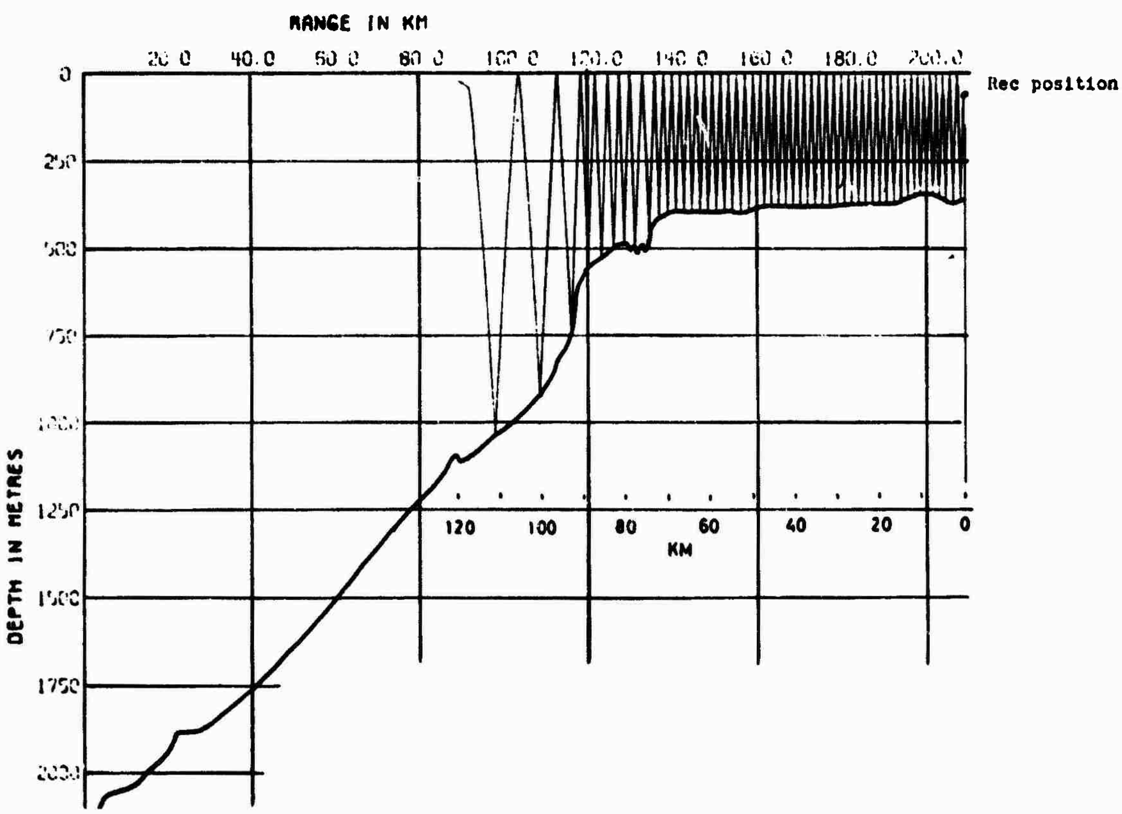

FIG. 15 TRACK 3. A SOUND RAY PATH OVER 120 km DISTANCE TAKING 51 BOTTOM REFLECTIONS

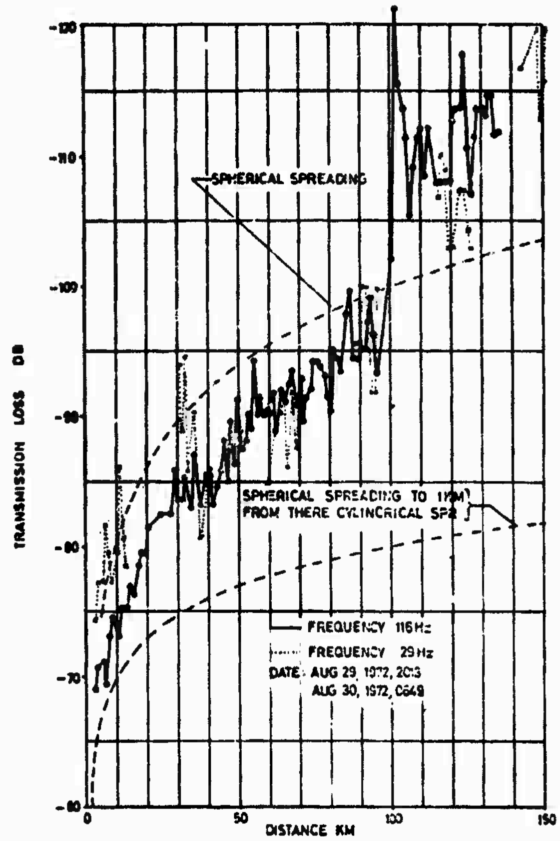

FIG. 16

TRACK 3. MEASURED TRANSMISSION LOSS

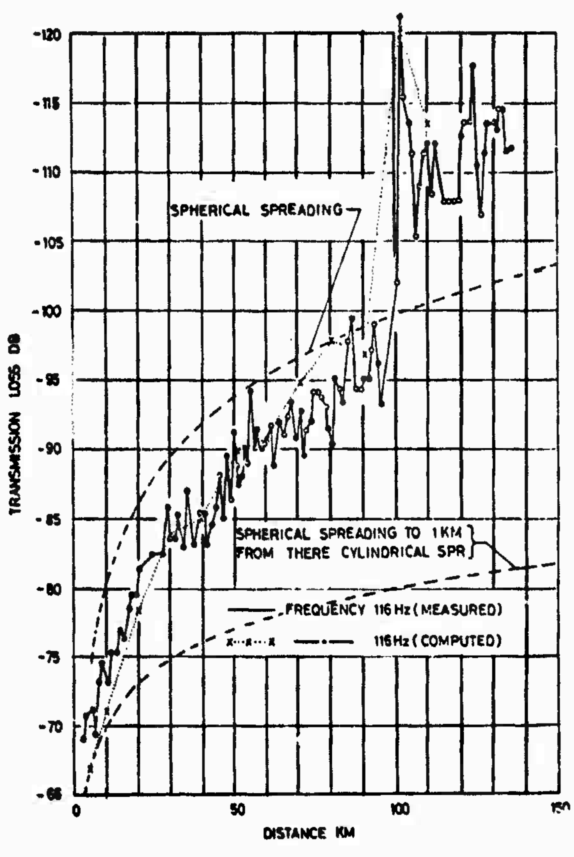

FIG. 17

TRACK 3. COMPARISON BETWEEN MEASURED AND COMPUTED TRANSMISSION LOSS

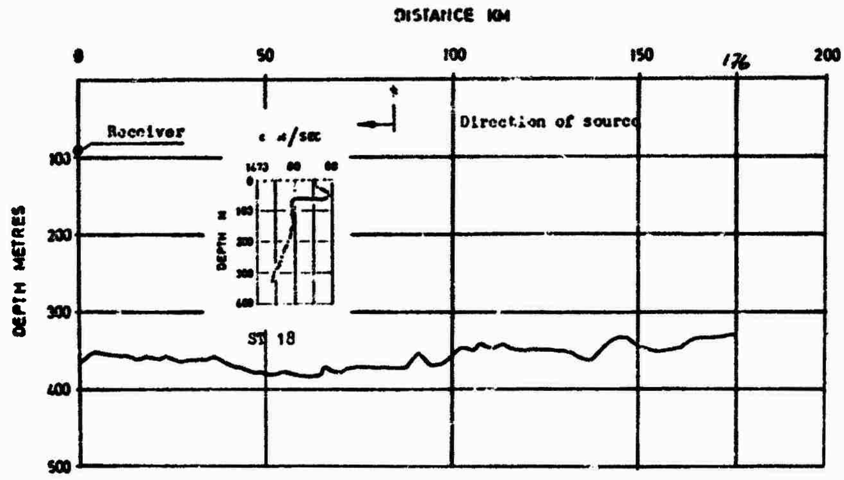

FIG. 18 TRACK 4. BATHYMETRIC PROFILE AND SOUND VELOCITY DISTRIBUTION

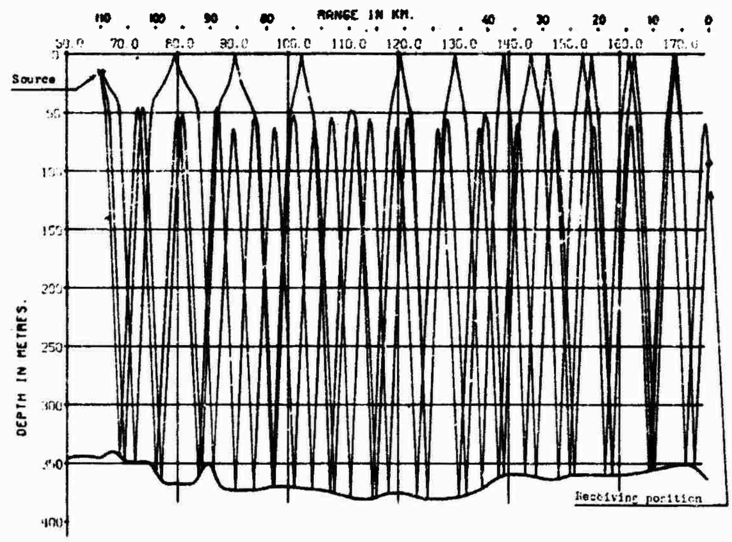

FIG. 19 TRACK 4. RAY PATHS OVER 110 km DISTANCE

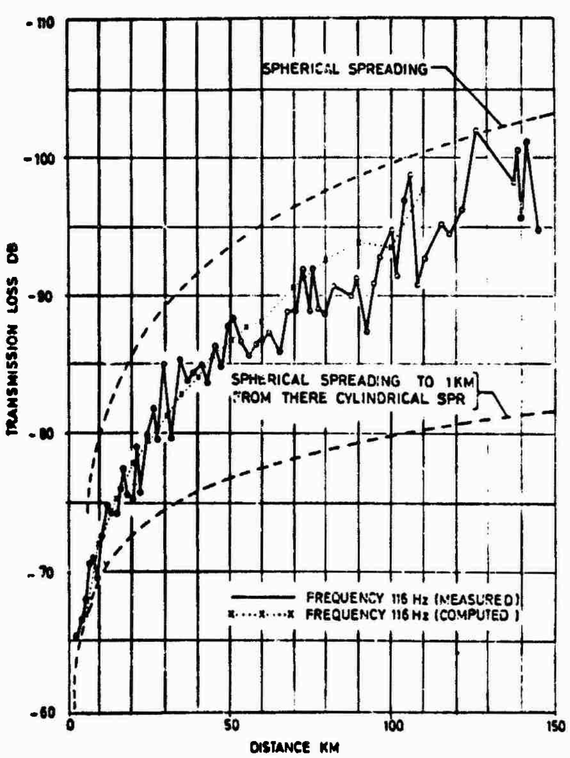

FIG. 20

TRACK 4. COMPARISON BETWEEN MEASURED AND COMPUTED TRANSMISSION LOSS

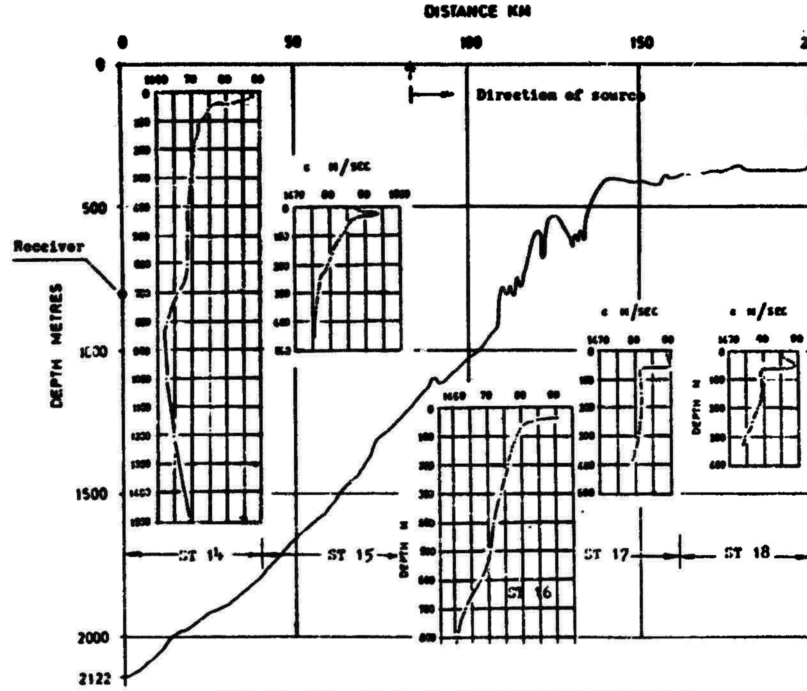

FIG. 21 TRACK 5. BATHYMETRIC PROFILE

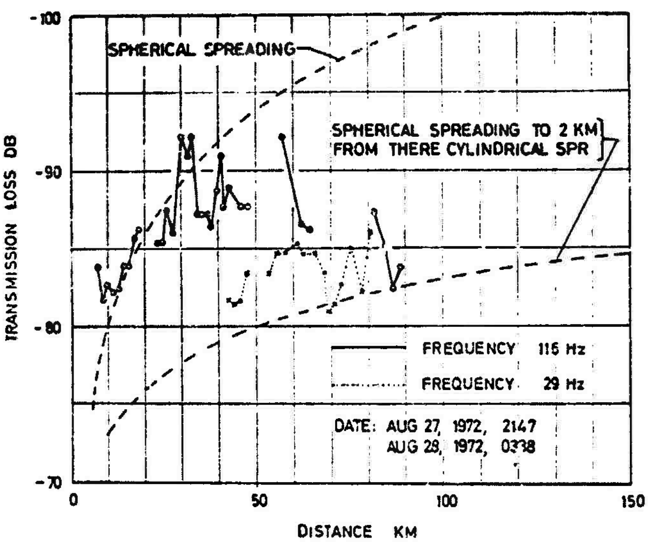

FIG. 22 TRACK 5. MEASURED TRANSMISSION LOSS

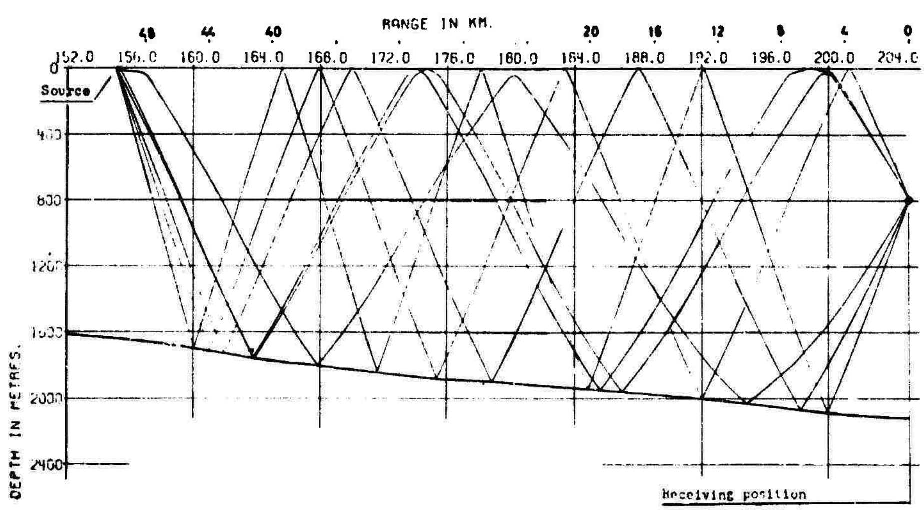

FIG. 23 TRACK 5. RAY PATHS OVER 50 km DISTANCE – RECEIVING POSITION

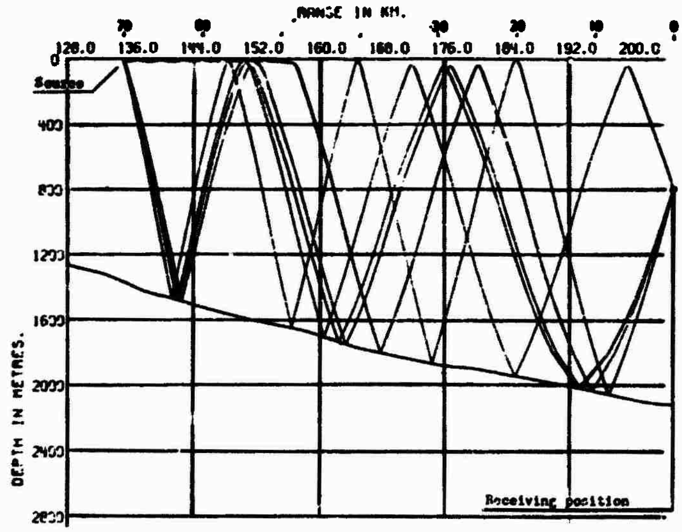

FIG. 24 TRACK 5. RAY PATHS OVER 70 km DISTANCE – RECEIVING POSITION

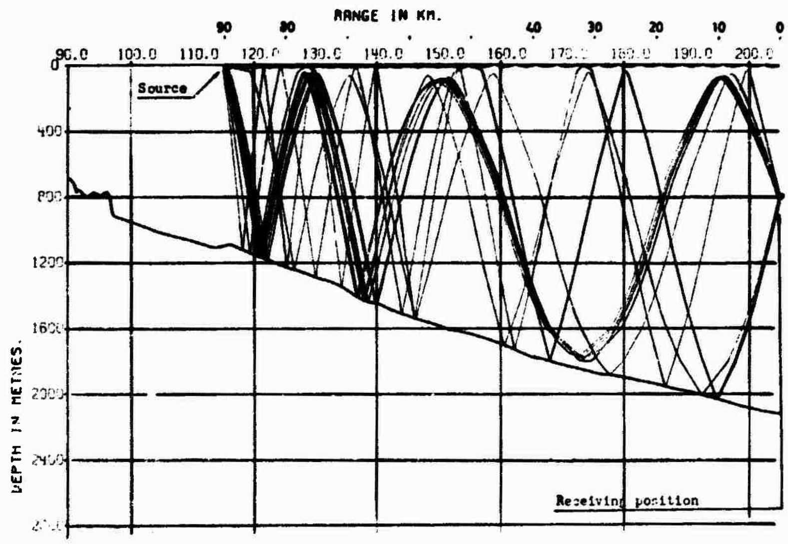

FIG. 25 TRACK 5. RAY PATHS OVER 90 km DISTANCE – RECEIVING POSITION

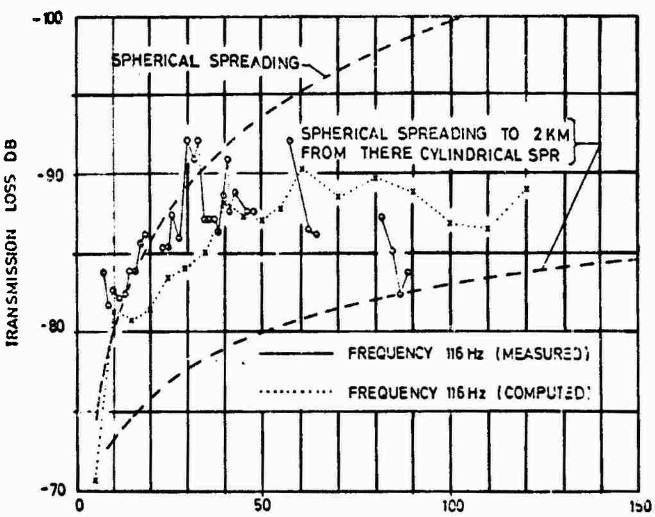

FIG. 26 TRACK 5. COMPARISON BETWEEN MEASURED AND COMPUTED TRANSMISSION LOSS AT 116 Hz FREQUENCY

A STATISTICAL RAY TRACING ROUTINE

by

H.G. Schneider and W. Kroll
Forschungsanstalt d. BW für Wasserschall
und Geophysik, Kiel, Germany

ABSTRACT

As a first step towards predicting sonar ranges in shallow water a ray-tracing computer program has been written, which includes the possibility of handling stochastic influences on underwater sound by Monte Carlo methods. For example, sound scattering by the sea surface or leakage of energy from sound channels can be accounted for. The program serves to model the measured acoustical fields and to gain a better understanding of the involved physical mechanisms. In the paper the flexible module structure of the program will be sketched shortly. The idea of introducing Monte Carlo methods in a ray-tracing computation will be discussed for sound scattering at the sea surface. Data from experiment and calculation will be compared to this point concerning propagation loss.

INTRODUCTION

It is well known that ray-tracing models provide a good basis to gain considerable insight in the propagation characteristics of underwater sound. Moreover, these models enable us to do some forecasting of acoustic quantities if a certain set of environmental parameters is known.

The aim of the work, the beginning of which is reported here, is to establish some kind of material (functions, tables, programs or whatsoever) from which sonar ranges can be read. This material is of practical interest to SW and ASW only if the number of input parameters is fairly small and if all situations which may occur are accounted for. Thus, a parameter reduction or classification is necessary and the criteria for this must be specified from the acoustical field characteristics.

A first step towards solving this task is to model performed experiments by ray-tracing techniques. The modelling should, from the very beginning, be based on those parameters which the user of the forecasting material can readily obtain. On the other hand, we should limit our investigation to that degree of refinement and exactness which the user really needs, even though from the scientific point of view it is often challenging to go into further details. This does not mean we have only to do a data sorting and fitting job, but on the contrary, we are in the lucky situation that our task can be

solved easier if we gain more understanding of the involved mechanisms from the physical standpoint or that of information theory. This seems to be the best way to reduce and standardize the number of input parameters.

The following three quantities are of main interest to us at the present stage ofthe model:

1. The overall propagation loss.
2. The propagation loss as a function of receiver depth.
3. The angular density distribution of energy at the ocean bottom and/or sea surface, from which we want to provide input data for reverberation.

These quantities are functions of the seasonal sound-speed profiles, acoustic frequencies, bottom impedance and geometry, sea-surface roughness and the source depth.

1. THE MODEL

1.1 The Ray-Tracing Routine for Shallow Water

For shallow water conditions the propagation loss can hardly be calculated by ray divergence methods even if the ocean bottom and the sea surface are assumed to be flat. Moreover, in most shallow water areas at least one of these boundaries influences the sound propagation stochastically. We determine the energy in a certain depth interval at a given distance from the source by adding the energy of single rays penetrating this interval. It is therefore not necessary for the ray-tracing computations to approximate the sound-speed profile by differentiable functions, but piecewise linear seg nts connecting the main data points will do.

The question, "Which are the main data points of a measured sound speed profile", has been discussed by Cdr Dr Sluyterman van Langeweyde. He classifies sound-speed profiles by means of acoustic criteria. This includes the task to find the most simple profile of a certain set of profiles which generate the same type of acoustical field. Thinking of this task as beeing solved we use the most simple profile as representative of its class in this computation.

Deterministic horizontal variations of sound-speed profiles may be accounted for in the usual way by lining up several profiles along the propagation path. Horizontal and vertical gradients are allowed. (Care must be taken in case of steep vertical gradients which change depth along the propagation path, this is important for propagation in ducts for example.)

Stochastic variations in sound speed, either vertical or horizontal, may be accounted for by a Monte Carlo method, this part of the program is in the stage of being developed.

As mentioned above, the stochastic roughness of the sea surface or the ocean bottom may be of importance for propagation loss. The scattering of sound at these random rough surfaces is simulated by, in principle, the same Monte Carlo Method as just mentioned. Let me give some comments on this method. The main point is that we do not model the stochastic process itself in the ray-tracing routine, as for example Brochelman and Hagfors did. We use, in case of random rough boundary a scattering coefficient which has been obtained from the theory of sound rather than from ray theory. This scattering coefficient is interpreted as a probability density for the re-radiation angles. For every ray which contacts the boundary a re-radiation angle is determined at random from the corresponding probability density. If the random process is stationary for the time of the acoustic transmission and over the propagation path this method is exact.

Since the scattering coefficient is obtained from the theory of sound and not from ray theory it is frequency dependent, and at least valid for all acoustic wave lengths where ray tracing techniques hold. Moreover, it is possible to simulate the effect of interactions with such processes that may not be treated by ray theory. For example the influence of resonant or Bragg scattering from a rippled sand bottom on propagation loss may be accounted for by this method.

1.2 Model Parameters

1.2.1 Output Parameters

The quantity which dominates our interest at this stage of the model is the propagation loss defined as follows.

Let w denote the energy measured at distance r from the source at a depth interval about z. We assume a function

$$w(r, z) = \frac{a}{r} e^{-d(z) \cdot r} \qquad \text{[Eq. 1]}$$

by which the measured data is to be described.

After eliminating the term for cylindrical spreading we may write:

$$10 \lg\left(\frac{w \cdot r}{w_0 \cdot r_0}\right) = 10 \lg \frac{a}{a_0} - \alpha \cdot 10 \lg(e) \cdot r \qquad \text{[Eq. 2]}$$

or with the new quantities:

$$E(z, r) = A(z) - B(z) \cdot r \, . \qquad \text{[Eq. 3]}$$

The quantity to be compared with the calculations is $B(z)$, the propagation loss in dB/km for a certain depth interval and at a certain frequency. The depth interval may extend over the total water depth.

The quanaity B(ᴌ) depends on whether the data can in principle be described by the assumed function or not. If not, B is a function of the range over which the curve fitting is done. To limit this influence a constant range has been assumed.

As input data for reverberation computations, we compute the angular distribution of energy from $0°$ to $30°$ grazing angles in one nautical mile segments at the ocean bottom and/or sea surface, at distance of 5, 10, 15, 20, 25 n.mi from the source.

1.2.2 Input Parameters

The input parameters of the model are given by the experimental and environmental conditions.

a) Experimental conditions:

The range is 30 n.mi; source depth is 26 m below the sea surface; the broadband signals from explosive have been evaluated from 15 Hz to 10 kHz. Model computations have been made for the following four centre frequencies:

0.5 kHz, 1.0 kHz, 2.0 kHz, 4.0 kHz

b) Environmental conditions:

Because of constant salinity in the North Sea Standard Area the medium attenuation is taken to be constant. We used the values:

Frequency	0.5	1.0	2.0	4.0	
Attenuation	0.02	0.07	0.17	0.32	dB/km

which are taken from Thorp. These attenuation values are added to the computed ray tracing results for comparison with the experimental data.

The bottom impedance has been calculated from sandcore data taken in the Standard Area on the assumption of homogeneous layering. The reflection coefficient is to be seen in Fig. 1.

Other parameters do change from experiment to experiment and will be given with the comparison of the computational results. In general those parameters which have been measured or estimated in situ will be introduced in the model.

For the sea-surface roughness the estimated values of $h_{1/3}$ were used. Since the root mean square elevation $\sigma = \frac{1}{4} h_{1/3}$ and the correlation length of the sea state have to be supplied to the model, the latter quantity has been calculated from σ and the assumption of a Pierson and Moskowitz spectra.

The wave height of the swell was assumed to be the same as that of the wind sea; the root mean square slope was set to 0.015 times that of the wind sea (approximately $0.12°$).

2. COMPARISON OF EXPERIMENTAL AND COMPUTATIONAL RESULTS

2.1 Large-Scale Bottom Topography

The North Sea experiments were conducted in an area of relatively constant water depth. To obtain information on the influence of the large scale bottom topography, computations were made with two bottom profiles as given in Fig. 2 (denoted by 1 and 2) and for comparison with a flat bottom (denoted by 3). The propagation loss was the same for all three cases for winter conditions with isothermal water and a flat sea surface. Because of this, in all the following computations the bottom was assumed to be flat.

2.2 Winter Conditions

The term winter conditions is equivalent to isothermal water over the total water depth. The sound speed increases from the sea surface to the ocean bottom because of the increasing pressure with 1/63 m/s/m.

Measurements have been made during three different sea state conditions with wave heights $h_{1/3} = 0.5$ m, 1.5 m and 3.0 m.

In Fig. 3 the measured propagation loss is plotted with continuous lines. The computational results correspond to the dashed lines. The computation with the flat sea surface $\sigma = 0$ yields the lowest propagation loss. Obviously, the dependence of the propagation loss on frequency and sea state is the same for the measured and computed data. This becomes even more evident in Fig. 4 which contains the same data.

The agreement of computational and experimental data is rather good. The relatively large deviation of the point at 2 kHz/$h_{1/3}$ = 2.5 m is due to an insufficient number of rays.

This demonstrates the necessity to consider a frequency-dependent scattering mechanism.

This agreement in propagation-loss data is only of any value if other measured field characteristics are modelled with the same accuracy. One measurement was conducted with a vertical hydrophone line array. From this a depth-independent propagation loss was inferred. In Fig. 5 the propagation loss is plotted vs depth for $h_{1/3} = 1.5$ m ($\sigma = 0.38$ m). For the 4 kHz data the standard number of 4000 rays has to be increased to 8000 rays to yield a smooth curve. Agreement of measured and computed data is very good. In the upper left corner the size of the depth interval (6.4 m) used in the calculation is depicted. One has to ensure that the energy penetrating one depth interval is due to a sufficiently large number of rays to yield statistically relevant results.

The only loss mechanism except the constant medium attenuation is provided by the bottom-reflection coefficient. Hence the increase in propagation loss with higher sea states must be due to a change in the angular energy density at the bottom caused by the scattering of sound at the sea surface.

Because of the increasing sound speed towards the bottom, the rays which leave the sea surface with grazing angles of less than 2.5° do not reach the bottom. Since we want to obtain information on all rays we depicted the angular energy density at the sea surface. In Fig. 6a, this energy density in one nautical mile segments is plotted vs the grazing angle (1° interval) for five distances from the source. For a flat sea surface ($\sigma = 0$) (Fig. 6a) the energy density becomes continuously smaller for increasing distances from the source. If the sea surface is rough (Fig. 6b) the energy density becomes nearly constant for angles greater than 5° and does not concentrate the energy towards smaller grazing angles. This means the roughness of the sea surface continuously converts energy from smaller to greater re-radiation angles. This process has been assumed in the paper of Wille, Thiele, Schunk published in J.A.S.A. to explain a range-independent propagation loss.

In conclusion of this chapter the model proves to be a powerful tool to calculate sonar ranges for these isothermal water conditions with constant water depth.

It is known that for a reflection coefficient of the bottom which is linearly dependent on the grazing angle, ray-tracing computations with flat boundaries yield a propagation loss which is independent from the water depth. But measurements have shown that the propagation loss increases with smaller water depth. This result has been obtained too with our model assuming a rough sea surface and isothermal water.

With $h_{1/3} = 1.5$ m and a frequency of 2 kHz the propagation loss was computed to

0.34 dB/km	for	120 m	water depth
0.42 dB/km	for	64 m	water depth
0.94 dB/km	for	30 m	water depth

The source depth was half the water depth. With a flat sea surface the propagation loss was (0.30 ± 0.02) dB/km for all three depths.

2.3 Early Summer Conditions

In June, the sound-speed profile in the North Sea usually appears as shown in Fig. 7. The thickness of the isothermal surface layer depends strongly on the weather. In this case there was a sea state of $h_{1/3} = 1.5$ m. In Fig. 8 the continuous lines denote experimental propagation loss data: series No. 33 has been measured in cross-wind and series No. 34 in the up-wind direction. The dashed curve has been computed with $\sigma = 0$ and $\sigma = 0.38$ for a receiver depth of 23 m, well below the surface layer. Since the main transmission path is of the RBR type these rays never reach the sea surface and so the model calculation is sea-state independent for this data.

In Figs. 9a and 9b the angular energy density at the bottom is shown. The energy which reaches the ocean bottom with grazing angles of less than 11° is not influenced by the sea-surface roughness only the remaining part of the energy is scattered to larger angles and damped

out very quickly. Since the same propagation loss has been computed for a rough and a flat sea surface in a depth of 23 m one of the following two possibilities must hold: in case of a flat sea surface the energy which reaches the bottom with grazing angles greater than 11° contributes either a neglegible part or a constant fraction to the total energy.

Obviously, there is a mechanism which has not been accounted for in the model and which is responsible for the discrepancy of experimental and computational results.

Since we have no measurements with a vertical hydrophone array for this early summer condition we have not calculated the dependence of propagation loss on depth but we have done this for the similar situation in August.

2.4 Later Summer Conditions

Figure 10 shows two typical sound-speed profiles measured in August, No. 1 has been measured after a period of warm weather with low winds, No. 2 after several days of gale winds (36 kn). Our investigation is done with profile No. 2. The dashed horizontal line denotes the source depth. Wave height was recorded and found to be $h_{1/3} = 1$ m. Figure 11 shows the measured (full line) and computed propagation loss. In the computation there is only a moderate influence of sea state on the propagation loss. Obviously, this is too little to achieve agreement between measurements and computation. The experimental results with a vertical hydrophone array yield a depth-independent propagation loss. The computational results showed a different behaviour.

If the sea surface is flat, the propagation loss in the surface layer is smaller than in the underlying layers. This is due to the SRBR rays which have maximum skip distance from bottom bounce to bottom bounce (Fig. 12). If the sea surface is rough these rays are scattered to large angles and undergo a stronger absorption at the bottom hence the propagation loss (Fig. 13) is increased in the top layer since no energy is allowed to enter the top layer from below. The energy from the surface layer is removed by scattering.

Since measurements show a depth-independent propagation loss, the next step of our model is to provide a non-zero probability for converting RBR into SRBR rays.

The probability for the mechanism must be taken from observed changes in the sound-speed profiles with respect to time, space and bottom roughness. We are able to account for this by the same Monte Carlo Method we utilized for the rough boundary scattering.

CONCLUSION

Finally I want to stress the following:

1. In this model every parameter has been set to the value corresponding to the experimental situation and the knowledge of the physical process. This means no artificial or free parameter has been introduced to gain a better agreement between experimental and computational results.

2. The idea of dealing with rough-boundary scattering in the way it is done here has been proven very successful and needs no further refinement to obtain results of practical interest. The sea state reports in half metre steps are exact enough, but more up-to-date information on swell would be good.

3. In the model a mechanism is missing which allows energy to penetrate steep gradients in those situations where ray theory forbids it. This does not question the value of ray tracing; on the contrary, we will use the developed Monte Carlo Method, which is based on ray tracing, to overcome this problem. In order to provide a basis for sonar forecasting we have to find a standardized quantity for the probability of energy penetrating steep gradients; again this function will be frequency dependent.

4. We have not even made the attempt to utilize this statistical Monte Carlo Method for other quantities of interest as for example the information content of the transmitted sound. Hence the possibilities inherent in the Monte Carlo Method, which does not model the stochastic processes themselves, provide a frame in which many limits caused by the ray-tracing concept may be overcome.

DISCUSSION

Replying to Mr Laval's question about the surface-scattering Dr Schneider explained that the model used was the Beckmann and Spizzichino two-dimensional scattering equation multiplied by the shadow function, because the small angles here are very important, and the specular or coherent part was added incoherently.

Dr Schneider assured Dr Wille that a varying bottom depth could easily be accounted for.

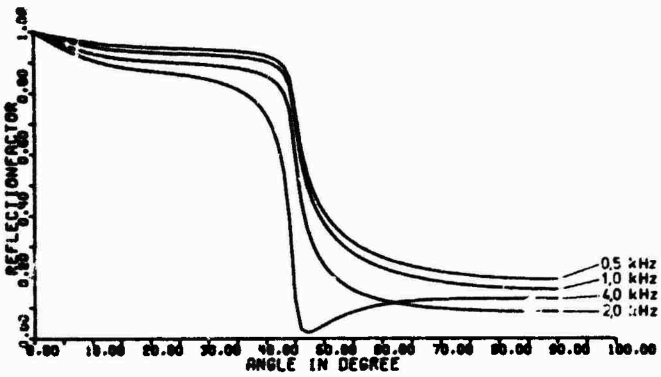

FIG. 1

FIG. 2

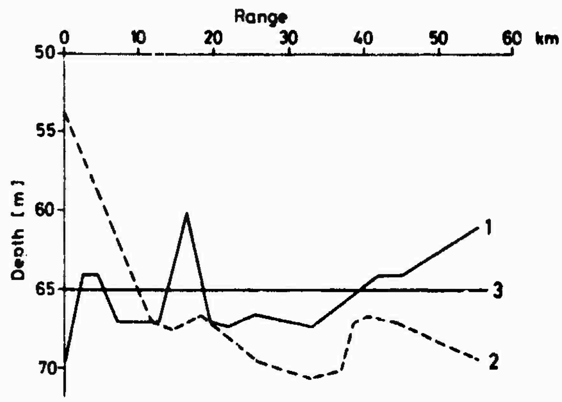

LARGE SCALE BOTTOM TOPOGRAPHY
TWO EXAMPLES NORTH-SEA

PROPAGATION LOSS
FEBRUARY, NORTH SEA

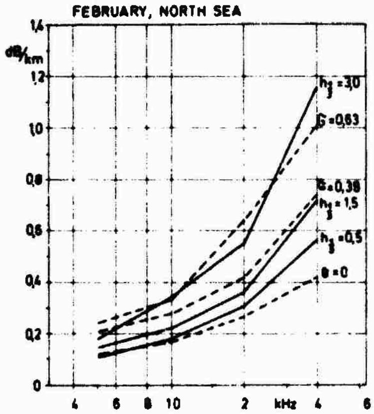

FIG. 3

PROPAGATION LOSS VERSUS SEA STATE
FEBRUARY, NORTH SEA

FIG. 4

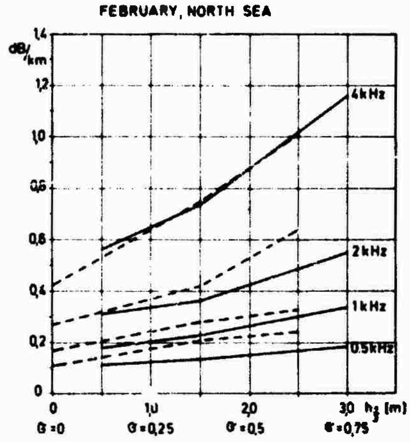

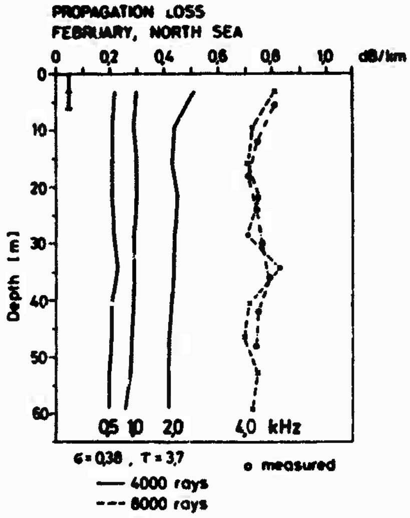

FIG. 5

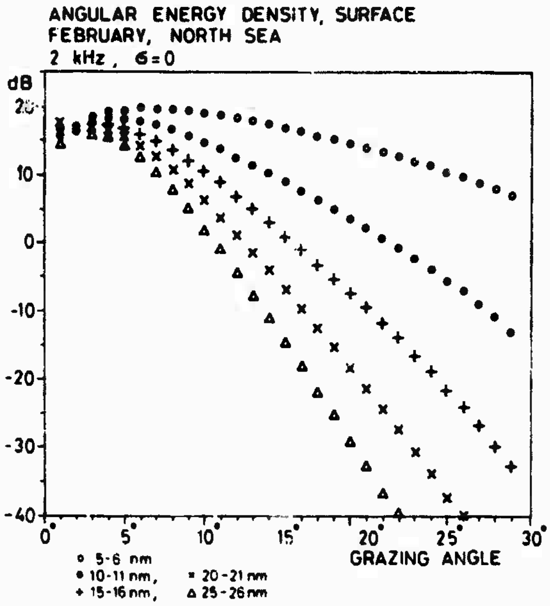

FIG. 6a

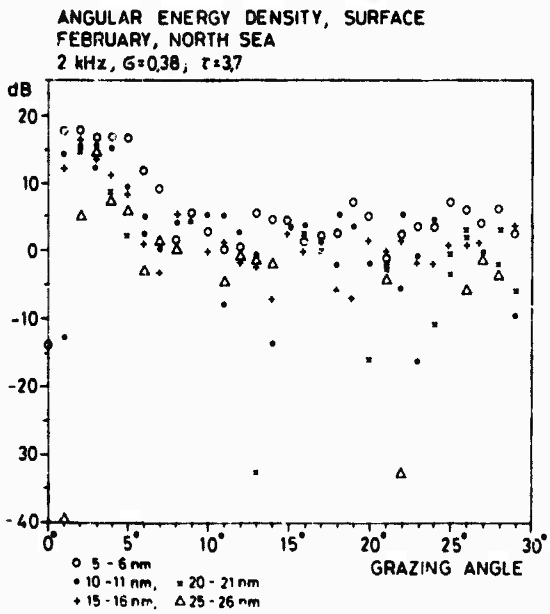

FIG. 6b

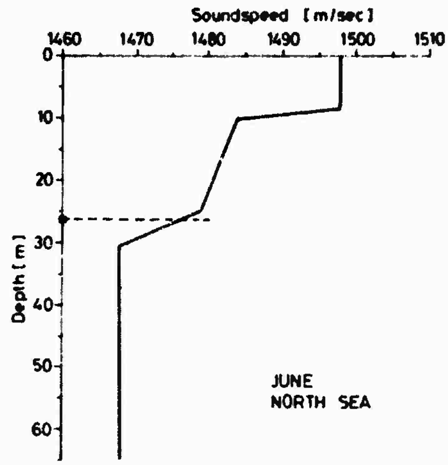

FIG. 7

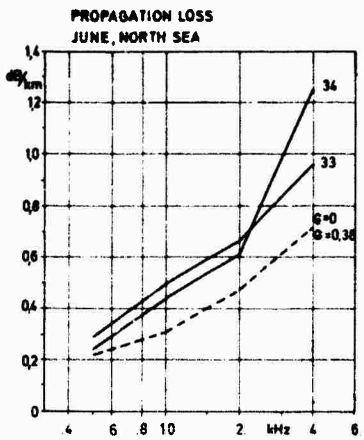

FIG. 8

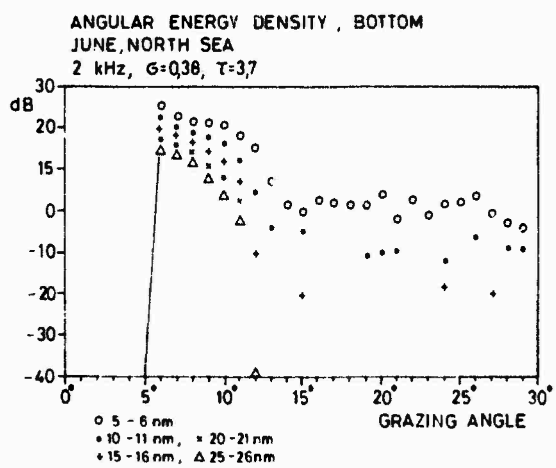

FIG. 9a

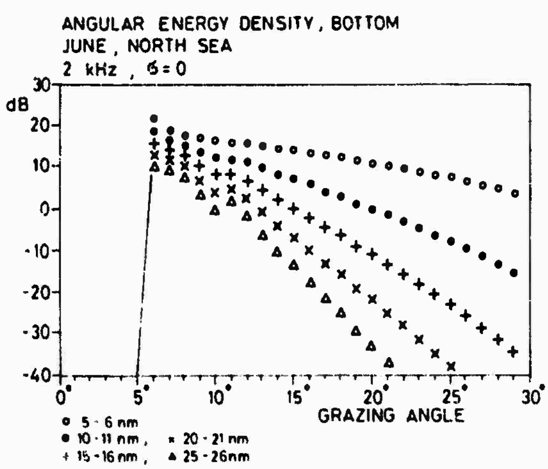

FIG. 9b

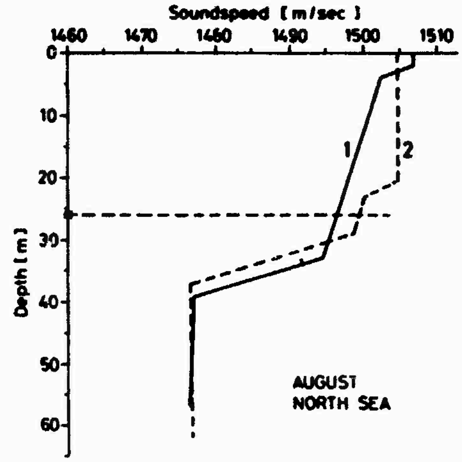

FIG. 10

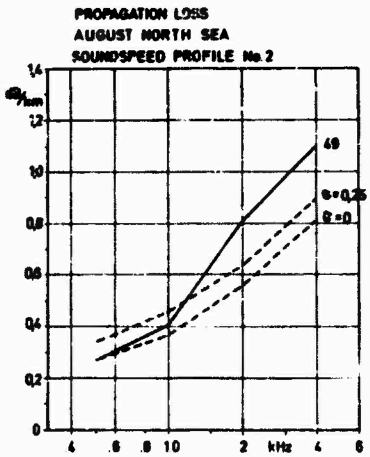

FIG. 11

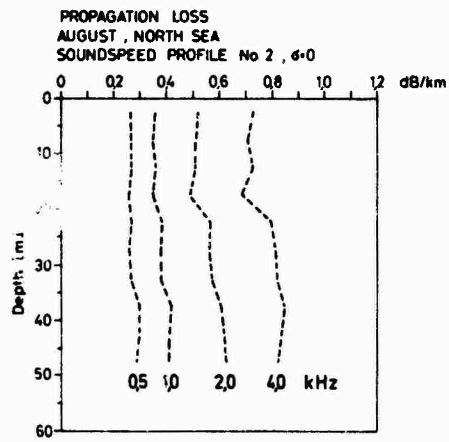

FIG. 12

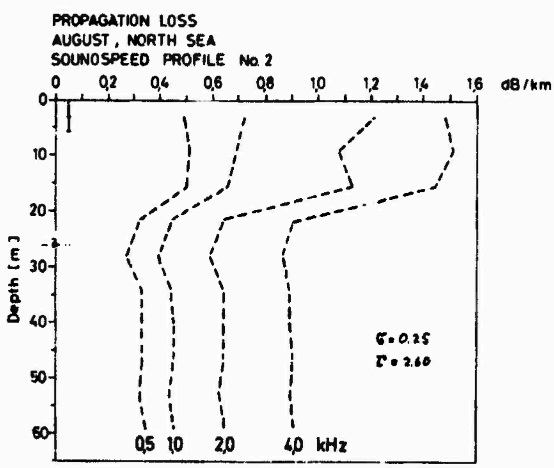

FIG. 13

SOURCES OF AMBIENT NOISE IN THE SHALLOW-WATER MARGINAL SEA-ICE ZONE*

by

O.I. Diachok
and
G.K. Long
U.S. Naval Oceanographic Office, Washington, D.C.

A series of synoptic measurements of the spatial variability of ambient noise and related environmental parameters in the shallow waters of the marginal sea-ice zone were made using sonobuoy and remote sensing techniques from aircraft. The primary physical sources of ambient noise were shown to be wave and swell interaction with ice floes at the ice/water boundary, and dynamic interactions between adjacent ice floes in the ice field, in accordance with the results of similar measurements in deep waters. Noise levels at ice/water boundaries protected from swell by land masses were found to be relatively low. It was also shown that biological sources of ambient noise, specifically high concentrations of beluga whales, seals and walrus, may at times be dominant at some shallow-water locations, in contrast with the results of measurements in relatively deep waters, where contributions to total noise levels due to biological activity are generally minimal.

INTRODUCTION

The marginal sea-ice zone may be defined as the partially ice-covered transition region between the totally ice-covered Arctic Ocean and the ice-free Atlantic and Pacific Oceans. This oceanic regime is situated in areas which may be as shallow as 50 m or as deep as 2000 m, but which are generally less than 500 m deep.

Aside from depth considerations, the physical configuration of the marginal sea-ice areas of the Arctic Ocean is characterized by complex and unique dynamic processes not found in either the open oceans or the ice-covered Arctic Ocean, with the most prominant one being the interaction of ocean waves with sea ice [Ref. 2]. As a result of this interaction, ocean waves are attenuated and the ice is broken up into relatively small floes by the waves. Furthermore ocean waves entering shallow marginal sea-ice areas are also affected by interactions with the ocean bottom. In order to determine some of the effects of environmental phenomena characteristic of marginal sea-ice areas on the spatial variability of ambient noise, a series of quasi-synoptic noise measurements was made with air-deployed sonobuoys during

* A significant portion of the results presented here has been published previously in Ref. [illegible].

the period 1971-1974 in the East Greenland Sea and in the Bering Sea [Ref. 1]. It is the purpose of this paper to describe and discuss some of the salient results of these experiments.

1. MEASUREMENT TECHNIQUE

Quasi-synoptic measurements of ambient noise levels in the vicinity of the ice/water boundary were made at the sites shown in Fig. 1. The measurements were accomplished by deploying calibrated sonobuoys from aircraft [Ref. 3] into open water and into polynas, i.e., water openings in the ice field. The hydrophone depth of the sonobuoys was 30 m.

Each sonobuoy was monitored for periods, which were generally longer than 10 minutes, from the aircraft which circled overhead. To avoid contamination of the data by aircraft noise, the telemetry distances to the aircraft were greater than 10 km and the altitudes were greater than 1 km. To check repeatability most of the sonobuoys were monitored more than once during the measurement periods. The data were tape-recorded in the aircraft and subsequently processed to determine average noise levels for consecutive 32-second samples in each one-third-octave frequency band over the range from 100 to 1000 Hz. Median ambient noise energy spectrum levels were then determined for each 10-minute period for each sonobuoy. Generally, the variability about the median levels was approximately 3 dB. No local ship traffic was observed during the course of the measurements which will be discussed in this paper.

All measurements were made in cloud-free sites, which were often selected by using real-time, in-flight reception of satellite imagery [Ref. 4], a technique especially developed for this airborne research programme. Measurements of the ice concentration and ice-floe diameters were made by using standard and infrared photographic techniques. Measurements of wind-generated ocean-wave profiles were made at some of the sites with an airborne laser profiler [Ref. 5]. The latter data have not yet been analysed, however, and will not be discussed here. Instead, the ambient noise data will be related to the observed sea state, and to hindcasts of the geostrophic wind velocity and the ocean wave conditions [Ref. 6]. Sea state (1-6) was determined visually with an estimated uncertainty of ±1. Hindcasts of wind velocity at sea level were made by reducing the geostrophic wind velocity computed from barometric pressure charts by a factor of 0.7. The estimated uncertainty in the resultant geostrophic wind velocity at sea level is ±5 kn [Ref. 7]. The uncertainties in the corresponding hindcasts of dominant wave periods and amplitudes are estimated to be ±1 s and ±1 m, respectively [Ref. 6]. The water depths at the measurement sites were determined from bathymetric charts.

2. NOISE GENERATION AT THE ICE/WATER BOUNDARY

In order to determine the relative magnitudes of physical phenomena characteristic of marginal sea-ice areas on the generation of ambient noise, several sets of measurements of the spatial variability of ambient noise were made under the following environmental conditions: relatively compact and diffuse boundaries, and relatively high and low sea states.

The most pronounced feature of the measurements, which appears to be a universal property of the ice/water boundary, is a relative maximum in noise levels at the boundary [Ref. 1]. Hypothetically, the mechanisms responsible for high ambient-noise generation are related to wind-generated ocean wave interactions with sea ice at the ice/water boundary.

The magnitudes of ocean waves incident at the ice/water boundary may be considered to be a function of local and distant meteorological conditions [Ref. 8]. The magnitude of locally-generated ocean waves is a function of the wind velocity, fetch and duration. The magnitude of the contributions from distant sources of ocean waves is a function of the magnitudes of the sources, their range, the orientation of the sources, and the oceanographic conditions along the propagation paths.

Sea ice at the ice/water boundary is generally composed of individual ice floes, which are generally between 10 m to 100 m in diameter, and are on the order of 1.0 m thick [Ref. 9]. The spatial extent of the ice/water boundary, which may be defined as the region between 1/8 to 7/8 ice cover, may vary from 1 to 100 km. Diffuse ice/water boundaries, being a relatively disordered environmental configuration, have a higher probability of occurrence than compact boundaries.

Theoretically, ocean waves incident at the ice/water boundary are partly reflected and partly transmitted [Ref. 10]. The transmission/reflection coefficients are a function of the angle of incidence, the ice thickness and the wave period. For the case of normal incidence and for an ice thickness of the order of 1 m, nearly all of the energy of the ocean waves with periods greater than 4 s is transmitted into the ice field, whereas ocean waves with periods less than 4 s are nearly totally reflected. Experimentally, it has been observed that ocean waves in the ice field are rapidly attenuated when the half-wavelength of the waves is smaller than the ice-floe diameter [Ref. 2]. In particular, for ice floes about 100 m in diameter rapid attenuation of ocean wave energy occurs when the half-wavelength of the waves is smaller than 100 m, which corresponds to an ocean wave period of 11 s. The energy of the ocean waves which have shorter wavelengths are apparently attenuated by interactions with individual ice floes by the action of flexing and breaking the floes and by the generation of turbulence [Ref. 2]. Each of these ocean-wave/ice interaction mechanisms is potentially a source of underwater sound. Consequently, it may be hypothesized that ocean waves which interact with sea ice to generate high noise levels at the ice edge correspond to periods which are between 4 s and 11 s, or to wavelengths which are between 25 m and 200 m. The characteristics of such waves, specifically the wind dependence and the energy spectrum, are

independent of the ocean depth for depths greater than 50 m, and are highly dependent on ocean depth for depths smaller than 10 m [Ref. 11]. Consequently, the noise levels generated at the ice/water boundary by the interaction of ocean waves with sea ice should be expected to be dependent on the state of the sea, and to be independent of depth for depths greater than approximately 50 m.

In order to illustrate some of the qualitative features of the spatial variability of noise as a function of distance from the ice/water boundary, measurements made at a compact ice/water boundary in June 1971 will be considered in some detail. The measurements were made using eight sonobuoys deployed into open water and into relatively small water openings in the ice field at approximately 28 km intervals in a line normal to the ice/water boundary as illustrated in Fig. 2. The ice concentration changed from 1/8 to 7/8 over a distance of about 1 km. Sea state was estimated to be 2, and the 6-hour average geostrophic wind velocity was determined to be 5 kn, approximately normal to the boundary. Representative 3-minute data samples for each of the eight sonobuoys are shown for a frequency of 315 Hz in Fig. 3. Two characteristics of ambient noise in the region of the ice/water boundary are evident in this figure. First, the noise level is greatest at the ice/water boundary (sonobuoy A), as might be intuitively expected, with the levels decreasing more rapidly with distance from the ice edge in the ice field than in the open water. Second, the ambient noise recorded at sonobuoys C and D in the ice field is intermittently spiky, probably indicative of ice floes colliding and cracking, compared to the more uniform nature of the data obtained in open water at sonobuoys W, X, Y and Z. The noise at the ice edge appears similar to the open-water data and to the ear it resembles the sound of the sea on the beach. In agreement with previously-reported arctic ambient-noise measurements under comparable wind conditions [Refs. 12, 13], noise levels in the ice field are significantly lower than open-ocean noise levels.

Figure 4 illustrates the spatial dependence of the median ambient-noise levels as a function of distance from the ice edge for frequencies of 100, 315 and 1000 Hz. From this figure it is evident that the relative maximum at the ice/water boundary occurs over the entire frequency range of 100 Hz to 1000 Hz and that the low-frequency sound generated at the ice edge affects the ambient noise levels at significantly greater ranges than does the high-frequency sound.

Quasi-synoptic ambient noise measurements were made in the vicinity of a diffuse ice/water boundary in April 1972. At this site, the ice concentration changed from 1/8 to 7/8 over a distance of about 100 km and the geostrophic wind velocity was determined to be about 3 kn, nearly normal to the ice/water boundary. The sea state was estimated to be one. The spatial variability of the median ambient noise levels as a function of distance from a diffuse ice/water boundary for frequencies of 100, 315 and 1000 Hz is shown in Fig. 5.

As for the previously-discussed compact ice-edge environmental configuration, the open-water ambient noise levels far from the ice edge are significantly higher than the ice-covered levels, and a relative maximum in the ambient noise levels occurs in the vicinity of 4/8 concentration of ice and water. From a comparison of Figs. 4 and 5

it is apparent that the magnitude of the relative maximum measured at the ice/water boundary is relatively large at a compact edge (12 dB) and small at a diffuse edge (5 dB) compared to open-water values. From these results it may be concluded that the relative magnitude of the noise levels generated at the ice/water boundary are a function of the rate of change of ice concentration with distance.

To gain some insight into the dependence of the magnitudes of noise levels generated at the ice edge on other environmental parameters, viz. sea state and ocean depth, several sets of ambient noise measurements were made in the vicinity of diffuse ice/water boundaries, where the ice concentration changed from 1/8 to 7/8 over a distance of approximately 100 km, in December 1971 in the East Greenland Sea and in April 1974 in the Bering Sea. A comparison of some of these measurements at a frequency of 1000 Hz as a function of the observed sea state is shown in Fig. 6. Wenz' standard ambient-noise levels [Ref. 14] as a function of sea state at a frequency of 1000 Hz are also shown. At distances which are far from the ice/water boundary it is evident that the measured noise levels under open-water conditions for sea states 1, 3 and 5 are in good agreement with Wenz' standard levels.

The measurements corresponding to sea state 1, which were discussed previously, were made at a site in the Greenland Sea which was 2000 m deep. The measurements corresponding to sea state 3 were made at a site in the Bering Sea which was 50 m deep; the corresponding geostrophic wind velocity was determined to be 20 kn. The measurements corresponding to sea state 5 were made at a site in the Greenland Sea which was 1000 m deep; the corresponding geostrophic wind velocity was determined to be 20 kn. From a comparison of these data it may be inferred that the relative magnitudes of the noise levels generated at a diffuse ice edge at a frequency of 1 kHz are generally about 5 dB higher than noise levels in the open water, about 9 dB higher than noise levels in the ice field and are apparently independent of depth for depths greater than 50 m. These experimental results are qualitatively in accordance with theoretical considerations regarding the depth dependence of ocean waves discussed previously.

The three data sets shown in Fig. 6 also suggest that an empirical relationship exists between the absolute magnitudes of noise levels generated at the boundary and the sea state of the contiguous open ocean [Ref. 2].

To gain some insight into the dependence of the absolute magnitudes of noise levels generated at the ice edge on specific ocean wave characteristics, noise measurements made at diffuse ice/water boundaries were related to hindcasts of the dominant ocean-wave periods and amplitudes at the measurement sites. Only those data sets which correspond to winds and waves directed toward the ice field were considered.

The ambient-noise data at 100 Hz are plotted as a function of the dominant ocean-wave period (in seconds) in Fig. 7. Also shown are the corresponding ocean-wave amplitudes in metres. The straight line is an empirical fit to the data points. From an examination of Fig. 7 it may be inferred that the absolute values of ambient noise levels generated at a diffuse ice/water boundary increase with the dominant

period of the incoming ocean waves, a result that is qualitatively in accordance with theoretical considerations regarding the transmissivity of ocean waves as a function of period at an ice/water boundary.

Unfortunately, there are insufficient data at present to investigate possible correlations between the measured noise levels and the magnitudes and directions of the ocean waves incident at either diffuse or compact ice/water boundaries. It is noteworthy that the lowest ambient noise level shown in Fig. 7 was measured in the Denmark Strait, at a site which was protected from long-period ocean-wave energy from distant sources due to its proximity to land [Ref. 6].

Theoretically, the shapes of the ambient noise with distance curves are a function of sound propagation conditions which, in turn, are a function of ocean depth, sound velocity structure and the nature of the ocean boundaries. Sound propagation under ice occurs primarily by RSR paths and the signal attenuation with distance is controlled to a large extent by reflection losses from the ice/water interface [Ref. 15], which are generally much higher than reflection losses from the sea surface [Ref. 16]. Unfortunately, no transmission loss measurements were made during the course of the ambient noise measurements. However, ray theoretical computations of the spatial variability of noise with distance have been shown to be generally in fair agreement with the results reported here [Ref. 17].

3. COMMENTS ON BIOACOUSTIC SIGNALS IN THE MARGINAL SEA-ICE ZONE

Bioacoustic phenomena, specifically vocalization by marine mammals indigenous to the marginal sea-ice zone significantly complicates the relatively simple model of the spatial variability of ambient noise in the marginal sea-ice zone presented here. In order to illustrate some of the characteristics of the effects of biological sound generation on the spatial variability of ambient noise some of the results of an experiment conducted in the shallow waters of the Bering Sea in April 1973 will be discussed in some detail. This particular experiment was designed primarily to provide data on sound propagation conditions in the shallow-water marginal sea-ice zone. The results of the propagation loss measurements, however, will not be discussed here. The ambient noise measurements were made between the hours of 1000 and 1500 local time using air-deployed sonobuoys in the area shown in Fig. 8. Depth contours at 100, 200, 1000 and 2000 m, the ice/water boundary and the locations of the sonobuoy sites are shown. Each sonobuoy was monitored several times for continuous 1/2 hour periods. The wind velocity at sea level, which was measured from an ice-breaker in the vicinity of the measurement sites, was 7.5 ± 2.5 kn. The ice concentration varied from 4/8 at the ice/water boundary to 7/8 at site I.

The resultant ambient noise measurements are illustrated in Fig. 9 as a function of distance from the ice/water boundary for a frequency of 100 Hz. Also shown are a curve of the spatial variability of noise in relative dB near the boundary, which was computed for the environmental configuration of the measurement site [Ref. 17], and a straight line designating the average asymptotic value of ambient noise at large distances from the boundary.

It is apparent that at site F, which is approximately 130 km from the boundary, noise levels were at times much higher than the average asymptotic value. The high levels during noisy periods were primarily due to marine mammal sounds, which will be discussed subsequently.

The temporal variation of the noise at site F is illustrated in Fig. 10, which shows a 10-minute sample of the variability of the measured data in relative dB at a frequency of 100 Hz. The bioacoustic sounds, which correspond to the noisy periods, were hypothesized to be generated by the Pacific walrus (Odobenus rosmarus divergens), which were visually sighted in the vicinity of site F, in roughly 100-member pods surrounding water openings in the ice field. A comparison of a spectrograph of the recorded bioacoustic sounds and previously-measured spectrographs [Ref. 18] of the Atlantic walrus (Odobenus rosmarus rosmarus), sounds, which were made under controlled conditions, is shown in Fig. 11. A comparison between these data is valid, since the latter set of measurements are virtually identical to previously measured, but unpublished spectrographs of Pacific walrus sounds [Ref. 19].

The previously-reported spectrographs of "clicking" and "bell-like" sounds of the walrus shown at the bottom of Fig. 11 appear to be nearly identical to the spectrograph of "clicking" and "bell-like" sounds obtained by the authors, shown at the top of Fig. 11. However, the previously-reported spectrograph of the "rasp" of the walrus could not be identified with the observed "rasp-like" noise in the centre of the spectrograph because this particular signal overloaded the tape.

The walrus sounds were heard at several locations, but were loudest at site F, which was the shallowest location, being approximately 100 m in depth. Since walruses are bottom feeders and are restricted to water depths shallower than 100 m [Ref. 20], the measured result is qualitatively in accordance with previously-reported biological data regarding depth constraints on the spatial distribution of walrus herds.

Walruses, which are common in the Bering Sea, migrate seasonally with the ice edge, staying generally near water openings in the ice field [Ref. 20]. Unlike walruses, seals are neither restricted to staying near water openings because they can form and maintain breathing holes through the ice, nor are they restricted to shallow water depths because they may feed on organisms found either on the ocean bottom or in mid-water [Ref. 20].

Bearded seal (Erignathus barbetus) sounds, described as "warbling" sounds [Ref. 21], were heard frequently at various locations, viz. at sites D, D_3, A, I and F. Identification of the bearded seal sounds recorded during the conduct of this exercise was made in the same manner as described above [Ref. 22]. The bearded seal, which is a native of the northern seas, including the Bering Sea, is a solitary but vociferous creature. The loud "warbling" sounds discussed above are made only by mature males during the spring courtship period [Ref. 20], which coincided with the time of the measurements.

Other distinctive sounds described as "bellowing", "chirping" and "whistling" were recorded near the ice/water boundary predominantly at site I, and to some extent at sites D_3 and D_4. Beluga whales, which were visually sighted in 10-30 member pods in water openings in the vicinity of these sites, may have been responsible for generating these sounds [Ref. 23]. In this case, however, the spectrographs of the recorded sounds could not be matched with previously-published spectrographs of sounds generated either by beluga whales [Ref. 24] or by any other marine mammal indigenous to the Bering Sea [Ref. 25]. Beluga whales migrate into the Bering Sea between March and May, travelling in pods numbered by the thousands. They generally do not enter deeply into ice-covered areas, staying in partially ice-covered areas in large water openings [Ref. 23].

The discussion of the bioacoustic measurements merely illustrates a few aspects of the complexity of bioacoustic phenomena as it affects the spatial variability of ambient noise in the marginal sea-ice zone. Due to the lack of sufficient data on the source levels and the behaviour and migration patterns of marine mammals indigenous to the marginal sea-ice zone, meaningful prediction of the frequency of occurrence and levels of sound generated by marine mammals in these areas as a function of time and space is not possible at the present time [Ref. 25].

CONCLUSION

The data presented in this paper suggest that a universal feature of the marginal sea-ice zone environment is a relative maximum in ambient noise levels at the ice/water boundary. The absolute magnitudes of noise levels at the boundary appear to be a function of the state of the contiguous open ocean, and the rate of change of ice concentration at the boundary appear to be a function of the state of the contiguous open ocean, and the rate of change of ice concentration at the boundary, and appear to be independent of ocean depths for depths greater than 50 m. Measurements made at an ice/water boundary in the Denmark Strait suggest that noise levels generated at the boundary may be affected by the proximity of land to the boundary, being significantly lower than measurements at boundaries far from land. At some times and at some locations ambient noise levels may be measurably affected by sound generation by marine mammals.

ACKNOWLEDGEMENTS

This research was supported by the US Advanced Research Projects Agency.

The authors are sincerely grateful to Mr Robert Winokur and Mr Kenneth Mackenzie for reviewing the work. Thanks also go to Mr Larry Pugh for his constructive criticisms, and to Mr Walter Wittmann, for his encouragement.

The author is also deeply indebted to the Officers, especially Cdr R.L. Barr, and the crew of the US Oceanographic Development Squadron VXN-8, Patuxent, NAS, and to the participating scientists and technicians of the US Naval Oceanographc Office, especially Messrs P. LaViolette, F. Taylor, W. Renshaw, J. Kerling, P. Parrott and W. Martin, and to Chief Noel Belcher of the US Fleet Weather Facility, for their cooperation and assistance throughout the course of the measurement programme.

Special thanks also go to the following personnel of the US Naval Oceanographic Office: Messrs Tom Kozo and Terry Tucker of the Polar Oceanography Division for many helpful discussions on remote sensing of sea ice characteristics, and Mrs Judy Albrittain for typing the manuscript.

REFERENCES

1. O.I. Diachok and R.S. Winokur, "Spatial Variability of Ambient Noise at the Arctic Ice/Water Boundary," J. Acoust. Soc. Am. 55, 750-753 (1974).

2. G. De Robin, "Wave Propagation through Fields of Pack Ice," Phil. Trans. Roy. Soc., London 255, 313-339 (1963).

3. R.J. Urick and C.E. Kelly, "Underwater Sound Measurements from Aircraft," Naval Ordnance Laboratory Technical Report No. 68-99 (1968).

4. P.E. LaViolette and O.I. Diachok, "The Use of Real Time Satellite Imagery in a Subarctic Airborne Oceanographic Survey," 54th Meeting of the American Geophysical Union, Washington,DC (1973).

5. V.E. Noble, R.D. Ketchum and D.B. Ross, "Some Aspects of Remote Sensing as Applied to Oceanography," Proceedings of the IEEE, 57, 594-604 (1969).

6. R.W. James, Personal Communication.

7. L. Hasse and V. Wagner, "On the Relationship between Geostrophic and Surface Wind at Sea," Monthly Weather Review, 99, 255-266 (1971).

8. W.J. Pierson, G. Neumann and R.W. James, "Practical Methods for Observing and Forecasting Ocean Waves by Means of Wave Spectra and Statistics," U.S. Navy Hydrographic Office Pub. No. 603, Suitland, MD, 284 pp. (1960).

9. T.L. Kozo and O.I. Diachok, "Spatial Variability of Topside and Bottomside Ice Roughness and its Relevance to Underice Acoustic Reflection Loss, "AIDJEX Bulletin No. 19, 113-122 (1973).

10. A. Shapiro and L.S. Simpson, "The Effect of a Broken Icefield on Water Waves," Trans. Amer. Geophys. Union 34, 36-42 (1953).

11. B. Kinsman, "Wind Waves," Prentice-Hall, Englewood Cliffs, N.J., 126-133 (1965).

12. C.R. Greene and B.M. Buck, "Arctic Ocean Ambient Noise," J. Acoust. Soc. Am., 36:1218 (1964).

13. A.R. Milne, "Sound Propagation and Ambient Noise Under Sea Ice," in Underwater Acoustics, Vol. II, V.M. Albers, Ed. Plenum Press, New York, Chap. 7, pp. 103-137 (1967).

14. G.M. Wenz, "Acoustic Ambient Noise in the Ocean Spectra and Sources," J. Acoust. Soc. Amer., 34, 1936-1956 (1962).

15. O.I. Diachok, "Effects of Sea Ice Ridge Characteristics on Under-Ice Reflection Loss in Arctic and Sub-Arctic Waters," Proceedings of the 8th International Congress on Acoustics, Symposium on Underwater Acoustics, London, England (1974).

16. H.W. Marsh, M. Schulkin and S.G. Kneale, "Scattering of Underwater Sound by the Sea Surface," J. Acoust. Soc. Amer., 33, 334-340 (1961).

17. M.S. Weinstein, Unpublished Manuscript.

18. W.E. Sheville, W.A. Watkins and C. Ray, "Analysis of Underwater Odobenus Calls," Zoologica, 51, 103-106 (1966).

19. C. Ray and W.A. Watkins, "The Social Function of Underwater Sound in Odobenus (Walrus)," Proceedings of the Symposium on the Biology of the Seal, 14-17 August (1972) (in press).

20. R. Perry, "The Polar Worlds," Taplinger Publishing Co., Inc., New York, New York, 166-192 (1973).

21. C. Ray, W.A. Watkins and J.J. Burns, "The Underwater Sound of Erignathus (Bearded Seal)," Zoologica: New York Zoological Society, 54(2), 79-83 (1969).

22. G.K. Long and O.I. Diachok, "Bioacoustic Measurements in the Bering Sea," (in preparation).

23. Mowbary and Fish, "Production of Underwater Sound by the White Whale or Beluga, Delphinapterus leucas (Pallas), "Journal of Marine Research, 20(2), 149-162 (1962).

24. C. Ray, Personal Communication.

25. B. Cummings and J.F. Fish, "A Synopsis of Marine Animal Sounds in Eight Geographic Areas," Informal Report, Naval Undersea Center, San Diego, Calif. (1971).

DISCUSSION

Answering a question by Ir Vettori about the asymptotic noise levels under ice and open water Dr Diachok explained that the only part investigated quantitatively was the sound propagating into the open water but that he expected to find a higher attenuation coefficient under ice. This implies that the noise level will decrease more quickly with range and more rapidly reach an asymptotic level that should be lower than the asymptotic level found in the open sea.

Dr Diachok agreed with Dr Wille that the spiking noise found under ice far from the ice edge was most likely associated with temperature gradients.

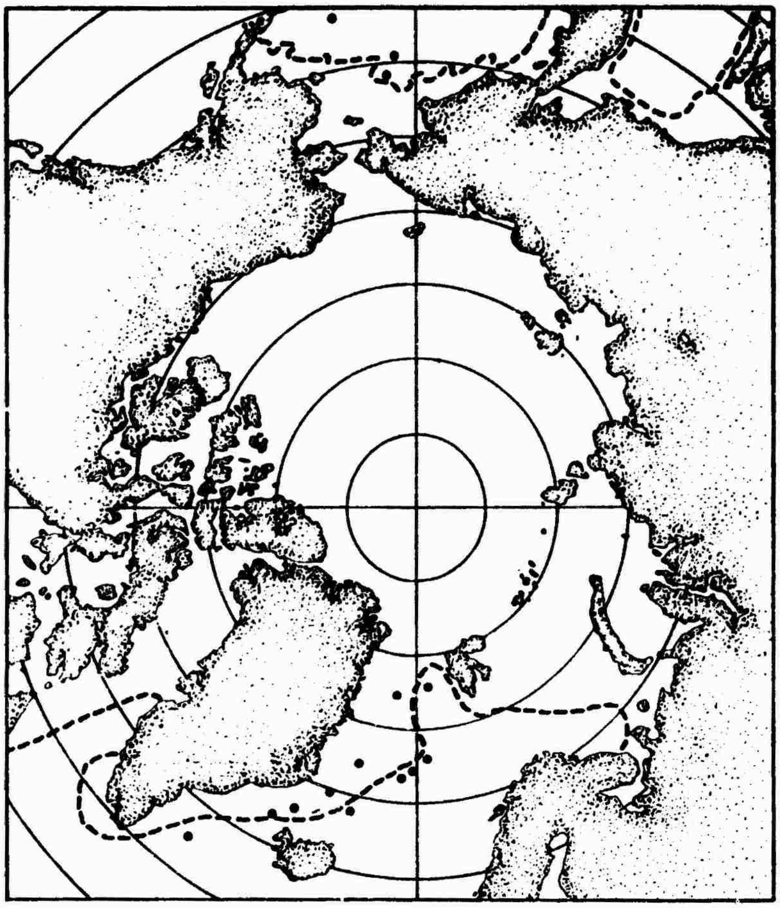

FIG. 1

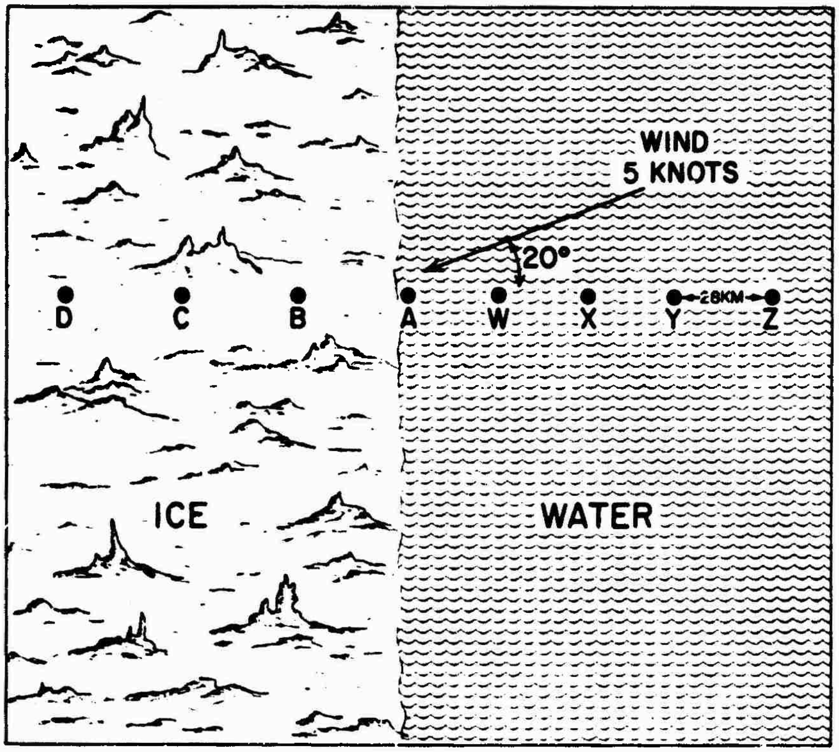

FIG. 2

FIG 3

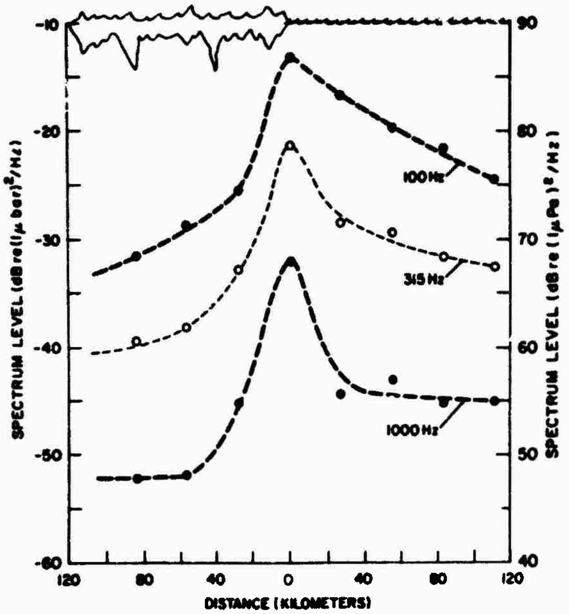

FIG. 4

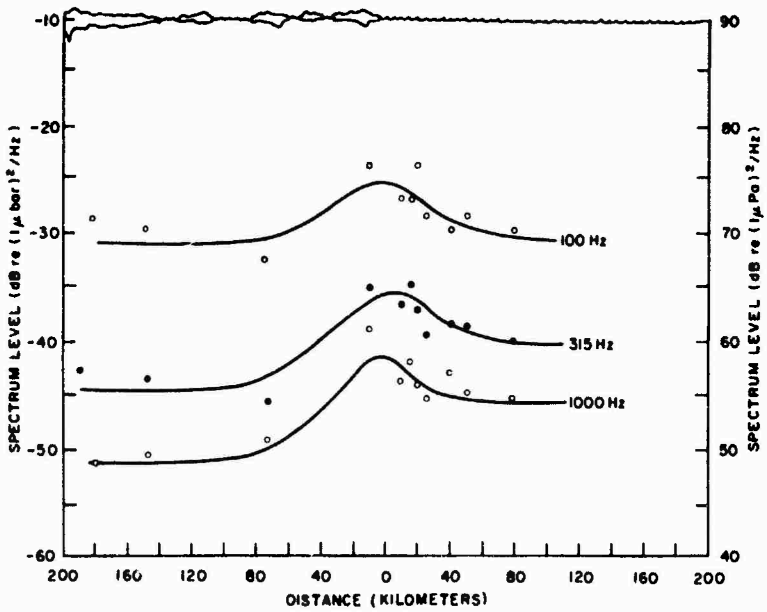

FIG. 5

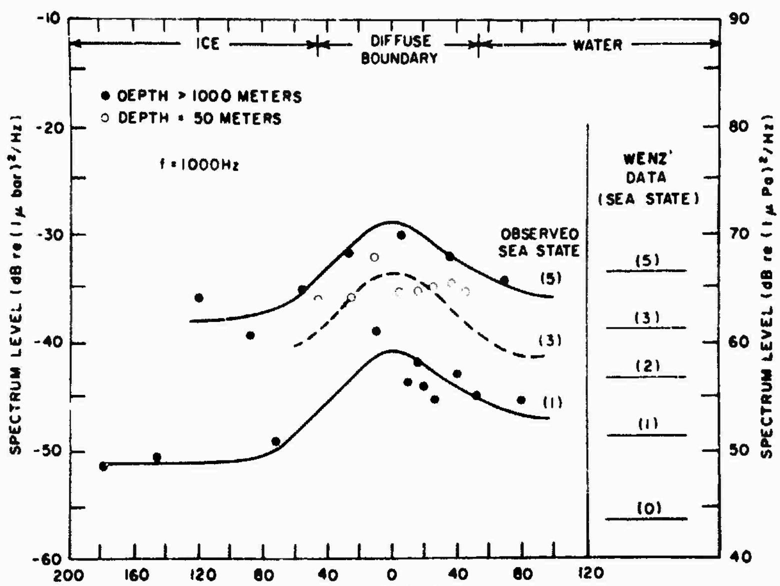

FIG. 6

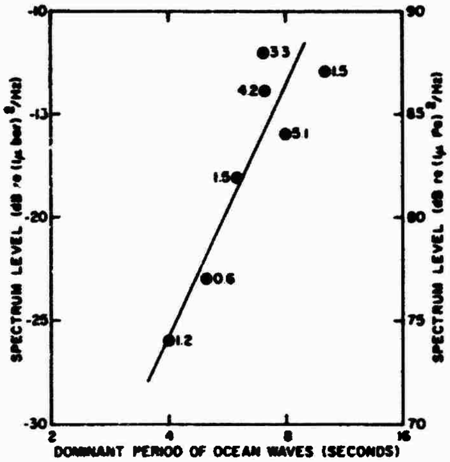

FIG. 7

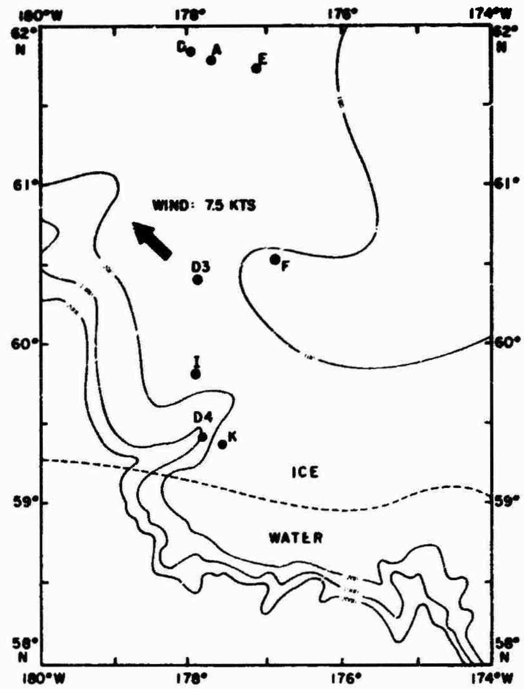

FIG. 8

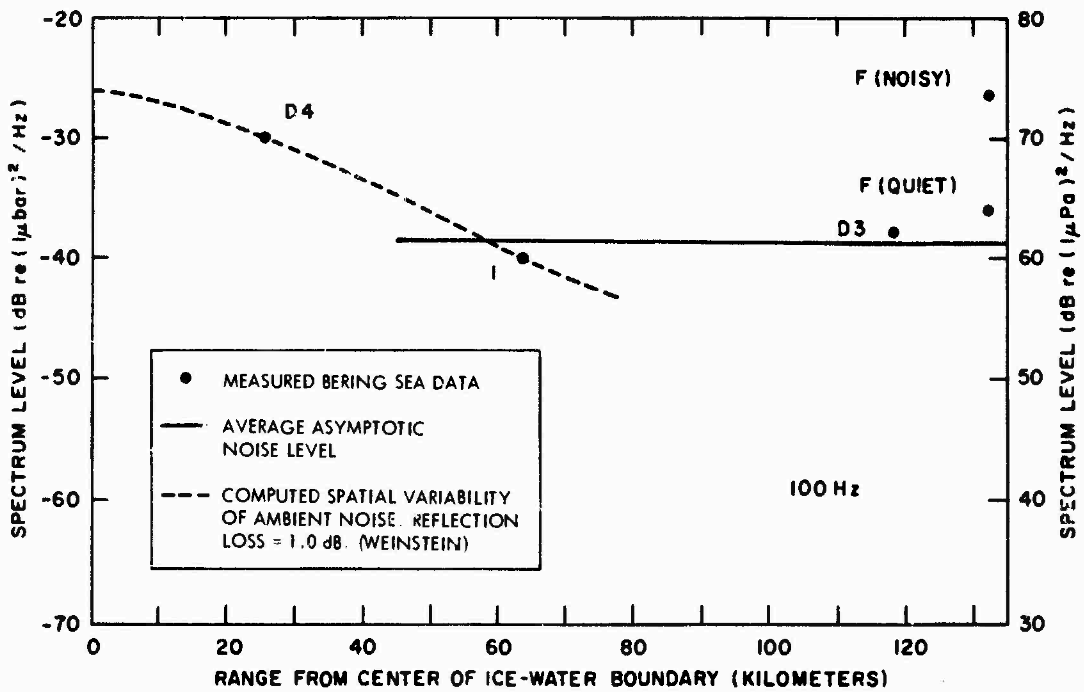

FIG. 9

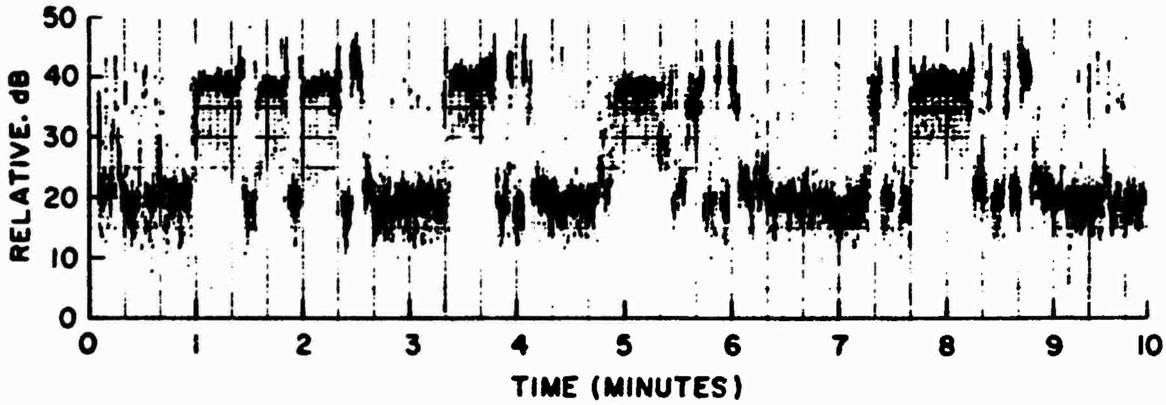
RELATIVE, dB
TIME (MINUTES)

FIG. 10

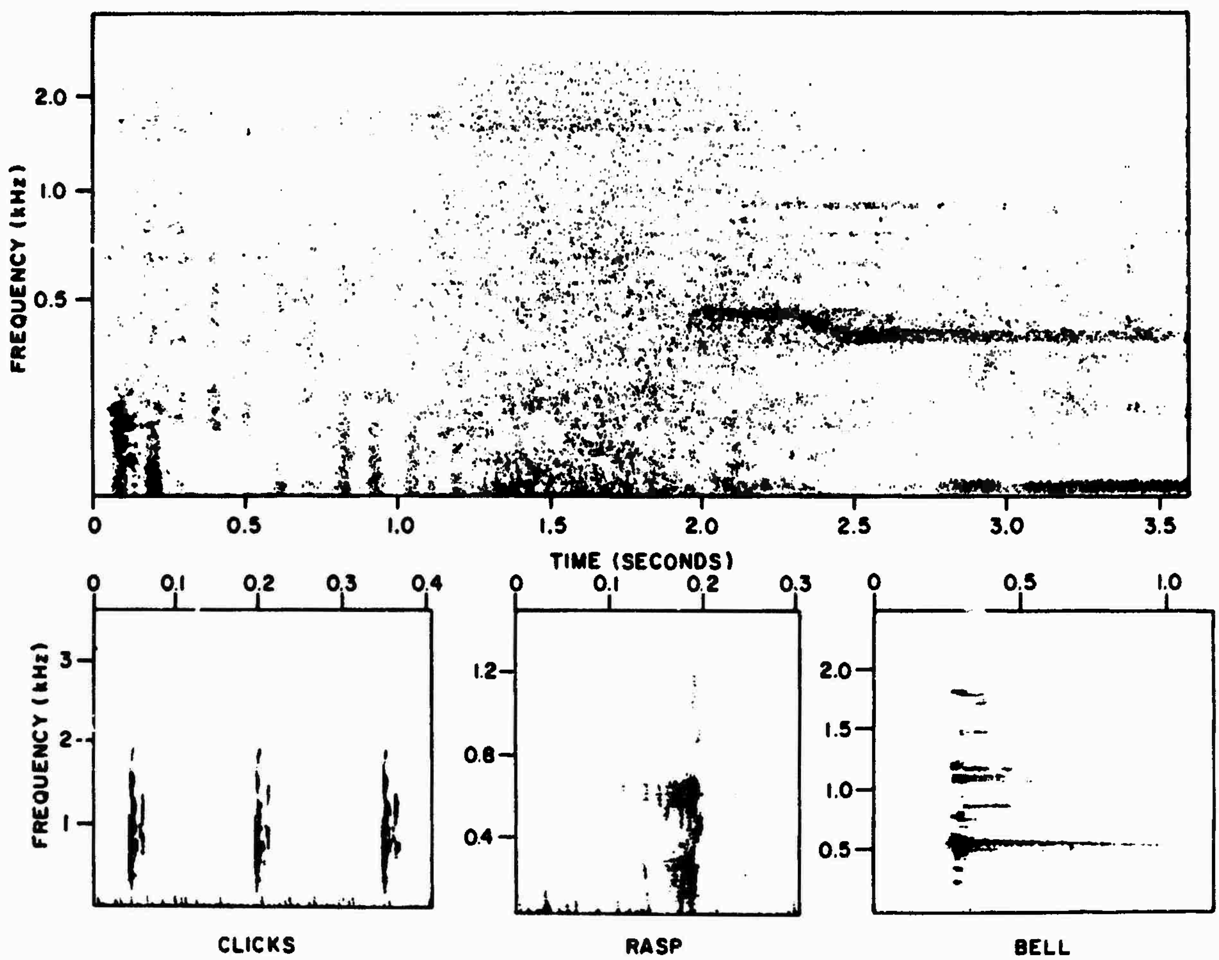
FREQUENCY (kHz)
TIME (SECONDS)
CLICKS
RASP
BELL

FIG. 11

SPATIAL HORIZONTAL COHERENCE OF EXPLOSIVE SIGNALS IN SHALLOW WATER

by

A. Wasiljeff
SACLANT ASW Research Centre
La Spezia, Italy

ABSTRACT

An important parameter in shallow water sound propagation is the influence of the transmitting medium and its boundaries on the spatial coherence of acoustic signals. Spatial coherence has been studied with a 30 m horizontal array by measuring the crosscorrelation function of explosive signals between various pairs of hydrophones on the array. The experiments have been performed under isothermal winter conditions in the Strait of Sicily over flat and rough bottom. The results are compared with data which had been collected in the shallow water area near the island of Elba under different seasonal conditions. The angular uncertainty of the medium gives limitations on the classification range of target classification procedures.

1. ARRANGEMENT OF THE EXPERIMENTS

SACLANTCEN's Shallow Water Group has been investigating shallow water sound propagation in the areas north and southeast of the island of Elba and in the Strait of Sicily north of Pantelleria and south of Lampedusa.

The areas around Elba had a flat bottom which has been described in the paper of T. Akal, whereas the Strait of Sicily has a high velocity bottom which consists of sand and silt in the area north of Pantelleria (Adventure bank) and of sand with patches of rock and gravel in the area south of Lampedusa.

The water depth was nearly constant along the tracks of Elba (115 to 120 m in the north, 110 to 115 m in the southeast), varied between 80 and 60 m north of Pantelleria and was almost constant about 80 m along the tracks south of Lampedusa.

Explosives of 180 g TNT were used as broadband acoustic sources. They were launched from a source ship at different ranges and fired electrically by means of a sea water activated battery and a pressure device which allowed their detonation at a preset depth.

Figure 1 gives an illustration of the operational procedures.

The signals were received with an horizontal array. The array was suspended to midwater depth from a spare buoy, which was floated away from the Centre's research vessel.

They were preamplified and transmitted to the ship through cables that were connected to the spare buoy. On board the research ship they were amplified and low pass filtered at a 6 dB cut off frequency of 8 kHz.

They were fed to an analogue-digital converter of 24 kHz sampling rate. The digitized values were recorded on magnetic tapes with the Centre's digital recording system. The processing was done ashore using the Centre's Elliott 503, which is now replaced by a UNIVAC 1106.

The measuring array consisted of a rigid line of 9 omnidirectional hydrophones with a total length of 30 m. The spacing of the different hydrophones is shown in Fig. 2. The positioning of the hydrophones allows 36 pairs of spacing combination. Some of the spacings were chosen identical in order to allow a check on stationarity in space and to back up possible failures of hydrophones.

The vertical branch was used for transmission loss measurements but will not be considered here.

2. ANGULAR UNCERTAINTY

If a source signal is distorted by the transmitting medium the shape of the received signal will in general depend on the location of the receiver.

The influence of the medium can be understood with the aid of the angular scattering function ASF. It describes the average spread of signal power in the angular space that is defined by the wave number coordinates [Ref. 1].

The ASF is thus the power directivity function of a δ-source in angular space after distortion by the medium. The medium behaves like a random space channel. The output of such a channel (in angular space) can be found by convolution of the power directivity function of the source with the ASF of the medium.

If a source emits a plane wave, which corresponds to a δ-function in angular space, the medium will distort its wavefronts unless the ASF is a δ-function itself.

If the receiving device has a power directivity function that is not a δ-function in angular space, we have to convolve it with the ASF of the medium and the power directivity function of the source in order to know the average power distribution in angular space that is seen by the receiver.

If we were able to know exactly the ASF of the medium we could by deconvolution determine the power directivity of the source, which might be for example a submarine, and thus classify the target.

Unfortunately, due to practical reasons we can not determine the exact ASF of the medium. But like very often in statistics, where we content ourselves with the mean and the standard deviation, although we know in principle that we ought to know all higher moments in order to give a complete description, we shall try to measure the "effective beamwidth" of the ASF, which we shall call the "angular uncertainty" of the medium (AUM).

Here we can make use of the acoustic analogue to the van Cittert-Zernicke theorem, which is known from optics [Ref. 2]. It states that there exists a Fourier transform relationship between the angular scattering function and the spatial correlation function of the transfer function of the medium under the assumption of stationarity in space.

If we measure the effective width of the spatial correlation function we can make use of the following uncertainty principle: for simple functions that decrease fast enough not to cause trouble when using Fourier transforms the product of the effective width of such a function and the effective width of its Fourier transform is of the order of one. (The communication engineer knows that the time band-width product of nonsophisticated signals is of the order of one).

Thus the AUM can be estimated from the inverse of the correlation length of the spatial correlation function. The assumption of a Gaussian scattering function [Ref. 3] is very useful but it is not essential for this result.

3. CROSS-CORRELATION

Usually we do not measure directly the spatial correlation function but the cross-correlation function between two time signals received at two different points in space. It can be shown for narrow-band signals that the maximum of this correlation function is a good estimate for the spatial cross-correlation at the given distance.

Thus we can by choosing different spacings built up a sampled space correlation function and then determine its effective width. Its inverse will give us an estimate for the desired AUM.

The temporal cross-correlation function between signals received at two different points in space is a measure for the similarity of the signal structure at these two points.

A maximum of this normalized correlation function, which is close to one, indicates a high degree of similarity. The calculation of the CCF was performed digitally.

The digitized time domain records were transformed to frequency domain with the aid of the FFT. Conjugate multiplication gave after inverse transformation and normalization the cross-correlation function.

The maximum of the CCF is usually displaced from zero. This can be used to determine the signal delays at the different hydrophones of an array and from this one can determine the angle by which the array is declined from the direction perpendicular to the main direction of sound propagation.

To illustrate the correlation procedure we regard in Fig. 3 an example of a shot fired at a range of 0.5 km and recorded at two hydrophones 8 m apart in the Strait of Sicily.

The structure of the signals is very similar. There are some slight differences that are hardly visible. Figure 4 shows the broadband cross-correlation function of the signals on these two hydrophones. The main peak is very close to one.

The strong side-lobes are due to the bubble pulse. To study the dependence of the cross-correlation function on the carrier frequency of a narrow band signal, digital filtering was applied in the frequency domain at different centre frequencies varying from 800 Hz to 6.4 kHz and with a bandwidth of 200 Hz.

Figure 5 shows an example of the cross-correlation function of two filtered signals. The centre frequency was 3 kHz, the bandwidth 200 Hz.

In the actual calculations envelope detection was performed by using the Hilbert transform. From the envelope the maximum can be much more easily determined, than from the rapidly oscillating cross-correlation function itself.

This maximum as a function of the spacing of the various hydrophones gives the spatial coherence function. An example is given in Fig. 6. The acoustical length at which this maximum decreases below 0.6 is the width of the coherence function. The reciprocal of this width gives the angular uncertainty of the medium. Sometimes the correlation is so good that the width is larger than 1000, (see Fig. 7).

4. STRAIT OF SICILY

The cruise to the Strait of Sicily was conducted in February 1973. There we have during winter isothermal conditions, in which the increase of the sound speed profile towards the bottom is only due to static water pressure. Under these upward refracting conditions the bottom plays a less important part. After a few kilometres the boundaries are hit by the acoustic rays at a very long grazing angle. Therefore we were not surprised to find a low angular uncertainty in spite of a very rough sea.

Figure 8 shows the angular uncertainty versus range at different centre frequencies for the Adventure Bank north of Pantelleria. For close range shots, the angular uncertainty is higher than 1° for the frequencies from 0.8 to 3.2 kHz. This is due to the separation of multipath arrivals which makes the arriving wavefronts very sensitive

to variations in boundary structure. For ranges beyond 3 km the AUM is lower than 1/2 degree. The acoustic rays do not see the "roughness of the boundaries" because of the low grazing angles or to talk in a wave picture the whole water column is exited and "rings", thus giving a high horizontal correlation of the sound field which corresponds to a low AUM. Slight variation beyond 3 km may be due to the varying water depth of this run, which varied as said before between 80 and 65 m. They did not exist over flat bottom as may be seen in Fig. 9 where the run was performed over an almost flat bottom of constant water depth of 80 m south of the Island of Lampedusa.

Here the "near field" effect is even more pronounced giving at close ranges an AUM between 4° and 7°. At ranges beyond 3 km the AUM is lower than 0.1° up to 35 km. It should be mentioned again that the experiment was performed in a very rough sea of sea state 3 to 5.

Figure 10 displays the signals received at one hydrophone of the horizontal array versus range. Between 25 and 35 km it is to be seen that there is a clear separation between the response of the medium to shock and to bubble pulse. If we cut the signal before the arrival of the bubble pulse we get an approximation to the impulse response of the medium.

Correlating these impulse responses from two adjacent shots gives a good correlation in space and time as seen in Fig. 11, between two shots at a distance of 31.7 km and 33.6 km with a time difference of 8 minutes.

This is still the case at even larger time and space intervals as seen in Fig. 12 where the shot distances from the receiver are 27.4 and 33.6 km respectively and the time difference was 24 minutes.

This proves that beyond a certain range in shallow water the propagation conditions can be very stable regardless of the roughness of the surface, thus giving a high reproduceability of the transmitted signal.

5. ELBA ZONE

The data discussed so far have been collected under isothermal winter conditions. In summer we have a strong thermocline, however, due to the heating of the surface.

Figure 13 shows the sound speed profiles of the area near the island of Elba.

Figure 14 gives the corresponding ray diagrams. The upward refracting conditions in winter cause a smaller grazing angle and a larger cycle distance than under downward refracting conditions in summer, where the bottom is hit by a steeper grazing angle. Therefore the influence of the boundaries and specially the bottom on the propagation conditions is much higher in summer than during the winter season. During summer the attenuation of the sound field is higher and since

the propagation is more complicated one expects to find a higher angular uncertainty than under winter conditions. Due to technical reasons we did not measure horizontal coherence in the Strait of Sicily during summer conditions. Some experiments, however, have been performed in the area near the island of Elba.

Figure 15 shows the AUM versus range southeast of Elba.

A pronounced decrease of AUM with range for short range data can only be seen at the low frequency of 0.8 kHz contrary to the winter conditions of the Strait of Sicily where it appears on almost all frequencies processed. This may be explained by the absence of rough boundaries in the Elba area during this experiment.

For long wavelengths, the source is very close to the receiver so that a plane wave has not yet been built up. For higher frequencies this is not the case and the AUM is influenced in a random way by the boundary parameters.

Nevertheless it varies between 0.2° and 1° for ranges between 500 m and 20 km. For longer ranges there is a much higher AUM. But here the signal-to-noise ratio may be not high enough to give a good estimation of spatial cross-correlation.

Figure 16 shows a similar behaviour of AUM for the area north of Elba for the frequencies of 1.6, 2.4 and 3.2 kHz and Fig. 17 gives the AUM for 4.8, 5.6 and 6.4 kHz.

No significant difference could be found between the areas north and southeast of Elba and an obvious frequency dependence does not seem to exist for ranges larger than 3 km.

Figure 18 gives a comparison of the AUM of the two areas averaged over frequency with some data reported by the Laboratory of Le Brusc from the Gulf of Lions [Ref. 4]. It seems that the coherence of signals in the Gulf of Lions is slightly poorer than for the Elba area, but the angular uncertainty of the medium is still below 1°. The small difference may be due to the different experimental set up. Our array has been suspended from a buoy to mid-water depth whereas the hydrophones in the Gulf of Lions were put on the bottom of the sea. A boundary that is very close to the receiver may have some influence on the coherence of the signals.

6. CLASSIFICATION RANGE

The classical target classification procedures that use the line structure of a submarine as classification clue are based on a SONAR-interferometer technique which makes it possible to distinguish the submarine from a school of fish and to determine the aspect angle φ of the submarine (see Fig. 19). In the multihydrophone technique an array of at least two hydrophones form a base line D. The frequency response of a target looks slightly different on the two hydrophones. It can be measured either by using a FM-sweep as

source signal (STARLITE) or by explosives that are Fourier-analysed on line. From the shift of the spectral response the aspect angle can be determined. This frequency shift corresponds to a phase change in time domain. This is used in the split-beam or SONAR-interferometer technique. Although these methods differ with respect to technical realization they are based on the same physical principle.

The classification device has to be able to resolve the angle α which for fixed aspect angle depends on the range R.

The angular uncertainty of the medium σ has to be smaller than the resolution angle α otherwise the classification procedure will not work.

This leads to the concept of classification range as the maximum range up to which the classification procedures may be expected to be operational.

Figure 20 gives a display of classification range versus angular uncertainty of the medium for different aspect angles φ of a 100 m long submarine.

In the Strait of Sicily we can expect for winter conditions a classification range of 8 to 30 km whereas forthe summer conditions that we have found in the area of Elba the classification range will vary between 1 and 10 km.

REFERENCES

1. LAVAL, R. Sound propagation effects on signal processing, SACLANTCEN M-79. La Spezia, Italy, SACLANT ASW Research Centre, 1972.

2. KO, H.C. Coherence theory of radio astronomical measurements. IEEE Trans. on Antennas and Propagation, AP-15 (1), Jan 67: 10-20.

3. WILLE, P. and THIELE, R. Transverse horizontal coherence of explosive signals in shallow water. Jnl Acoustical Society America, 50, 1971: 348-353.

4. ANCEY, R. Coherence spatiale de signaux acoustiques propagés par petits fonds. Quatrième Colloque sur le Traitement du Signal et ses Applications, Nice 1973.

DISCUSSION

In answer to a question by Mr Schneider about the season of the Gulf of Lions data, Dr Wasiljeff explained that those data had been presented by Mr Ancey from Le Brusc Laboratory during a colloquium in Nice. They had been collected during summer in an area with a flat bottom covered with mud and clay where the water depth was about 100 m.

In reply to Mr King's question, Dr Wasiljeff said that during SACLANTCEN's Elba summer experiments all shots had been fired below the thermocline.

Dr Wasiljeff explained to Dr Kuperman that it was difficult to keep the array perpendicular to the propagation direction in the horizontal plane but that the angle of orientation of the array was measured afterwards and when the deviation from the perpendicular direction was considered too large, the data from that shot were not used. Dr Ziegenbein asked whether array depth and shot depth had been changed. In reply it was said that the depth of the array was not changed but two different source depths of 25 and 50 m were used and yielded similar results.

Dr Wille noted that for passive measurements a better angular resolution than one degree may be needed, which will make further investigation necessary on the influence of the bottom, the sea state and all the ambient parameters.

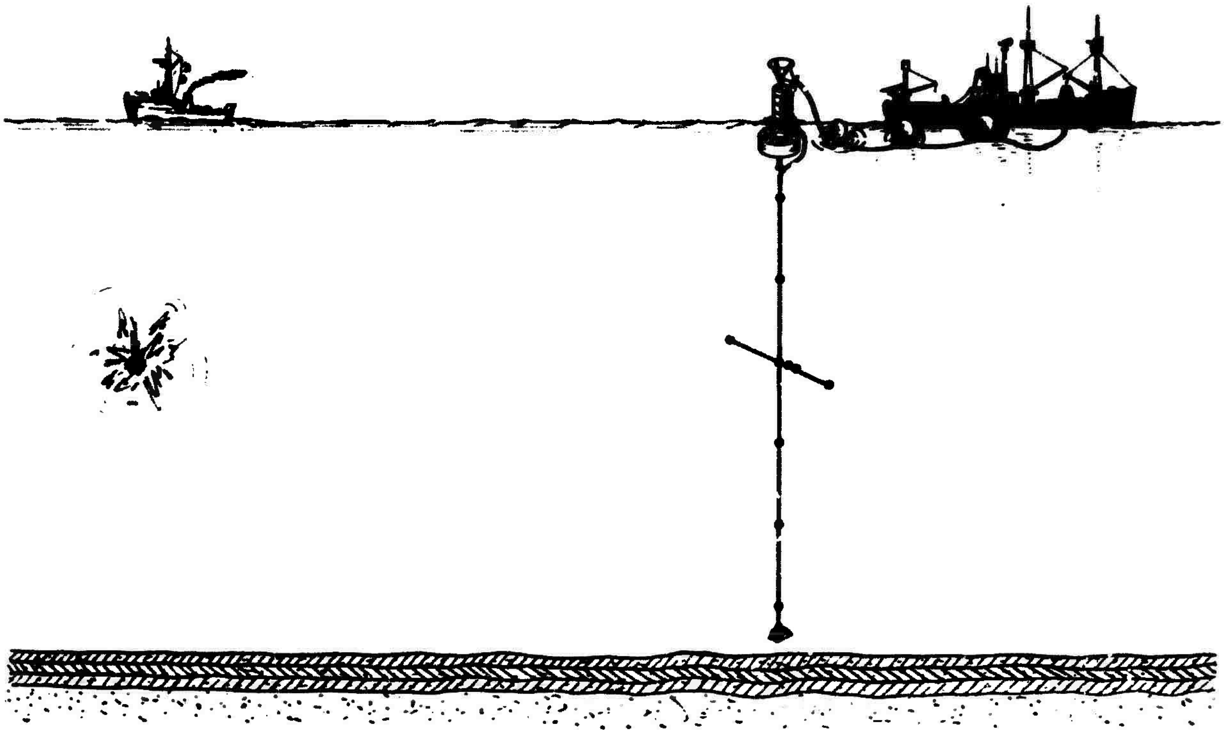

FIG. 1 EXPERIMENTAL ARRANGEMENT

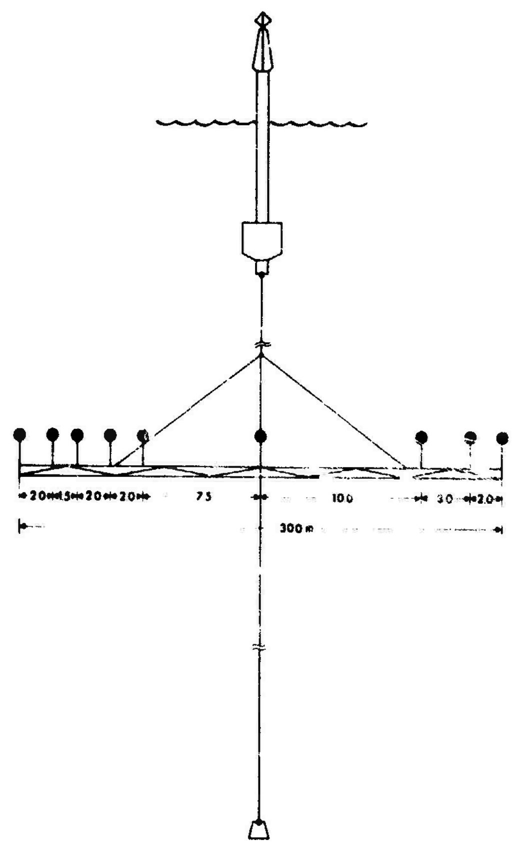

FIG. 2 ARRAY CONFIGURATION

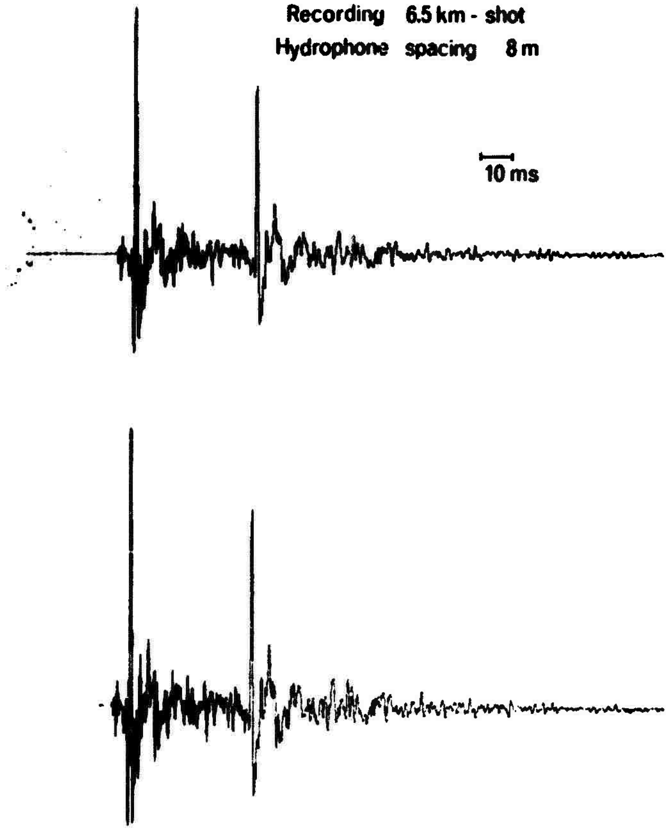

FIG. 3
RECORD OF A SHOT ON TWO HYDROPHONES

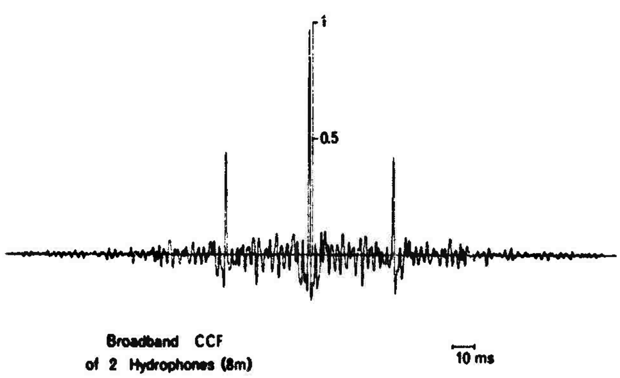

FIG. 4
BROADBAND CROSS-CORRELATION FUNCTION

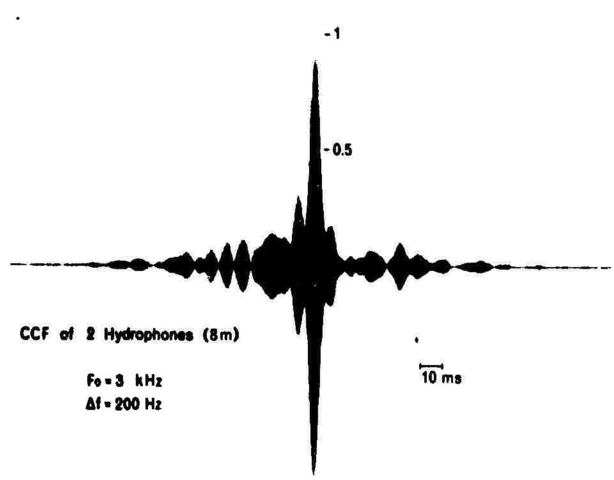

FIG. 5
NARROW BAND CROSS-CORRELATION FUNCTION

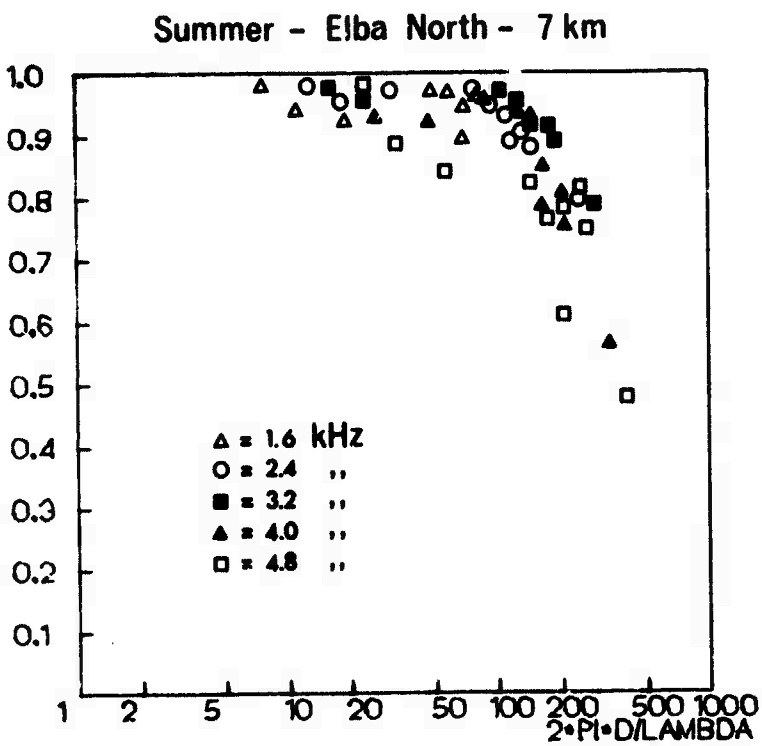

FIG. 6 MAXIMUM OF CROSS-CORRELATION vs ACOUSTICAL LENGTH ELBA SUMMER

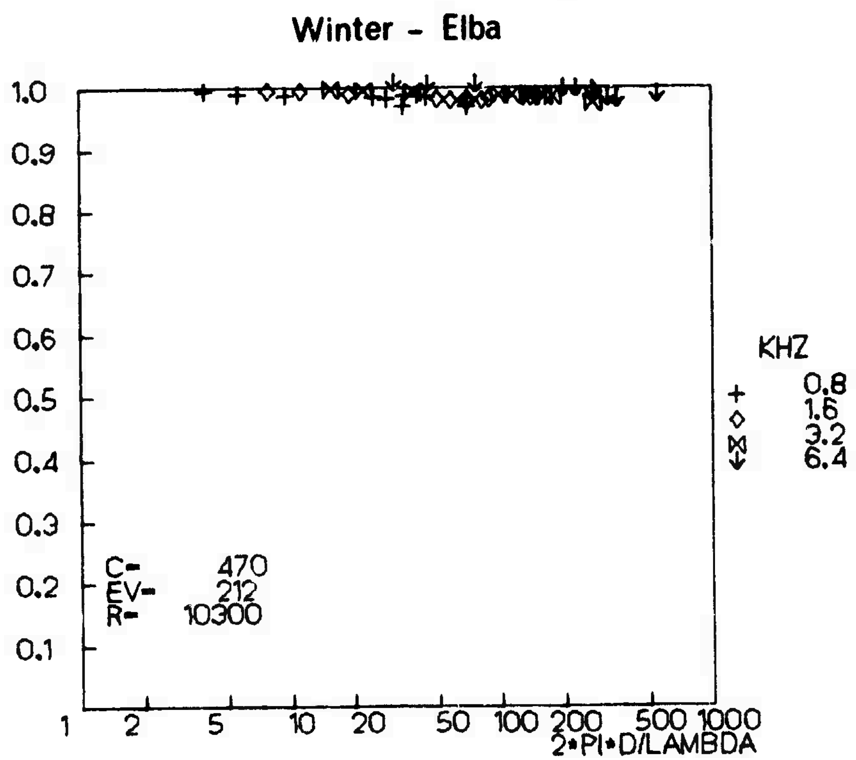

FIG. 7 MAXIMUM OF CROSS-CORRELATION vs ACOUSTICAL LENGTH ELBA WINTER

FIG. 8

ANGULAR UNCERTAINTY vs RANGE NORTH OF PANTELLERIA

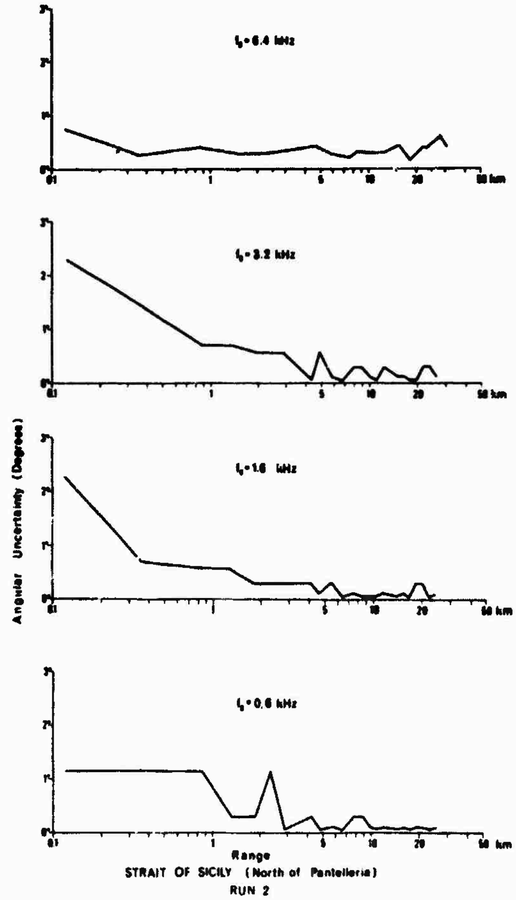

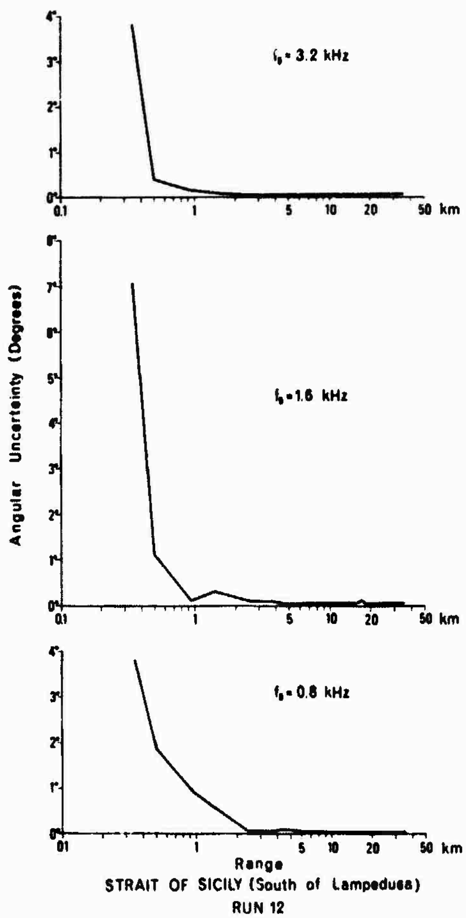

FIG. 9

ANGULAR UNCERTAINTY vs RANGE SOUTH OF LAMPEDUSA

FIG. 10
SAMPLE SIGNALS SOUTH OF LAMPEDUSA

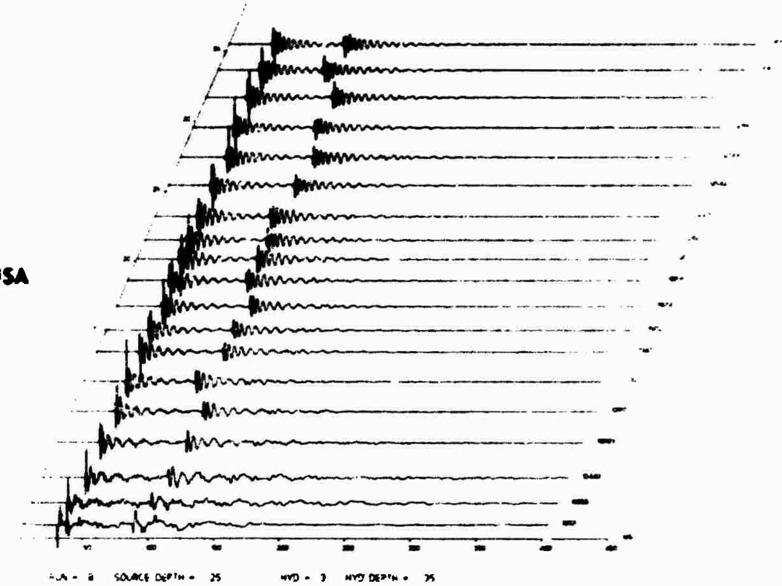

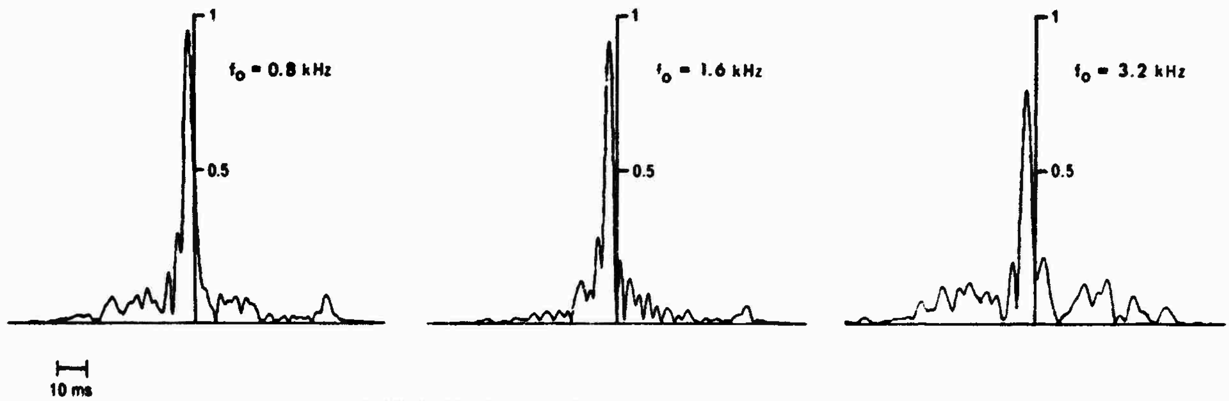

ENVELOPE OF CROSSCORRELATION OF TWO SHOTS

Distance 31.7 km and 33.6 km

Time difference 8min ; Δf 200 Hz

South of Lampedusa (run # 8)

FIG. 11 CROSS-CORRELATION OF TWO SHOTS: TIME DIFFERENCE 8 min

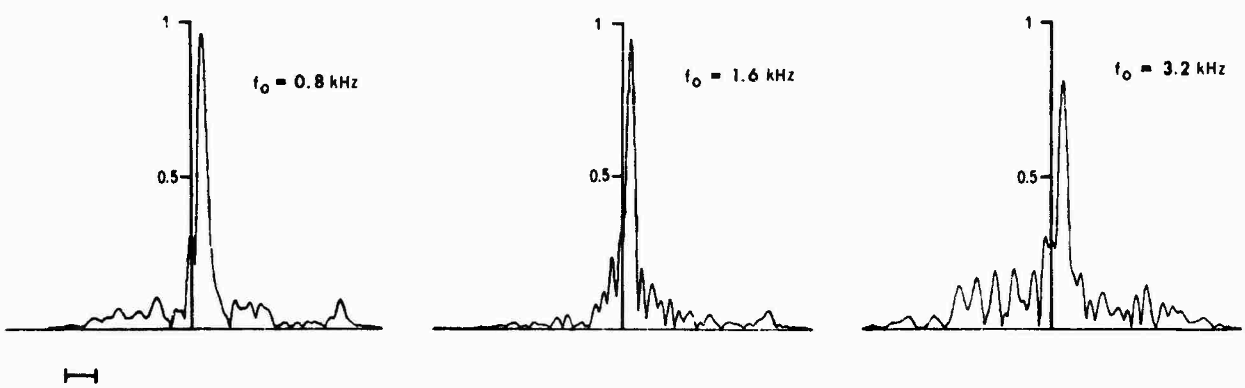

ENVELOPE OF CROSSCORRELATION OF TWO SHOTS

Distance 27.4 km and 33.6 km

Time difference 24 min ; Δf 200 Hz

South of Lampedusa (run # 8)

FIG. 12 CROSS-CORRELATION OF TWO SHOTS: TIME DIFFERENCE 24 min

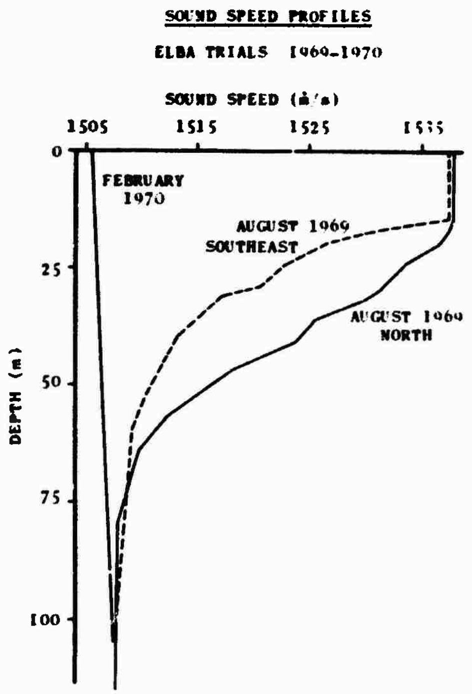

FIG. 13 VELOCITY PROFILE

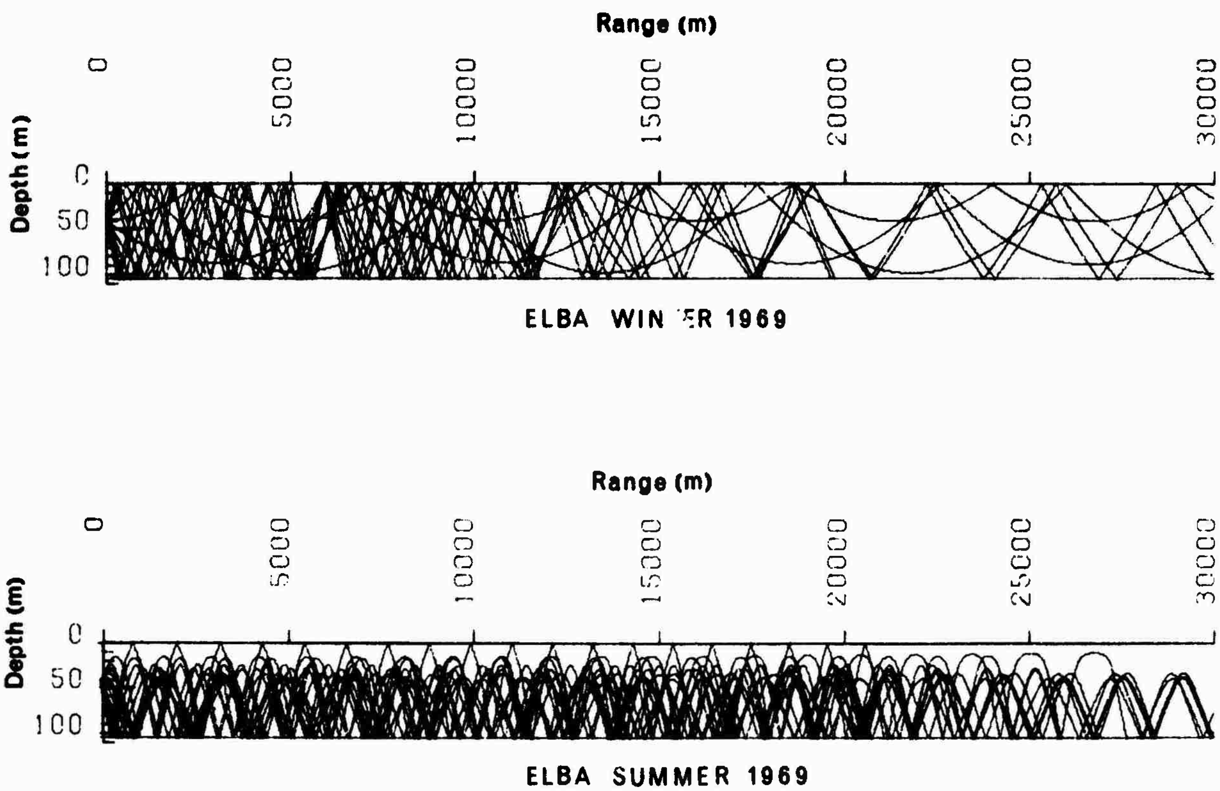

FIG. 14 RAY DIAGRAM

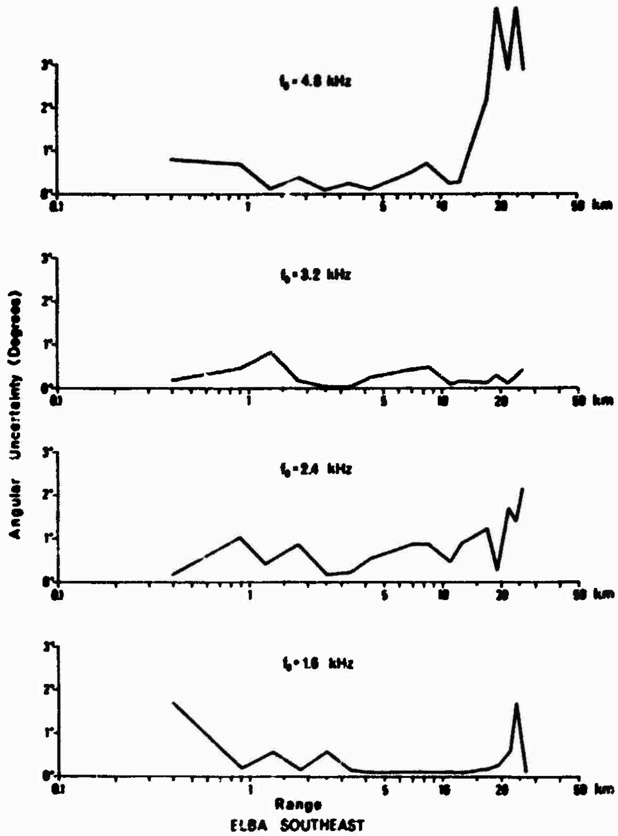

FIG. 15

ANGULAR UNCERTAINTY vs RANGE SOUTHEAST OF ELBA

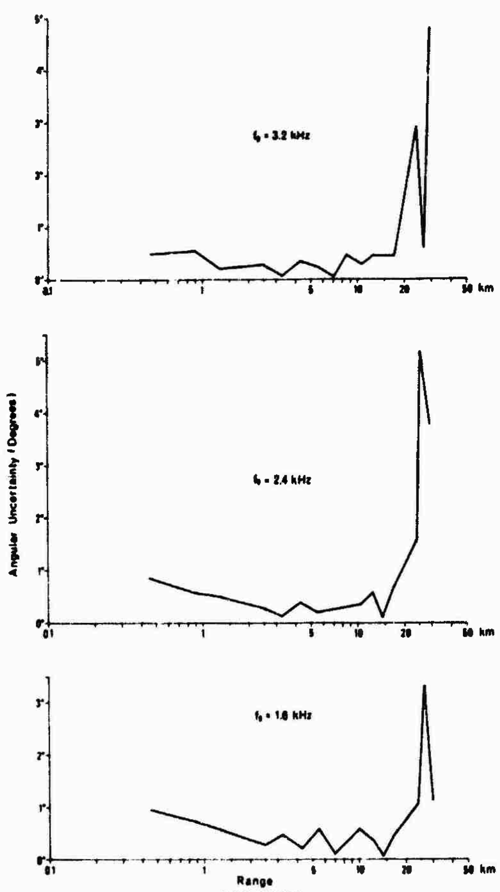

FIG. 16

ANGULAR UNCERTAINTY vs RANGE NORTH OF ELBA

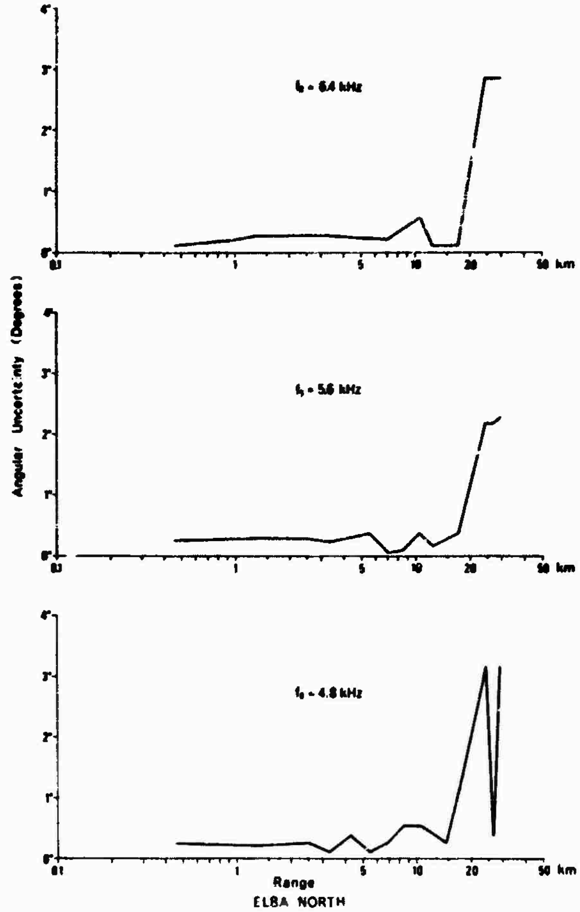

FIG. 17
ANGULAR UNCERTAINTY vs RANGE NORTH OF ELBA

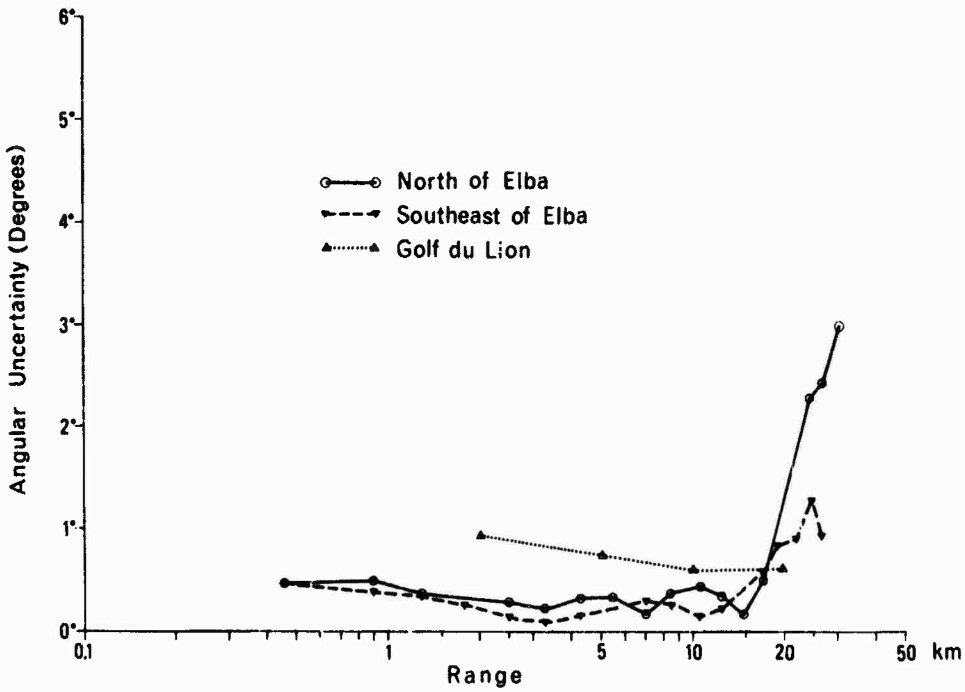

FIG. 18 AVERAGE ANGULAR UNCERTAINTY vs RANGE

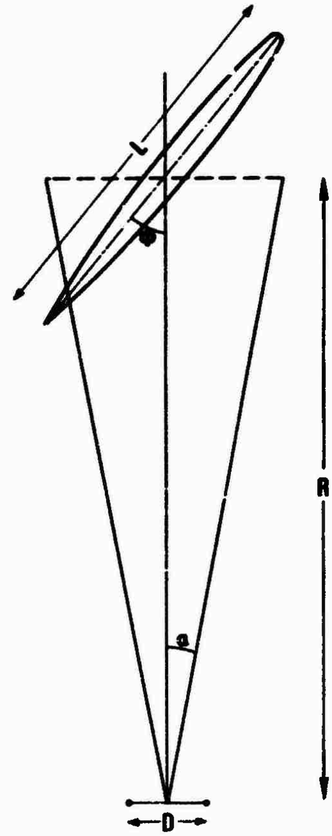

FIG. 19
SONAR INTERFEROMETER

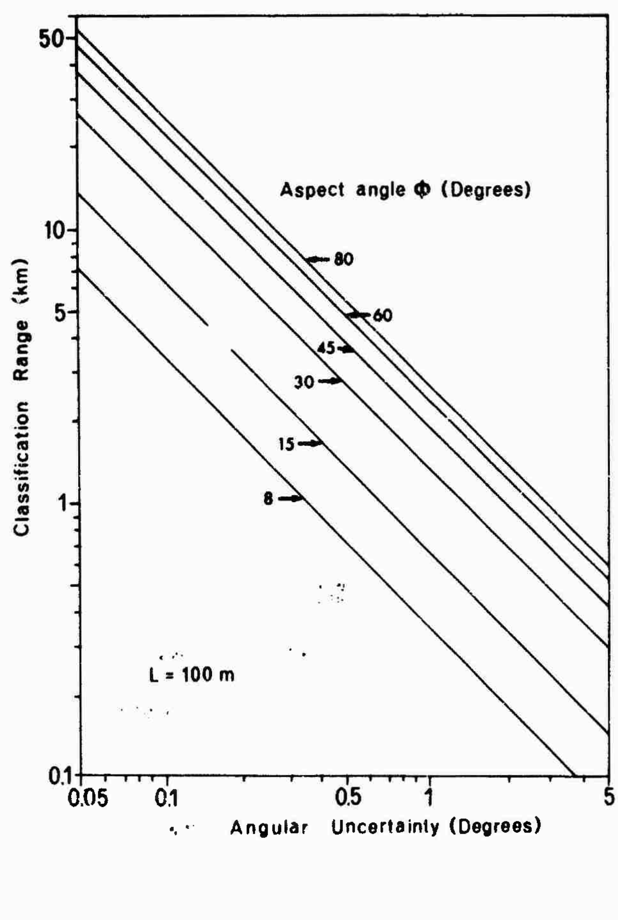

FIG. 20
CLASSIFICATION RANGE vs ANGULAR UNCERTAINTY

SHALLOW WATER CHANNEL ANALYSIS BY THE TIME VARIANT WEIGHTING FUNCTION

by

R. Thiele
Forschungsanstalt d. BW für Wasserschall
und Geophysik, Kiel, Germany

ABSTRACT

The transmission properties between a transmitter and a remote receiver are completely described by the time variant weighting function of this channel. The weighting function itself is not measurable and not to determine by a finite set of numbers. Therefore, we use a model function with the same effect as the weighting function in a certain measuring time and frequency band. This model function needs a large set of numbers too. It is only possible to display certain expectation or sample functions. Some of these expectation functions — as the scattering, the average pulse power, the amplitude fluctuations, etc. — are shown and compared with the eigenray structure of the channel. Thereby we get mainly information about the physical effects involved in the propagation process, but also some information about the relationship between transmitted and received signals.

1. THE OUTLINE OF THE WEIGHTING FUNCTION MEASUREMENT METHOD

Experimental studies in underwater acoustics are usually connected with special physical questions, for example, propagation loss, reverberation, ambient noise, etc. To learn more about the nature of sound propagation, I would like to add another method. This method is particularly suitable to shallow water because the mutual influence of surface and bottom reflection, as far as the sound velocity variations in space and time, are more complicated than in deep water.

The principle idea is not to present a well defined question to the medium but to use a simple well defined experiment. The acoustical situation of the experiment is transformed and stored by a digital computer. Now we can pose different questions to the computer, utilizing each time the same experimental situation.

The physical situation of this simple experiment will be a sound transmitter and a distant receiver, located at specific places in shallow water (a shallow water range).

To transform the acoustical content into a form which the computer may read, we use the well known transmission formula for a time-variant linear channel

$$y(t) = \int_{-\infty}^{\infty} g(t,\tau)\, x(t-\tau)\, d\tau$$

where $x(t)$ is an arbitrary transmitted signal and $y(t)$ the resulting received signal for the individual channel described by $g(t,\tau)$. A digital computer operates with sets of numbers. For a complete description we need a set of numbers infinite in both the τ and t parameters. Because we can only handle finite sets of numbers in the computer, we must use a segment of the complete set.

The weighting function has a small extent in the travel time direction τ. But it is a generalized function in τ with a correlation distance of zero. After filtering a certain frequency band of $g(t,\tau)$ a finite sampling rate is allowed by Shannon's theorem. The segment in t-direction will be the duration of the experiment. The needed sampling rate in t is rather low. When a cw-signal is transmitted, the spectrum of the received signal is associated with the variation in t (Fig. 1). These spectra show the well known modulation by the seastate [Ref. 1]. In any case, with fixed transmitting and receiving platforms, a sample frequency of 10 Hz will be sufficient.

This sampling frequency can easily be made with a train of short pulses and a repetition rate of 100 ms. For example Fig. 2 shows a segment of the received signals from such a train of pulses. The first part of these signals shows no variations.

Without stable platforms, the main variations are made by platform motions [Ref. 2]. When we use an anchored ship the motions are due to the seastate. Travel time changes will also be made by the ship tending her anchor. Because of these variations the total signal is time shifted. With the computer an invariant part of the received signal may be used to eliminate these time shifts and thereby the influence of ship motions. This ability to remove the effects of platform motion extends the range of environmental parameters over which these types of experiments can be conducted.

2. EXPERIMENTAL APPLICATION

Three experiments are presented and some evaluations of them are shown (see Table 1).

2.1 Frequency Spread

Figure 3 shows the frequency spread for the AFAR-experiment. This is not the frequency spread of a certain individual transmitted frequency but of the total applied bandwidth. By this averaging in the frequency direction we get a high frequency resolution with a short measuring time and a low statistical variation.

The modulation of the transmission by the wind waves and the swell is well distinguishable. To get the same statistical degree of freedom for the same frequency resolution with a single frequency experiment, we would require many hours of measuring time and difficulties about the stationarity of the seastate would arise. A further advantage of this method is that more refined evaluation procedures are applicable.

Figure 4 depicts the same kind of evaluation with the Baltic Sea experiment. This cruise was originally made for other purposes hence no precautions were taken to insure adequate time stability of the tape recordings. The method of elimination of travel time variation does not work at higher variational frequencies, therefore the spectral irregularities at 2 Hz will be erroneous.

For comparison Fig. 5 shows a series of 200 short time spectra of a single frequency signal at 15 kHz with the WFS PLANET hull mounted sonar [Ref. 2]. The horizontal scale is 2.5 Hz/div. and the vertical 8 s/div. These momentary Doppler shifts are completely eliminated in the spectrum of Fig. 4 and of Fig. 6 from the North Sea experiment.

2.2 Average Time Structure

Characteristic of shallow water sound transmission is multipath propagation with reflections at the rough boundaries. The differences in travel time between the paths are small. An impression of the multipath structure may be obtained by averaging the received signals of each pulse over the time t with τ as a parameter (Fig. 7). For the Great Fisherbank experiment there are three well distinguishable travel time groups. The upper curve shows the total signal power over τ and the lower that part of energy which was invariant during the measuring time.

The eigenray structure computed for this experiment (Fig. 8) shows the first group with a direct path and a single surface reflection, a second group with one bottom reflection and a third group with two bottom reflections [Ref. 3]. In this case at least one surface reflection will occur.

In Table 2 of the computed eigenray travel times we can find these three groups, however individual paths in each group are not separable with the applied bandwidth.

Due to a lack of knowledge of the exact transmitter and receiver location, sound velocity distribution, water depth and their slow variations in time and space there is no exact agreement between the computed and measured time structure.

When the multipaths are not distinguishable by the signal bandwidth interference by deterministically unknown phase differences will occur. It may vary with tides, internal waves, seiches, etc. These variations can introduce an unstationarity of the statistical properties of the weighting function during the measuring time.

TABLE 1

Name	Date	Duration	c.f.	b.w.	Repet.	Number of Values	Distance	Depth	Transm. Depth	Receiver
Gr. Fisherbank	13.8.70	10 min	15 kHz	1 kHz	120 ms	$0{,}64 \cdot 10^6$	1300 m	65 m	4,5 m	6 m
Baltic	24.10.71	10 min	15 kHz	2 kHz	80 ms	$1{,}25 \cdot 10^6$	1500 m	80 m	4,5 m	8 m
AFAR	17.8.72	40 min	.8 kHz	.2 kHz	1 sec	$0{,}9 \cdot 10^6$	19 nmi	600 - 2000 m	540 m	740 m

TABLE 2

W_1 degree	T-863,214 ms	Path
- .066	0	TR
.463	0.028	TSR
- 2.27	10.37	TBR
2.89	11.11	TSBR
- 3.10	11.21	TBSR
3.70	11.57	TSBSR
- 8.04	25.01	TBSBR
8.61	25.88	TSBSBR
- 8.80	26.18	TBSBSR
9.35	27.12	TSBSBSR

The very simple time structure is typical for shallow water propagation with small to intermediate ranges and flat bottom. In the deep water AFAR experiment with a rocky bottom the structure is very complicated (Fig. 9). Because the weighting function has a large time extent, the applied pulse repetition rate of 1 s was not sufficient. The first part of the signal is at 750 ms. The parts before are from the previous impulse. The large number of eigenrays is not resolvable with the signal bandwidth. There is no group structure as in the previous depiction.

2.3 Variations of the Time Structure

The small and slow variations of the phase interference result in slow variations of the time structure, which are visible in Fig. 10. During the measuring time of 45 min the transmission seems to be very stationary.

These variations are much lower in the Great Fisherbank experiment (Fig. 11). There are two possible reasons for these slow changes, either oceanic variations or the tending of the anchored ship whose time shift is eliminated.

2.4 Level Fluctuations

While the previous depictions are smoothed in the time direction, Fig. 12 gives the unsmoothed level fluctuations of a broadband signal in comparison to a cw signal with the same weighting function. The cw signal shows the well known interference fading. The variations of the broadband signal will be caused by the interference of eigenrays with small travel time differences.

The same evaluation of the Great Fisherbank measurement (Fig. 13) shows level fluctuations of the broadband signal in the same order of magnitude but no significant interference pattern of the highly varying cw transmission. It is to be supposed that we have fast varying interferences by vertical motions of the ship mounted transmitter. This is a principal limitation of the method for elimination of ship motions.

2.5 Scattering Function

We have the possibility of removing arbitrary travel time groups. Figure 14 shows the frequency spread of the second travel time group of the Great Fisherbank experiment. For this kind of evaluation we can use the travel time τ as a second independent variable of time spread in addition to the frequency spread variable μ, which gives the so called scattering function. With a wide sense stationary uncorrelated scattering Gaussian channel the scattering function represents the complete statistical expectation of the transmission.

There is an important relation to Woodward's ambiguity function of the transmitted signal

$$\overline{|\chi_{xy}(\mu, \tau)|^2} = \int_{-\infty}^{\infty}\int_{-\infty}^{\infty} \sigma(\mu_1, \tau_1)\, |\chi_{xx}(\mu - \mu_1, \tau - \tau_1)|^2 \, d\mu_1 \, d\tau_1$$

which gives the mean square of the cross ambiguity function between transmitted and received signal [Ref. 4].

A rather simple scattering function was obtained with the Baltic Sea experiment (Fig. 15). The interrelation of time and frequency spread makes a detailed study of the small grazing angle scattering and the dependence of the scattering angle with the frequency spread possible. This interrelation is more pronounced with the fixed platform AFAR experiment (Fig. 16) though the structure is more complicated and the time resolution rather low [Ref. 5].

In the Great Fisherbank experiment (Fig. 17) we find no distinct time-frequency-interrelation but evident differences in the properties of the three travel time groups. For a more explicit study we need a set of shallow water experiments with well defined environmental parameters and stable platforms.

3. FURTHER APPROACHES

These experiments are proposed with the ongoing Baltic Sea traverse experiment in coastal waters east of Fehmarn and the North Sea experiment with an open sea range in preparation. It is proposed to extend the weighting function sketch to a multi-receiver experiment. The purposes of the experiments are

a. To define the statistical category of shallow water transmission for realistic assumptions to the optimization of signal processing.

b. To separate the involved sound propagation effects, as for example multipath transmission and angular dependent rough boundary scattering.

c. To simulate different signal transmissions for comparison with exactly the same environmental conditions.

d. To standardize the experimental procedures for certain scientific questions.

REFERENCES

1. RODERICK, W.I., CRON, B.F. "Frequency Spectra of Forward-Scattered Sound from the Ocean Surface", J. Acoust. Soc. Am., Vol. 48, 759-766 (1970).

2. THIELE, R. "Anwendung der Theorie zeitveränderlicher Filter zur Beschreibung des Flachwasser-Schallkanals", Dissertation Hannover 1972, also FWG-Bericht 71-4 (1971).

3. SLUYTERMAN VAN LANGEWEYDE, W. "Ein Schallstrahlenprogramm für den Tischrechner Hewlett-Packard 9810", Interner FWG-Bericht 72-12 (1972).

4. PRICE, R., GREEN, P.E. Jr., "Signal Processing in Radar Astronomy", M.I.T. Lincoln Lab., T.R. 234 (1960).

5. THIELE, R., HELMER E. "AFAR 72, Acoustic Measurements on Time Variability", Interner FWG-Bericht 73-3b (1973).

DISCUSSION

Dr Wasiljeff asked about the limits of the assumptions for stationarity in time and frequency that are necessary for the concept of the presented scattering function. Dr Thiele replied that time stationarity can be assumed for approximately 1 hour, depending on the sea state, and that stationarity in frequency is assumed to have been fulfilled for the band-limited signals used; however, the main problem lies in the non-deterministic, slowly-varying part of the scattered field, which is not gaussian distributed.

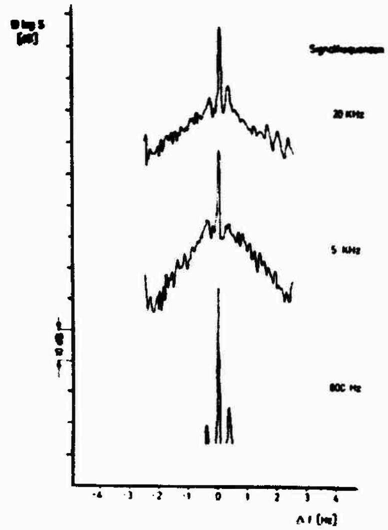

FIG. 1
FREQUENCY SPREAD OF CW-SIGNALS.
PROPAGATION DISTANCE 500, WATER DEPTH ca. 10 m

FIG. 2
PARTS OF RESPONSES OF A CW-PULSE SEQUENCE

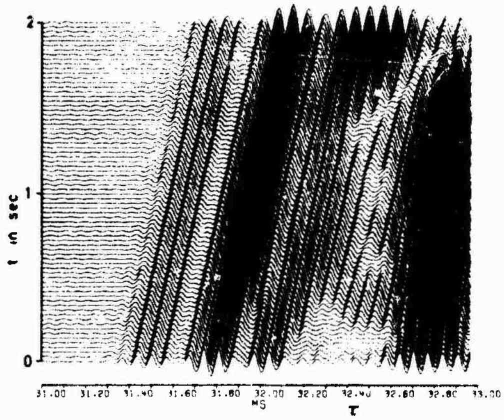

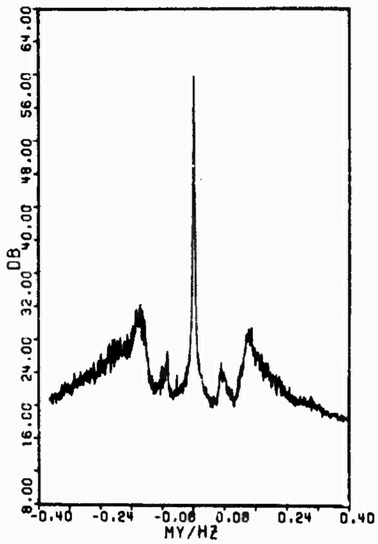

FIG. 3
AFAR 800 Hz POWER DENSITY SPECTRUM

FIG. 4
BALTIC SEA 15 kHz POWER DENSITY SPECTRUM

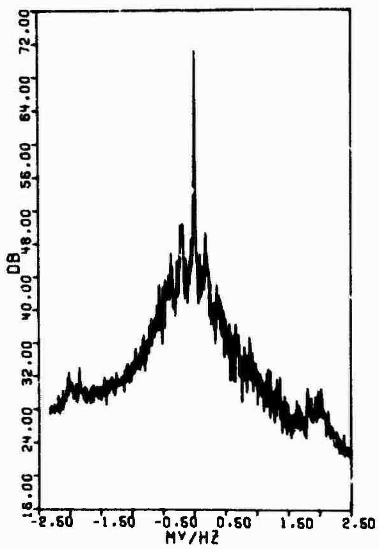

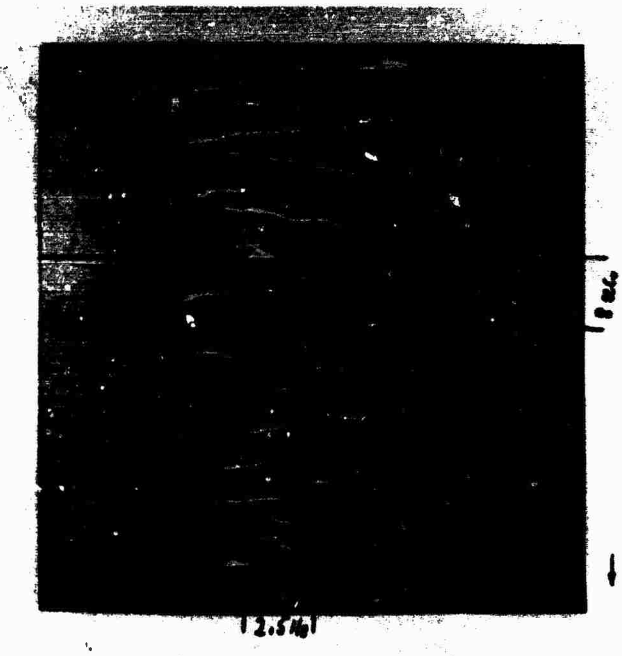

FIG. 5
SERIES OF SHORT-TIME SPECTRA OF A CW-TRANSMISSION WITH A SHIP MOUNTED TRANSMITTER OF 15 kHz

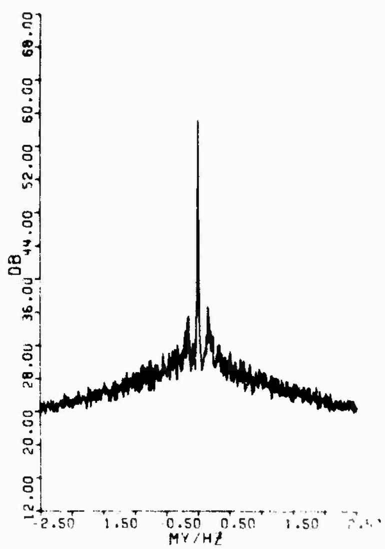

FIG. 6
POWER DENSITY SPECTRUM
(GREAT FISHER BANK)

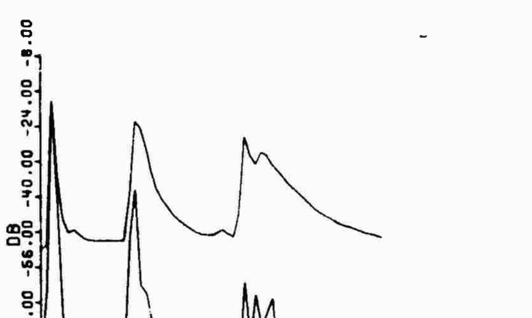

FIG. 7
AVERAGE PULSE RESPONSE
(GREAT FISHER BANK)

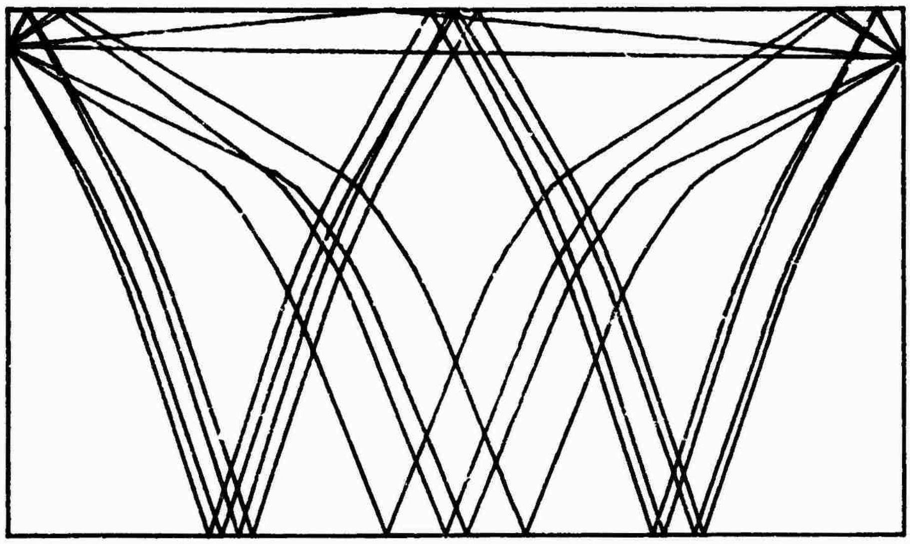

FIG. 8 EIGENRAYS

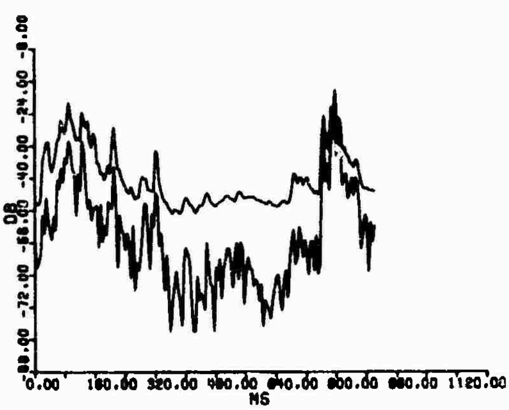

FIG. 9
AVERAGE PULSE, AFAR

FIG. 10
TIME VARIATIONS OF THE PULSE RESPONSE LEVELS IN dB, AFAR

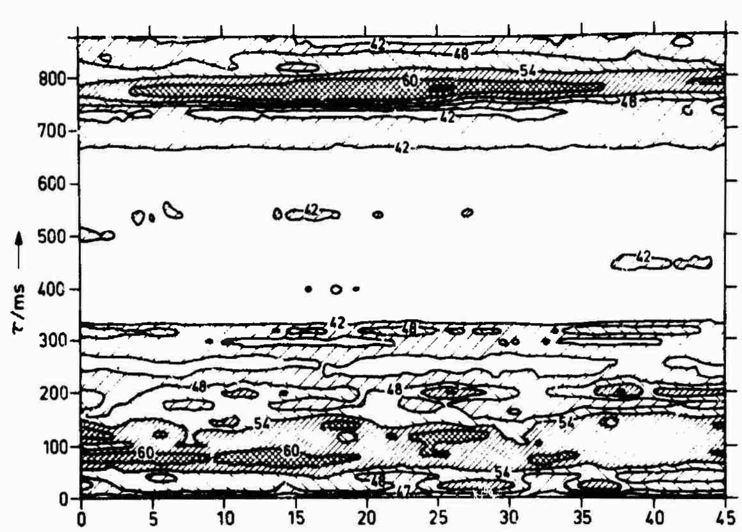

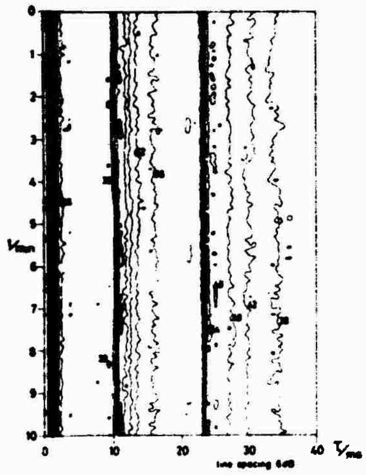

FIG. 11
TIME VARIATION OF THE PULSE RESPONSE
(GREAT FISHER BANK)

FIG. 12
AMPLITUDE FLUCTUATIONS OF A CW- AND A 200 Hz-BANDWIDTH-SIGNAL WITH THE SAME WEIGHTING FUNCTION

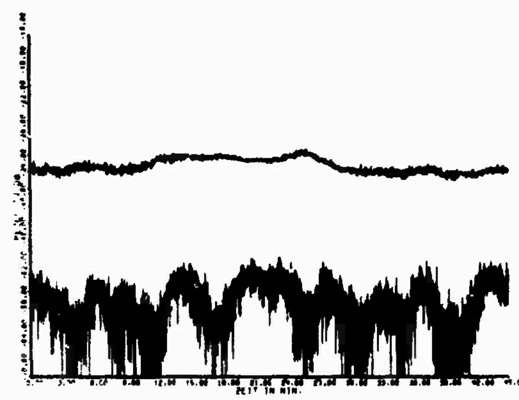

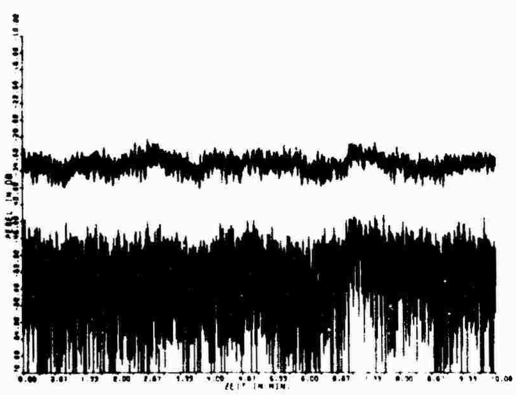

FIG. 13
AMPLITUDE FLUCTUATIONS
(GREAT FISHER BANK)

FIG. 14
POWER DENSITY SPECTRUM – SECOND GROUP
(GREAT FISHER BANK)

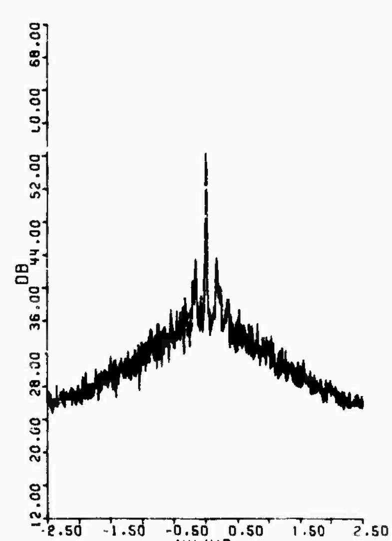

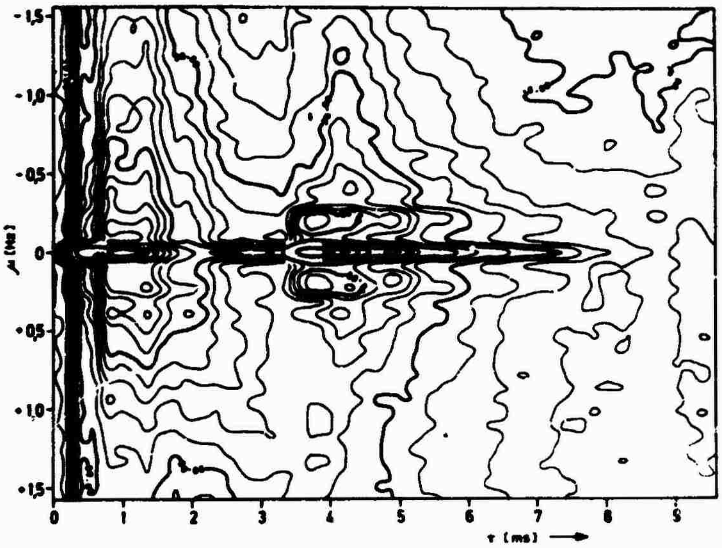

FIG 15 SCATTERING FUNCTION, BALTIC SEA

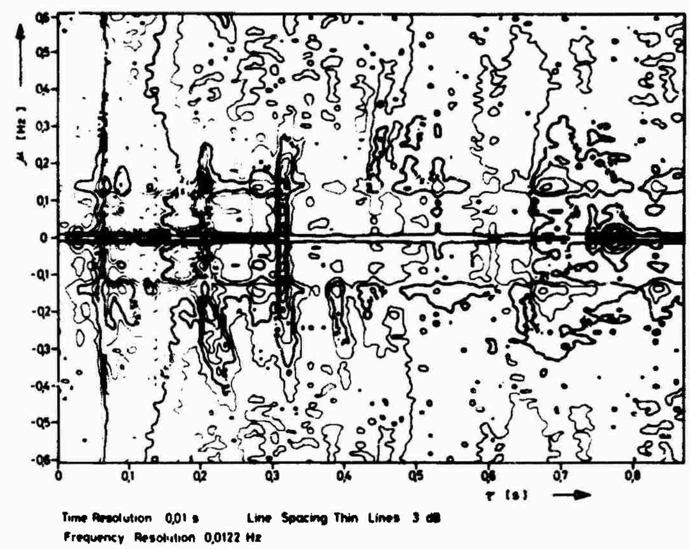

FIG. 16 800 Hz SCATTERING FUNCTION, AFAR

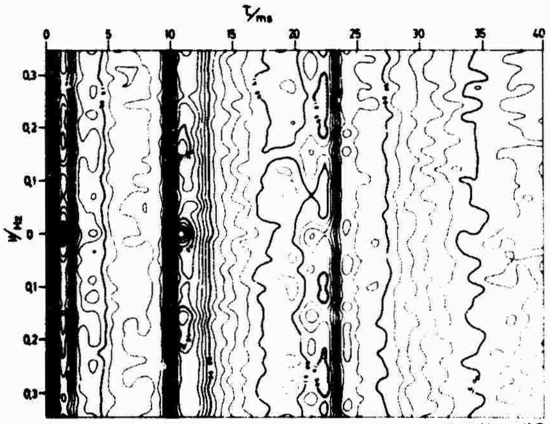

FIG. 17 SCATTERING FUNCTION (GREAT FISHER BANK)

EXPERIMENTAL MODEL STUDIES OF NONLINEAR EFFECTS IN NORMAL MODE PROPAGATION

by

T.G. Muir, R.L. White and J.R. Clynch
Applied Research Laboratories
The University of Texas at Austin, Austin, Texas, USA

ABSTRACT

Nonlinear acoustic phenomena associated with parametric sonar are examined in the light of modal propagation in shallow seas. An analysis of the end-fire generation of difference-frequency sound in this type of environment has identified several potential advantages and limitations of the parametric technique. Among the advantages is the selective narrow-beam excitation of discrete modes with a resulting smoothing of the propagation curve. Among the limitations are the destructive interference effects brought about by phase reversals at boundary reflections within the zone of interaction. These problems have been studied in some experiments at ultrasonic frequencies in a large model tank. The results are interpreted with regard to theory developed for the application of parametric arrays to shallow-water propagation.

INTRODUCTION

The propagation of sound in shallow water is governed by many complicated effects that tend to progressively destroy the coherence of the field radiated by the sound source. Eventually, multipath reflections from the surface and bottom undergo a mutual interference process in which several modes of propagation are usually emphasized at the expense of others. This leads to dispersion effects that limit the effectiveness of acoustic systems that must operate in shallow water.

In order to reduce these difficulties, one might employ conventional high-frequency systems having narrow-beam transmissions. These are impractical, however, due to the severe high-frequency absorption losses that reduce range capability.

One might also consider employing large transducers to achieve good directivity at reasonably low frequencies. This approach is also impractical, as the size of the transducers required is simply too large for use in shallow water.

We propose a new solution to this problem, based on recent developments in the field of nonlinear acoustics. It is now possible to nonlinearly generate highly-directive, low-frequency sound beams by use of Westervelt's parametric acoustic array [Ref. 1]. This device requires only a small primary sound source that is well suited to shallow-water work. The directive, low-frequency beams are generated by nonlinear interaction in the water itself, in the sense of a virtual end-fire array. By vertically tilting this array at incident angles appropriate for the excitation of one or more preferred modes of propagation, it is possible to maximize the energy coupled to that mode. In doing so, energy radiated in adjacent modes is greatly reduced, thereby reducing the undesirable effects of dispersion. The parametric process also offers the realization of wider bandwidth and greater horizontal directivity than can be achieved by conventional linear processes.

This paper is intended to demonstrate the potential of our proposed solution through the presentation of theory and experiment on the application of parametric arrays to normal mode propagation. Simplicity in the theory has been stressed, in order to bridge the difficult gap between nonlinear acoustics and shallow-water propagation. A brief resumé of the nonlinear phenomenon is given to provide background information on its essential features. These principles are then combined with some fundamental shallow-water concepts presented by Weston [Ref. 2], in order to define the approach. The results of model-tank experiments done at ultrasonic frequencies are simultaneously discussed with the theory to verify and further demonstrate these methods. Measured data on parametric beam generation, ray/mode coupling and propagation are presented and compared with the performance of a conventional linear system.

1. NONLINEAR ACOUSTICS

Since it will be necessary to refer to several developments in nonlinear acoustics that may not be widely appreciated, it is convenient to review some of the more important concepts that are fundamental to the subject matter.

1.1 The Equations of Fluid Mechanics

For lossless media*, the three concepts of fluid mechanics that form the basis of acoustics are those of continuity, conservation of momentum, and the physical equilibrium or state of the medium.

---

* The presentation here assumes lossless media for purposes of theoretical simplicity. Absorption appropriate for real media will be subsequently incorporated in an ad hoc manner.

These concepts may be stated mathematically as follows.

Continuity Equation

$$\frac{\partial \rho_T}{\partial t} + \nabla \cdot (\rho_T \vec{u}) = 0 \,, \qquad \text{[Eq. 1]}$$

Momentum Equation

$$\frac{\partial}{\partial t}(\rho_T \vec{u}) + \rho_T \vec{u}(\nabla \cdot \vec{u}) + (\vec{u} \cdot \nabla)\rho_T \vec{u} + \nabla p = 0 \,, \qquad \text{[Eq. 2]}$$

Isentropic Equation of State

$$p = \sum_{n=1}^{\infty} \frac{1}{n!} \left(\frac{\partial^n p}{\partial \rho^n}\right)_{\rho = \rho_0, S} \rho^n \,, \qquad \text{[Eq. 3]}$$

where

ρ_T	=	$\rho_0 + \rho$, total density, ρ_0 = static or equilibrium density,
ρ	=	excess density, ∇ = the vector differential operator,
$\vec{u}$	=	the particle velocity, t = time, p = acoustic or excess pressure,
n	=	a summation index, and S = entropy.

The equation of state shown here is a Maclaurin series expansion of the pressure/density relation. It is usually approximated by retaining only the first two terms in the series, i.e.,

$$p = c_0^2 \rho + \frac{1}{2} \frac{c_0^2}{\rho_0} \left(\frac{B}{A}\right) \rho^2 \,, \qquad \text{[Eq. 4]}$$

where

$$c_0^2 = \left(\frac{\partial p}{\partial \rho}\right)_{\rho=\rho_0, S} \,, \qquad \text{[Eq. 5]}$$

and

$$\frac{B}{A} = \frac{\rho_0}{c_0^2} \left(\frac{\partial^2 p}{\partial \rho^2}\right)_{\rho=\rho_0, S} \,. \qquad \text{[Eq. 6]}$$

Equation 5 is the definition of the small-signal sound speed, c_0, whereas Eq. 6 may be taken as the definition of the "parameter of nonlinearity" of the medium, following the nomenclature of Beyer [Ref. 3]. The results of several measurements indicate that B/A has the value 5.2 for water at 30°C.

1.2 Theory of Parametric Arrays

In 1960, P.J. Westervelt [Ref. 1] at Brown University developed the theory for a sound source that he called a parametric acoustic array. This type of source allows the creation of highly-directive sound at relatively low operating frequencies through the nonlinear interaction of acoustic waves. The original theory treated the problem of the interaction of two plane, collimated, monochromatic primary waves emitted simultaneously from a high-frequency projector. A sketch of the geometry is shown in Fig. 1. The primary waves were postulated to interact nonlinearly in the medium within a zone of modulation that is bounded by the collimated beam and extends a distance along the acoustic axis determined by the small-signal absorption of the primaries. In this sense, the parametric acoustic array may be thought of as a volumetric end-fired array that occupies a portion of the medium directly in front of the projector.

Experimental evidence of the existence and character of parametric arrays was first reported in 1963 by Bellin and Beyer [Ref. 4] and has continued to appear [Refs. 5 to 17] since that time, with recent emphasis on applications [Refs. 18 to 27].

The engineering significance of the parametric array is due to its great directivity: specifically its narrow beamwidth and the absence of minor lobes in its radiation patterns. The narrow beamwidth is a result of the shape of the zone of interaction. By analogy to the ordinary end-fired array, it can easily be seen that the longer the zone of interaction, the smaller is the beamwidth of the parametric array. Since the zone of interaction is usually very long in comparison with its width, the parametric array produces a radiation much narrower than that which would be produced by the source transducer were it operating linearly at the difference frequency. The parametric array is shaded by virtue of the naturally smooth decay in the conversion of carrier-frequency sound to difference-frequency sound with increasing distance from the electroacoustic source. This inherent form of array shading, which is due to the absorption of the primary waves and to diffraction within the zone of interaction, gives rise to an angular response that decays monotonically with increasing angle from the acoustic axis. The beam pattern of the parametric array therefore contains none of the undesirable minor lobe structures common to conventional piston-type transducers.

Although the generation of difference-frequency sound is of the greatest current interest, it should be pointed out that parametric arrays also generate sound at frequencies equal to the sum of the original primary frequencies.

The theory underlying the parametric array problem has its roots in the basic equations 1 to 3, as do other problems in nonlinear acoustics. In working with these equations, Westervelt [Ref. 1] found an inhomogeneous wave equation appropriate for the description of parametric interaction. This is

$$\Box\, p_s = -\frac{\beta}{\rho_0 c_0^4}\frac{\partial^2}{\partial t^2}\, p^2 , \qquad \text{[Eq. 7]}$$

where $\square$ is the d'Alembertian operator, $= \nabla^2 - 1/c_0^2 \dfrac{\partial^2}{\partial t^2}$,

p is the sum of the two primary pressures, and

p_s is the amplitude of difference-frequency sound.

Westervelt solved Eq. 7 for the case of two highly-collimated plane-wave primaries in the steady state. The result, which is valid at long ranges from the interaction volume, may be written in the form

$$p_d(R_0, \theta) = \frac{\beta \omega_d^2 p_1 p_2 S_0}{8\pi R_0 \rho_0 c_0^4} \; \frac{1}{[\alpha^2 + k_d^2 \sin^4(\theta/2)]^{1/2}} \qquad \text{[Eq. 8]}$$

where α is the mean carrier or primary wave-attenuation coefficient,

S_0 is the cross-sectional area of the primary beam,

p_1 and p_2 are the primary-wave amplitudes, and

d indicates difference-frequency parameters.

The half-power beamwidth of the difference-frequency radiation can be obtained from Eq. 8 as

$$\theta_{HP} = 4 \sqrt{\frac{\alpha}{k_d}} \; . \qquad \text{[Eq. 9]}$$

Equation 9 can be used to show that the beamwidth is reduced by reducing the primary frequencies and increasing the difference frequency. This dependence is illustrated in Fig. 2, which plots the half-power beamwidths as a function of the primary and difference frequencies for sea water, using the Schuldin-Marsh absorption formula [Ref. 27]. Since the assumptions underlying Eq. 9 require highly-collimated, plane-wave primaries, Fig. 2 should not be used for primaries of large sphericity and beamwidth. In particular, the primary beamwidth should be smaller than the predicted difference-frequency beamwidth in order to satisfy these assumptions.

Refinements to the solution represented by Eq. 8 have also been made. One of these [Ref. 16] has been especially helpful to the authors of this paper as it allows the extension of theory to spherical and cylindrical wave interaction in the farfield of the primary electro-acoustic source(s). This modification utilizes a numerical integration to provide for an exact description of the directivities of these sources. The numerical solution also allows the difference-frequency sound field to be predicted within the zone of interaction.

Other numerical approaches [Refs. 31, 32] have also been used with success, especially in calculations of finite-amplitude sound-pressure levels. Approximate solutions, based on empirical evidence, have also been developed [Ref. 33] in graphic form for use in design studies.

1.? Measurements on Parametric Arrays

It is convenient to illustrate the parametric-array concept by presenting some free-field measurements on the parametric system to be used in the shallow-water model-tank experiments to follow. This system operates in accordance with the block diagram shown in Fig. 3. A carrier frequency of 1.63 MHz is electronically-modulated at 100 kHz, producing a double-sideband, suppressed-carrier primary signal having sideband components at 1.53 and 1.73 MHz. This signal is applied to an electronic gate to produce modulated cw pulses that are subsequently amplified to peak powers* ranging up to 80 W. The amplified signal is then used to drive an air-backed ceramic piston, 3.3 cm in diameter, producing peak primary source levels ranging up to 222 dB re 1 μPa at 1 m. Nonlinear interaction of the two main-band components of the primary signal occurs in the water, producing a difference-frequency signal centred at 200 kHz, with equivalent peak source levels up to 183 dB.

Free-field propagation data are presented in Fig. 4, which plots the primary and difference-frequency levels as a function of range for four input power levels. It can be seen that increasing the input power increases the sound-pressure levels of the difference-frequency radiation. The difference SPL is proportional to the product of primary-wave amplitudes and is therefore directly dependent on input power. At low power, the difference-frequency generation continues out to about 4 m, where the propagation curve reaches the spherical spreading asymptote of the farfield. This is a measure of the effective length of the end-fired parametric array, which is here determined by the thermoviscous absorption of the water at the primary frequencies. (The −3 dB and 1/e absorption lengths for a 1.63 MHz primary are shown on the horizontal axis.) As the power is increased, the length of the parametric end-fire array becomes shorter as the interaction becomes limited to the near-field region of the primary source. (The near-field distances of the primary source are also shown on the horizontal axis.) The shortening effect is due to another nonlinear acoustic phenomenon associated with finite-amplitude distortion, shock formation, and eventual saturation of the primary field [Ref. 33]. This process has the effect of increasing the effective attenuation with increase in radiated power.

Beam-pattern data on the primary and difference-frequency radiations are shown in Fig. 5, as a function of input power. These were taken at a range station of 4 m. The high-amplitude primary patterns demonstrate the aforementioned saturation effect in that the main lobes are progressively attenuated and blunted with increase in power. This also causes a progressive reduction in side-lobe suppression. The difference-frequency patterns demonstrate their characteristic monotonic shape, with no side lobes, that is the hallmark of parametric arrays. The beamwidths are also quite narrow considering that an electroacoustic source with a diameter of only 3.3 cm or four difference-frequency wavelengths was used to produce these fields. A beam pattern of the electroacoustic source operating linearly at 200 kHz is also shown in Fig. 5 for purposes of comparison. It can be seen that the linear pattern is about six times broader than the parametric patterns, thereby demonstrating a 6:1 improvement in resolution for this particular parametric example.

* [illegible] primary powers [illegible] measured [illegible] interference phase [illegible] pulse.

Parametric beam patterns were also recorded at the other range stations in the propagation curves of Fig. 4. Most of these patterns differ only slightly from the low-amplitude patterns of Fig. 5. This is due to the fact that the nearfield beamwidths of an exponentially-shaded, end-fire array approach the farfield beamwidth in accordance with an exponential range dependence [Ref. 16]. One therefore realizes the farfield beamwidth of the array at fairly short ranges within the interaction region.

2. MODEL-TANK EXPERIMENTS

Over the past 20 years, a considerable development of scientific experimentation in shallow-water propagation has occurred. Two approaches have been taken: (1) full-scale measurements at sea, and (2) model-tank measurements in the laboratory. Unfortunately, neither of these approaches is fully satisfactory in the experimental sense. The full-scale measurements are limited by their great expense, and they are also subject to uncontrollable environmental fluctuations that are difficult to account for. Although the model-tank experiments are much less expensive and easier to control, they are beset with difficulties in scaling the crucial oceanographic parameters. It was nonetheless felt that the application of nonlinear acoustics to shallow-water propagation was sufficiently new and difficult so as to be best suited to experimentation under controlled conditions. The design of our model-tank system was greatly assisted and influenced by the work of A.B. Wood [Ref. 35] and by the work of Eby, Williams, Ryan, and Tamarkin [Ref. 36].

2.1 The Apparatus

A sketch of the mechanical apparatus is shown in Fig. 6. A tank, 10-m long, 5-m wide, and 4-m deep was chosen. Since the horizontal beamwidth of the parametric source is quite narrow, the width of the shallow area in this type of experiment need not be large. A continuous aluminum plank, 2-cm thick, 50-cm wide and 8-m long was therefore chosen as the bottom surface. This plank was suspended in the tank in a horizontal position, 11.4 cm beneath the water surface. This "shallow sea" is fifteen wavelengths in depth at our 200 kHz frequency. The electroacoustic source is located at one end of the water column and is mounted on a device that rotates and tilts the projector about its acoustic centre. A spherical hydrophone, 1.3 cm in diameter, is used as a receiver. This sensor can be mounted on a motorized car that runs up and down the plank or it can be suspended from an overhead tram travelling on a monorail. All of the angular and linear movements are monitored by servomechanisms connected to the data-plotting machines. A titanium block, 3-cm thick, 50-cm wide and 11.4-cm high is also used as a reflector at the end of the plank. This increases the effective length of the shallow area to 16 m, for pulsed operation of the system.

2.2 Pulse Propagation in the Time Domain

Measurements on the time arrivals of pulses radiated into the shallow-water model sea are perhaps the clearest indicator of the interesting role parametric techniques may play in both experimental work and in possible system applications. Some photographs of this type of data are presented in Fig. 7. These were taken with a delayed time-base oscilloscope so as to expand the detail about the arrival times. Two photos are shown; one for the system operating linearly and the other with the system in parametric operation. In each case, a 200 μs pulse was transmitted horizontally into the shallow water at mid-depth. The hydrophone was also located at mid-depth at a range of 5.1 m. The horizontal scale on both photographs is 0.5 ms per division.

In the linear case shown in Fig. 7 considerable interference and smearing in the pulse arrival can be seen. The early arrivals show interference resulting from multipath reflections in the intermediate ray/mode regime. This is visible in the "dip" or "notch" appearing in the first of the linear pulses. Most of the later arrivals arose from relatively wide-angle scatterers in the tank, i.e. the plank suspension wires, the tank sides, etc. Such scatterers are always a source of difficulty in tank work with linear systems having their usual side lobes.

The data for the parametric case shown in Fig. 7 show practically no interference or smearing. In fact, clean pulses of this type were obtained for the mid-depth orientation at ranges out to 16 m, despite the fact that the water column was only 11.4 cm, or 15 λ_s in depth. No significant reflections from unwanted scatterers in the tank are obtained. This illustrates the value of the narrow-beam parametric system, with its side-lobe-free radiation field, in model-tank experiments. Applications to systems operating in other reverberant environments are also worthy of consideration.

2.3 Pulse Propagation in the Spatial Domain

Measurements on the amplitude of the peak-pulse arrivals for both linear and parametric operation are shown plotted in Fig. 8 as a function of range. These are simply propagation curves with amplitude plotted in the decibel format and range plotted on a linear scale. They were acquired with the projector and receiver at mid-depth with a horizontal orientation, as before. The hydrophone was displaced horizontally in a continuous fashion, and a synchronous electric plotter was used to record the peak amplitude of the received signals. The pulse lengths, power, etc. are the same as for the data of the previous section.

The data for linear operation of the system were acquired with a time-gated receiver adjusted to reject most of the unwanted reflections from scatterers in the tank. The resulting propagation curves for the linear case in Fig. 8 are therefore fairly representative of the fluctuations brought about by modal interference. The propagation characteristics are quite complicated, illustrating the general difficulties of shallow-water work.

It was not necessary to gate-reject unwanted echoes in the acquisition of the parametric data shown in Fig. 8, as there was none. The parametric propagation curve is very smooth and well-behaved. Note that the amplitude of the difference-frequency radiation is essentially zero at zero range and then grows rapidly, reaching a maximum at a range of about 50 cm. This behaviour illustrates the phenomenon of nonlinear sound generation in the water itself. The behaviour of the remainder of the propagation curve illustrates the immunity of the difference-frequency radiation to the acute modal-interference phenomena associated with the linear system. If modal interference exists at all in this parametric data, it must not only play a minor role but also one with minimal excursion.

2.4 Analysis

Before proceeding with more experimental data, it will be convenient to return briefly to the theory in order to establish an analytical basis for further interpretation of the measurements. A simplified ray approach to modal theory presented by Weston [Ref. 2] will be blended with some of the nonlinear acoustic solutions to postulate two important criteria. These will then be used to clarify the experimental situation.

By reference to Fig. 9a, we accept the definition of the ray-theory cycle distance as

$$D = 2H/\varphi \, , \qquad \text{[Eq. 10]}$$

where H is the water depth and φ is the grazing angle. The allowed eigenvalues in the waveguide may easily be found from the "rays-with-phase" form of the WKB approximation,

$$2\int \frac{2\pi}{\lambda}\varphi \, dh + \theta_s + \theta_B = 2\pi n \, , \qquad \text{[Eq. 11]}$$

where λ is the wave length,

dh is the incremental height,

θ_s and θ_B are the phase shifts at the surface and bottom, and

n is the modal number.

While θ_s has the value π, θ_B is usually π or zero, depending on the boundary conditions. With the solid bottom of the present experiments, $\theta_B = 0$. The subscripts "s" (for soft) and "h" (for hard) will be used to denote each boundary condition, respectively.

The solution of Eq. 11 yields the eigenvalues in terms of allowed rays, cycle distance and phase velocities. These are

$$\varphi_s = n\lambda/2H \quad \text{and} \quad \varphi_n = (n-1/2)\lambda/2H \, , \qquad \text{[Eq. 12]}$$

$$D_s = 4H^2/n\lambda \quad \text{and} \quad D_n = 4H^2/(n-1/2)\lambda \, , \qquad \text{[Eq. 13]}$$

and

$$c_n = c_0 \sec\varphi \qquad \text{[Eq. 14]}$$

For the $H = 15\lambda$ water column of our model-tank experiments, Eqs. 12 and 13 predict the quantities shown in Table 1.

TABLE 1

n	φ_n	D_n
1	0.93°	14.04 m
2	2.79°	4.58 m
3	4.66°	2.80 m
4	6.53°	1.99 m
5	8.40°	1.54 m

We next postulate that to concentrate the maximum amount of parametric energy into a given mode we must achieve a parametric beam having a half-width that is smaller than the modal separation angle. This criterion may be expressed, with the aid of Eq. 12, as

$$1/2\ \theta_{HP} \le \varphi_{n+1} - \varphi_n = \lambda_d/2H\ , \qquad \text{[Eq. 15]}$$

where λ_d is the difference-frequency wave length.

Use of Eq. 9 then yields

$$\alpha \le \frac{\pi\lambda_d}{8H^2}\ , \qquad \text{[Eq. 16]}$$

where α is again the mean absorption coefficient at the primary frequencies. This result merely states a rough minimum length for the parametric end-fire array appropriate for the development of a sufficiently narrow beam. This criterion is fairly-well satisfied for the experiment at hand in that the left-hand side of Eq. 15 amounts to about 1° while the right-hand side is about 2°.

Our second postulation concerns the amplitude and phase of difference-frequency sound generation within each mode. Without going into great detail, it is important to note that phase reversals within the zone of interaction of a parametric array create difficulties that should be avoided, if possible. This problem has been studied theoretically and experimentally [Ref. 23] and it has been found that the phase reversals can cause destructive interference effects that are counter-productive to difference-frequency generation. This difficulty is qualitatively illustrated in Fig. 9b. It can there be seen that difference-frequency sound generated after a phase reversal is simply 180° out of phase with that reflected from the previous segment of the interaction zone. This is due to the fact that 180° phase shifts in each primary have no effect on the phase of difference-frequency generation, thereby emphasizing the phase reversal of the difference frequency in the superposition process.

A handy criterion to estimate the possible onset of difficulties wrought by phase reversals for parametric operation in modal propagation is therefore required. Experience has shown that parametric generation is effectively terminated at a range corresponding to the -3 dB absorption distance of the primaries. By requiring this range to be ≤ the range to the first phase reversal, we can develop a fairly-conservative estimate of the bounds of the phase problem. Use of Eq. 13 for a projector at mid-depth leads to

$$L_{-3\ dB} \le \frac{1}{4} D_s$$

or [Eq. 17]

$$L_{-3\ dB} \le \frac{3}{4} D_n ,$$

the latter formula being appropriate for a downward-oriented beam. If the projector is located at the surface, the right-hand sides of Eq. 17 may be increased by a factor of 4/3. Algebraic reduction enables Eq. 17 to be written in the form*

$$\alpha \le \frac{n\lambda_d}{3H^2}$$

or [Eq. 18]

$$\alpha \le \frac{(n-1/2)\ \lambda_d}{4H^2}$$

Again, the right-hand sides of Eq. 17 may be increased by a factor of 4/3 for projectors located at the surface. For the experiment at hand, the inequality of the second form of Eq. 17 is satisfied in the ratio of 1 : 3.2, for propagation in the first mode.

Comparison of the beamwidth criterion, [Eqs. 15 and 16], with the phase criterion, [Eqs. 17 and 18] shows the former to be more restrictive. These may all be relaxed however, as we examine these two important effects in greater detail. It would seem, for example, that scattering losses at the boundary would reduce the severity of the phase problem as they would effectively reduce the strength of one of the interfering fields.

The analysis presented in this section indicates that we should have a fairly good chance of coupling most of the parametric energy into the first mode of our shallow-water experiment. The beam is relatively narrow with respect to the mode-angle separation and the zone of interaction is shorter than the distance to a phase-reversed bounce. The problem of parametric modal coupling will now be illustrated with the presentation of more experimental data.

---

* *The first form of Eq. 17 is for modes having a "soft" reflection at the first bounce, while the second form is appropriate for a "hard" reflection.*

2.5 Beam Formation

The water column's evolutionary acceptance of the parametric beam in a modal sense is first illustrated by the beam-development data of Fig. 10. Here, the amplitude of the parametric signal was measured at mid-depth as a function of the angular position of the projector in the vertical plane. Data were acquired at seven ranges, logarithmically-spaced. The pulse length was 200 μs at an input power of 22.5 W, as before. The results are presented in a series of plots showing tilt angle versus received level, with range increasing to the right. It can be seen that several unrelated beam reflections occur at the short ranges, resulting in prominent lobes in the tilt patterns. As the range increases, however, these lobes progressively die out, leaving a narrow beam peaked at about 1° of downward tilt.

An enlarged view of the evolved beam is shown in Fig. 11. The peak at 1° of downward tilt corresponds to the ray angle of the first mode, shown previously in Table 1. These data appear to indicate that the water column prefers a main beam oriented at the first-mode ray angle. This occurs despite the fact that the hydrophone was located at mid-depth throughout the measurement.

2.6 Beam Behaviour

Additional data extracted from Fig. 10 are presented in Fig. 12.

The plot in Fig. 12a shows the range-dependence of the peak amplitude of the main beam. It can be seen that after the parametric-generation region, the beam enters a regime governed by spherical spreading. This is not surprising since the cycle distance of the first mode is about 14 m for the experiment at hand.

The plot in Fig. 12b shows the trend in downward deflection of the main beam with increase in range. Although there is some scatter in the data, a progressive shift toward the first modal angle is evident.

2.7 Depth Profile

One of the most descriptive eigenfunctions of a normal mode process is the vertical distribution of sound amplitude permitted by modal selection. Data on the depth profile at a range of 13.5 m are shown in Fig. 13. This curve was measured by raising the hydrophone in 1 cm increments, keeping the projector tilt constant at a 1° downward orientation. Other parameters of the measurement are the same as for the previous data. The curve peaks at about 1 cm above mid-depth and goes to zero at the water surface. It does not appear to approach zero at the bottom surface, although it is there rather small.

The depth profile of the first mode for the experiment at hand should be zero at the surface and should progress to a value of unity at the bottom. Some interference from perhaps the second mode or the residual direct-path radiation may be responsible for a non-unity value

in the eigenfunctions at zero depth. The difference in arrival time for the first and second mode pulses at the range of measurement is about 10 μs. This corresponds to two periods of the difference-frequency measurement, which is too short to be resolved by the present system. Data acquired at greater ranges would therefore be of interest in separating cause and effect in the eigenfunction behaviour.

SUMMARY AND CONCLUSIONS

This paper has examined the application of nonlinear parametric arrays to shallow-water propagation by means of theory and experiment on a model-tank scale. The possibility of using the parametric endfire array to couple to discrete modes was proposed and analysed with a view toward the reduction of multipath reflections and modal interference.

The fundamental theory of parametric arrays was reviewed and illustrated by presentation of free-field measurements on a difference-frequency radiation. A model-tank facility designed for parametric work in shallow water was described.

Initial results obtained in this tank demonstrate several advantages of narrow-beam parametric arrays when compared with conventional linear systems. These advantages include increased immunity to multipath interference in the transmission and reception of short pulses, with a corresponding smoothing of the propagation curves. These advantages are not only due to the narrow beamwidth of parametric radiations, but also to their side-lobe-free radiation patterns.

A simple analysis was presented to help quantify the possibilities and limitations of the approach. In so doing, criteria were established by relating (1) the parametric beamwidth to the modal ray angles and (2) the length of the parametric array to the mode-cycle distance. It was argued that discrete modal coupling is increased when (1) the parametric beam is smaller than the modal separation angle and (2) the array length is less than the range to the first phase-reversed reflection.

Detailed experimental results on the formation of a parametric beam at depression angles near that for the first mode were presented. It was shown that the water column itself preferred a beam oriented at an angle appropriate for the first mode. Measurements on the depth profile of difference-frequency sound amplitude in the water column were presented for a depression angle appropriate for excitation of the first mode. These data show the depth function to be zero at the surface, progressing to a value of unity near mid-depth and then falling off to a reduced but non-zero amplitude at the bottom. Although this behaviour has not yet been fully explained,

its character indicates the possible excitation of the first mode, with residual energy in only a few other modes.

In conclusion, it appears that parametric end-fire arrays are well suited to shallow-water propagation work. It makes sense to consider these long, narrow arrays for use in waters that are themselves long and narrow. Many new and interesting features of this approach have already arisen, and others are likely to develop with continued research.

ACKNOWLEDGEMENTS

The authors are indebted to Teddy Cloer and Walter Birchfield for their assistance in constructing the model-tank experiment. Many helpful discussions with P.J. Westervelt and D.E. Weston are also acknowledged. This work was supported by the U.S. Office of Naval Research.

REFERENCES

1. P.J. Westervelt, "Parametric Acoustic Array," J. Acoust. Soc. Am. 35, 535-537 (1963).

2. D.E. Weston, "Rays, Modes, Interference, and the Effect of Shear Flow in Underwater Acoustics," J. Sound Vib. 9, 80-89 (1969).

3. R.T. Beyer, "Parameter of Nonlinearity in Fluids," J. Acoust. Soc. Am. 32, 719 (1960).

4. J.L.S. Bellin and R.T. Beyer, "Experimental Investigation of an End-Fire Array," J. Acoust. Soc. Am. 34, 1051-1054 (1962).

5. H.O. Berktay, "Possible Exploitation of Nonlinear Acoustics in Underwater Transmitting Applications," J. Sound Vib. 2, 435-461 (1965).

6. H.O. Berktay, "Parametric Amplification by the Use of Acoustic Nonlinearities and Some Possible Applications," J. Sound Vib. 2, 462-470 (1965).

7. H. Hobaek, "Experimental Investigation of an Acoustical End-Fired Array," J. Sound Vib. 6, 460 (1967).

8. V.A. Zverev and A.I. Kalachev, "Measurement of the Scattering of Sound by Sound in the Superposition of Parallel Beams," Sov. Phys. Acoust. 14, 173-178 (1968).

9. H.O. Berktay, "Nonlinear Interactions between Acoustic Waves in Liquids — Possible Applications," Application of Finite Amplitude Acoustics to Underwater Sound, Proceedings of a Seminar held at the U.S.Navy Underwater Sound Laboratory on 27 May 1968, NUSL Rpt. No. 1034, 15-38 (1970).

10. T.G. Muir and J.E. Blue, "Acoustic Modulation of Large Amplitude Waves," J. Acoust. Soc. Am. 46, 227-232 (1969).

11. See, for example, Nonlinear Acoustics, Proceedings of the 1969 ARL Symposium, T.G. Muir (ed.), Applied Research Laboratories, The University of Texas at Austin (1970).

12. Proceeding of the British Acoustical Society Specialist Meeting on Nonlinear Acoustics, University of Birmingham (1971).

13. H.M. Merklinger, "High Intensity Effects in the Nonlinear Acoustic Parametric End-Fire Array," Ph.D. Thesis, University of Birmingham (England), June 1971.

14. M.B. Moffett, P.J. Westervelt, and R.T. Beyer, "Large-Amplitude Pulse Propagation — A Transient Effect," J. Acoust. Soc. Am. 49, 339-343 (1971).

15. R.H. Mellen, D.G. Browning, and W.L. Konrad, "Parametric Sonar Transmitting Array Measurements," J. Acoust. Soc. Am. 49, 932(L) (1971).

16. T.G. Muir and J.G. Willette, "Parametric Acoustic Transmitting Arrays," J. Acoust. Soc. Am. 52, 1481-1486 (1972).

17. See, for example, Proceedings of the 1973 Symposium on Finite-Amplitude Effects in Fluids, L. Bjørnø, (ed.), Technical University of Denmark, IPC Science and Technology Press Surrey, England (1974).

18. H.O. Berktay, "Some Proposals for Underwater Transmitting Applications of Nonlinear Acoustics," J. Sound Vib. 6, 244-254 (1967).

19. See, for example, G.M. Walsh, Ref. 12.

20. T.G. Muir, "The Potential of Sonar Surveys in Marine Archeology," Applied Research Laboratories Prospectus, (June 1972).

21. T.G. Muir and R.S. Adair, "Potential Use of Parametric Sonar in Marine Archeology," J. Acoust. Soc. Am. 52, 122(A) (1972).

22. T.G. Muir, "A Parametric Model for Porpoise Sonar," Unpublished manuscript, Applied Research Laboratories, The University of Texas at Austin, January 1973.

23. T.G. Muir, et al. "Parametric Echoscanner for Biomedical Diagnostics," J. Acoust. Soc. Am. 53, 382(A) (1973).

24. T.G. Muir and D.L. Folds, "Parametric Acoustic Lens Sonar," Paper V2, 86th Meeting of Acoustical Society of America.

25. See, for example, Ref. 17.

26. T.G. Muir, "Nonlinear Acoustics and its Role in the Sedimentary Geophysics of the Sea," in Physics of Sound in the Sediments, L.D. Hampton (ed.), Plenum Press, New York (1974).

27. See, for example, W.L. Konrad, Ref. 17.

28. M. Schulkin and H.W. Marsh, "Sound Absorption in Sea Water," J. Acoust. Soc. Am. 30, 864 (1962).

29. V. Lauvstad, J. Naze and S. Tjötta, "Nonlinear Interaction of Two Soundwaves," Acta Universitatis Bergensis Series Matematica, (Norwegian Universities Press, Oslo) 12, 1-24 (1964).

30. See, for example, Refs. 9, 11, 12, and 17.

31. F.H. Fenlon, "A Recursive Procedure for Computing the Nonlinear Spectral Interactions of Progressive Finite-Amplitude Waves in Nondispersive Fluids," J. Acoust. Soc. Am. 50, 1299-1313 (1971).

32. F.H. Fenlon, "On the Derivation of Zone I Spectra for a Pulsed Finite-Amplitude Source Operating in a Nonviscous Nondispersive Medium," J. Acoust. Soc. Am. 54, 465-473 (1973).

33. R.H. Mellen and M.B. Moffett, "A Model for Parametric Sonar Radiator Design," Naval Underwater Sound Center Tech. Memo PA 41-229-71 dated 14 September (1971).

34. J.A. Shooter, T.G. Muir, and D.T. Blackstock, "Acoustic Saturation of Spherical Waves in Water," J. Acoust. Soc. Am. 55, 54-62 (1971).

35. A.B. Wood, "Model Experiments on Propagation in Shallow Seas," J. Acoust. Soc. Am. 31, 1213-1235 (1959).

36. R.K. Eby, et al., "Study of Acoustic Propagation in a Two-Layered Model," J. Acoust. Soc. Am. 32, 88-99 (1960).

DISCUSSION

Dr Kuperman asked how the narrow beam could create the necessary plane waves, with constant phase over their fronts, for the formation of modes. Dr Muir explained that the geometry of the tank experiments was such that at the end of the tank, which is at a distance of half a cycle, the beam is 8 in high and the water column only 4½ in tall, so that although at the source the beam was smaller than the water column it does not take long before it becomes plane waves and can insonify the water column.

Dr Weston suggested the possibility of an alternative non-linear method for selecting the first normal mode in which, although the beamwidth can be greater than the angular separation of the modes, the acoustic interaction distance is arranged to be about equal to the cycle distance for the first mode. The interaction distance is then greater than the cycle distance for the higher modes, which are therefore not efficiently excited. This mechanism could act in different circumstances to Dr Muir's first mechanism, or it could reinforce it. Dr Muir agreed that this could be an applicable mechanism.

Mr Laval pointed out that with a horizontal end-fire array it is possible to select a given mode in the axial direction by having a phase weighting corresponding to the phase velocity of this particular mode. Such a phase weighting, however, corresponds to the projected phase velocity of other lower modes propagating in different directions and the array actually selects various modes, each corresponding to a particular propagating direction. He therefore asked whether such a propagation might be occurring with a parametric array, which is a type of end-fire array and, if not, whether is it something in the mechanism of non-linearity that prevents it. Dr Muir agreed that there is a good possibility that this type of propagation might be occurring, which may explain why he obtained more of mode two than he expected in his experiments.

Dr Kuperman said that in shallow water it should be possible to expand the excitation of the non-linear sound mathematically as the sum of the normal modes and asked whether this had been attempted. Dr Muir said that he had a rigorous theoretical model that takes this into account but felt that it was too complicated to take time in explaining it here.

FIG. 1

PARAMETRIC TRANSMITTER, GEOMETRY

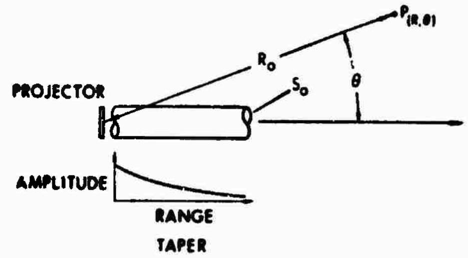

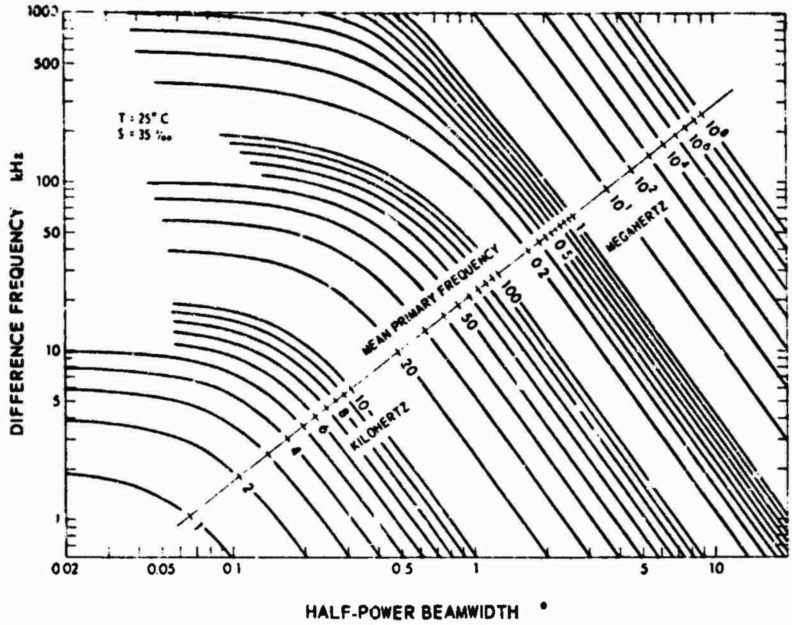

FIG. 2 NOMOGRAPH OF PARAMETRIC TRANSMITTING ARRAY BEAMWIDTHS AS CALCULATED FROM THE WESTERVELT FORMULA

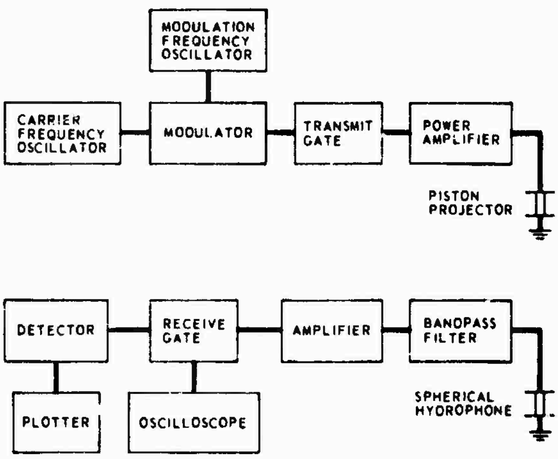

FIG. 3 BLOCK DIAGRAM OF THE EXPERIMENT

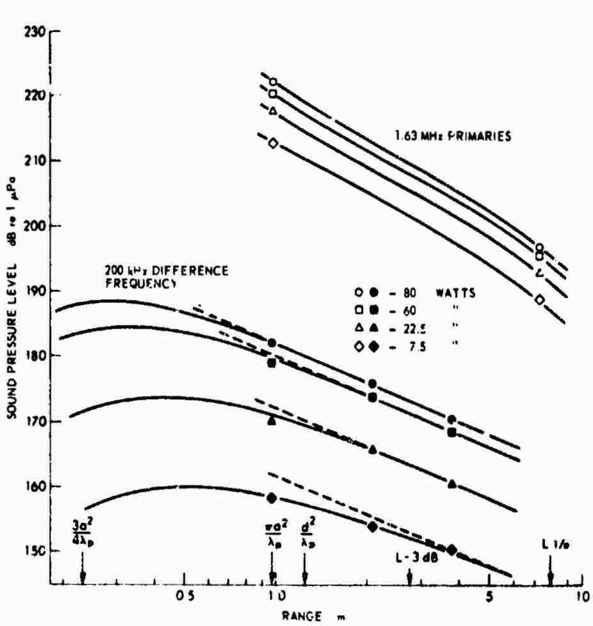

FIG. 4 FREEFIELD PROPAGATION

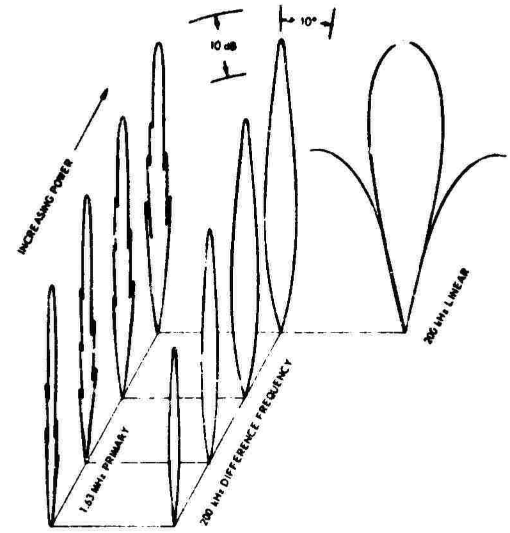

FIG. 5
BEAM PATTERNS

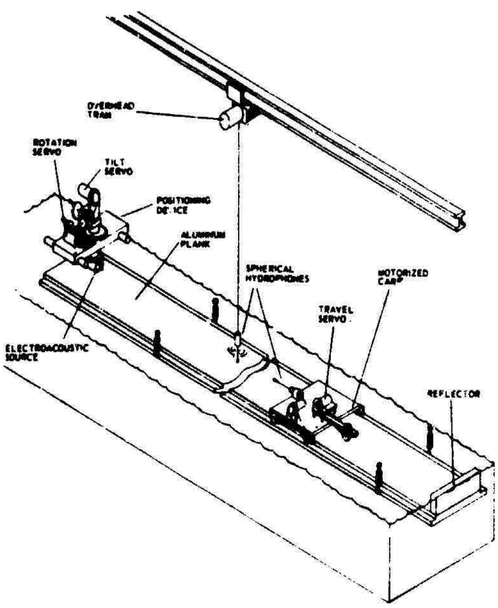

FIG. 6
MODEL TANK APPARATUS

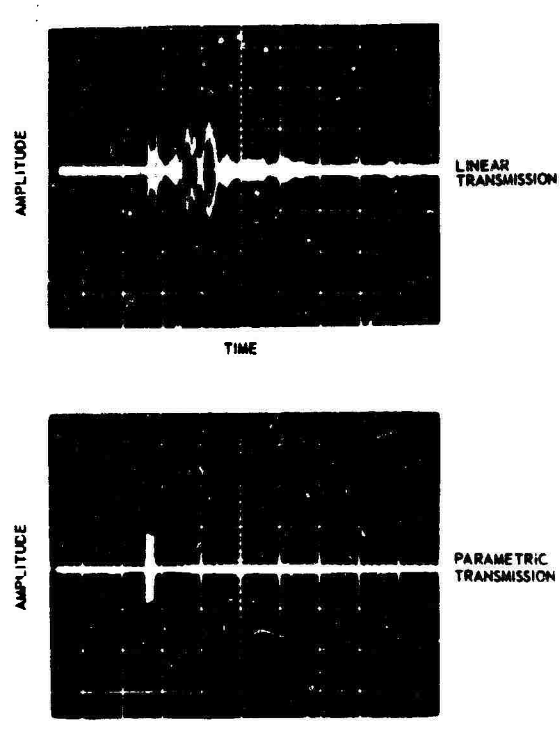

FIG. 7
PULSE ARRIVAL DATA

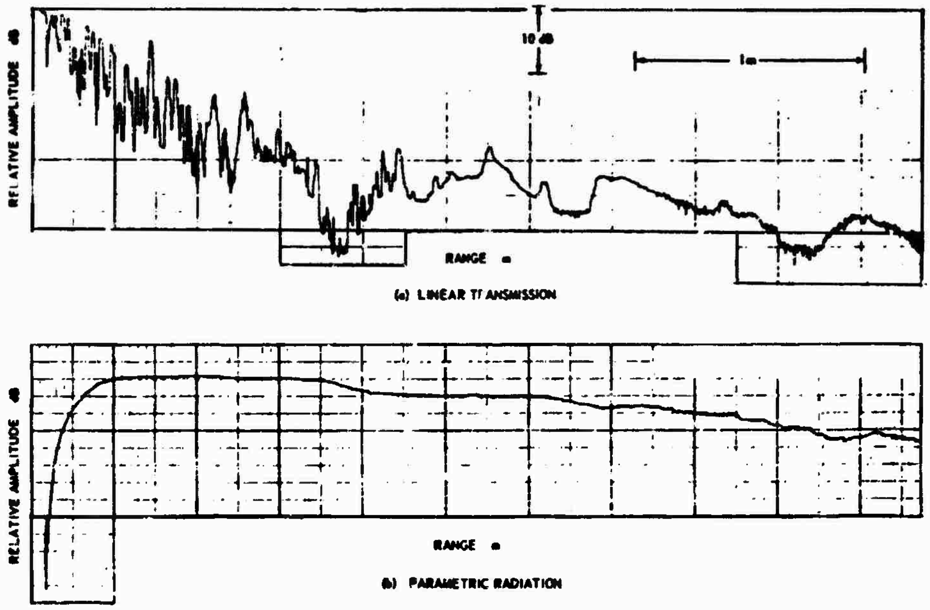

(a) LINEAR TRANSMISSION

(b) PARAMETRIC RADIATION

FIG. 8 MODEL TANK PROPAGATION CURVES

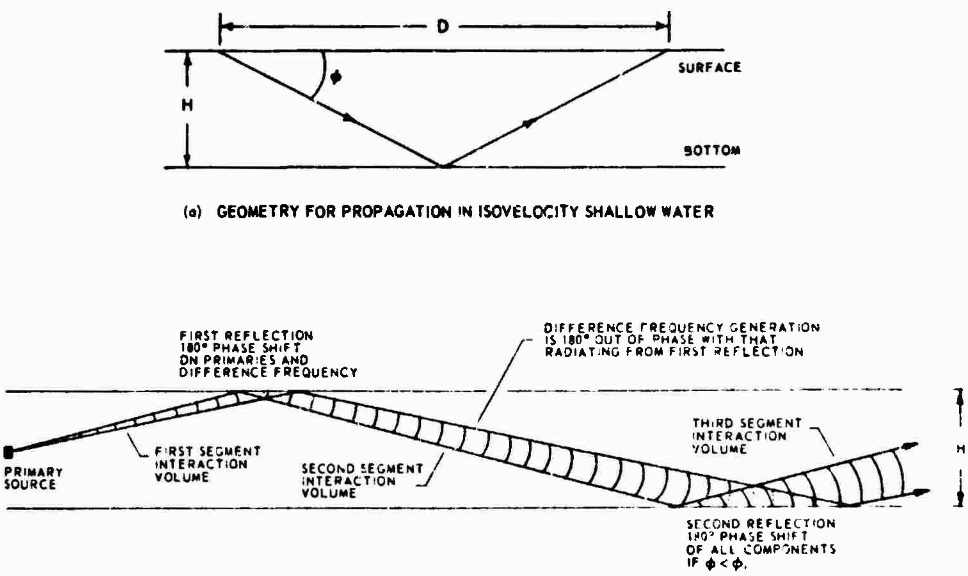

(a) GEOMETRY FOR PROPAGATION IN ISOVELOCITY SHALLOW WATER

(b) GEOMETRY OF PARAMETRIC INTERACTION VOLUME IN SHALLOW WATER

FIG. 9 SHALLOW WATER PROPAGATION GEOMETRIES

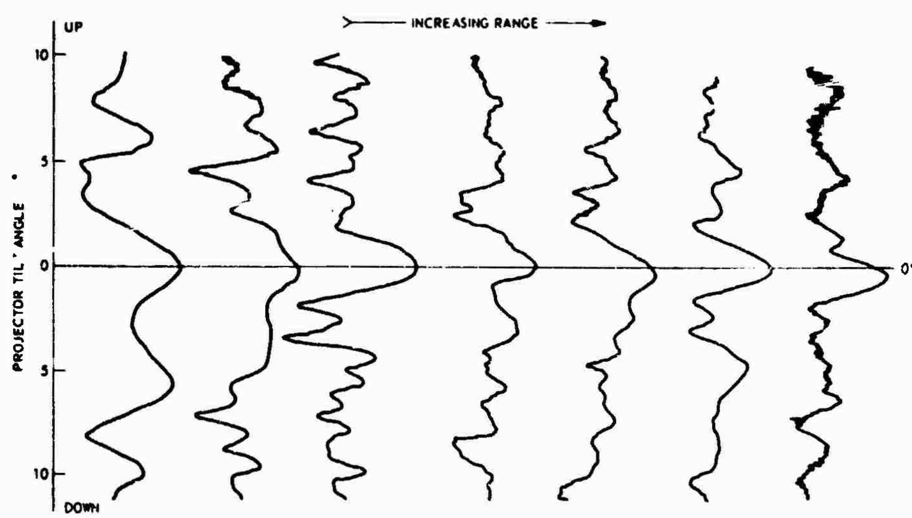

FIG. 10 PARAMETRIC BEAM FORMATION IN SHALLOW WATER

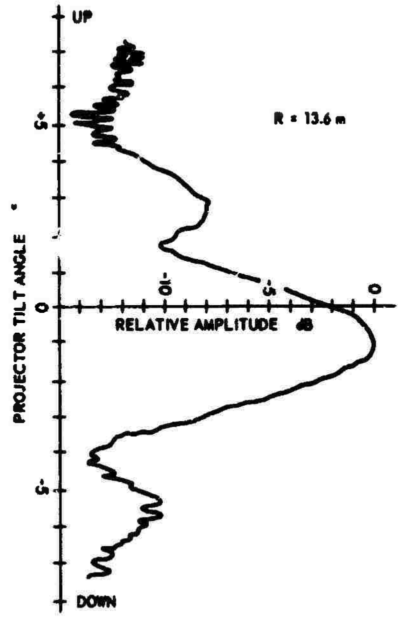

FIG. 11 DEPENDENCE OF RECEIVED AMPLITUDE AT MID-DEPTH ON PROJECTOR TILT ANGLE

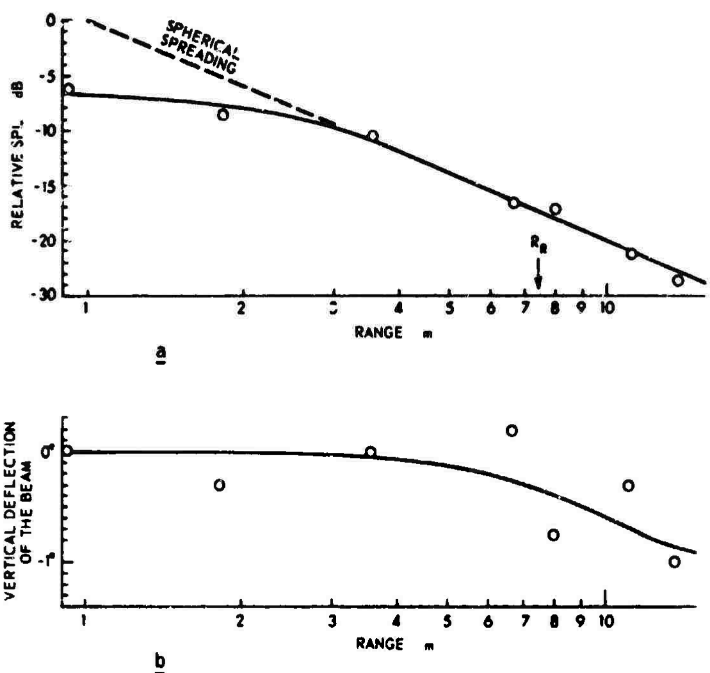

FIG. 12 EARLY PROPAGATION OF THE PARAMETRIC BEAM AS IT IS LAUNCHED INTO THE FIRST MODE

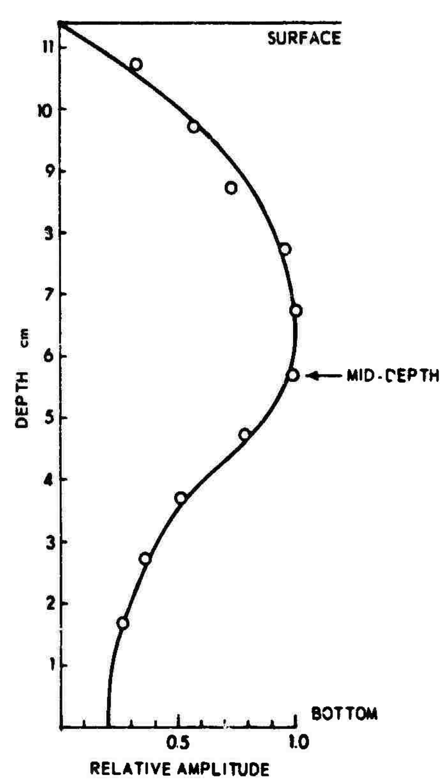

FIG. 13 DEPTH PROFILE FOR PROJECTOR TILTED 1° DOWN AT A RANGE OF 13 5 m

THE INFLUENCE OF OCEANOGRAPHIC PARAMETERS ON THE RANGE DEPENDENCY OF UNDERWATER REVERBERATION AND TARGET ECHO INTENSITY

by

Hans J. Arens
Erprobungsstelle 71 der Bundeswehr
Eckernfoerde, Germany

INTRODUCTION

A series of experiments was suggested by E 71 to clarify the influence of oceanographic parameters on target echo intensity- and reverberation decay. The purpose of these experiments is to determine the limitation of target detection of sonars, which can either be reverberation or background noise, under a variety of different oceanographic and topographic conditions. The results presented, especially all the target detection ranges, are valid for a recognition differential of 0 dB which indicates a sonar without an optimized receiver. The available literature related to the range-dependent decay of reverberation and target-echo intensity was a paper by R.P. Chapman on "Reverberation in shallow water" [Ref. 1] and the NATO Standardization Agreement (STANAG) No. 4118 [Ref. 2]. A prediction model for the reverberation decay is included in Chapman's report but there is no correlation to target-echo-intensity decays presented. STANAG 4118 shows in its appendix a rough graph of parallel decay of target- and reverberation levels. This, as will be proved, cannot be a representative model for more than simple oceanographic conditions.

Experimental results discussed in this paper were gathered in the Baltic Sea, east of the Island of Bornholm, in August 1973. The validity of the model will then be proved by a set of data measured under simpler conditions in the North Sea, 30 km west of Heligoland Island in January 1974.

1. EXPERIMENTAL

The Baltic Sea experiment used a sonar type M4 by Friedr. Krupp Atlas (FKAE), installed on a vessel of the E 71 laboratory. It is a searchlight sonar operating at 8.2 kHz carrier frequency with 50 ms pulses continuous wave (cw). The target for the experiment was a double triplane, consisting of two 1 m^2 triplanes of synthetic material, stiff connected and horizontally twisted by an angle of 22.5° against each other. The target strength of this setup is almost independent of angle of incidence; its absolute value was calculated at 8.2 kHz and results in +9 dB. Fluctuations of the target strength depend on the directional changes in value and are less than or equal to 3 dB, as shown in Fig. 1. The depth of the

target was chosen according to the vertical sound-velocity profile in the area of the experiment. The sound-velocity profile was found to be independent of time during the first part of the experiment, and independent of position within a certain area. A sample is shown in Fig. 2. It indicates a weak surface channel limited by the almost flat surface and a layer with an extreme sound-velocity gradient of 36 m/s within 7 m in about 25 m depth. Since the sonar transducer could not be extended further than 5 m below the surface, the surface channel should be used as a propagation channel and the target was placed 15 m deep. The target position was determined after a survey of the bottom homogeneity in the area, using a sub-bottom profiler. The exact target position was 55°16.5'N; 15°51'E, as indicated in Fig. 3. The water depth in the area was 94 m. The ship made repeated runs towards the target, closing range, starting out at a range of 4 km; it transmitted pulses at a source level of 113 dB re 1 μbar in 1 m. The horizontal-beam half-angle of the directivity pattern was 15°. For data-reduction purposes the receiving signal path of the sonar was tapped off following the uncontrolled preammplifier. It was amplified and displayed on a level recorder as well as tape recorded for off-line data analysis.

2. DATA ANALYSIS

The data analysis procedure for the received signal after pulse transmission included the following steps: The decaying reverberation- and the background noise levels were averaged on a ping-by-ping basis, see Fig. 4. The correct method to do this is convertion of levels to absolute intensities, calculation of the arithmetic mean and reconversion. This procedure performed on 2800 pings of the whole experiment is of course extremely time consuming. We therefore calculated the bias error introduced through averaging levels. As long as the peak-to-peak fluctuations stay below 10 dB, the error by averaging levels stays less than 3 dB. The arithmetic mean estimated in this way is in general too small.

The absolute reverberation-intensity levels for certain distances were averaged over a complete run to give representative mean reverberation levels. The standard deviation σ was calculated and both the mean and the confidence interval with $\pm 3\sigma$ were plotted in a logarithmic scale of distance r. The graph was then completed by adding the target-echo intensities for the whole run. Superposition of all runs under equal oceanographic conditions enlarges the statistical security of the results concerning target echoes. In general, for the range-dependent intensity levels of reverberation and target echoes, the same sound propagation model must be assumed. This model is represented in sonar equations through the propagation function $2H(r)$, as stated in Urick's "Principles of underwater sound for engineers" [Ref. 3]. It basically consists of two terms, one part concerning spreading, which can be expressed by some exponential function of range in the form of r^{-x}. A second part takes care of the frequency-dependent sound absorption in sea water as a function of distance in the form of ar, where "a" is given as a constant for one frequency in dB/m. As one corrects the values of the reverberation and target-echo-intensity levels by the sound absorption in sea water

and plots them in a logarithmic scale of distance, both the reverberation decay and the limiting curve to the target echoes will appear as straight lines. This will be presented as a result a little later. From the decay itself the exponent of distance in the spreading term of $2\,H(r)$ can be calculated and leads to a propagation model for the experimental case. The exponent and the value of the maximum reverberation range will then be used as an explanation for the source of reverberation.

There remains one point for discussion. What is an appropriate number of pings to average and lead to reliable results of mean reverberation levels. The criterion for it is the central limit theorem of statistics. The distribution of a stochastic process that is governed by more than one statistic parameter with different distribution functions tends to approach a Gaussian distribution if the number of events observed becomes high enough. A suitable test for it is that of plotting on probability paper the cumulative relative frequency distribution as percentages of the mean values for a certain reverberation range of all pings of one run. The outcome should be a straight line, which signifies a normal distribution. 170 pings was found as the necessary number for a suitable statistic evaluation. A presentation of this test for a reverberation range of 1000 m is shown in Fig. 5, valid for the first run on 12 August 1973. This test was systematically performed on all runs and reverberation ranges of 250, 500, 750, 1000 and 1250 m.

3. RESULTS

A superposition of data of three runs under equal oceanographic conditions on 12 August 1973 is shown in Fig. 6. The absolute values of target-echo intensity and reverberation are presented in a logarithmic scale of range. They are corrected by the frequency-dependent absorption to enable first graphic determination of the spreading part of a propagation function. This will result from the calculation of a limiting line to the target echoes. A second line represents the average reverberation level, which decays with range and finally crosses the constant background-noise level at the maximum reverberation range. The exponent of the range-dependent decay of the mean reverberation level was calculated; it comes out as -5.2.

The decay of the limiting line to the target echoes is proportional to $r^{-3.5}$, indicating cylindrical spreading with lossy boundaries. The losses are mainly caused at the lower boundary by channel leakage. Penetrating energy into and through the high gradient layer is refracted towards the bottom. The reflection-loss coefficient of the soft bottom in the area can be assumed to be greater than 0.5. Therefore bottom-reflected sound energy has reduced influence on the target-echo intensity.

The maximum reverberation range of 1500 m in connection with the ray diagram shown in Fig. 7 indicates that the bottom is the major source of reverberation. The decay exponent agrees very well with the model by Chapman, which states that for bottom reverberation in the presence of a high reflection-loss coefficient, layers with strong gradients

and irregularities of the sound velocity in the water column can approach values even in excess of -6. Five days later, on 17 August 1973, the surface was more and more heated and the weak subsurface channel disappeared. This is shown in the vertical sound-velocity profile of Fig. 3. The ray diagram, Fig. 9, calculated for this case indicates that again the bottom is the main source of reverberation. The exponent of the decay did not vary but the maximum reverberation range decreased to 1000 m. The target could no longer be detected. The correction of target-echo levels by the frequency-dependent absorption results, as pointed out before, in straight lines. This procedure allowes two important values to be calculated. Extrapolation from the level of the limiting line to the target echoes at 1000 m over three decades leads to the equivalent echo level at 1 m. If the source level is subtracted, this results in the target strength. The target strength, however, is known, and a comparison of this approximation and the calculated value gives a measure for the reliability of the statistic evaluation.

A second, even more important calculation, concerns the linear decay of the average reverberation levels. Extrapolation of the mean level at 1000 m over three decades, deduction of the factor 10 lg Area for bottom reverberation, which depends only on known sonar parameters, and subtraction of the source level according to the equation

$$R_L = S_L - 2\,H(r) + S_S + 10\ \lg A$$

results in the value of scattering strength for surface or bottom reverberation. This value depends only on oceanographic parameters like bottom structure, surface roughness and sound-velocity profile. Knowing the target strength for surface or bottom reverberation for a variety of different conditions, and knowing the range-dependent decay of the mean level, the possible maximum target-detection range for a given recognition differential and target strength can be predicted. E 71 therefore proposes to continue this kind of experiments under a variety of different conditions. One additional experiment has already been performed and the results gained up to now are presented, as a conclusion, in Fig. 10.

DISCUSSION

Answering a question by Dr Wasiljeff about the 400 dB dynamic range Mr Arens explained that tests made with the sonar in the passive mode prior to the runs had shown that no better ambient noise level could be found for the speed used and the noise was believed to be due to water flow around the sonar.

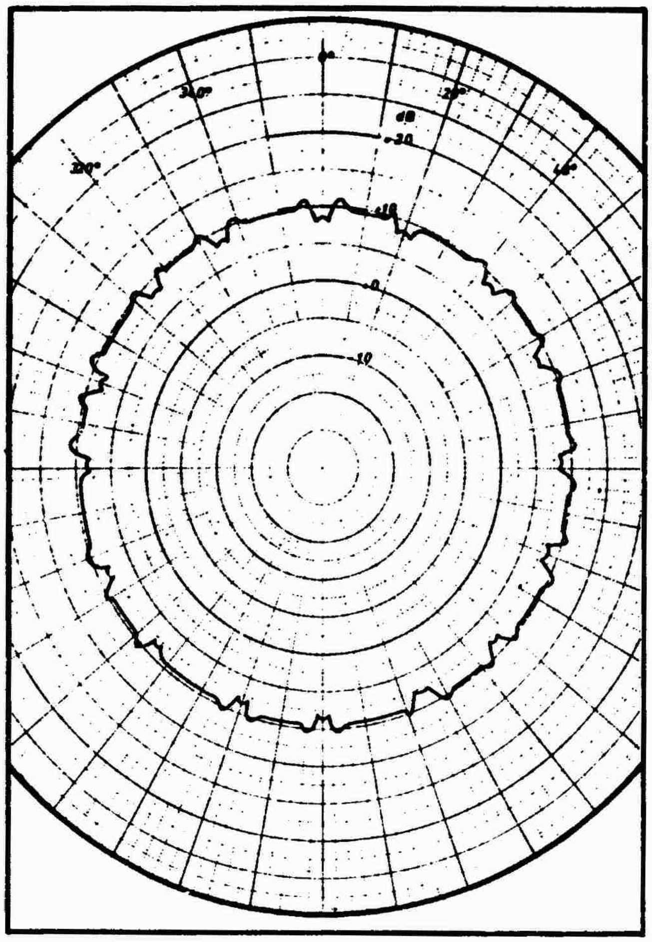

FIG. 1 TARGET STRENGTH OF DOUBLE TRIPLANE CALCULATED FOR 8.2 kHz AS A FUNCTION OF ANGLE OF INCIDENCE

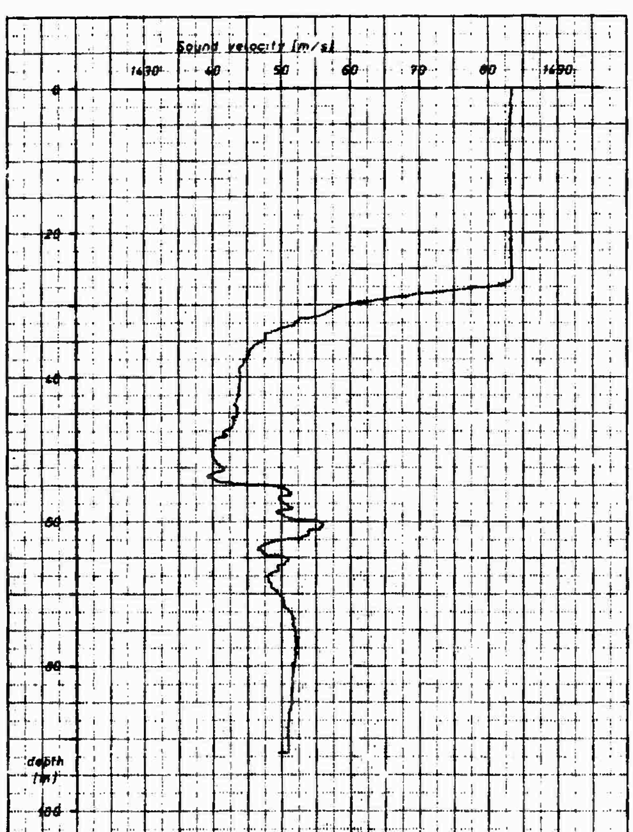

FIG. 2 SOUND VELOCITY PROFILE MEASURED ON 12 AUGUST 1973 AT THE POSITION OF THE TRIPLANE

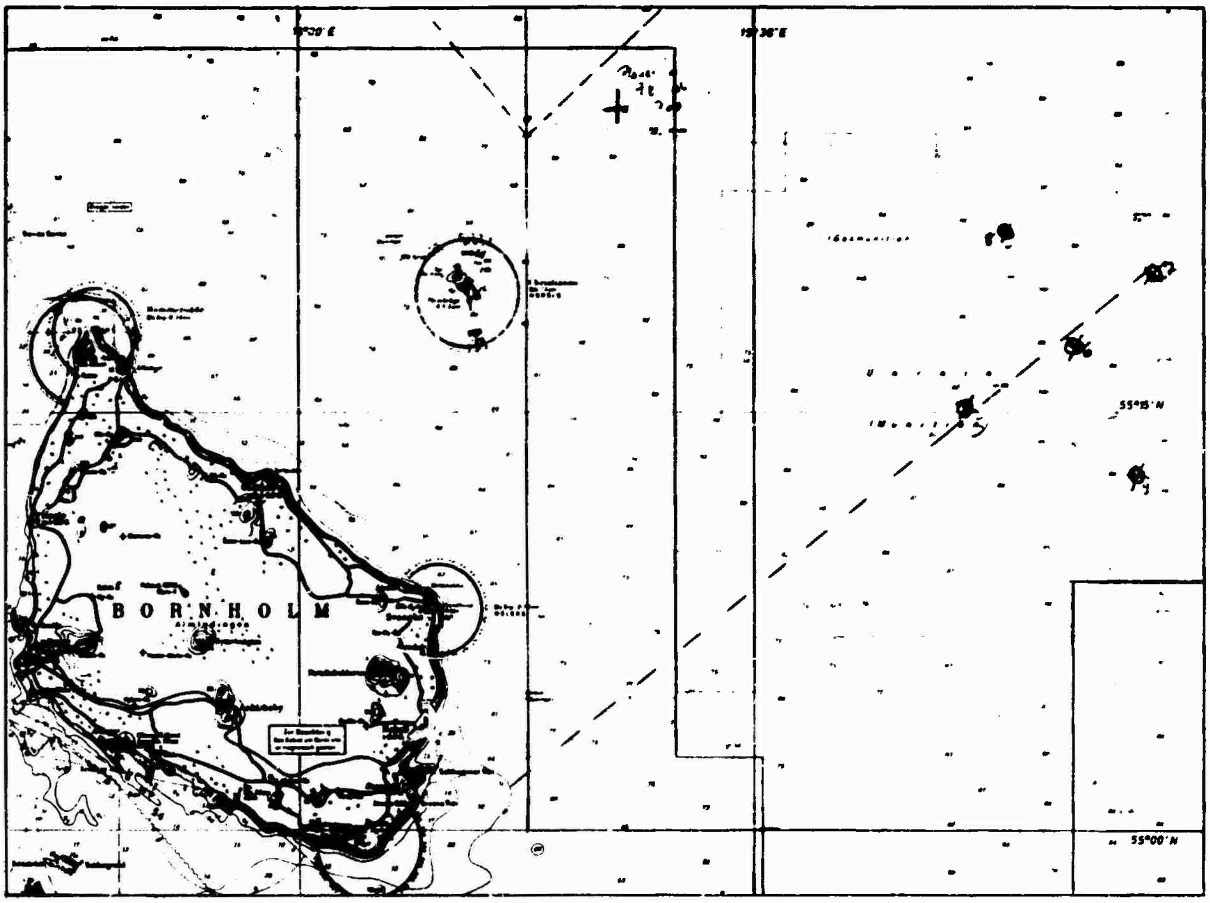

FIG. 3 AREA FOR EXPERIMENT

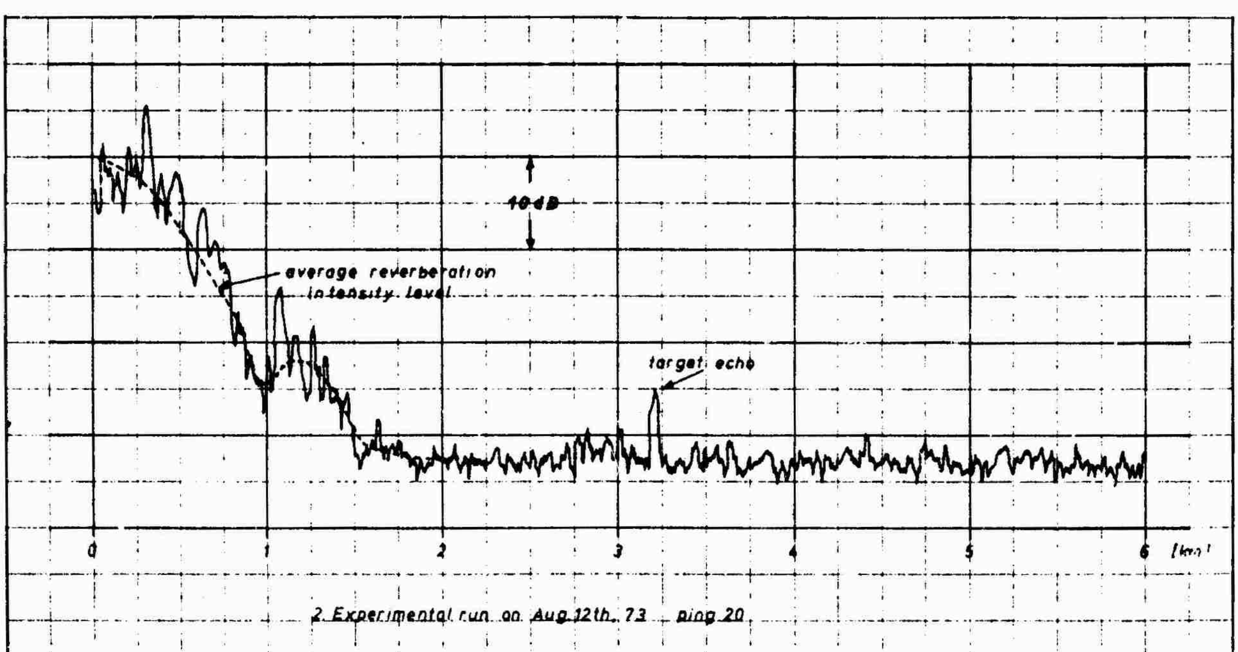

FIG. 4 SAMPLE OF UNCONTROLLED RECEIVED SIGNAL

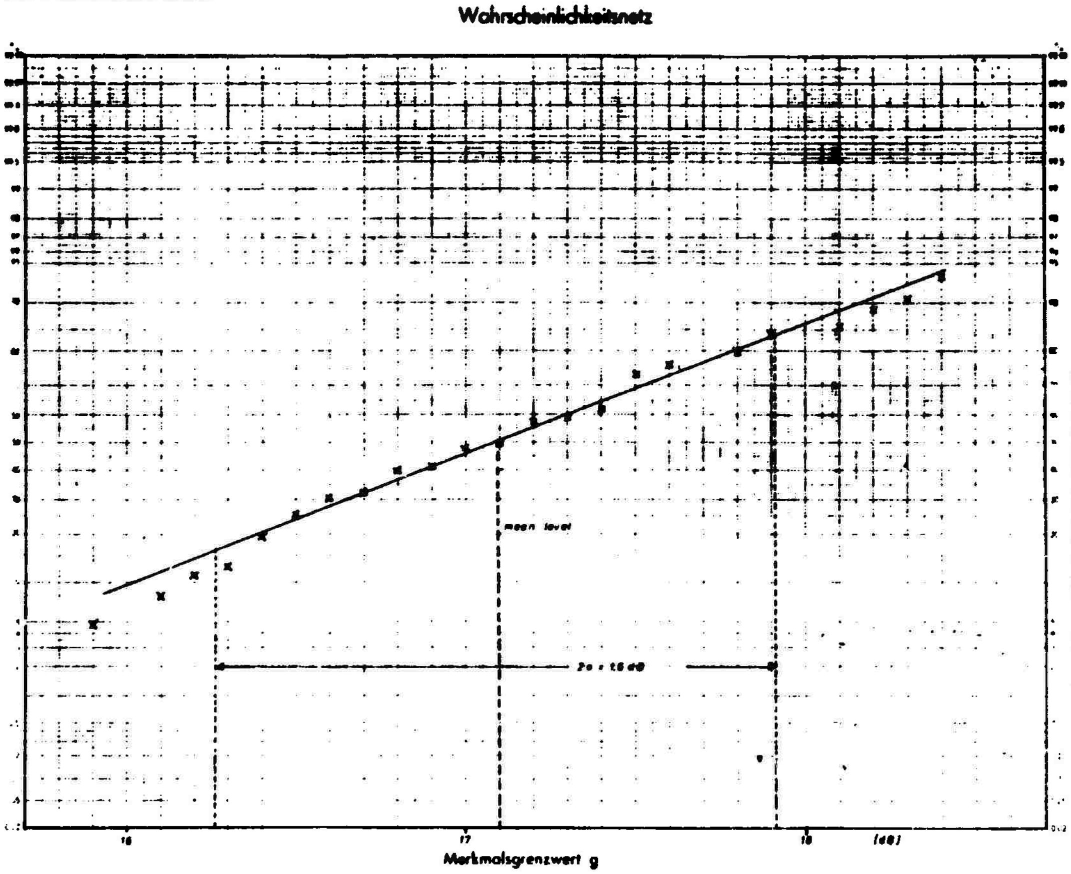

FIG. 5 SAMPLE OF CUMULATIVE RELATIVE FREQUENCY DISTRIBUTION (Reverberation range 1000 m, 1st Run 12 August 1973)

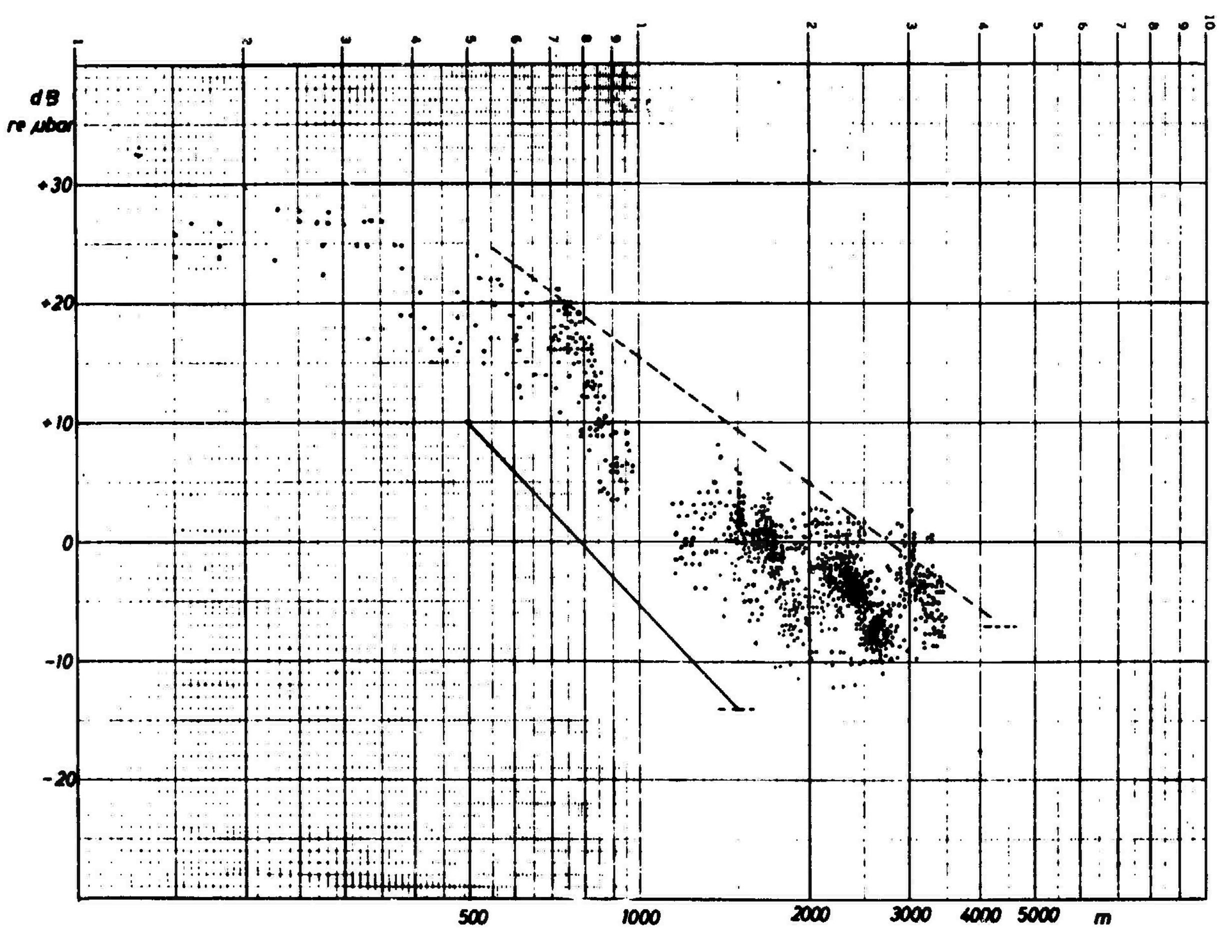

FIG. 6 SUPERPOSITION OF THREE RUNS ON 12 AUGUST 1973

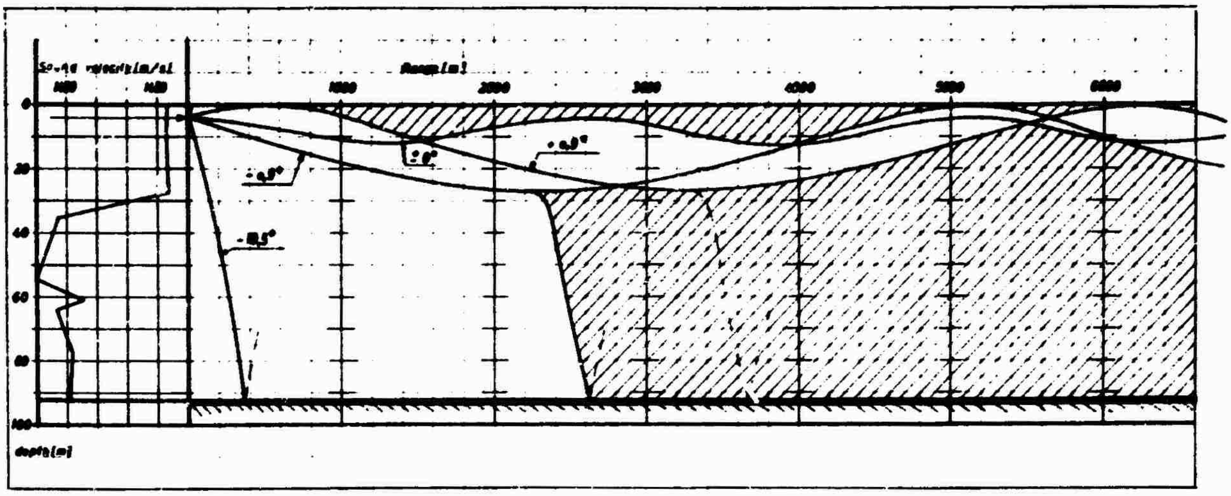

FIG. 7 RAY DIAGRAM CALCULATED FOR EXPERIMENTS ON 12 AUGUST 1973

FIG. 8 SOUND VELOCITY PROFILE MEASURED ON 17 AUGUST 1973

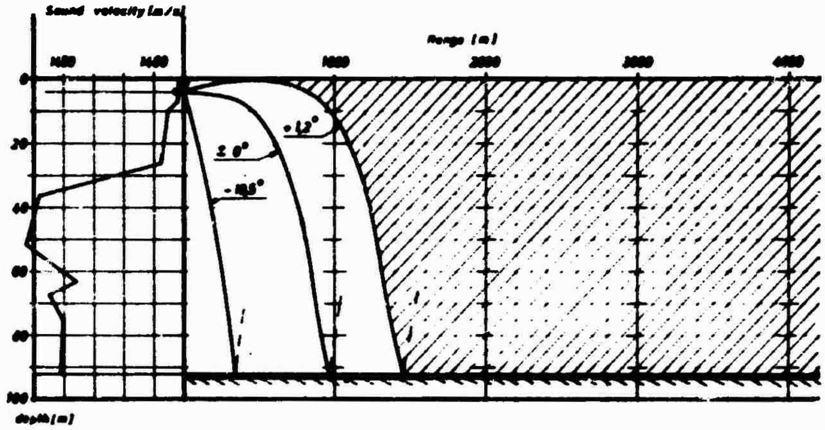

FIG. 9 RAY DIAGRAM CALCULATED FOR EXPERIMENTS ON 17 AUGUST 1973

Description of the experiment	date of experiment	sound velocity profile	main source of reverberation	bottom description	predicted reflection loss coefficient of bottom	sea state	description of target and source geometry	scatter strength of reverb [dB]	target	decay exponent of reverb	decay exponent of limiting line to echoes	optimum range for target detection [km]	target range with 50% probability of detection	optimum reverberation range [km]
Baltic Sea summer conditions	Aug 12th, 73	negative gradient weak surface channel	bottom	soft, mud	> 0.5	0 - 1	source depth 5m target depth 15m		double triplane	5.2	3.5	4.5	38km	1.5
Baltic Sea summer conditions	Aug 17th, 73	negative gradient no channel	bottom	soft, mud	> 0.5	0	source depth 5m target depth 15m		double triplane	5.2				10
North Sea winter conditions	Jan 17/18th,74	positive gradient almost isovelocity	surface	hard, sand	< 0.5	4	source depth 5m target depth 20m	-20	double triplane	3.2	3.4	6.3	35km	3.7
North Sea winter conditions	Jan 21st 74	positive gradient almost isovelocity	surface	hard, sand	< 0.5	3	source depth 5m target depth 20m	-53	double triplane	2.5	3.0	6.5	51km	4.1

FIG. 10 CONCLUDING RESULTS OF BALTIC SEA AND NORTH SEA EXPERIMENTS

TIME RESPONSE OF EXPLOSIVE SIGNALS IN SHALLOW WATER

by

Harvey S. Piper
Applied Research Laboratory
The Pennsylvania State University, Pennsylvania, USA

ABSTRACT

For a real-valued transmitted signal which can be represented by

$$f(t) = \frac{1}{2\pi} \int_{-\infty}^{\infty} F(\omega)\, e^{i\omega t}\, d\omega = \frac{1}{2\pi} \int_{-\infty}^{\infty} F^*(\omega)\, e^{-i\omega t}\, d\omega ,$$

the received pressure time signature is computed from

$$R(t) = \frac{1}{2\pi} \int_{-\infty}^{\infty} F^*(\omega)\, p(r_r, r_z, \omega)\, e^{-i\omega t}\, d\omega ,$$

where,

$$p(r_r, z_r, \omega)\, e^{-i\omega t}$$

is the pressure at $r = r_r$, $z = z_r$ for a harmonic source at $r = 0$, $z = z_0$. Since $R(t)$ is the Fourier transform of $F^*(\omega)\, p(r_r, z_r, \omega)$, the procedure used is to approximate $R(t)$ by a discrete Fourier transform and compute the received pressure time signature using the FFT algorithm. A normal mode program is used as a subroutine to compute $p(r_r, z_r, \omega)$.

Comparisons are made between the computed time signatures and some experimental time signatures obtained in shallow water.

INTRODUCTION

An analytical model will be described which can be used to calculate the received pressure time waveform due to an arbitrary source function. This model has been developed in order to study long-range propagation of broadband acoustic signals in shallow water. The procedure used is to represent the source function by a finite discrete Fourier transform, and calculate the received pressure due to each component in the transform by using a normal mode program. The sum of the responses due to each component is the Fourier transform of the received pressure and the Fast Fourier Transform (FFT) algorithm is then used to obtain the received pressure time signature.

This model has been used to calculate received signals for comparison with experimentally-obtained results in a shallow-water environment. In November and December 1973, the Applied Research Laboratory participated in a field experiment conducted by the Naval Research Laboratory in an area approximately 40 miles east of Daytona Beach, Florida. In one of the tests, explosive sources were used at ranges up to 100 miles along a path with essentially constant water depth of about 43 m. The data from this test has been analysed by using various one-third octave filters, and envelope-detecting the filter outputs. The computer program described here has been used to obtain the received signals and the processing performed on the field data has been simulated on the computer. The calculated results show good agreement with the measured results.

1. PROCEDURE FOR OBTAINING TIME WAVEFORM

We will assume an ideal two-fluid model of the shallow-water environment. A constant-depth layer of water is bounded above by a pressure-release surface, and below by a fluid half-space with constant density and sound velocity. The density of the water layer is assumed constant, and its velocity is allowed to vary with depth, but not range. We will use a cylindrical coordinate system with the surface at $z=0$ and the bottom interface at $z=H$. For a harmonic point source with unit source strength located at $r=0$, $z=z_0$, the pressure at long ranges can be found in terms of normal modes in the form [see Ref. 1],

$$p(r,\zeta,\omega)e^{-i\omega t} = \frac{\rho_1}{H}\left(\frac{1}{8\pi r}\right)^{1/2}\sum_{n=1}^{M}\frac{u_n(\zeta_0)u_n(\zeta)}{k_n^{1/2}}\, e^{i(k_n r-\frac{\pi}{4})}\, e^{-\delta_n r}\, e^{-i\omega t} \qquad \text{[Eq. 1]}$$

where $\zeta=\frac{z}{H}$, ρ_1 is the density in the water layer,
M is the number of discrete modes,
$u_n(\zeta)$ is the mode amplitude,
k_n is the wavenumber and
δ_n is a mode attenuation coefficient.

We now consider a real-valued transmitted signal, $f(t)$, with a representation of the form

$$\begin{aligned} f(t) &= \frac{1}{2\pi}\int_{-\infty}^{\infty} F(\omega)\, e^{i\omega t}\, d\omega \\ &= \frac{1}{2\pi}\int_{-\infty}^{\infty} F(-\omega)\, e^{-i\omega t}\, d\omega \\ &= \frac{1}{2\pi}\int_{-\infty}^{\infty} F^*(\omega)\, e^{-i\omega t}\, d\omega\,, \end{aligned} \qquad \text{[Eq. 2]}$$

where

$$F(\omega) = \int_{-\infty}^{\infty} f(t)\, e^{-i\omega t}\, d\omega \,. \qquad \text{[Eq. 3]}$$

Since the response of the channel described above to $e^{-i\omega t}$ is given by $p(r,\zeta,\omega)\, e^{-i\omega t}$, the response to $f(t)$ is given by

$$R(t) = \frac{1}{2\pi} \int_{-\infty}^{\infty} F^{*}(\omega)\, p(r,\zeta,\omega)\, e^{-i\omega t}\, d\omega \,. \qquad \text{[Eq. 4]}$$

We can interpret $R(t)$ as the Fourier transform of $\frac{1}{2\pi} F^{*}(\omega)\, p(r,\zeta,\omega)$. The procedure is to approximate this transform by a discrete finite Fourier transform and use the FFT algorithm to obtain sample values of $R(t)$.

In computing $R(t)$, sample values of $F(\omega)$ are obtained from Eq. 3 for the source function of interest, while a normal mode program [Ref. 2] is used to find $p(r,\zeta,\omega)$. A 4096 point FFT was used, yielding 4096 sample values of $R(t)$, and requiring 4096 sample values of $\frac{1}{2\pi} F^{*}(\omega)\, p(r,\zeta,\omega)$. Note that since $R(t)$ is real valued,

$$F^{*}(-\omega)\, p(r,\zeta,-\omega) = [F^{*}(\omega)\, p(r,\zeta,\omega)]^{*},$$

and consequently we only need to obtain $p(r,\zeta,\omega)$ for positive frequencies. In addition, since $p(r,\zeta,\omega)$ is a relatively slowly varying function of ω, it is not necessary to calculate response functions at each of the sample frequencies. For the results presented here, the source was an explosive charge, which was represented by a shock wave plus two bubble pulses. The parameters for the explosive signal were obtained from Weston [Ref. 3]. The data from the field experiment was limited to 60 Hz to 1300 Hz and $p(r,\zeta,\omega)$ was obtained at 20 Hz intervals and the intermediate points obtained by interpolation. Thus, the 4096 sample inputs to the FFT subroutine were obtained by running the normal mode program at 63 different frequencies.

The results to be presented here were calculated using the IBM system 370/168 computer at The Pennsylvania State University Computation Center.

2. FIELD EXPERIMENT

During November and December 1973, ARL participated in a field program conducted by NRL in a shallow-water area about 40 miles east of Daytona Beach, Florida. The particular experiment to be considered here was conducted on November 29 and consisted of long range transmission of explosive signals. The sources were 1.8 lb charges of TNT dropped by an aircraft at 5 mile intervals at ranges of 10 to 100 n.mi, along a northerly leg from the receiver. The charges were detonated at a depth of 18.3 m. The water depth varied along this path between 33.5 and 70.1 m. The water depth at the receiver was 42.7 m. Figure 1 shows the bottom contour along the path and the location of the sources. The sound velocity profile measured near the receiver is shown in Fig. 2.

The receiving array consisted of a vertical string of 12 hydrophones suspended from a buoy, spaced about 3 m apart. The received signals from each hydrophone were transmitted from the buoy by radio to the support ship located about 10 miles from the buoy, and were recorded on magnetic tape. The telemetry system bandwidth was about 60 Hz to 1300 Hz, and thus this is the bandwidth used for the computer calculations to be presented. Figure 3 illustrates the experimental procedure.

3. LABORATORY PROCESSING OF RECORDED DATA

The data that was collected from the field experiment was processed in the laboratory by passing the signals through various one-third octave band filters, full-wave rectifying the filtered data and logarithmically amplifying to reduce the dynamic range. The signals were then averaged over 20 ms. Figures 4 and 5 show the envelope detected signals in one-third octave bands centred at 160, 400 and 800 Hz, as well as the full band from 60 Hz to 1300 Hz, at ranges of 10 and 40 n.mi. These signals were recorded on the hydrophone at a depth of about 33.5 m. In Fig. 6 we see the measured results at 60 n.mi for the hydrophone at a depth of about 15.2 m, as well as the hydrophone at 33.5 m. In Fig. 6, the results for the one-third octave band filter centred on 160 Hz is not shown since the signal is not distinguishable from the noise.

The detected envelopes in the one-third octave bands shown in Figs. 4, 5 and 6 clearly show the shock-wave arrival and the first two bubble-pulse arrivals. In addition, these figures illustrate the dispersion in the received signal. For example, at 40 n.mi, the shock-wave peak in the one-third octave band centred at 160 Hz arrives about 150 ms later than the peak of the detected signal in the band centred at 800 Hz.

4. COMPUTER MODEL

The computer model described here was used to simulate the field experiment described above. The sound velocity profile measured near the buoy, and shown in Fig. 2, was used in the normal mode program. The model used for the source function was computed using expressions given by Weston [Ref. 3], and consisted of a shock wave plus two bubble pulses. The water depth was assumed to be a constant 42.7 m. For the fluid bottom half-space, a density of 2.1 and a sound velocity of 1720 m/s were used. Several different values for the volume attenuation of the fluid half-space were used and will be discussed later.

The first tests run consisted of obtaining the pressure time waveform at various ranges. These results were compared with the recorded field data, and good agreement was obtained.

The program was then extended to model the laboratory processing of the field data. The one-third octave filters used in the laboratory were a 6-pole Butterworth design. The computed samples of the Fourier transform of the received signal were multiplied by the appropriate filter transfer function and then the FFT was computed. The logarithm of the absolute value of the sampled time function was calculated and the result was averaged over 20 ms.

In Fig. 7, we see the calculated envelopes for the broadband signal at 40 n.mi using four different values for the volume attenuation in the bottom; namely 0.2 dB/m/(kHz)$^{0.7}$, 0.25 dB/m/kHz, 0.3 dB/m/(kHz)$^{1.3}$ and 0.4 dB/m/(kHz)$^{1.7}$. These values were chosen to give equal attenuation at 500 Hz. This figure clearly shows the effect of the frequency dependence of the bottom attenuation on the received envelope pulse shape. In comparing this figure with the measured broadband envelope shown in Fig. 5, we see that the best agreement is obtained using a volume attenuation of 0.25 dB/m/kHz for the bottom. Consequently, this value of bottom attenuation was used for the remaining calculated results to be shown.

In Figs. 8 and 9 the calculated results are shown at ranges of 10 and 40 n.mi for the various one-third octave bands, as well as the broadband case. If we compare the calculated results shown in Figs. 8 and 9 with the measured results shown in Figs. 4 and 5 we see that good agreement is obtained, and that the major features of the measured signals are predicted correctly by the calculated results. Note in particular that the time of arrival of the detected shock wave peak and first bubble peak in the different frequency bands agrees extremely well with the observed results. Note also that the calculated results consistently show less contribution from the second bubble pulse than was actually observed, indicating that better agreement with the measured results could be obtained by modifying the model used to represent the signature of the explosion.

In Fig. 10, we show the received envelopes at 60 n.mi for receiver depths of 15.2 and 33.5 m. This figure should be compared with Fig. 6. Again, good agreement is obtained, and we see practically no effect due to receiver depth on the received signal. The approximate measured ambient noise level is indicated on Figs. 8, 9 and 10.

It should be noted that in performing these calculations, no attempt was made to improve the agreement with the measured results by varying any input parameter, other than the frequency dependence of the bottom attenuation. As noted, the agreement could almost certainly be improved by changing the explosive source time signature — in particular by increasing the level of the second bubble pulse and possibly by adding additional bubble pulses. The agreement might also be improved by changing other parameters such as the sound velocity in the bottom, water depth or sound velocity profile in the water layer. The particular values used for the various input parameters in the calculations presented here were chosen since they represent the best estimates of these parameters that existed during the field experiment.

Work is continuing on developing the model described here, and the effects of varying various input parameters will be investigated. In addition, the model will be extended to include the signal-plus-

noise case, as well as the signal-only case considered here. That is, computer-generated noise samples will be added to the signal samples generated by the computer.

SUMMARY

A computer program has been described which calculates the time response due to an arbitrary broadband source. Results have been shown for an explosive source which show good agreement with measured results.

This program should be useful not only for studying the propagation of broadband signals, but also in investigating signal processing techniques for broadband receivers. For example, the envelope detecting of one-third octave bands modelled here could be replaced by some other processing to model a receiver front end, and its characteristics evaluated.

ACKNOWLEDGEMENTS

This work was done under contract with the US Naval Ordnance Systems Command. The cooperation of the US Naval Research Laboratory, both for providing their normal mode program and allowing ARL to participate in their field experiment, is greatly appreciated. The excellent programming provided by Walter Caswell made the results presented here possible.

REFERENCES

1. I. Tolstoy and C.S. Clay, Ocean Acoustics [McGraw-Hill, New York, 1966], p.84.

2. A.V. Newman and F. Ingenito, "A Normal Mode Computer Program for Calculating Sound Propagation in Shallow Water with an Arbitrary Velocity Profile", Naval Research Laboratory Memo, Rep. 2381 [1972].

3. D.E. Weston, "Underwater Explosions as Acoustic Sources", Proc. of the Physical Soc., London, 76 (pt.2), 1960, p.233.

DISCUSSION

Dr Weston commented that simple calculations in recent papers by Preston Smith and by Weston and Stevens suggest there is a very close link between the dispersion and the geometrical plus boundary-loss components of transmission loss, showing that it is basically the magnitude rather than the nature of the bottom loss that matter and it therefore might be necessary to look elsewhere for an explanation of the discrepancies. Dr Piper said that he had not yet taken shear waves into account but was interested in trying it.

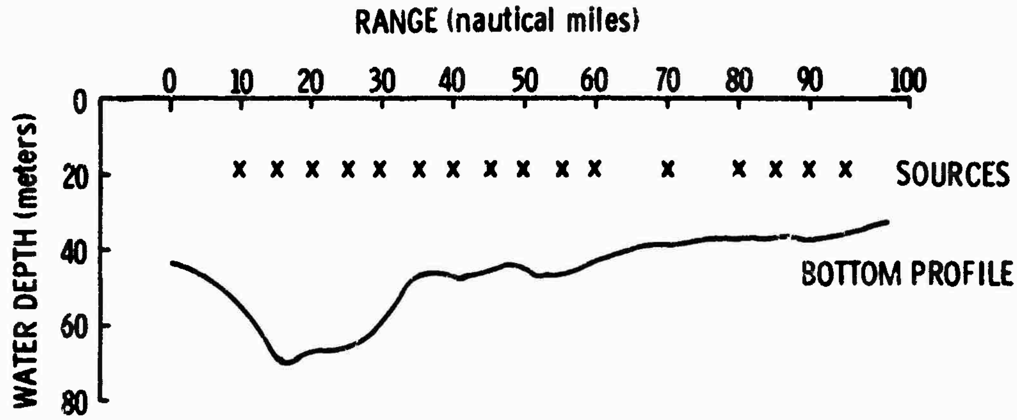

FIG. 1

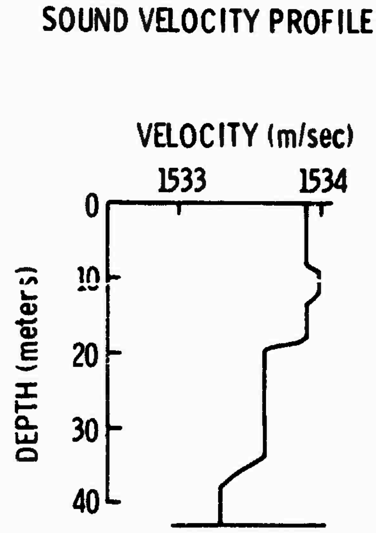

FIG. 2

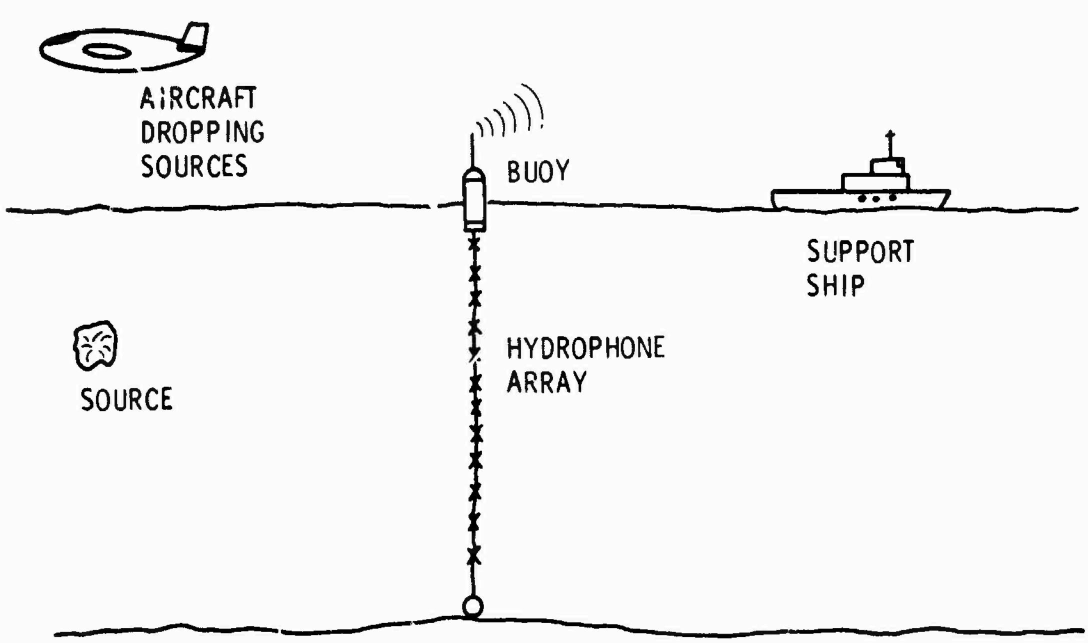

FIG. 3

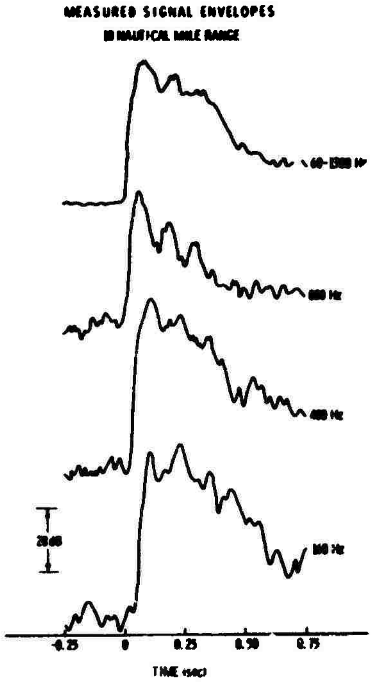

FIG. 4

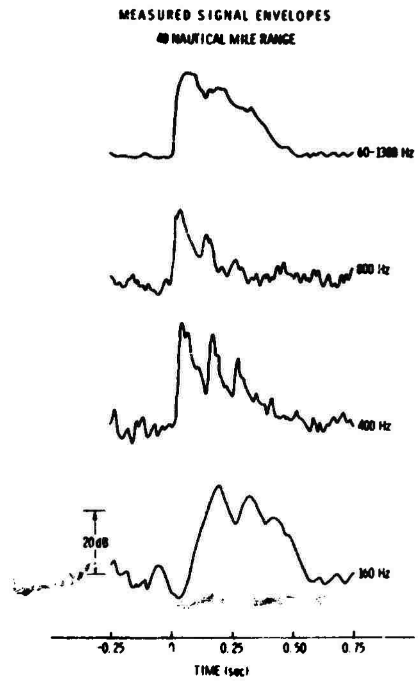

FIG. 5

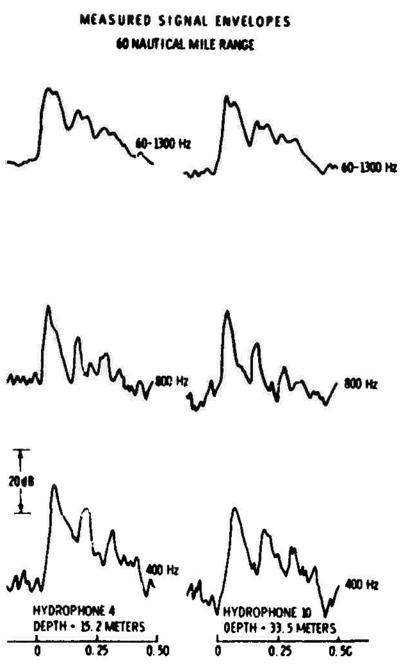

FIG. 6

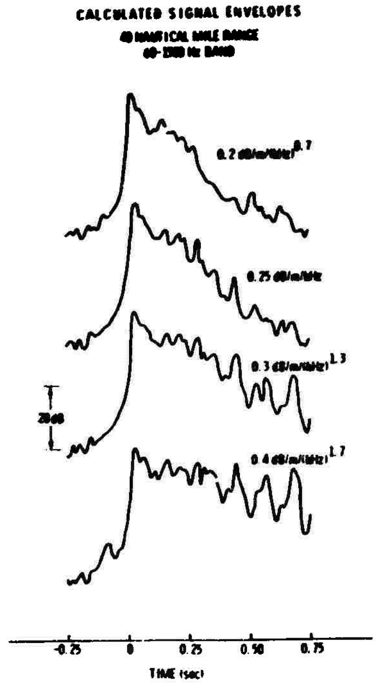

FIG. 7

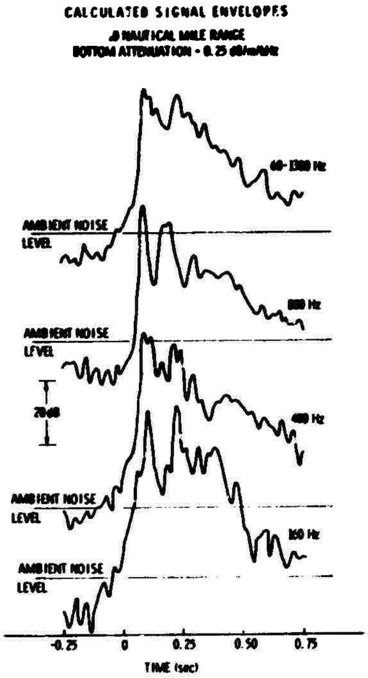

FIG. 8

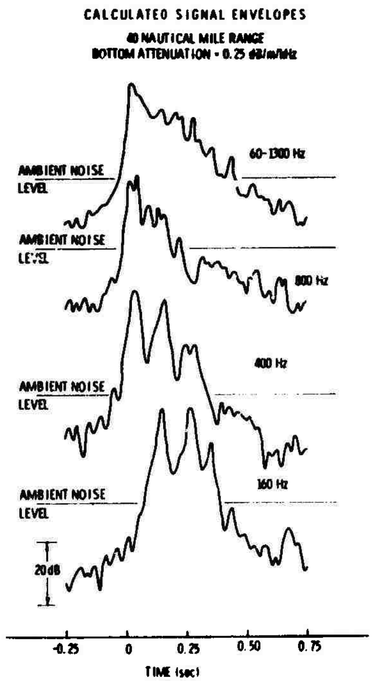

FIG. 9

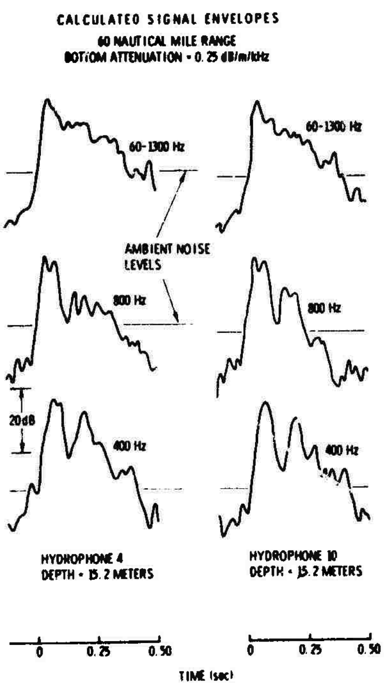

FIG. 10

ENHANCEMENT TECHNIQUES IN TRANSMITTING AND RECEIVING UNDERWATER ACOUSTIC MODES

by

L.A. King
New London Laboratory, New London, Conn., USA

ABSTRACT

Modes or eigenfunction solutions to the scalar wave equation have been useful in understanding acoustic interference phenomena observed in shallow water. The premise that one can enhance modes compatible with propagation conditions to suit ones purpose is the basis for current investigation in shallow-water acoustic propagation at NUSC. Mode Enhancement Techniques (METS) in transmitting and receiving acoustic signals are described. Also described is the use of a vertical array of transducers as a novel experimental tool in developing METS. When receiving, the individual signals can be weighted and summed to reject unwanted modes. When transmitting, the signal amplitude and phase distribution over the array can be varied to manipulate end enhance particular modes.

This paper is organized into essentially three parts. The first presents pertinent results of several propagation experiments in the Baltic Sea and the Gulf of Aden. The results reveal modal properties which when controllable can be exploited in active or passive sonar situations. The second presents the results of CW experiments in Block Island Sound where a multi-element array was used in the further study of controlling these modal properties. Various array configurations were tested for their effectiveness in producing modes. In several cases, compensation for propagation conditions was achieved. The third part compares with measurements the results of an approach to predict the modes generated by the multi-element array.

The work referred to above is part of a shallow water acoustics program at the Naval Underwater Systems Center (NUSC) concerned with the influence of shallow water on sound propagation. The concept to utilize modal properties to improve signal-to-background levels in various segments of the water column has been termed Mode Enhancement Techniques (METS). A parallel effort has been to expand a propagation loss model based on normal mode theory — itself developed in the program — for application to multi-element transmitting and receiving situations. Once validated, the model can be used not only to predict the sound fields, but also to serve as an aid in generating desired sound fields. However, although the accuracy of METS increases with the accuracy of the model incorporated, it is not solely dependent on

such accuracy to be useful. Knowing the properties of sound propagation in shallow water — even qualitatively — can be of tactical value.

Before presenting the propagation data, some further explanation is given relating the modal properties of interest to the concept of METS. A key assumption underlying METS is that an acoustic pattern is formed from interfering wave trains whose angle of propagation can be related to modes. The pattern then can be manipulated by changing either the direction of the wave trains or the frequency of the acoustic waves.

Figure 1 illustrates how directionality plays a role. Pictured on the left are two sets of wave trains; one propagating downward and the other upward. Chosen as a parameter is the angle, the downward train makes with the horizontal. The wave trains interfere to produce a pattern of destructive and constructive interference zones. The vertical separation between two interfering wave fronts, say producing nulls, defines λ_z, the vertical component of the wave length associated with the formed mode. In this manner an angle of direction can be associated with a mode. The right hand side of the figure shows the angle decreased resulting in an increase in the vertical separation between the null regions. The greater the separation, the lower order the mode. Then as one manipulates the angle of the interfering wave trains one manipulates the sound field. From the same illustration, one can also see that the grid pattern can be altered by changing the frequency of wave length of the wave train. For a fixed direction; the higher the frequency, the closer the grid points and the higher the order mode. From another aspect, for a fixed vertical pattern, the higher the frequency, the shallower would be the wave trains.

Propagation experiments in the Baltic Sea and the Gulf of Aden have revealed such modal properties. Figure 2 shows the geographical area of the Western Baltic region. At the southwest end of the Baltic is the town of Eckernförde, West Germany where located is a test facility of the MOD designated as E-71. NUSC and E-71 have participated in a joint program to study sound propagation in the Western Baltic. The sites for the experimental work are indicated as stations 1 and 2, 1 being in the Kiel Bay area where waters are approximately 25 m deep and 2 being in the Arcona Basin west of the Danish Island of Bornholm where waters are approximately 50 m deep.

A typical summer sound speed profile for the Bornholm area is shown in Fig. 3. At mid-depth is a strong internal duct about 10 m in breadth, having a maximum contrast in sound speed of 20 m/s. The sound speed profile measured at the Kiel Bay site showed a similar but shallower internal duct.

Since these internal ducts should be the prime influencing features on the propagation of sound, the hydrophone and charge depths were selected to border and lie within these ducts. The influence of the duct on propagation and its sensitivity to frequency were revealed in the measurements.

Figure 4 shows the propagation loss with range at the 1/3-octave frequency of 200 Hz as measured at the three depths of 12, 20, and 40 m. The source depth for this event is 20 m placing the detonation within the duct. At 200 Hz the difference in received levels between the hydrophones outside the duct and the hydrophone within the duct is 4 to 5 dB.

Figure 5 shows that for the same source and receiver geometries, but for a frequency of 4000 Hz, some 6 to 10 dB difference in level occurs between the in-duct and out-of-duct hydrophone arrivals. The remainder of the data showed consistently that when the source was on axis, the spatial variation in level increased as the frequency increased. This suggests that at the higher frequencies, the chief contributors to the sound field are the lower order modes propagating in the form of shallow-going wave trains confined to the internal duct. The lower frequency energy travels in wave trains having a broader band of angles resulting in less level variation over the water column.

Figure 6 shows the propagation loss with range measured for the 1/3-octave centre frequency of 200 Hz when the source was off axis. The three curves correspond to the three receiving depths of 12, 20, and 40 m and the charges for these events were detonated at a depth of 10 m. The maximum difference in levels observed at the three depths is less than 5 dB. This suggests that the off-axis source excited higher order modes steeper going wave trains resulting in a more uniform energy pictture over the receiving aperture.

Figure 7 shows the loss curves for the same geometry but for the 1/3-octave centre frequency of 4000 Hz. The difference in levels over the 30 m receiving aperture now shows a variation from a few to 7 dB. The lower insonification of regions outside the duct suggests again that propagation at this higher frequency is favourable in the form of shallow-going wave trains.

Another area where stringent propagation conditions exist is near the Strait of Bab El Mandeb located between the Red Sea and the Gulf of Aden (see Fig. 8). The summer water at the mouth of the strait, in comparison to the 15°C summer waters of the Western Baltic, reaches a temperature of 30°C to 35°C and has about three to four times the salinity (36‰). Of the number of acoustic tracks made during the operation, of interest is track number four which starts from a point in the Gulf and ends at a point at the mouth of the Strait. A two ship operation, the receiving ship lay anchored at the mouth of the strait in 50 m of water. Suspended over her side were three hydrophones set at depths of 6, 18, and 49 m. The source ship, closing range, dropped 1.8 lb TNT charges set to detonate at a depth of 6 m.

On the right-hand side of Fig. 9 is a linear-segmented version of the measured sound speed profile. This profile features a surface duct 32 m in depth, disclosing that the charges were detonated within the duct. The signal arrival structure observed at all three depths had characteristically two distinct segments. The first segment was sharp and impulse-like. This was followed by a reverberant segment which one could audibly perceive as having lower frequency content than the impulses. The left side of the graph shows the peak received levels

of the impulses at the three hydrophone depths as a function of the ship's range at the time of detonation. The bathymetry along the acoustic track is also shown but not proportionately. The steepest slope occurs at the shallow end and has a value of 0.052 or an angle of approximately 3°. Clearly evident from the differences is the strong channelling by the surface duct of the high frequency acoustic energy. Better than 20 dB marks the difference in level received on the near-surface and near-bottom hydrophones.

The peak received levels of the reverberant portion of the signal are shown in Fig. 10. Although these peak levels varied, channelling was still evident in that they tended to be greatest on the near-surface hydrophone and least on the near-bottom hydrophone. The differences in level however, are about 10 dB — 1/2 the dB level of the impulse arrivals. This energy, having lower frequency content, was more readily distributed over the water column.

Thus similar modal properties are evident in both the Baltic Sea and the Gulf of Aden data. The low order modes of the higher frequency components consisted of wave trains propagating within cones of shallow angles and were confined to the ducts. The low order modes at the lower frequencies were formed from wave trains with steeper angles resulting in a measurable distribution of energy beyond the extent of the duct.

Given such channelling, one asks how one can use these modal properties to direct or redirect a worthwhile amount of acoustic energy to various segments of the water column? To pursue this question and explore the METS concept, a multi-element array was designed, built, and implemented to electronically tailor the amplitude and phase of the transmitted or received signals (see Fig. 11).

In Fig. 12 the array was implanted in NUSC's shallow water acoustic range located in Block Island Sound. The signal to each element was tailored in amplitude and phase to produce and alter acoustic patterns. Environmental and acoustic measurements were made as a function of depth and range in order to relate configuration and propagation conditions to observed patterns. An accurate model permitting a quantitative approach is presently being validated; however, presented are several cases whereby experimental trials, acoustic levels were enhanced in desired segments of the water column.

Figure 13 shows measurements of received levels made in Block Island Sound during a day in January. A typical sound speed profile shown at the left has a positive gradient. With such a profile, the acoustic energy is expected to propagate along the upper segments of the water column. The intention is to enhance the signal level along the lower segment. To the right of the figure, the lower curve is of levels received at a depth of 80 ft when the transmitting array was weighted uniformly, or equivalently, when the array had zero depression angle. The upper curve shows the received levels when the signals to the array were time delayed as one would to steer a beam downward. Even though the total input power to the array was the same for each case, a 4 to 6 dB increase in level was achieved at this depth by steering downward.

To the left of Fig. 14 is a sound speed profile displaying a downward refracting gradient typical for a day in August. To the right are the received levels measured at this time as a function of depth. The maximum difference in sound speed over the water column for this summer condition is approximately 25 ft/s or 7.4 m/s — much less than the vertical changes of 20 m/s in the Western Baltic or the 40 m/s in the Gulf of Aden. The measured vertical acoustic profile that resulted when the array was uniformly weighted (a depression angle of zero) is shown as indicated. The maxima in received levels at this range (1 n.mi) were observed at depths below 50 ft. The signals applied to the array were then time delayed as done to steer a beam upward. The acoustic levels received as a result of the steering are shown as the curve of x's. An increase in acoustic level of approximately 8 dB can be observed in the upper 25 ft of the water column.

These are examples where signal levels were enhanced while going against the grain,' suppose one now intends to go with the grain and seeks to increase the signal level at a depth segment that is favoured by the propagation conditions.

Figure 15 presents just such a case. To the left is the typical sound speed profile for an experiment that took place during the end of June. Downward refracting conditions existed and one would expect the acoustic energy to propagate along the lower portion of the channel. The solid line indicates the aperture of the transmitting array relative to the profile. The small square at 80 ft indicates the receiver depth, the data points shown on the right are the received levels at the indicated depth for two trial configurations; cosine amplitude shading and uniform amplitude shading. The amplitudes for these configurations were adjusted so that each drew the same electrical input power. Even though both had zero depression angles, the uniform shading produced a 5 to 8 dB increase in the received level. In explanation, it is submitted that the predominant mode is generated by wave trains propagating from the array at zero or near-zero degree angles. The cosine shading produces a broader main lobe than the uniform shading and directs less energy along the main axis-less energy available for exciting the predominant mode. These experiments have shown that signal levels at depths favoured by the propagation conditions as well as less favoured by the propagation conditions can be increased by spatially tailoring the acoustic signal.

The eventual question to be answered is whether one can manipulate the acoustic pattern in a quantitative way. If one can provide a valid propagation model one can use the model as an aid in manipulating the acoustic field. A first approach at the multi-element case was simplified by assuming that only wave train directions within the main lobe of the array would generate the predominant contributors to the signal field down range. These directions can be related to the allowed modes and fix the number of modes to be synthesized in producing the theoretical field.

One result of this approach is shown in Fig. 16. The sound speed profile is shown at the left and indicates an upward refracting condition. The measured acoustic profile for the indicated range, sound speed profile, and acoustic frequency is shown at the extreme

right. The depth-dependent amplitude function for each mode was calculated for the same conditions and are shown in the central part of the figure. Only the first four modes were synthesized since they were calculated to be from wave trains within the main lobe of the array. The theoretical acoustic profile is shown next to the measured profile. The major characteristics in both these acoustic profiles, shown on the right hand side of the figure, compare relatively well in that the maxima in each occur at depths above 50 ft.

Another result is shown in Fig. 17, where again, only the first four modes were needed to synthesize the field. Again, the major characteristics in the derived and observed acoustic profiles agree reasonably well. The maxima in each curve occur at depths between 50 and 60 ft. The measured acoustic profile disclosed a secondary maximum occurring in the upper 25 ft of the water column. The theoretical curve also shows a secondary maximum in the upper quarter of the water column.

This simplified analysis resulted in acoustic profiles displaying major characteristics found in the observed acoustic profiles. Although a more accurate model is needed to produce more detailed results, even these results, in so far as maxima occur, are of tactical use. The Block Island results also demonstrate the point that to obtain an increase in signal level one need not merely resort to increasing input source level.

In summary, this paper presented and pointed out similar modal properties in the results of several propagation experiments conducted in the Baltic Sea, Gulf of Aden, and Block Island Sound. The modal approach, in agreement with experimental results, reveals that the influence of stringent propagation conditions on the signal field is sensitive to acoustic frequency and source-receiver geometries. Even though the propagation conditions may be stringent, the approach suggests ways to compensate for these conditions to improve and manipulate signal levels within the water column. It was shown by experiment in Block Island Sound that METS using a multi-element array can be used to manipulate the signal field. The full impact of METS rests upon incorporation of an accurate shallow water propagation model — a task which NUSC is currently pursuing.

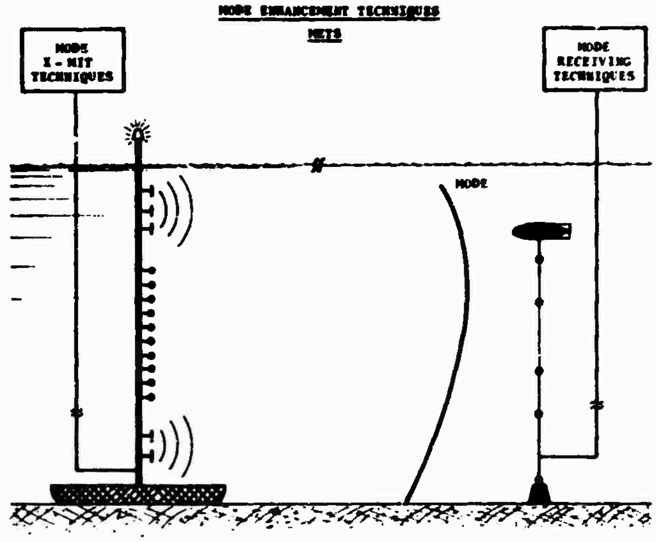

FIG. 1

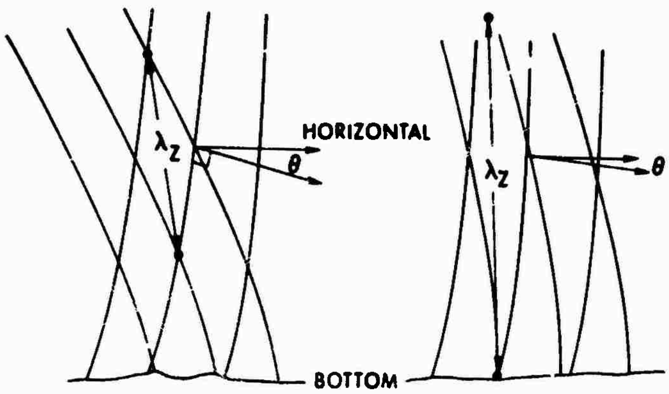

IDEALIZATION OF MODE FORMATION

FIG. 2

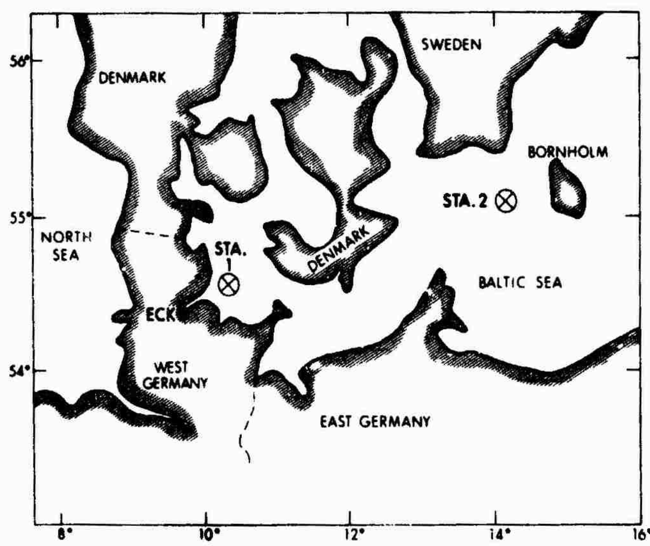

FIG. 3

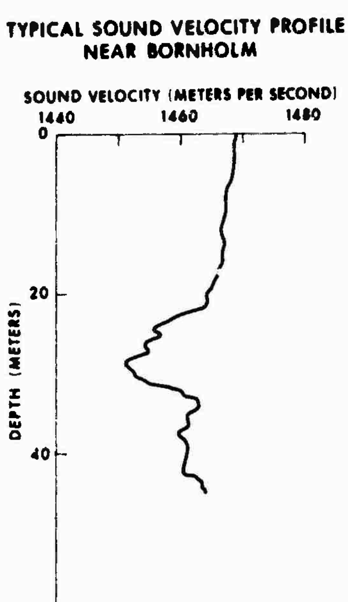

FIG. 4

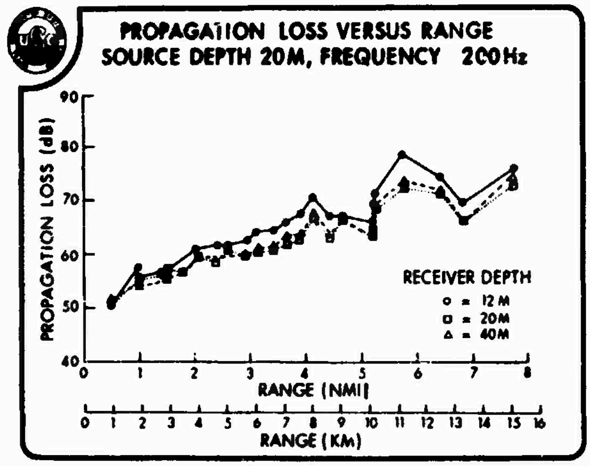

FIG. 5

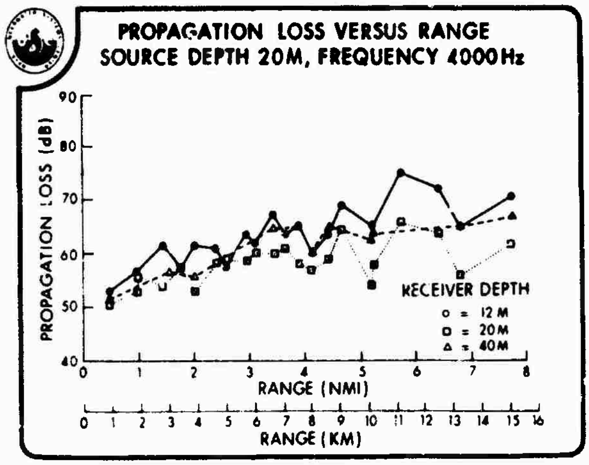

FIG. 6

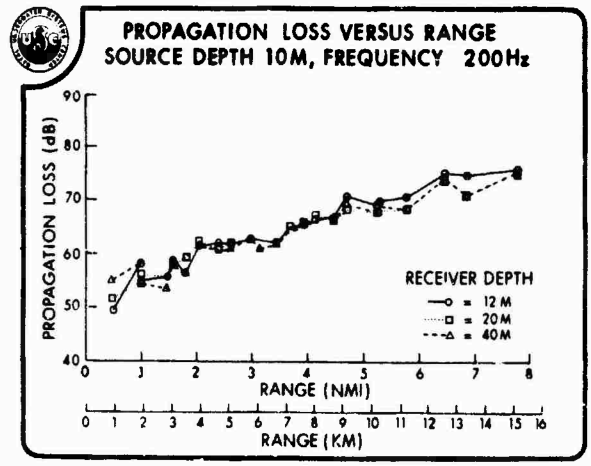

FIG. 7

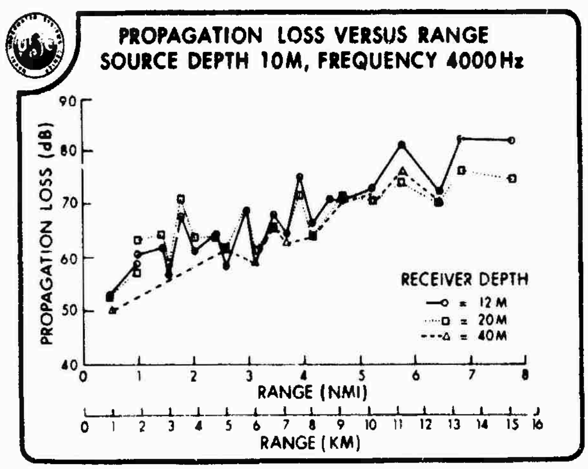

FIG. 8

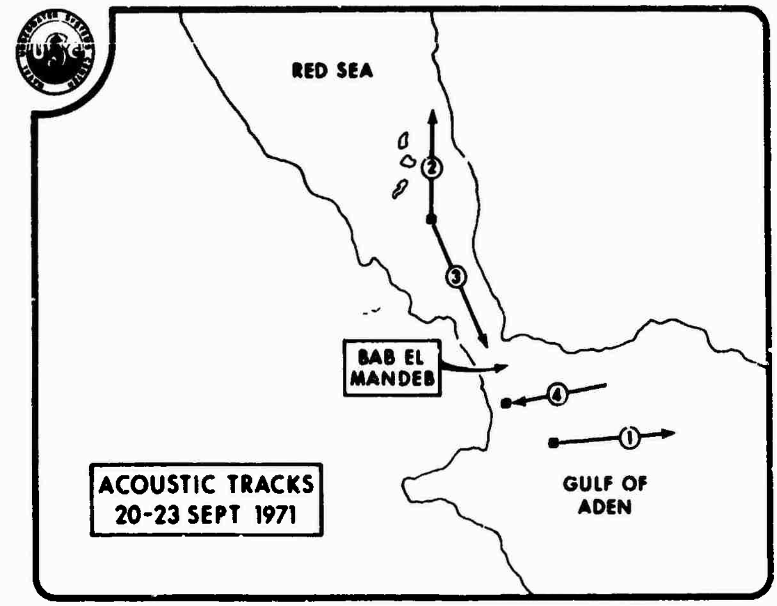

FIG. 9

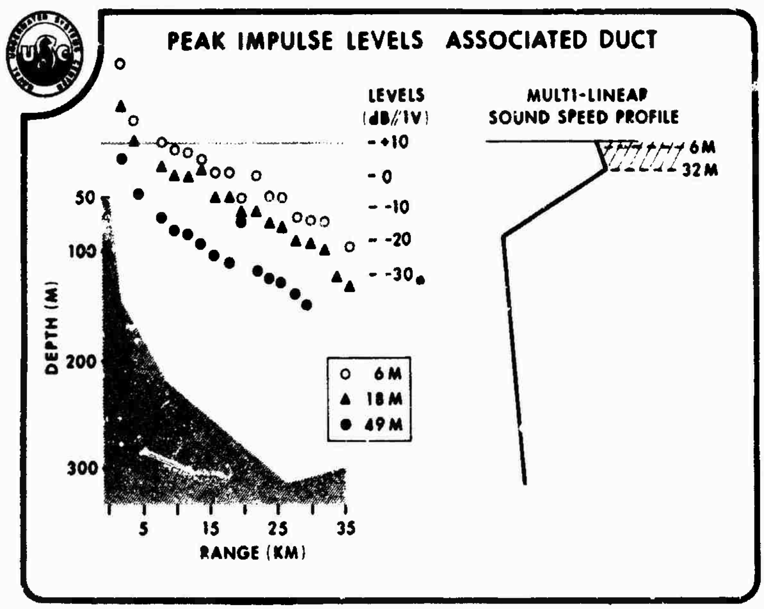

FIG. 10

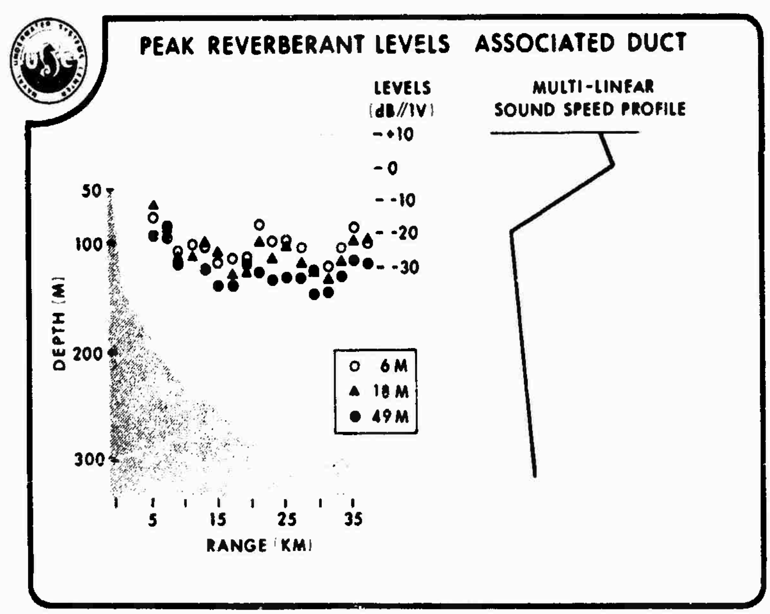

FIG. 11

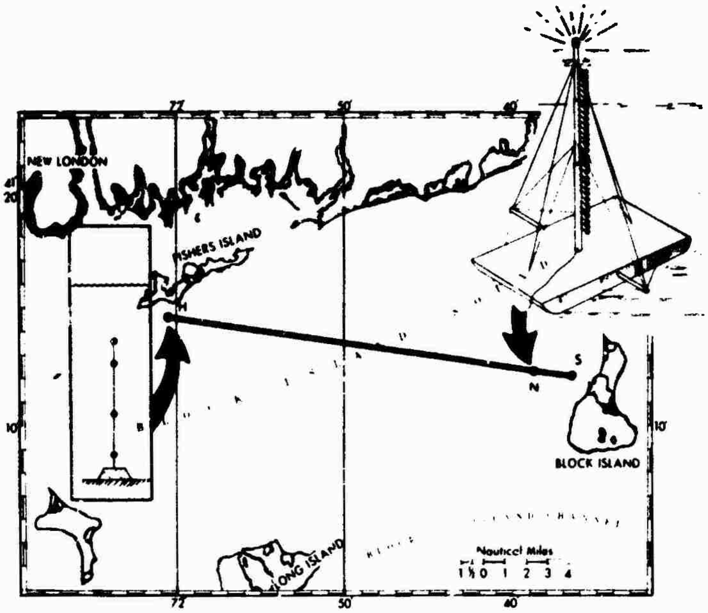

FIG. 12

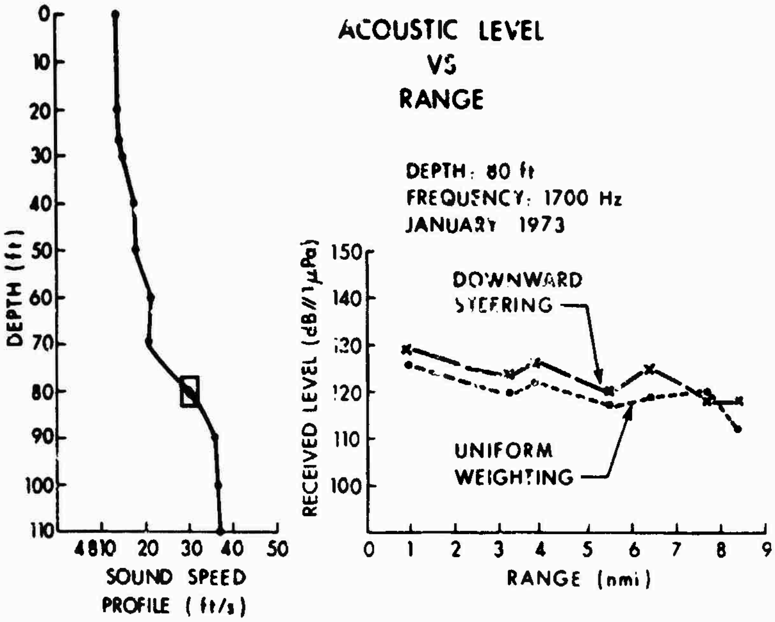

FIG. 13

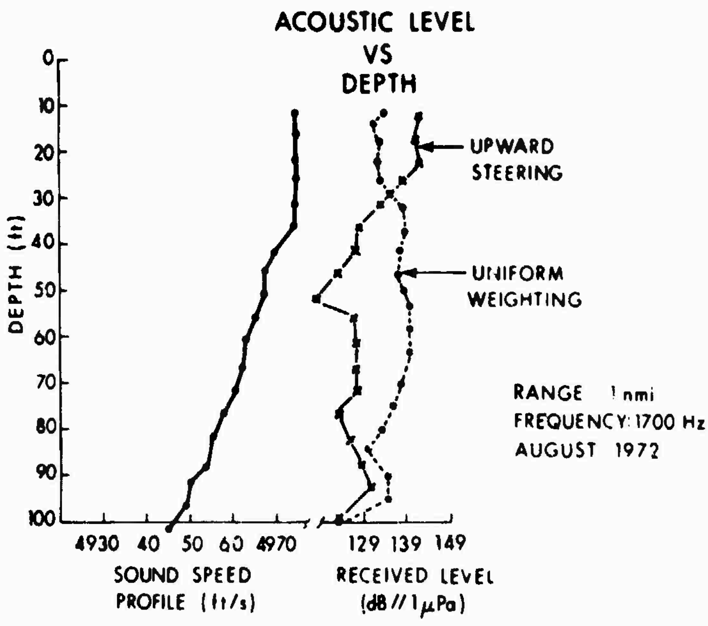

FIG. 14

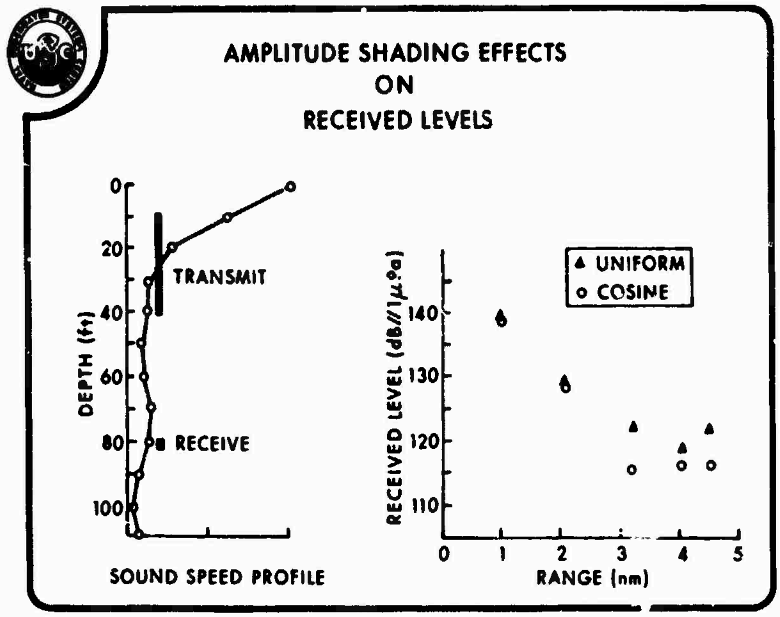

FIG. 15

COMPARISON OF ACOUSTIC PATTERNS
THEORY & OBSERVED
FREQUENCY: 1700 Hz
RANGE: 2.02 nmi (3.7 km)

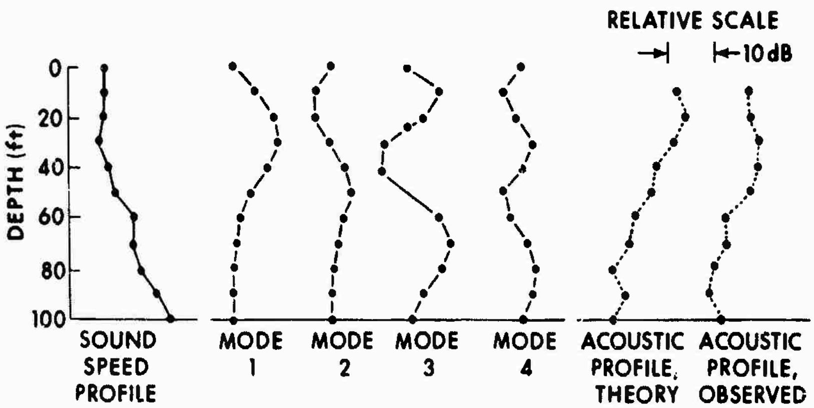

FIG. 16

COMPARISON OF ACOUSTIC PATTERNS
THEORY & OBSERVED
FREQUENCY: 1700 Hz
RANGE: 3.88 nmi (7.1 km)

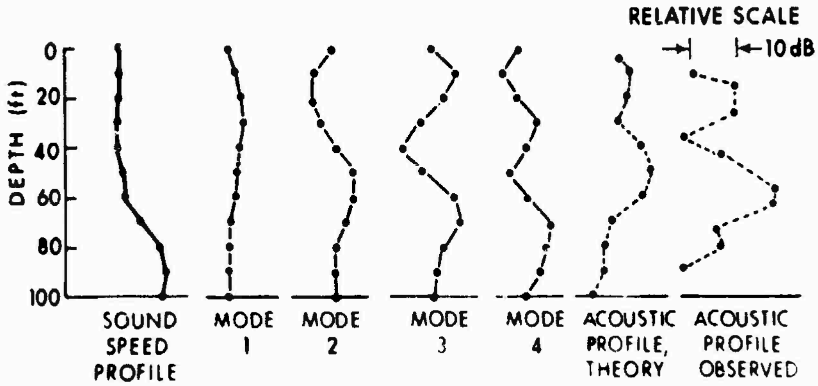

FIG. 17

VARIOUS CONCEPTS FOR FUTURE SONARS IN SHALLOW WATER

by

R. Laval
SACLANT ASW Research Centre
La Spezia, Italy

ABSTRACT

Most of the time, the performances of active sonars in shallow water are drastically limited by the high reverberation level and the difficulties of classification. There is not much hope that any substantial improvement may be obtained by keeping the concept of a hull-mounted sonar operated from a surface ship in motion. On the other hand, it may be possible to define a variety of new concepts which could offer much higher performances for detection and classification, but would introduce some restriction in operational flexibility. The various approaches which could be followed in order to get these improvements are discussed.

INTRODUCTION

The detection of submarines in shallow water with active hull mounted sonars is rather problematic, mostly for two reasons: the high reverberation level, and the difficulties of classification.

Experience has shown that the echo/reverberation ratio in shallow water is relatively independent of the range. The reverberation level superimposed on the echo is due to the energy scattered from the bottom, the surface and the volume in the immediate vicinity of the target, within an elementary "resolution cell". The echo and the reverberation level are thus affected in the same way by the variations of propagation loss. The fact that the area of the resolution cell increases proportionally with the range is more or less compensated by the decrease of the scattering strength which is associated with the progressive reduction with range of the mean grazing angles of the rays reflected at the surface and the bottom (or, in terms of mode theory, by the larger attenuation of the highest modes with respect to the lowest).

In reverberation-limited conditions, the probability of detecting a submarine with a given sonar is thus relatively independent of the range. If the echo/reverberation ratio is high enough, detection will occur at all ranges, up to a maximum range where background noise is the limiting factor. This maximum range will then depend on the transmission level. On the contrary, if the echo/reverberation ratio is below a certain critical threshold, it will be impossible to detect a submarine at any range, whatever the transmission level is.

The detection of submarines in shallow water is thus a kind of go-nogo process. Depending on the geographical location (the bottom properties) the sound-velocity structure, the sea state, maybe the biological conditions, and of course the submarine target strength (which means the submarine aspect), the "detection channel" will be either open up to a rather long range, or will be completely closed.

In shallow water, improving the signal/reverberation figure of sonars means improving the probability (or the percentage of cases) of finding "open" detection conditions.

The other limitation is the classification problem, which is more difficult in shallow than in deep water for the following reasons:

a. The higher density of false targets, mostly due to bottom irregularities: rocks, sea mountains, wrecks, but also to the higher biological life, shoals of fishes, bubble clouds etc.

b. The higher complexity of the acoustic communication channel, in terms of pulse elongation, frequency spread, angular spread, spatial coherence losses, etc. Some of the classification methods which may prove to be satisfactory in deep water may not work in shallow water because of the various types of signal distortion occurring during propagation.

The detection and classification performances of sonars in shallow water are therefore not so dependent on the transmission level; most of the time the propagation loss falls between the cylindrical and the spherical spreading law and so is inferior to what it would be in deep water. It is essentially a problem of information: The acoustic channel should be used in the best possible way in order to distinguish the echo of a submarine from the reverberation back-ground and the various types of false target.

Some limited improvement of the actual sonar performances may be expected by developing more efficient signal processing techniques for detection and classification (a combination of various types of transmitted signals, automatic signal extraction, tracking, etc.). The continuous progress of digital computers in the field of signal processing will undoubtedly allow better use to be made of the acoustic information collected by a given sonar.

Apart from these possible improvements in signal processing, any further progress can only be obtained from an increase in the quantity of information collected by the system. From this point of view, it is probable that the hull-mounted sonar has already almost reached the limits which are compatible with its practical restrictions, such as the array and transducer size, the doppler discrimination from a mobile platform and the total bandwidth.

On the other hand, it is possible to imagine different systems which would not be subject to the same restrictions and could thus be given the capability of collecting much more acoustic information,

at the cost of some revisions of the operational concepts of ASW in shallow water [Ref. 1].

Various approaches could be followed in order to get these improvements:

1. Improve the techniques of doppler resolution and fixed echo elimination in the case of fixed systems.

2. Optimize the operating frequency.

3. Use very broadband signals (such as explosive charges).

4. Use large arrays in order to increase the horizontal directivity.

5. Make use of vertical directivity.

6. Use mode selection techniques:
   a. at the transmission only
   b. at the reception only
   c. at both the transmission and the reception.

7. Use bistatic or multistatic techniques.

The combination of some of these different approaches suggest a number of possibilities to be considered for the design of new systems.

Let us first consider briefly these various approaches one by one.

1. IMPROVEMENT OF DOPPLER RESOLUTION AND FIXED ECHO REJECTION IN THE CASE OF FIXED SYSTEMS

For targets presenting an appreciable doppler the echo can be separated from the reverberation and the fixed false targets by using CW pulses and frequency resolution. With mobile platforms, however, the efficiency of this method is limited by two factors:

a. The ship's own doppler, which is a function of the bearing, which has an appreciable bandwidth due to the width of the main beam and to the side lobes of the receiving array.

b. The spatial variations of the propagation "transfer function" which become time variations when the ship is in motion and cause a doppler spreading of both the echo and the reverberation. These time variations are not associated with any time-variant properties of the medium; the roughness of the bottom, for instance, does produce a frequency broadening when a monochromatic wave (or a long CW pulse) is transmitted or received by a ship in motion.

With a fixed system the two above effects no longer affect the reverberation. The doppler spread will only be due to the motion of the scatterers (surface waves or fishes) and the purely time-variant properties of the propagation channel. Very substantial improvements may thus be expected from the techniques of frequency rejection (prewhitening equalization) provided the transmitted signal itself presents a very narrow ambiguity function in the frequency domain. A long CW pulse, gaussian shaped in order to avoid any side lobes in frequency, is probably the most convenient.

Furthermore, ping-to-ping comparison and tracking techniques are much more efficient and precise with fixed than with mobile systems, which gives the former a considerable advantage for the elimination of fixed echoes and the classification of mobile targets.

2. OPTIMIZATION OF THE OPERATING FREQUENCY

For a given environmental and geometrical situation, the signal/background ratio is a function of the operating frequency which should reach a maximum value in a given frequency band. This optimum frequency band is probably rather variable with the environment and with the geomtry, and it may be interesting to consider the possibility of choosing the frequency of operation in function of the local conditions. A flexibility in the choice of the frequency may be particularly useful when the reverberation has a biological origin and the scattering appears to be concentrated within some well-defined frequency bands corresponding to the resonance frequencies of various species of fish.

This optimization may tend to the use of lower frequencies than those commonly used in present sonar, provided larger arrays can be used in order to maintain the horizontal directivity within reasonably high values.

3. USE OF BROADBAND SIGNALS (Explosive Charges)

By using very broadband signals such as those produced by explosive charges, the information concerning the echo and the reverberation may extend over 3 to 5 octave bands.

The processing can be continually adapted in order to match the optimum frequency band of any particular situation, for detection and/or for classification. Furthermore, the frequency dependence of the target strength can be estimated on several octave bands, which may be an interesting element of classification.

For targets presenting an appreciable doppler, the comparison of the signal/reverberation performances which can be obtained by such broadband signals (using time resolution) and with CW pulses (using frequency resolution) requires a rather complex study based on a detailed knowledge of the time and frequency propagation spread, the target extension and aspect, and the statistical properties

of the reverberation. The conclusions of such a study will depend on the geometrical and environmental conditions.

On the other hand, broadband signals offer the only chance of detecting a submarine with a low doppler.

In any case, using acoustic signals with a spectrum extending over several octaves would obviously constitute a considerable improvement with respect to the FM pulses normally used by conventional sonars with a maximum bandwidth of the order of 1/3 octave.

Explosive charges may offer a relatively cheap and powerful source of energy for operations of limited duration, (for instance when associated with expendable buoys). They can be easily used in bistatic or multistatic operations.

Other types of broadband signals, such as those produced by pneumatic hammers, sparkers etc. could be considered when continuous operation over long periods of time is required.

4. INCREASE OF THE HORIZONTAL DIRECTIVITY (Large Arrays)

The echo/background ratio is proportional to the horizontal directivity index of the receiving array. By using larger arrays the directivity index at a given frequency can be increased, or it can allow lower frequencies to be used for a constant directivity index.

Two types of large arrays may be considered in practice:

a. Linear arrays. They may be towed from a ship in motion (flexible arrays) or be anchored on the bottom (rigid arrays). These arrays are "side-looking", i.e. their operation being limited to an angular domain of $\pm 30^\circ$ or $\pm 45^\circ$ around the direction perpendicular to their axis. With present technology, it is possible to construct long towed arrays (up to several hundred metres) which are hydrodynamically stable. These could be towed at relatively high speeds by a surface ship, a hydrofoil or a surface effect ship. These arrays would have a rather high directivity even at low frequencies. This directivity, however, would be limited by the linearity of the array (the "snaking" effect). The technique of a constant-beamwidth-broadband-array [Ref. 2] which allows a constant directivity to be maintained on several octave bands seems to be particularly interesting when such arrays are planned to be used with explosive sound sources.

b. Circular arrays. Above a certain size, they could no longer be operated from a ship in motion. however, they could probably be "foldable", i.e. constructed as a kind of umbrella, and be operated in the "sprint and dip" mode from various types of high-speed platforms such as helicopters, hydrofoils, surface-effect ship, etc. They could also be used for expandable buoys provided they could be folded into small enough packages.

Above certain dimensions, however, and independently of the technological limitations, the performances of large arrays would be limited by several factors:

a. The physical size of the submarine: when the directivity of the array is such that the target is resolved in bearing, the gain in signal/background is no longer proportional to the directivity index. In compensation, the angular resolution of the target may be an element of classification.

b. The spatial coherence of the sound field associated with the spatial inhomogeneities of the medium and the boundaries (surface and bottom). This limitation in spatial coherence can be described in terms of angular spreading [Ref. 3]. The angular resolution of the array-plus-medium is obtained by convolving the theoretical directivity pattern of the array by the angular-spread function of the medium, (which is the Fourier Transform of the spatial coherence function). When the size of the array is larger than the actual spatial coherence length of the propagation channel, the beamwidth of the array becomes narrower than the angular-spreading width of the medium. A point target is no longer seen as a point but as a cloud which extends over several successive elementary beams. The signal/reverberation per beam does not increase any more when the length of the array increases beyond this size, but the signal is received on an increasing number of elementary beams. The information coming from these different beams can be combined together in an incoherent way. The gain in signal-to-background ratio will then tend to a law in $5 \lg \ell$ instead of $10 \lg \ell$ (ℓ being the length of a line array, or the diameter of a circular array).

5. USE OF VERTICAL DIRECTIVITY

In shallow water, the vertical directivity is imposed by the medium itself. The acoustic energy can only propagate within a small angular domain of a few degrees around the horizontal. The vertical beamwidth of a conventional hull-mounted sonar is generally of the order of $\pm 10^{\circ}$ to $\pm 15^{\circ}$, so much larger than the medium's natural directivity. All the energy which is transmitted outside the small central angular domain is lost in the bottom.

From a signal/noise point of view a waste of energy could be avoided by using a directivity at the transmission which would match the directivity of the medium.

Still from the point of view of signal/noise ratio, the effect of increasing the vertical directivity at the reception would depend upon the vertical directivity of the background noise. The gain would be very large if the directivity pattern of the noise was vertical, i.e. if the noise was generated by the surface in the vicinity of the receiver. On the contrary, the vertical directivity would not reject the long-range traffic noise coming within the same angular domain as the echo. Here there seems to be an open field for further research.

From the point of view of signal/reverberation, as the echo and the reverberation both come from a small angular domain, the vertical directivity of the transmitter or the receiver have no influence as long as the medium is more directive than the system. The conclusions would be different however if the system were more directive than the propagation channel. As the scattering strength of the surface and the bottom increases rapidly with the grazing angle, the most-inclined rays are responsible for the largest part of the reverberation. An appreciable gain in signal/reverberation could therefore be obtained by selecting the rays which deviate from the horizontal as little as possible (provided they can reach the target at its maximum immersion).

Speaking in terms of the selection of rays by vertical directivity, however, is without much meaning, except at relatively high frequencies. The departure and arrival angles of the eigenrays joining a point source and receiver vary with the depth of the source and/or the receiver. The vertical size of the array has to be small enough that the variations of the ray inclination from one extremity of the array to the other is small compared to the beamwidth of the array. When this is not the case, ray theory is not directly applicable, and it is more convenient to use mode theory.

As an example, an array giving a directivity of $\pm 1^{\circ}$ at 1 kHz is about 50 m long, which is the order of magnitude of the water depth considered.

6. USE OF MODE SELECTION TECHNIQUES

The behaviour of long vertical arrays can be better described in terms of their selective properties with respect to acoustic modes rather than in terms of their directivity, which is a free-field concept not applicable to the description of the vertical pressure distribution in a shallow wave-guide.

The principle of the decomposition into orthogonal modes of the waves propagating in a horizontally layered medium is well-known, and is widely covered in several papers presented at this conference. In very physical terms, any given mode can be considered as the result of an interference between an up-going and a down-going wave of equal (opposite) inclination with the vertical. These waves are not plane, except for the case of iso-velocity layers, but are distorted by the variations with depth of the sound velocity in accordance with Snell's law. The angle of these elementary waves with the vertical increases with the mode number and decreases with the frequency. The vertical distribution of pressure associated with a given mode presents a succession of zero and maxima, with a phase inversion of π occurring at each zero crossing. The number of zero crossings between the surface and the bottom represents the order of the mode, the first zero being always at the surface.

A vertical array extending from the surface to the bottom may excite or receive any particular mode by having its weighting adapted in such a way as to reproduce the vertical pressure distribution of the mode. Because of the orthogonality of the modes, an array which is matched for a given mode will not excite or receive any other. The vertical profile of the mode has to be computed from the knowledge of the sound velocity profile in the water, and the acoustic properties of the bottom. It varies with frequency, which means that the weight of any single element of the array has to be a function of frequency in case of broadband application.

The selection of one particular mode (or group of modes) at the transmission, at the reception, or both, may present some advantages for the detection and classification capabilities of active sonars. The various modes, indeed, present different properties with regards to propagation and reverberation, and also time-frequency spread (scattering function and the spatial coherence of the channel).

Let us try to understand how mode selection could work:

If a mode selective array is used to transmit the mode i at a point A, and another mode selective array is used at some distance from the first to receive the mode j at a point B, a transmission coefficient L_{ij} can be defined which gives the level of the mode j which is received at point B, when mode i is transmitted at point A with a transmission level equal to unity. When $i = j$, the coefficient L_{ii} then represents the inverse of the attenuation of mode i. When i and j are different, L_{ij} represents the energy which has been converted from mode i to mode j during propagation. Mode conversion results from the inhomogeneities in the volume and the bottom, from the surface waves, and from the variations of water depth between source and receiver. The L_{ij} coefficients from a matrix which completely describe the propagation in terms of mode attenuation and mode conversion. They are functions of both the frequency and of the range between source and receiver.

The mode transmission terms L_{ii} (diagonal terms of the matrix) generally decrease with the order of the mode. (The attenuation increases with the order of the mode). The mode conversion terms L_{ij} (with $i \neq j$) are generally much smaller than the L_{ii} terms. They tend to become larger and larger when the order of the modes i and j increases, as the equivalent grazing angle of the modes with the surface and the bottom increases.

A similar matrix can be defined for the reverberation. If mode i is transmitted at point A, and the corresponding reverberation energy is measured on mode j at the same point A (or in another point C if bistatic applications are considered) a coefficient R_{ij} can be defined which is the normalized reverberation level measured on mode j when a signal of unit energy is transmitted on mode i. R_{ij} is again a function of frequency and range (time).

A mode dependent echo/reverberation ratio $(E/R)_{ij}$ can then be defined, which is the echo/reverberation observed at a mode-selective receiver tuned for mode j when a mode-selective source has transmitted mode i.

Assuming the transmitter to be at point A, a submarine of target strength TS at point B, and the receiver at the same point A of the transmitter (in case of monostatic) or at a point C (in case of bistatic) the $(E/R)_{ij}$ terms can be computed from the L_{ij} and R_{ij} terms.

The energetic level at point B (averaged over the water column) will be the sum of the j modes:

$$\sum_{j=1}^{j=N} L_{ij} = L_{i\Sigma} .$$

(N being the highest mode containing an appreciable energy).

A submarine at point B will act as a secondary source, which will reradiate the intercepted energy on all modes, whatever the transmitted mode is. The coupling between the submarine and any given mode is function of the submarine depth.

Considering that the submarine has a rather large vertical extension, and taking an average value for all possible submarine depths, simply we may assume that the coupling with the submarine is equal to 1 for all modes.

In this case the submarine secondary source level for any arbitrary mode will be (in logarithmic scale, with the L terms being negative)

$$TS + L_{i\Sigma}$$

and the echo level received at point A will be

$$TS + L_{i\Sigma} + L_{\Sigma j}$$

with

$$L_{\Sigma j} = \sum_{i=1}^{i=N} L_{ij} .$$

$L_{\Sigma j}$ represents the energy received on mode j at point A when all the modes are simultaneously transmitted at point B with unit source level.

The signal/reverberation term is therefore:

$$(E/R)_{ij} = TS + L_{i\Sigma} + L_{\Sigma j} - R_{ij} .$$

This term can be compared with the signal/reverberation ratio $(E/R)_{\Sigma\Sigma}$ which would be obtained without any selection of modes, (assuming that all modes are transmitted and received simultaneously.

Let us call $L_{\Sigma\Sigma}$ and $R_{\Sigma\Sigma}$ the transmission factor and reverberation level corresponding to this case:

$$(E/R)_{\Sigma\Sigma} = TS + 2\ L_{\Sigma\Sigma} - R_{\Sigma\Sigma}.$$

The principle of the mode selection method lies in the hope that some of the $(E/R)_{ij}$ terms may be substantially larger than $(E/R)_{\Sigma\Sigma}$. This should generally happen for the lowest modes, i.e. for the low values of i and j, if we assume that the reverberation is mostly associated with the high modes.

Furthermore, on the receiver side, all the modes can be processed individually, and the results recombined incoherently after detection.

It is possible to limit the mode selection to the transmission only. The signal reverberation term will then be:

$$(E/R)_{i\Sigma} = TS + L_{i\Sigma} + L_{\Sigma\Sigma} - R_{i\Sigma}$$

or to the reception only, which gives the term:

$$(E/R)_{\Sigma j} = TS + L_{\Sigma\Sigma} + L_{\Sigma j} - R_{\Sigma j}\ .$$

Various mixed systems could be considered:

Mode selective transmitters could be associated with large horizontal receiving arrays, which would probably constitute an extremely efficient system combining part of the advantages of mode selection with the high horizontal directivity of the receiver.

Broadband mode selective receivers could be activated by explosive charges.

It has to be pointed out that the selection of a single mode requires a vertical array which really does extend from the surface to the bottom. Such an array should not deviate from the vertical for more than a very small fraction of the wavelength. Deviations from the vertical would introduce an apparent phase weighting (dependent of the horizontal bearing), which has to be kept smaller than one radiant in order not to destroy its matching with the selected mode. From a practical engineering point of view this condition is extremely hard. At 1 kHz it means a maximum deviation of the order of twenty centimetres. With water 50 m deep the tolerance on the verticality would have to be within 2/10 of a degree. This tolerance can only be reached by building rigid bottom mounted arrays.

However, if instead of a single mode a group of several modes is to be selected (for sintance the 4 or 5 lowest ones) the tolerance on the verticality becomes less critically and the length of the array can be reduced. (It is no longer necessary for it to extend from the surface to the bottom).

7. USE OF BISTATIC OR MULTISTATIC TECHNIQUES

One of the most variable terms in the sonar equation is the target strength which varies as much as 15 dB as a function of the submarine aspect.

If the position of the transmitter and the receiver are separated, the target strength becomes a function of the bistatic angles.

A single transmitter can be used to activate several receivers, with the purpose that at least one receiver will be in a favourable angular position of bistatic angle and range to detect the submarine.

Conversely a single receiver may be activated by several transmitters. Such transmitters may just be explosive charges which are thrown some distance from the receiver in different directions.

More complex configuration can be used involving several receivers and transmitters (or explosive charges) in order to cover large areas.

Bistatic and multistatic methods have the advantage of confusing the evasion tactics of the submarine which does not know the position of the receivers.

CONCLUSION

The various approaches which have been considered can be combined in several ways in order to define new systems which would be more efficient than the present hull-mounted sonars for the detection of submarines in shallow water.

It appears, however, that all progress made in the acoustic domain would occasion a reduction in operational flexibility.

Mobile platforms, such as surface ship hydrofoils or hovercraft, could use long towed arrays at the cost of limiting the coverage to a lateral sector.

Large arrays covering all directions and advanced techniques of doppler resolution could only be used from non-moving platforms (dipped systems or buoys).

The technology of large foldable arrays still has to be developed.

The use of broadband explosive charges would be limited to relatively short operations by the quantity of charges which could be carried by the launching platforms (and by price considerations).

Broadband repetitive sound sources would be excellent for detection against reverberation, but would probably have their maximum detection range limited by their relatively low transmission level.

The techniques of mode selection probably have to be limited to the case of fixed or semi-fixed installations, due to the very high precision required for the verticality of the array.

Operations involving multistatic techniques are complex and. if they are to be successfully conducted, require highly skilled teams of operators.

The future methods of ASW in shallow water have therefore to be studied from the combined aspects of acoustics, technology and operational research. If this is done there is great hope that a variety of new techniques and tactics may be defined in the years to come which will give satisfactory solutions to this difficult problem.

REFERENCES

1. LAVAL, R. Some thoughts on the possible evolution of sonars in shallow water. Paper presented at the Long Term Scientific Study Panel on ASW in Shallow Waters. NATO Headquarters, Brussels, 17-21 March 1969.

2. REQUICHA, A.G. Broadband hydrophone arrays for use with explosive sound sources. Paper presented at the NATO Advanced Study Institute on Signal Processing. Loughborough, England, August 1972. Edited by Academic Press London and New York, 1973.

3. LAVAL, R. Sound propagation effects on signal processing. Paper presented at the NATO Advanced Study Institute on Signal Processing. Loughborough, Englamd, August 1972. Edited by Academic Press London and New York, 1973.

DISCUSSION

Dr Weston believed that mode selection should help considerably against ambient noise but will sometimes be limited by reverberation. This is because the medium itself selects a low mode and artificial selection may not be of much further help, especially if the reverberation is primarily from mid-water fish whose coupling for all modes is comparable with that of a submarine. Mr Laval replied that mode selection is probably only effective against surface and bottom reverberation, where the coupling with the modes is different from that of a submerged submarine. He agreed that at very long ranges the medium itself would select even the lowest mode, thereby indicating that artificial mode selection is probably most effective at intermediate ranges where several modes can propagate without excessive absorption. This appears to apply to the ranges and frequencies being considered for active sonars. Dr Muir liked the idea of vertical arrays but was afraid of the mechanical-engineering problems involved. Mr Laval pointed out that if a combination of several modes is selected, rather than a single mode, a complete surface-to-bottom array may not be necessary and the required angular accuracy may become less critical.

SOUND PROPAGATION MEASUREMENTS IN SHALLOW WATER

by

ISC B. Grandvaux
(presented by IPA F. Lefadeux)
Laboratoire de Détection Sous-Marine
Le Brusc, France

SUMMARY

The purpose of the sound propagation measurements in shallow water undertaken in France is to provide the data needed for a parametric study of sonar systems (which is the subject of Mr Roy's presentation).

When the study was started in 1970, the approach was the usual one:

- Survey of oceanographic parameters
- Modelling
- Experimental verification at sea.

Two geographical areas had been chosen for the experiments, one off the coast of Brittany, the other in the Gulf of Lions. It was very soon realized that modelling of sound propagation in shallow water was going to be a lengthy business (that would have to be performed, not prior to the study of sonar systems, as one would have wished, but simultaneously). Furthermore the characteristics of propagation and reverberation differed markedly from one area to the other.

It was therefore decided to modify the staging of the work and to use a shorter-term approach, by carrying out on the continental shelf a systematic survey of those data that are required for system design. These parameters are:

- Transmission loss
- Signal elongation
- Reverberation.

This survey is the objective of ESTHER, a programme of measurements performed by aircraft.

Parallel to this programme, conventional surface means are being used for localized measurements of bottom noise and spatial coherence.

The following points are made concerning the figures:

Fig. 1: The ESTHER programme has been spread over three years; the initial phase, in 1973, aimed also at developing the techniques of measurement.

Fig. 2: This geographical area has a most peculiar behaviour; it functions as a low-pass filter (the cut-off, at about 800 to 1000 Hz, is due to border reverberation). The lower the frequency becomes, the longer the elongation due to multi-path propagation. Reverberation is greatest at about 1 to 1.2 kHz, owing to the cumulative effects of the low-pass filter and of the increase of the scattering strength of the border at higher frequencies.

Fig. 3: This indicates good correlation of noise level, wind speed and sea state. However, the relation between wind speed and wave height does not correspond here to the standard laws, (violent winds causing only a moderate increase of wave height). This appears clearly when absolute noise levels are compared with standard values (noise level as a function of sea state is rather above normal, lower when seen as a function of wind speed).

Fig. 4: Among other results, vertical coherence is shown to decrease quicker than horizontal coherence.

DISCUSSION

Several questions concerning the experimental set up were answered by Mr Lefadeux as follows: The range of the radio link limited the runs to lengths of about 40 km. Ten to twelve bombettas were used at each depth for each run. The sonobuoys used were slightly-modified calibrated French sonobuoys with two gain settings and ceramic hydrophones of very good stability.

Mr Laval questioned the asymptotic level of 0.3 for the spatial coherence. It was thought to be due to noise limitations but as Mr Grandvaux was not present further details could not be determined; however Dr Bennett pointed out that coherence below 0.4 is statistically inconsistent.

Mr Lefadeux explained to Ir Vettori that the purpose of the table in the last figure is to create a databank from which various information can be retrieved for statistical analysis.

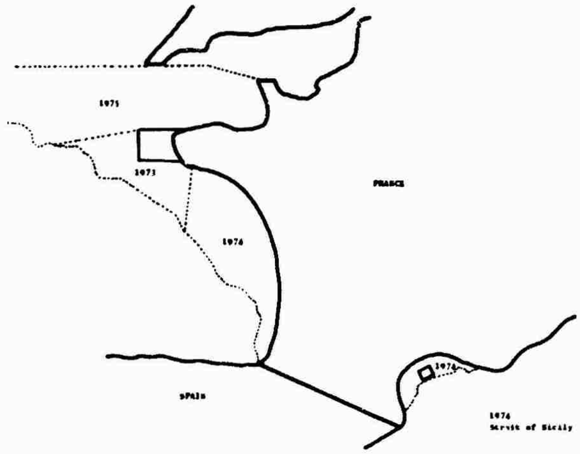

FIG. 1 ESTHER PROGRAMME
SHALLOW WATER PROPAGATION
GEOGRAPHICAL AREAS SELECTED

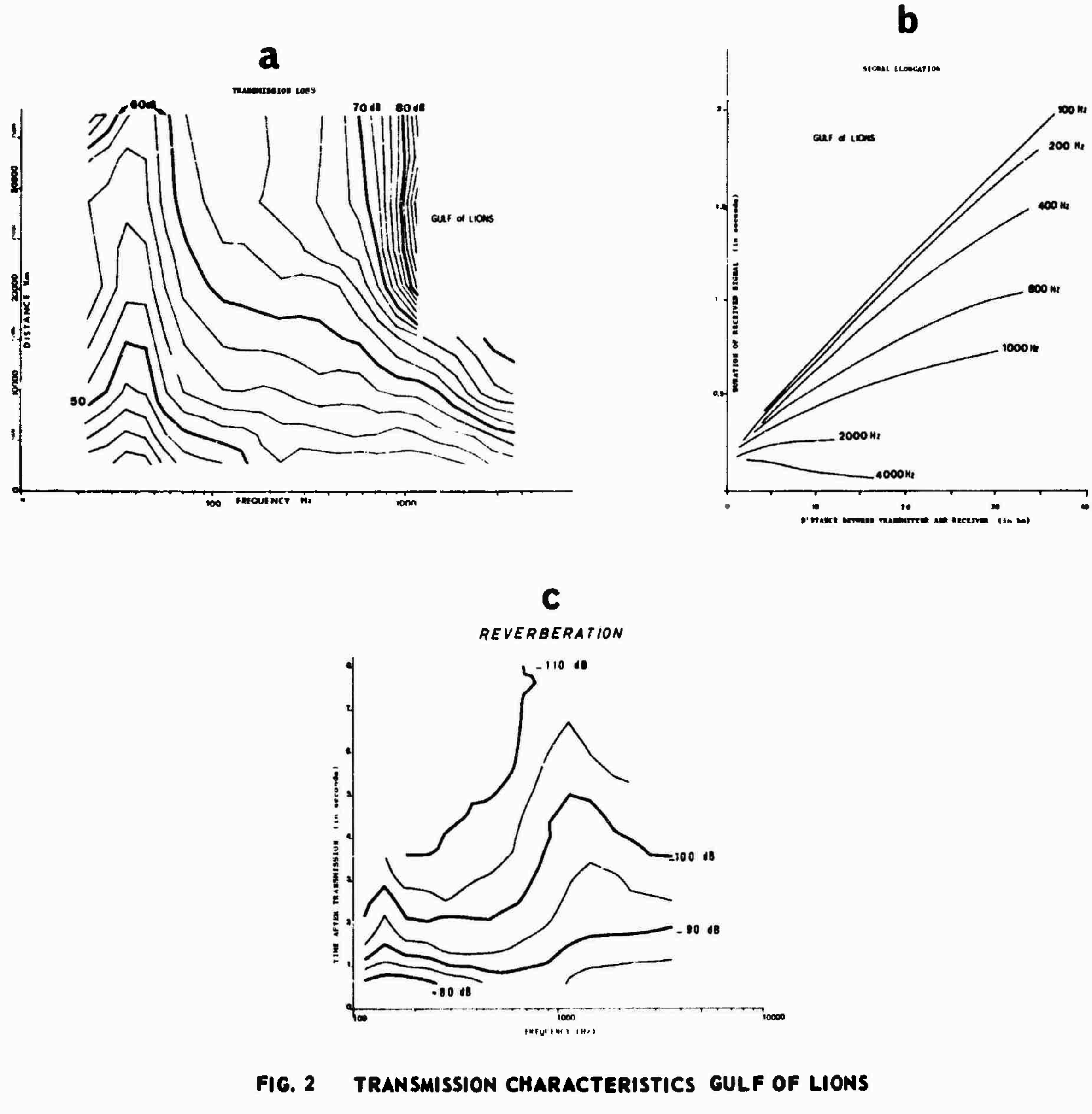

FIG. 2 TRANSMISSION CHARACTERISTICS GULF OF LIONS

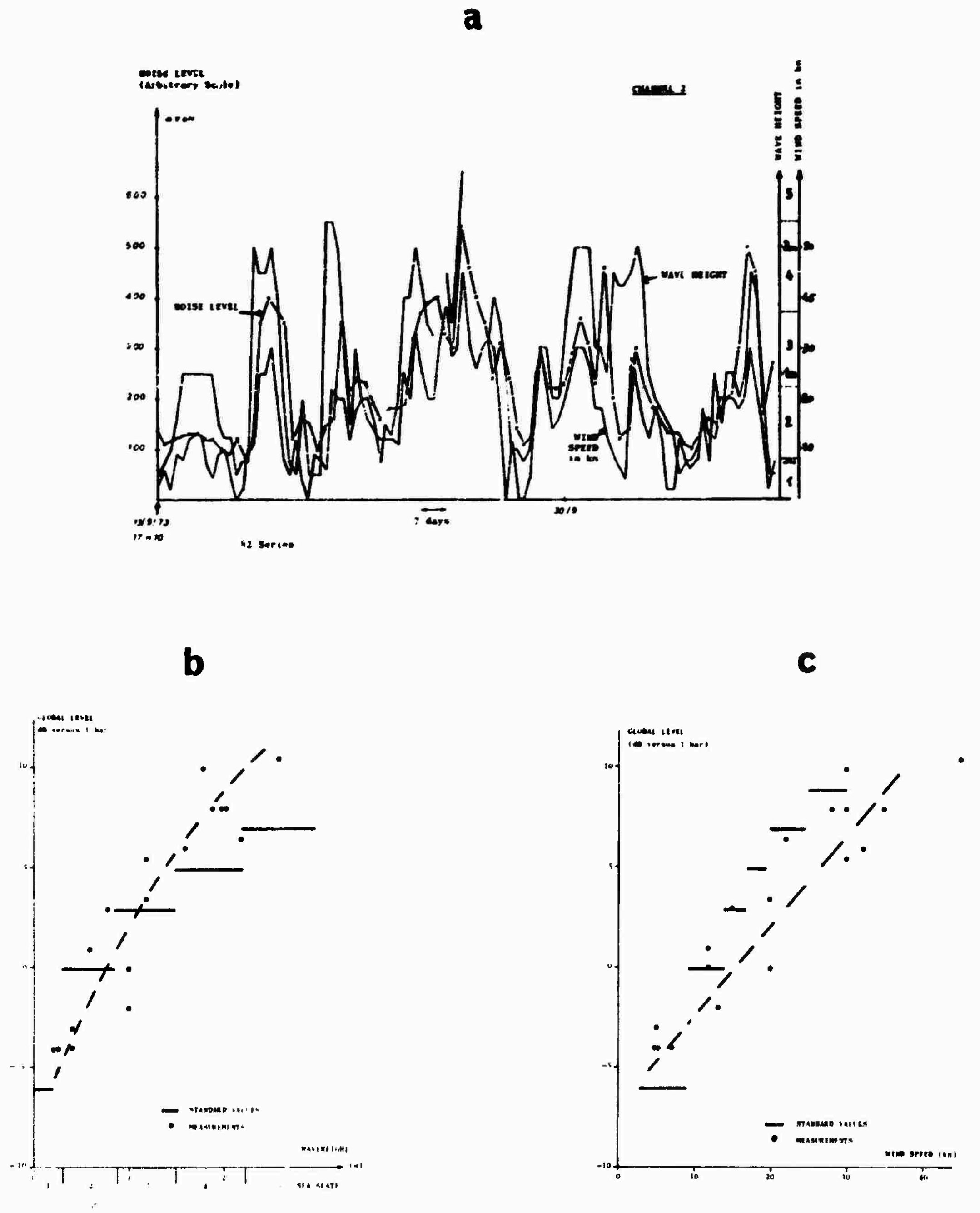

FIG. 3 MEASUREMENTS OF NOISE AS A FUNCTION OF WIND SPEED AND SEA STATE. GULF OF LIONS RESULTS

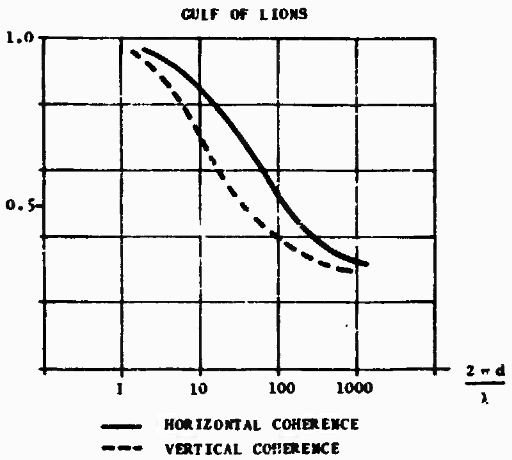

FIG. 4

SPATIAL COHERENCE MEASUREMENTS RESULTS, GULF OF LIONS

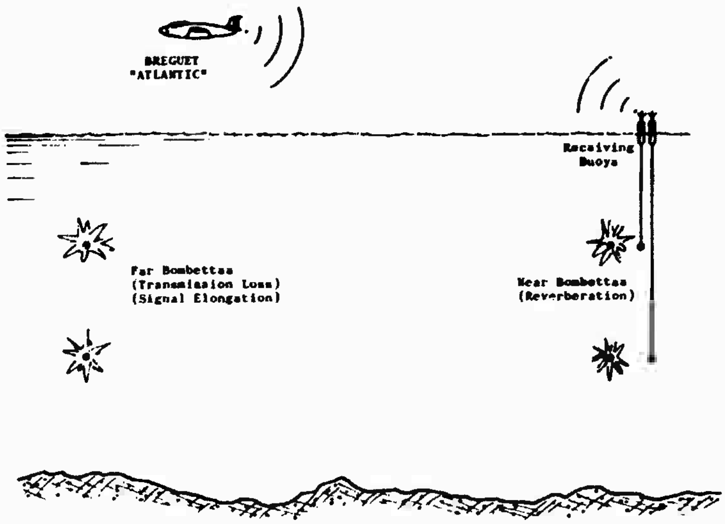

FIG. 5

ESTHER PROGRAMME MEASUREMENTS BY AIRCRAFT BASIC GEOMETRY

MESURES DE PROPAGATION PETITS FONDS FICHE D'EXPLOITATION

1. ORIGINE
   - THEORIQUE
   - EXPERIMENTALE
   - NON PRECISE

   LIEU (RECEPTION)
   - LATITUDE
   - LONGITUDE

   DATE
   - MOIS/ANNEE

2. DONNEES OCEANOGRAPHIQUES
   - PROFONDEUR (m)

   NATURE DU FOND
   - ABSORBANT
   - REFLECHISSANT
   - DIFFUSANT
   - NON PRECISE

   ETAT DE LA MER
   - FAIBLE
   - MOYEN
   - FORT
   - NON PRECISE

   BATHYTHERMIE
   - ISOCELERE
   - INDIA
   - PAPA
   - NOVEMBER
   - MIKE
   - NON PRECISE

   THERMOCLINE
   - IMMERSION MOYENNE
   - THERMOCLINE FORTE
   - THERMOCLINE FAIBLE
   - NON PRECISE

3. DONNEES ACOUSTIQUES
   - DIRECTION DE PROPAGATION
     - FOND PLAT
     - DIVERGENCE
     - CONVERGENCE
     - AUTRE SITUATION
     - NON PRECISE
   - POSITION DES CAPTEURS (PAR RAPPORT A LA THERMOCLINE)
     - EMETTEUR & RECEPTEUR AU-DESSUS
     - EMETTEUR & RECEPTEUR AU-DESSOUS
     - CROISES
     - NON PRECISE
   - TYPES DE SOURCE
     - SOURCES IMPULSIVES
     - SOURCE SONAR

4. RESULTATS
   - PERTE DE TRANSMISSION/DISTANCE
   - NIVEAU REVERBERE/TEMPS
   - ALLONGEMENT DU SIGNAL/DISTANCE
   - BRUIT AMBIANT/FREQUENCE/GISEMENT/SITE

FIG. 6 CARD FOR REGISTERING RESULTS OF SOUND PROPAGATION MEASUREMENTS IN SHALLOW WATER

PARAMETRIC STUDY OF SONAR SYSTEMS — APPLICATION TO SHALLOW WATER

by

ISC J.A. Roy
Laboratoire de Détection Sous-Marine
Le Brusc, France

ABSTRACT

The subject of the paper is the parametric study of the range which can be reached by a sonar, working by active or passive mode and using a monostatic or a multistatic system. At first the various hypotheses are presented and the most important parameters checked off. Then the two solutions (active or passive mode) are studied. The main conclusions are that for an active system, the reverberation soon becoming predominant, a very high emitting power is not necessary, the receiver directivity must be as good as possible, the detection frequency must be close to a particular value, and the multistatic system is more effective. For a passive system, the influence of the parameters is strongly bound to the medium (particularly when there is a noise-maker) and it is not very important for the surrounding conditions to be fitted to the hypothesis of the calculation.

INTRODUCTION

When it has been decided to realize a sonar system, it is obviously necessary to do previously a parametric study. The purpose of that study is to value the evolution of the performances in terms of the various parameters or of the system design, and to look for the best solution according to the foreseen uses.

The parameters acting on the efficiency of a sonar can be classified in three groups:

1. Those connected with the medium: propagation, reverberation and ambient noise.
2. Those connected with the target: echo and radiated noise.
3. Those connected with the sonar: size of the antennas, frequency range, signal processing and self noise.

The first characteristic of the system is the working mode: active or passive. In the active mode, we can consider a monostatic system (transmitter and receiver are put at the same place) or a multistatic system. With the passive mode, the detection can be adapted to the spectral anomalies (spectrum lines) of the target radiated noise or to a regular distribution of energy (principle of the optimum filter).

Then we must consider the working use:

- towed system
- dipped system from an inhabited bearer (ship, plane ...)
- independent dipped system
- permanent fixed system
- composite system (combination of the previous solutions).

In any case, a parametric study must be supplied with simultaneous studies of the various parameters:

- study of the medium for the propagation, the reverberation and the ambient noise
- technological studies to know the means at the present time (antennas directivity, transmitters power, possible gain of the signal processing ...)
- operational research studies to calculate the gain brought by a particular working mode (multistatic system for example).

At last, the results of the parametric study must be borne out by probative experiments.

1. ACTIVE MODE

1.1 General Remarks - Sonar Equation

We have to consider four cases in the theoretical study of the active sonar range in terms of the following choices:

- monostatic or multistatic system
- prevalence of noise or reverberation .

In any case, however, the sonar equation can be applied, providing that the parameters formulae are changed.

$$2\,H9r, f) = S + G_T - M + T(f) - B(r, \theta, f)$$

S = acoustic level of the emission signal

G_T = coherent processing gain

M = perception ratio (minimum signal-to-noise ratio) behind the signal processing

$B(r,\theta,f)$ = noise or reverberation term

$T(f)$ = targets strength (put in the form of $T = 10 \lg f + K$ with an upper limit f_c for the frequency and a lower limit $K = -5$ given by the target size and the hitting angle of the signal

$H(r,f)$ = transmission loss .

Then it is usual to select in this equation the terms in which we are particularly interested.

In the study upon which we entered, we chose:

- the transmitting acoustic power Pa which is very important if the noise is prevalent
- the mean backscattering strength R_f (including the boundaries) which becomes predominant when the reverberation level is higher than the noise level

- the bearing directivity index of the receiver ψ, defined by the ratio ℓ/λ for a linear array
- the frequency f
- the transmitter-receiver spacing R_0 in case of bistatic system
- the target strength T by the value of K.

In those conditions, the sonar equation will be written in the following ways, according to the chosen case:

1.2 Monostatic-Noise-Limited Conditions

$$2H(r, f) = A + 10 \lg P_a + T(f, K) + \psi$$

1.3 Monostatic-Reverberation-Limited Conditions

$$10 \lg r = A' - R + T(f, K) + \psi \,.$$

This equation is basically different from the previous one because the transmission term disappears. The geographic zone influence is only acting by the way of the reverberation.

Because of the simpleness, we can immediately pick out some conclusions:

- knowing that $\psi = 10 \lg \ell/\lambda$ + Cte, the range will be directly proportional to ℓ/λ as far as the spatial coherence allows it,
- R is not constant, but equal to $R_f + 10 \lg f$. Consequently, it is subordinate to the frequency on the one hand, and on the other hand to the medium and to the incidence of the rays hitting the borders (surface and bottom of the sea) by the way R_f (choice of the geographic zone and the sonar depth),
- $T(f,K) = K + 10 \lg f$ until a characteristic frequency $f = f_c$ and then $T(f, K) = K + 10 \lg f_c$. So we can assume that the frequency will not influence the range until $f = f_c$ (because of R and T which are opposite) and that the range will decrease when it will increase above this value.

1.4 Multistatic-Noise-Limited Conditions

$$H_1(r_1, f) + H_2, f) = A + 10 \lg P_a + T(f,K) + \psi$$

r_1 = transmitter - target spacing

r_2 = receiver - target spacing (chosen for the range).

This equation is very similar to the one written for the monostatic system. The transmitter-receiver spacing R_0 will influence the ranges through the difference between $2H(r,f)$ and $H_1(r_1, f) + H_2(r_2, f)$.

Moreover the target strength $T(f,K)$ changes its feature.

1.5 Multistatic-Reverberation-Limited Conditions

In that case, there is no longer a spherical symmetry around the sonar. This modification is particularly applied to the backscattering surface which becomes oval and of which the interaction with the receiver directivity pattern brings an integral shape in the formulae. Then, it is necessary to use two extra variables: the receiving bearing θ that we choose and the time (by the way of the product c . t)

$$H_1(r_1,f) + H_2(r_2,f) = A'' - R + T(f,K) - 10 \lg \int_0^{2\pi} F(\theta) \cdot d\theta \, .$$

To reduce the calculations, we limited the study to a receiving bearing put on the transmitter-receiver axis (major axis of the backscattering surface)... Yet some calculations have shown that the ranges were reduced in the second extremum case, when the target was put on the minor axis of the backscattering surface.

1.6 Conclusion

We have fixed reference conditions by the way of mean values for the various parameters and we have studied their influence on the reference range with independence from one to another (for example the influence of the spacing R_2 in the bistatic system was independent of the modification brought by that type of system on the target strength).

We have chosen two extremum cases of surroundings:

- a "bad medium" (pattern number one, Gulf of Lions for instance)
- a "good medium" (pattern number two, some parts of the continental shelf for instance).

1.6.1 Noise-Limited Conditions

In that configuration, most of the parameters have a small effect on the range. Figure 1 shows, for example:

- if the acoustic power is 10 times higher, the range is improved by 1.5,
- if the directivity is brought to the upper limit allowed by the lost of space coherence, there is no real effect,
- if the frequency is changed, the effect becomes evident only if the "bad medium" and, in relation to a mean value of the frequency range, brings a coefficient smaller than 1.4,
- the effect of increasing the transmitter-receiver spacing is not acting much against the range.

The only parameters which has a real important effect as well as a rather large variation range is the target strength.

1.6.2 Reverberation-Limited Conditions

The influence of the various parameters is more important in that case, as shown in Fig. 2:

- the range is directly proportional to the directivity (so that increasing the directivity index from 7 to 20, triples the range),
- as we have seen before, increasing the frequency beyond f_c is very badly acting (the range can be four times smaller).

But moving the receiver from the transmitter does not change the range (at least if the target is on the transmitter-receiver axis).

The most influent parameters are the backscattering strength R_f that we cannot modify and once again the target strength.

1.6.3 General Conclusions

- The detection frequency must be close to f_c.
- A very high emitting power is not necessary because the reverberation-limited conditions are soon reached.
- The receiver directivity must be as good as possible against the reverberation.
- A multistatic system will be certainly more effective because the separation of the receiver from the transmitter is not much influent when a good distribution of the system can highly increase the target strength which is always the most important parameter.

2. PASSIVE MODE

2.1 General Remarks - Optimum Filter

The way of calculation for this mode of detection is quite different from the previous one. For a passive sonar working with a detector-averager applied to the optimum filtering, it will be possible to detect if the signal-to-noise ratio at the end of the processing is higher than a fixed value.

Two possibilities must be considered:

- The surrounding conditions are fitted to the hypothesis of the optimum-filtering calculations.
- The conditions are not fitted to the hypothesis.

Three main parameters occur in the filtering definition:

- the radiated noise spectrum of the target,
- the surrounding-noise spectrum,
- the distance between the target and the sonar.

2.2 General Equations

If the conditions are fitted to the hypothesis of the optimum-filtering calculations:

$$\rho^2 = T \int_0^{\infty} \frac{A_S^2(\nu) \cdot \psi^{*2}(\nu)}{A_B^2(\nu) \cdot h^2(\nu)} \, d\nu \, .$$

If the conditions are not fitted to the hypothesis

$$\rho'^2 = T \cdot \frac{\left[\int_0^{\infty} \frac{A'_S(\nu)}{h'(\nu)} \cdot \frac{A_S(\nu)}{h(\nu)} \cdot \frac{\psi^{*2}(\nu)}{A_B^2(\nu)} \cdot d^2 \right]^2}{\int_0^{\infty} \frac{A'^2_B(\nu)}{A_B^4(\nu)} \cdot \frac{A_S^2(\nu)}{h^2(\nu)} \cdot \psi^{*2}(\nu) \cdot d\nu}$$

with:

$A_S(\nu)$ = spectrum density of the signal at 1 m from the target

$A_B(\nu)$ = spectrum density of the noise at the front of the antenna

$h(\nu)$ = transmission loss between the target and the antenna

$\psi^*(\nu)$ = receiving directivity of the sonar

which become $A'_S(\nu)$, $A'_B(\nu)$ and $h'(\nu)$ for the surrounding conditions when they are not fitted to the hypothesis.

T = integration time according to the crossing of the target through the main lobe of the antenna directivity pattern

2.3 Calculations

The integration time is limited by two ways: the technology possibilities and $4 \cdot 10^3 \cdot r \cdot \frac{1}{V} \cdot tg\, \theta_3$ (where r is the range in km, V the target speed in kn and $2\theta_3$ the size of the main lobe of the antenna directivity pattern).

The transmission loss is subordinate to the geographic situation of the detection zone. We have chosen two different surroundings patterns that we suppose to be the extreme types in shallow water;

a "good medium" and a "bad medium" previously described.

Two types of target have been selected:

- a weak signal according to a small submarine navigating silently,
- a rather strong signal according to a big submarine.

At last, we have chosen two types of ambient sea noise, spectra of which have the same slope but different levels. One agrees with a mean value of the sea state, the other agrees with a very strong noise.

The useful detection band, undefined in the formulae, must be limited. A first limit is fixed by the knowledge field of the various parameters. A second limit is chosen from the previous one by taking the boundary frequencies ν_1 and ν_2 as the signal-to-noise ratio lost 10% of its value. An arbitrary central frequency ν_0, needed by the definition of a directivity index, has been fixed by:

$$\int_{\nu_1}^{\nu_0} F(\nu)\cdot d\nu = \int_{\nu_0}^{\nu_2} F(\nu)\cdot d\nu = 0.5 \int_{\nu_1}^{\nu_2} F(\nu)\cdot d\nu \ .$$

To take into account the evolution of the directivity index inside the detection band, we have put it as:

$$\psi = 10 \lg \psi^* = cte + 10 \lg \nu \ .$$

2.4 Results

Figures 3 and 4 show that the range r_0 that we obtained with the chosen integration time and the detection threshold ρ_0, and with a directivity index in such a way that it is possible to detect a weak signal in a mean sea noise:

- becomes more than two (pattern No. 1) to three times (pattern No. 2) smaller for the same target in a very strong noise,
- increases in about 40% with the pattern No. 1 and does not change with the pattern No. 2 for a strong signal in the very strong noise,
- becomes 2 (pattern No. 2) to five times larger for a strong signal in the mean sea noise.

So, the influence of the target and the ambient noise characteristics are rather difficult, according to the propagation characteristics of the medium.

We can also notice that it is not so important for the surrounding conditions to be fitted to the hypothesis of the optimum-filtering calculation. However, that particularity is not unexpected because the radiated noise spectra of the various targets are very similar as well as the various ambient sea noise spectra (which is wrong for the levels).

At last the array directivity (or the antenna length for a linear array) does not influence much the range as long as we keep rather high values. On the contrary (Fig. 5), the range drops down very fast when the antenna becomes an omnidirectional receiver.

2.5 Noise-Maker Out of the Directivity Main Lobe

To enlarge that parametric study of the detection by a passive system, we have considered the possibility of a noise-maker coming out of the directivity main lobe (inside the lobe, it becomes impossible to detect the target). We have limited the study to a 50 000 tons oil-tanker, taking into account the ambient sea-noise.

Two cases have been considered:

- the optimum filtering is fitted to he noise-maker, according to its radiated noise spectrum as well as to its remoteness from the sonar,
- the optimum filtering is fitted to the sea noise.

Supposing that the antenna gain G towards the noise-maker is independent of the bearing and of the frequency, the equations become:

$$\rho^2 = T \int_0^\infty \frac{A_s^2(\nu)}{h_s^2(\nu)} \cdot \frac{d\nu}{\left[\dfrac{A_B(\nu)}{\psi^*(\nu)} + \dfrac{A_x(\nu)}{G^* \cdot h_x(\nu)}\right]^2}$$

in the first case, when the surrounding conditions are fitted to the hypothesis of the optimum-filtering calculations, and

$$\rho'^2 = T \cdot \frac{\left[\displaystyle\int_0^\infty \frac{A_s^2(\nu)\cdot\psi^{*2}(\nu)}{A_B^2(\nu)\cdot h_s^2(\nu)}\, d\nu\right]^2}{\displaystyle\int_0^\infty \frac{A_s^2(\nu)\cdot\psi^{*4}(\nu)}{A_B^4(\nu)\cdot h_s^2(\nu)} \cdot \left[\frac{A_B(\nu)}{\psi^*(\nu)} + \frac{A_x(\nu)}{G^*\cdot h_x(\nu)}\right]^2} .$$

In the second case, when the surrounding conditions (being of a noise-maker) are not fitted to the hypothesis (sea noise).

With:

$A_x(\nu)$ = noise-maker radiated noise

$h_x(\nu)$ = transmission-loss between the noise-maker and the sonar

$G = 10 \lg G^*$.

The main conclusions illustrated in Figs. 6 and 7 are:

- it is almost impossible to detect the target if the noise-maker is closer than $r_0/2$;
- the ranges become acceptable ($0.7\ r_0$ to $0.9\ r_0$ according to the geographic zone) only if the noise-maker is farther away than $2\ r_0$;
- the detection zone influences highly the results: in pattern No. 1 an unfitted filter is clearly bad for the range, but in pattern No. 2 it does not matter.

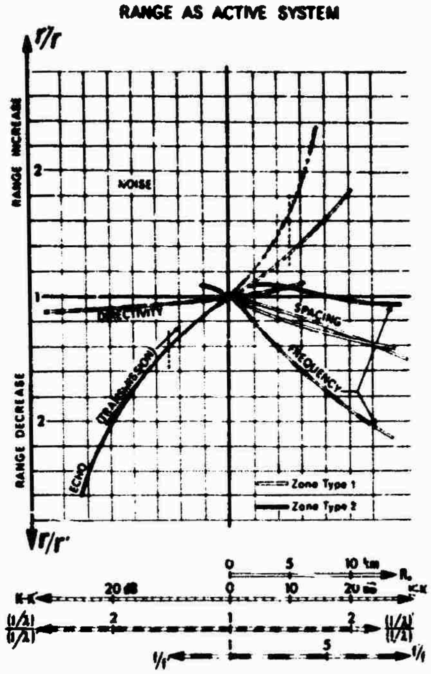

FIG. 1

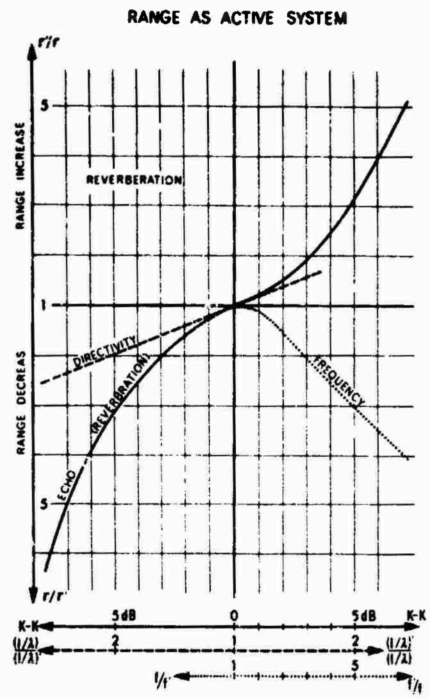

FIG. 2

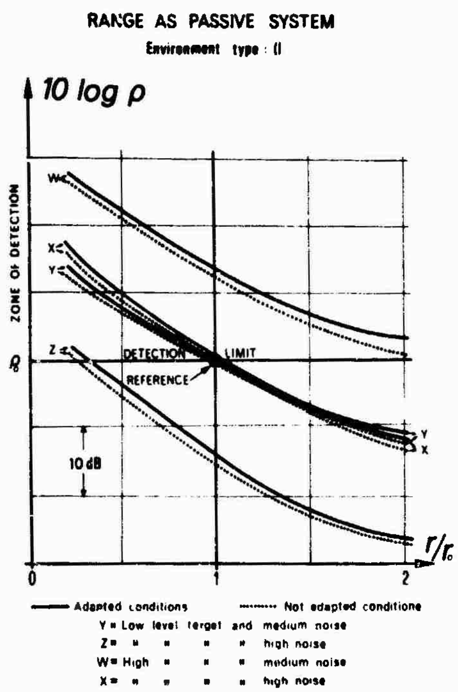

FIG 3

RANGE AS PASSIVE SYSTEM

Environment type 1

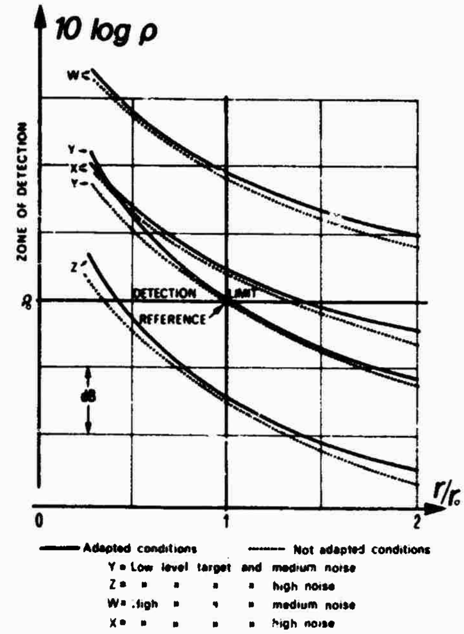

FIG. 4

RANGE AS PASSIVE SYSTEM

Influence of directivity

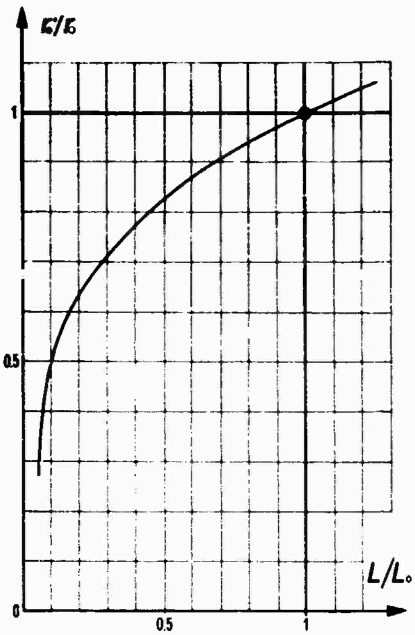

FIG. 5

RANGE AS PASSIVE SYSTEM

Precence of jammer out of beam

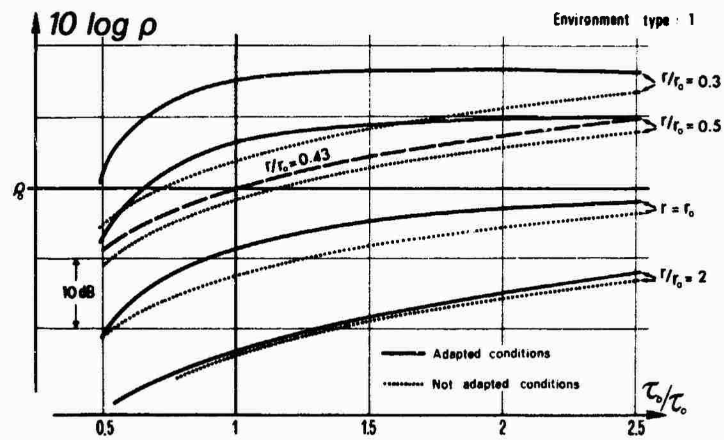

FIG. 6

RANGE AS PASSIVE SYSTEM

Precence of jammer out of beam

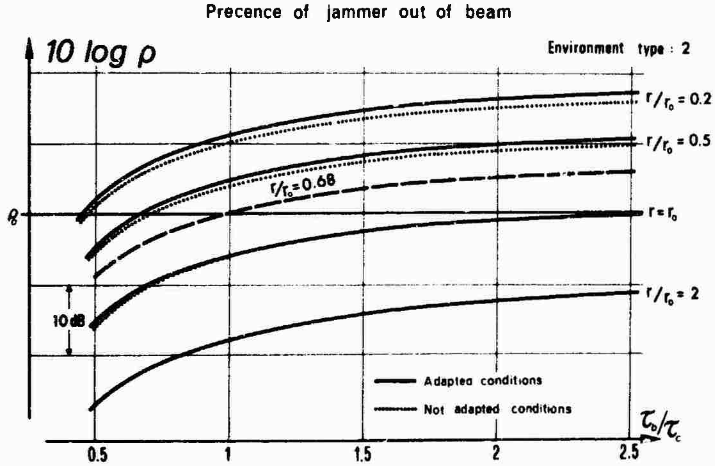

FIG. 7